Effects of Electric Forces on Rain Formation Processes in Tropical Clouds

Thesis Submitted for the Award of the Degree of

Doctor of Philosophy

in

Physics

by

DIPJYOTI MUDIAR

Indian Institute of Tropical Meteorology, Pune-411008, India

Internal Supervisor

Dr. Manoj Kr. Srivastava,

Professor, Department of Geophysics, BHU

External Supervisor

Dr. Sunil D Pawar,

Scientist-F, IITM

External Co-Supervisor

Dr. Anupam Hazra,

Scientist-F, IITM

External Co-Supervisor

Dr. D. M. Lal,

Scientist-D, IITM

Department of Geophysics, Institute of Science

Banaras Hindu University, Varanasi-221005, India

Enrollment No. 422928 **September, 2020**

विद्ययाऽमृतमश्नुते

काशी हिन्दू विश्वविद्यालय BANARAS HINDU UNIVERSITY

Effects of Electric Forces on Rain Formation Processes in Tropical Clouds

Thesis Submitted for the Award of the Degree of

Doctor of Philosophy

in

Physics

by

DIPJYOTI MUDIAR

Indian Institute of Tropical Meteorology, Pune-411008, India

Internal Supervisor

Dr. Manoj Kr. Srivastava,

Professor, Department of Geophysics, BHU

External Supervisor

Dr. Sunil D Pawar,

Scientist-F, IITM

External Co-Supervisor

Dr. Anupam Hazra,

Scientist-F, IITM

External Co-Supervisor

Dr. D. M. Lal,

Scientist-D, IITM

Department of Geophysics, Institute of Science

Banaras Hindu University, Varanasi-221005, India

Enrollment No. 422928 **September, 2020**

Dedicated to

The Curious Young Minds of Tomorrow

UNDERTAKING FROM THE CANDIDATE

I, DIPJYOTI MUIDAR, hereby declare that I have completed the research work for the full time period prescribed under the clause VIII.1 of the Ph.D. ordinance of the Banaras Hindu University, Varanasi and the research work embodied in this thesis entitled "**Effects of Electric Forces on Rain Formation Processes in Tropical Clouds"** is my own work.

Date: Dipjyoti Mudiar

Place: Varanasi

ANNEXURE-E

(Under Clause XIII.2 (b) (iii))

CANDIATE'S DECLARATION

I Dipjyoti Mudiar certify that the work embodied in this Ph.D. thesis is my own bona fide work carried out by me under the supervision of Dr. Manoj Kr. Srivastava (internal supervisor), Dr. Sunil D. Pawar (external supervisor), Dr. Anupam Hazra (external co-supervisor) and Dr. D. M. Lal (external co-supervisor) for a period from March 2017 to September 2020 at Banaras Hindu University, Varanasi and Indian Institute of Tropical Meteorology, Pune. The matter embodied in this Ph. D. thesis has not been submitted for award of any degree/diploma.

I declare that I have faithfully acknowledge, give credit to a referred to and referred to the research worker wherever their works have been cited in the text and the body of the thesis. I further certify that I have not willfully lifted up some other's works, para, text, data, results, etc. reported in the journals, books, magazines, reports, dissertations, theses etc. or available at websites and included them in this Ph.D. thesis and cited as my own work.

Date:

Place: Varanasi **Dipjyoti Mudiar**

Certificate from the Supervisor/Co-Supervisor

This is to certify that the above statement made by the candidate is correct to the best of our knowledge.

Dr. Anupam Hazra
External Co-supervisor

Dr. Sunil D Pawar
External Co-supervisor

Dr. D. M. Lal
External Co-supervisor

Porf. Manoj Kr. Srivastava
Supervisor

ANNEXURE-F

(See Clause XIII.1 (c) and XIII.2 (b) (iv))

COURSE WORK COMPLETION CERTIFICATE

This is to certify that **Mr. Dipjyoti Mudiar,** a bonafide research scholar of this department, has successfully completed his Course Work as per the guidelines of the University, which is a part of his Ph. D. program.

Date: 04/09/2020

Head

विभागाध्यक्ष / HEAD
भू-भौतिकी विभाग
Department of Geophysics
काशी हिन्दू विश्वविद्यालय
Banaras Hindu University
Varanasi-221005

Place: BHU, Varanasi

Department of Geophysics
Institute of Science, BHU
Varanasi-221005

ANNEXURE – F

(See Clause XIII.1 (c) and XIII.2 (b) (iv))

PRE-SUBMISSION SEMINAR COMPLETION CERTIFICATE

This is to certify that **Mr. Dipjyoti Mudiar**, a bonafide research scholar of this department has successfully completed his Pre – Submission seminar requirement on **05.08.2020**, which is a part of his Ph.D. programme on his thesis titled ***" Effects of Electrics Forces on Rain Formation Processes in Tropical Clouds"***.

Date: 04/09/2020

04/09/2020

Head

Department of Geophysics

Institute of Science, BHU

Varanasi- 221005

Place: BHU Varanasi

विभागाध्यक्ष /HEAD
भू-भौतिकी विभाग
Department of Geophysics
काशी हिन्दू विश्वविद्यालय
Banaras Hindu University
वाराणसी-२२१००५/Varanasi-221005

ANNEXURE-G

(Under Clause XIII.2 (b) (v))

COPYRIGHT TRANSFER CERTIFICATE

Title of the Thesis: Effects of Electric Forces on Rain Formation Processes in Tropical Clouds

Candidate's Name: Dipjyoti Mudiar

Copyright Transfer

The undersigned hereby assigns to the Banaras Hindu University all rights under Copyright that may exist in and for the above thesis submitted for the award of the Ph.D. degree.

Dipjyoti Mudiar

Acknowledgment

I deeply thank my external supervisor Dr Sunil D Pawar for the wonderful and exciting years that I have spent in IITM. You have provided me unique support, opportunities, scientific insight and most importantly the freedom to explore science. I remember our never ending discussion about scientific problems at hand and the healthy debates that has enlightened me as a young researcher. Thank you for a fantastic 7 years.

I would like to thank my internal supervisors at BHU, Varanasi Prof. Manoj K. Srivastava for continuous supervision of the work and assisting me in the registration process and for all the help during my visit to BHU, Varanasi. My deep gratitude to Dr Anupam Hazra (Co-supervisor) for introducing me to the world of numerical modeling of the atmosphere.

I would like to offer my sincere thank to Director, IITM, Pune for sponsoring me throughout to carry my research forward to obtain the degree of doctor of philosophy. I thank Department of Geophysics, Banaras Hindu University, Varanasi for allowing me to pursue my PhD research.

Special thanks to the scientific and support stuff of IITM, Pune for all the support during my stay in IITM.

I would like to offer my deep gratitude to Prof Bhupendra nath Goswami for his continuous guidance throughout the course of the study that resulted this thesis. It has been an honor to work with you, Sir.

I deeply acknowledge the support received from all my co-authors.

Although, not directly involved with this thesis work, I must acknowledge the invaluable contribution of Prof. Earl Williams, MIT, Cambridge as the first reviewer of all the manuscripts. I am grateful to those unknown reviewers without whose immensely valuable comments , my research work would have been of a much lesser quality than what it is now.

I would not miss this opportunity to acknowledge the contribution of Dr Akhil Ch. Das who has introduced me to the world of physics.

The work in this thesis wouldn't have been possible without the generous assistance of Dr Mahen Konwar, Subrata Mukherjee and Manoj Domkawale. I would like to offer my special gratitude to them.

I would like to also thank my family for the support and patience during this long pursuit to stand as a PhD holder.

Finally, I would like to thank my seniors and all my friends, especially Madhuparna Di ,Nanbanita Ba, Bidyut Da, Chinmayee, Bijita, Sangkha, Prodip, Arko, Bhupendra, Manmeet, Khunsang Da and Nipu. Thank you guys!

Contents

List of Figures

List of Tables

List of Abbreviations

AC :Alternating current

AEO :Atmospheric Electricity Obervatory

AWS :Automatic Weather Station

BMJ :Betts-Miller-Janjic

CAIPEEX : Cloud-Aerosol Interaction and Precipitation Enhancement Experiment

CAPE :Convective Available Potential Energy

LFC : level of free convection

CCNC : Cloud Condensation Nuclei Counter

CCN : cloud condensation nuclei

CG :cloud-to-ground

CIN : convective inhibition energy

CLOUD : Cosmics Leaving Outdoor Droplets

CLWC : cloud liquid wate

CPM :Convection Permitting Model

CTL : control

em :electromagnetic

Ens. Mean : Ensemble mean

ESC : electrified shower cloud

FNL :Final

GD :Grell-Devenyi ensemble

GFV : Gradient of Fall Velocity

HACPL :High Altitude Cloud Physics Laboratory

HF :High Frequency

HTI : Height Time Intensities

IC :intra-cloud

IST : Indian Standard Time

ITCZ : Inter-tropical convergence Zone

JWD :Joss-Waldvogel Disdrometer

K : Kelvin

kA :kilo-Ampere

KF :Kain-Fritsch

LIS :Lightning Imaging Sensor

LIS :Lightning Imaging Sensor

LNB : level of neutral buoyancy

LPCC : lower positive charge center

MAE : mean absolute error

MCS : Mesoscale convective systems

MeV : Mega electronvolts

MHz :Mega Hertz

MLLN :Maharashtra Lightning Location Network

MODIS : Moderate Resolution Imaging Spectroradiometer

Morr(M) :Morrison(Modified)

Morr :Morrison

MRR :Microrain radar

MSL :mean sea level

MVD : Median Volume Daimeter

MWD :Mass-Weighted Diameter

GHz :Giga Hertz

MWR :Microwave Radiometer

NCAR : National Centre for Atmospheric Research

NCEP :National Centre for Environmental Prediction

NIC : non-inductive charging

NWP : Numerical Weather Prediction

Obs : Observation

PT : Platinum resistance thermometer

QPF : quantitative precipitation forecast

RDSD :Raindrop Size Distribution

RLWC : Rain Liquid water Content

rpm :rotation per minutes

SE : strongly electrified

SMPS : Scanning Mobility Particle Sizer

TGF : terrestrial gamma-ray flashes

TRMM :Tropical Rainfall Measuring Mission

ic : initial condition

KHz : kilo Hertz

USA : United States of America

UTC :Universal Standard Time

VLF :Very low frequency

WE : weakly electrified

PREFACE

Precipitation, a product of complex cloud microphysical processes in the Earth's atmosphere has a profound influence on the Earth's geosphere as well as the biosphere. The quantity and intensity of precipitation at the Earth's surface influences the hydrological cycle as well as the social and economic activity of human. Historically persistent attempts have been made for accurate estimation of intensity and quantity of precipitation through multidimensional observational network, and also using numerical weather/climate prediction models. It has been recognized that for accurate estimation of rainfall with weather radar, it is very important to understand the prevailing cloud microphysical processes which leads to the raindrops. Although, the electrification mechanism of cloud in the Earth's atmosphere is understood reasonably well, the effect of electrification on the cloud processes still remain largely unexplored in the real atmospheric condition.

Although there are strong numerical and laboratory evidence of substantial electrical influence on rain formation processes in the Earth atmosphere, yet they are poorly modeled in most climate models. Also, over the Asian monsoon region, sufficient simultaneous observations of electrical and microphysical parameters under different precipitating environments are lacking. Attempts has been made in this thesis to quantify the electrical influences on the rain micro-physical processes inside tropical clouds and hence on the quantitative precipitation through observational investigations and numerical modeling. For evaluation and quantification of the possible electrical influence in the rain microphysical processes, observations at the upper level as well as at the ground have been analysed. Simultaneous measurement of cloud electrification and precipitation has been made to establish the anticipated association between the two observables. A few numerical simulations of electrically distinguished rain events have been performed using the Weather Research and Forecasting (WRF) model. This Thesis consists of seven chapters as follows

1. Introduction to tropical clouds, rain initiation and electrification.

2. Data and methodology adopted

3. Quantification of the Effect of in-cloud Electrical Forces on Raindrop Size Distribution (RDSD) in Stratiform Tropical Clouds

4. Association between Lightning and Intensity of Surface Precipitation

5. The Electrical Route to Realising Intensity Simulation of Heavy Rain Events in Tropics

6. The Laboratory Investigation of Electrical Influence on the Freezing of water drops in Perspective of Cloud Physics

7. Conclusions and summary

Chapter 1

Introduction

Chapter 1

1 Tropical Cloud, Dynamics and Microphysics

1.1 Introduction

Cloud, a visual manifestation of the general circulation of the Earth's atmosphere influences the hydrological cycle as well as radiation budget substantially. Particularly tropical clouds known to have profound importance in the global distribution of heat, momentum and water vapour vertically as well as laterally. Tropical clouds feedback to the general circulation through radiative forcing and latent heating. On the other hand, precipitation is the manifestation of complex microphysical interaction between the air dynamics and microphysical processes inside cloud. It drives the global atmospheric general circulations by redistributing the energy in the form of latent heat. The quantity and intensity of precipitation have substantial influences on the hydrology of earth *geosphere* apart from day to day impact on the *biosphere*. Proper understanding of the complex microphysical process that leads to precipitation is of profound importance in regard to the quantitative observational measurement and accurate numerical simulation and forecasting of precipitation in weather and climate models. There is considerable observational and laboratory evidence of substantial electrical influence on cloud microphysical processes. Yet they are poorly modeled in most climate models. Also, over the Asian monsoon region, sufficient simultaneous observations of electrical and micro-physical parameters under different precipitating environments are lacking. These gaps in observations and our understanding motivated this thesis to quantify the electrical influences on the rain microphysical processes inside tropical clouds and hence on the quantitative precipitation through observational investigations and numerical modeling. To set the stage, fundamentals of development of clouds, microphysical processes on precipitation and known facts on electrification within clouds are summarized in the chapter.

Large population density of cumulus cloud in tropics indicate that the tropical atmosphere is conditionally unstable and associated with larger Convective Available Potential Energy (CAPE) (*Xu and Emanue*l, 1989)

$$CAPE = \int_{LFC}^{LNB} g\frac{T_a - T_e}{T_e}dz \tag{1.1}$$

Where, g is the acceleration due to gravity and T_a and T_e are virtual temperatures of the parcel and the environment at the same level. LFC indicate the level of free convection while LNB indicate the level of neutral buoyancy as shown in Figure 1.1. Most of the deep convections are associated with CAPE greater than 1000J kg^{-1}. The air parcel has to overcome the convective inhibition energy (CIN) to reach the LFC so as to create favorable condition for deep convection.

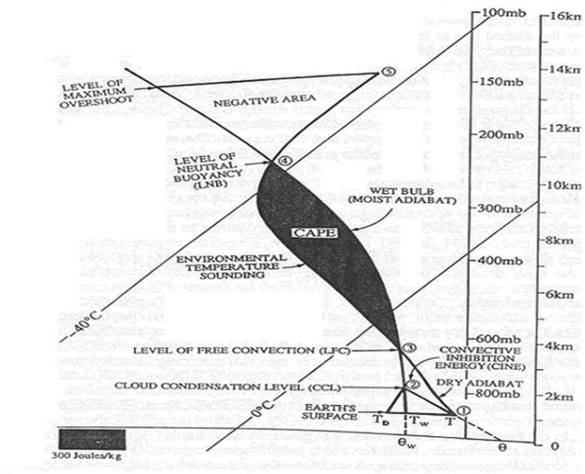

Figure 1.1: Illustration of conditional instability on a thermodynamic diagram (from *William*s, 1995).

In the Inter-tropical convergence Zone (ITCZ), about 40-45% of the total cloud is deep convective (*Gu and Zhang*, 2002). Observations suggest the deepest convective clouds in the earth atmosphere are thunderstorms, the genesis of which can be assigned to conditional instability. This set of clouds derive the required energy to generate deep convection primarily from the CAPE (*Williams*, 2001). The tropical atmosphere is essentially barotropic with modest lateral variations of air-temperature but is conditionally unstable. Deep convection can be triggered by initial lifting to LFC by surface heating and convergence by waves on easterlies where uplift of air parcels is nearly vertical with typical speeds of around 10-20 m s^{-1}. The baroclinic atmosphere in extra-tropics exhibits highly sheared environments causing the tilted updraft and laterally displaced from the downdraft. Extra-tropics is the budding ground of long-lived and most severe storms observed in the earth atmosphere. In severe storms, vertical velocities have been observed to exceed 50 ms^{-1}. This kind of updraft speed in severe storms can be explained by higher CAPE

$$W_{max} = \sqrt{2CAPE} \tag{1.2}$$

Although, in the barotropic environment, where entrainment is quite substantial, the parcel theory may not give an accurate prediction of vertical velocity as explained by *Williams,* (2001). Radar observation of convective storms suggests that the updraft profile increases monotonically from lower to the higher level (*Williams* et al., 1981).

In active convective system, the net vertical mass transport produces net latent heating at all levels from the ground and net horizontal convergence at the lower level and divergence at upper levels driven by mass continuity requirement (Figure 1.4) (*Houze*,1997). The boundary layer convergence decreases CIN, bringing down the LFC which triggers deep convection (*Mapes*, 1993). Gravity waves emanated from the active convective region as a compensation of upward mass transport can cause upward displacement at low levels forcing additional convection in the neighborhood. Mesoscale convective systems (MCS) are the largest and most organized convective cloud observed over the tropics, produced in response to convective instability. MCS accounts for a large proportion of precipitation in the tropical belt (*Houze*, 2004).

Figure 1.2: Cumulus stage of a storm observed over Pune, India.

The microphysical aspect of cloud could substantially affect the mean state of a convective atmosphere as suggested by *Grabowski and Smolarkiewicz* (1999), primarily through coupling between the convection and surface processes and by affecting the net radiative flux (The shape and size of precipitation particles). The smaller raindrops will evaporate effectively leaving the boundary layer cold and dry. Clouds with smaller drops will have a longer lifetime, thereby increasing the radiative cooling. Hence, precipitation intensity is anticipated to influence radiation as well as convective processes.

1.2 Precipitation Formation in Tropical Clouds

1.2.1 Warm rain

The warm rain originated in the warm phase of the cloud below the freezing level, the primary mechanism being the collision-coalescence growth cloud drops. In the tropical belt, warm rains account for 31% of the total rain amount and 72% of the total rain area (*Lau and Wu*, 2003). Conditionally unstable air parcel ascent and expand adiabatically which leads to condensation of water vapour. The condensational growth of a cloud droplet primarily depends on the ambient supersaturation. The growth rate of a micrometer size droplet is inversely proportional to radius of the droplet. Droplets growing by condensation first increases its size very rapidly. As the size of the droplets increase, the condensational growth diminishes. The cloud droplets must acquire a size of 20μm by condensational growth before raindrops start to grow by collision-coalescence methods in the warm phase of clouds. In the presence of higher cloud liquid water, precipitation particles grow by accretion of cloud liquid drops in the convective cloud (*Houghton*,1968) The collision efficiency, E of two colliding drops is defined as the ratio of collision cross-section (S$_C$) to the geometric cross-section (S_G) (Figure 1.11)

$$E = \frac{S_C}{S_G} \tag{1.3}$$

Here

$$S_G = \pi(r+R)^2 \tag{1.4}$$

r and R being the radius of smaller and larger drops. In the case of gravity induce collision between two clouds droplets, the collision efficiency usually remain less than unity (*Pinsky et al.*, 2001) (Figure 1.3).

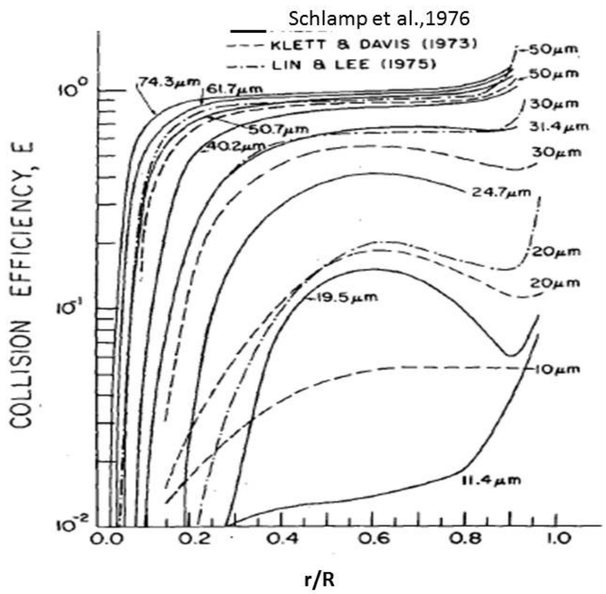

Figure 1.3: Numerically computed collision efficiency for a pair of cloud droplets as a function of the ratio of their radii. (From *Schalmp et al.*,1976)

The quantitative measure of droplet growth is the collection efficiency, a product of collision efficiency and coalescence efficiency. The collision efficiency primarily dominated by the separation of the colliding drops and the ratio of their respective sizes while the coalescence efficiency is depends on factors like the surface tension, ambient electrical forces etc. apart from the flow filed the particles are in. The drop which attains a radius of 0.1 mm stands a good chance to reach the ground before complete evaporation and called raindrops. The larger updraft advect the particles to higher altitude, increasing the residence time in cloud, thereby allowing the particles to grow to a size from where they drift downward contributing to the precipitation flux.

1.2.2 Cold Rain

It has been reported that substantial amount of continental precipitation form via ice phase mechanism (*Lau and W*u, 2003; *Lohmann and Feichter*, 2005; *Lohmann and Diehl*, 2006) indicating that cold rain processes could have a substantial influence on the hydrological cycle. Once the liquid phase precipitation particles reach the sub-freezing layer carried by the prevailing stronger updraft, cold rain processes initiate. In the deep convective cloud, precipitation originated from two dynamically and microphysically distinct regimes, one is the convective regime, and the other one is the trailing part of active convection, termed as stratiform regime (*Houze*,1997). Above the freezing layer of the convective regime, in the presence of larger supercooled water, the ice crystals primarily grow by collecting the super-cooled liquid drops producing graupels and snow particles. The *Clausis-Clapeyron* relation suggested the existence of two equilibrium vapour pressure in the mixed phase region, one for liquid water and the other one for ice. As the equilibrium vapour pressure for ice is less than that of liquid water at the same temperature ice crystal grows by vapour diffusion at the expense of liquid water droplets, the process famously known as *Bergeron process* of crystal growth. The stratiform regime is characterized by a weaker vertical velocity of around (1 ms^{-1}). In this regime, the upper atmosphere is dominated by a net upward velocity and the mid-levels below the melting layer is dominated by a net downward velocity. The upward mass transport in the upper levels allows the precipitation particles to grow by vapour deposition (*Rutledge and Houze*, 1987). The particles increase in their sizes by aggregation in the temperature range of 0 to $-5^{o}C$ (*Hobbs*, 1974). Upon drifting down, these aggregates melt and fall as raindrops and as the manifestation of complex microphysical processes in the form of precipitation.

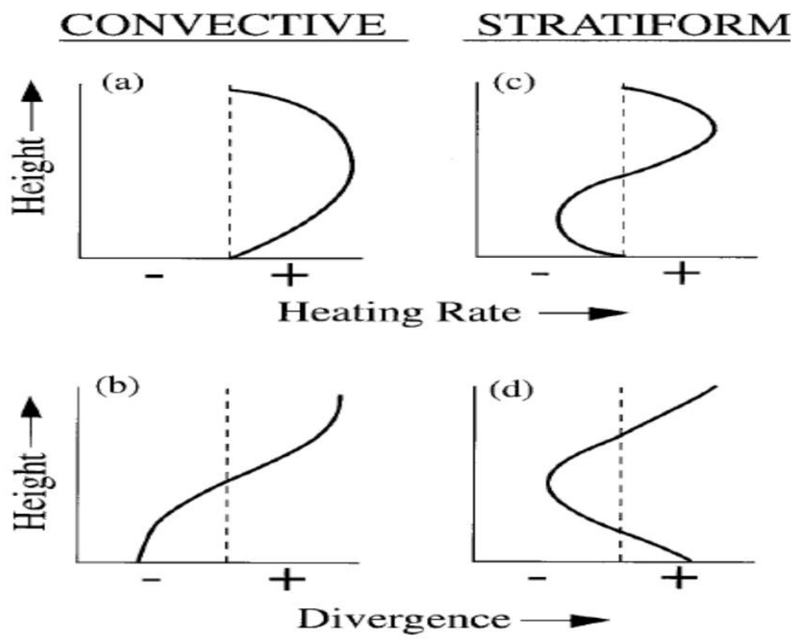

Figure 1.4: Characteristic Profiles of latent heating and horizontal mass divergence in convective and stratiform tropical clouds. (From *Houze*, 1997)

The distribution of cloud in the earth atmosphere is the manifestation of the general circulation of the atmosphere while the global atmospheric circulation is primarily maintained by tropical convection which transports moisture and heat vertically as well as laterally in the atmosphere. Primarily the interaction between the two mediated by phase change, radiative transfer and turbulent transfer of air parcels. The extent of interaction modulated by the vertical depth, lateral dimension, microphysical properties of cloud systems. One of the primary components of the general circulation of atmospheres is precipitation which substantially impacts the hydrological cycle and cloudiness of earth atmosphere. The latent heating associated with the precipitation is a primary driving force of circulation in the earth atmosphere (*Rutledge and Houze*,1987).

1.3 Precipitation Modification by aerosol

The presence of aerosols, both natural and anthropogenic, further complicates the precipitation formation process and its impact is found to be non-linear in precipitation modification. The cumulative precipitation may increase or decrease in response to aerosol and cloud condensation nuclei (CCN) concentration, primarily depending upon the size distribution of aerosol and the prevailing cloud microphysical and dynamical properties (*Rosenfeld*,1999; *Tao et al*., 2012; *Khain et al*.,2005). Distribution wise aerosols in the size range of $0.01 - 1\mu m$ leads to an increase in the number concentration of droplets making the droplet spectra narrower and delay the rain initiation by increasing the height of collision triggering levels (*Khain et al.* 1999; *Andreae et al,.* 2004) while aerosols of sizes above 1 μm produce larger droplets thereby enhancing the precipitation formation processes at lower levels (*Yin et al.,* 2000; *Rosenfeld et al*., 2002). CCN below the size of $0.01\mu m$ do not get activated usually and does not have much influence on the precipitation processes. *Rosenfeld* (2000) found that polluted atmosphere (with a high concentration of aerosol particles) can suppress precipitation by inhibiting the coalescence growth of cloud drops and formation of ice particles. However, a few investigations and observations suggested that the presence of high concentration of aerosol can invigorate the convection and produce intense thunderstorm with heavy precipitation by suppressing the warm rain processes (*Andreae et al*., 2004; *Rosenfeld and Woodley*, 2003). The simulation study of *Hazra et al*. (2013a) during the monsoon break and active phase over India suggest the invigoration of convective activity and enhancement of precipitation through the modification of cold rain microphysics in the presence of higher concentration of aerosol particles.

1.4 Electrification of Cloud in The Earth Atmosphere

One of the spectacular exhibitions of interaction between air dynamics and cloud is the cloud electrification and consequent lightning discharges. Curiosity-driven scientific exploration of the electrical aspect of earth atmosphere started back in the 17th century. Modern investigation of cloud electrification started with extensive laboratory experiments and field observation of *CTR Wilson* in early 20th century (*Wilson*, 1921; *Williams*, 2009), although century and half earlier, *Benzamine Franklin* had characterized the polarity of thunderstorms with his famous kite experiments (*Franklin*, 1751). Since then, the science of cloud electrification has been evolving in the backdrop of numerous laboratory and observational investigations. A thorough investigation through the available literature suggests, the electrification processes get substantially influenced by the prevailing meteorological processes; the primary factors included the air updraft, cloud liquid water (CLWC) in the mixed-phase region of cloud along with aerosol concentrations. The modern investigation of cloud electrification primarily germinated through the famous debate between two British physicist *C. T. R. Wilson* and *G. C. Simpson* on the polarity of thundercloud which lasted nearly 50 long years (*Williams*, 2009). Because of the inherent complexity of the charge separation processes inside cloud, a universal theory of cloud electrification remain illusive till date. The observation of electrical structure of strongly electrified cloud indicates a generalized *Tripole structure* (*Williams* 1989), a positive charge center at the top, a negative charge center near above the mixed phase and some positive charges at the bottom of the cloud (Figure 1.5).

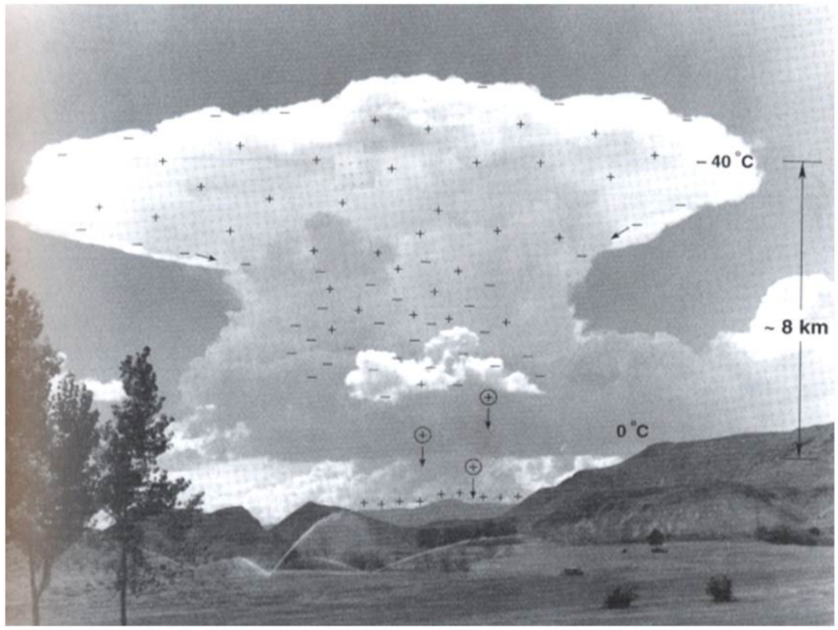

Figure 1.5: Simplified picture of charge distribution in strongly electrified clouds. (From *Krehbiel*, 1986)

The primary recipe of cloud electrification is the interaction between the larger size graupel particles and the smaller size ice crystal in the mixed phase region of cloud mediated by the differential velocity of the two species. The collision between the graupel and ice particles results in the selective transfer of negative charge to the larger particles and the differential separation of the two species produces the observed cloud-scale dipole structure (*Williams*, 2001) (Figure 1.6). The location of the positive charge is termed as main positive while that of negative charge is termed as the main negative charge center. The electrical pattern illustrated in Figure 1.6 is popularly known as the positive dipole.

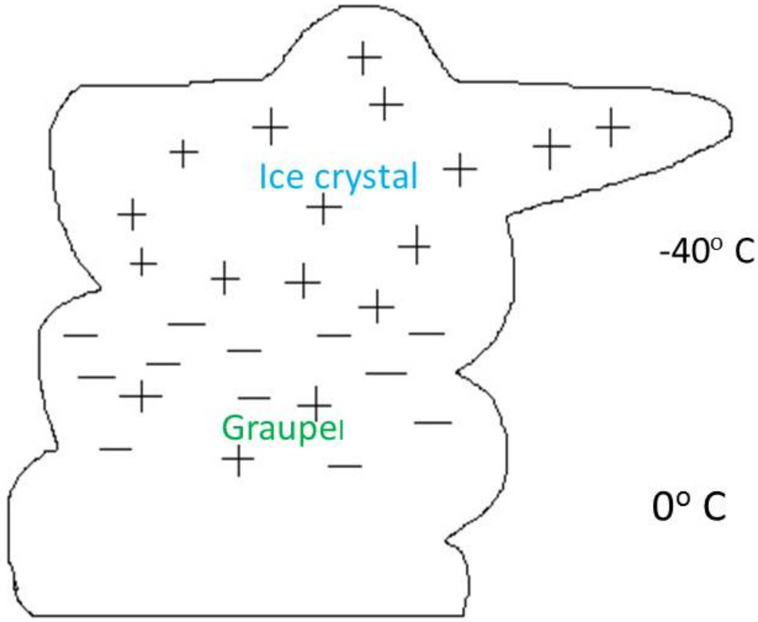

Figure 1.6: Illustration of cloud-scale dipole structure produced by differential charge separation.

This positive dipole is the most common and prevalent electrical characteristics of the ordinary thundercloud and is the primary producer of predominant lightning type, i.e. intra-cloud (IC) and cloud-to-ground (CG). In addition to this two main charge center, many observations reported a small accumulation of positive charge below the main negative charge known as lower positive charge center (LPCC) (*Simpson and Scrase*,1937; *Moore*,1976; *Krhebeil et al.*,1979; *Marshall and Winn*,1982; *Mo et al* ,2002). This lower positive charge possibly caused by the same macroscopic processes as in the upper level. One of the primary source of the LPCC may be the corona discharge from the sharp elevated objects below the thundercloud (*Vonnegut*, 1955; *Wilson*,1956). With their aircraft observations, *Mo et al.* (2002) suggested that this lower positive charge may be the result of charge deposition by lightning discharges.

1.5 The Charging Mechanism

The primary charging mechanisms of cloud postulated on the basis of numerous observation and laboratory experiments are discussed below

1.5.1 Convective Charging

According to the convective charging mechanism of cloud electrification, a growing cumulus cloud draws positive charge from below the cloud base and, prevailing updraft carries this charge upward (*Grenet*, 1947, *Vonnegut*, 1953). The updraft carries this positive charge to the cloud top. The positively charged cloud top attracts negative ions from the surrounding atmosphere where ions get attached to the cloud particles in cloud boundary forming a screening layer. The downward motion of the screening layer transported the negative charge to lower portion of the cloud. This causes enhancement of electric field on the Earth's surface. The enhanced electric field produces corona discharges on the earth surface producing positive ions near the earth surface. These positive ions again can provide positive feedback to the mechanism (*Vonnegut et al.*, 1962). The estimation made by *Schonland* (1928) and *Wormell* (1930,1953) suggested that the charges produced by corona discharges near the earth surface beneath a thunderstorm is sufficient to account for all the electrical energy inside the thundercloud. However, corona current observed to be less than 100*mA* which is quite small compared to the time averaged lightning current which is about 1 A measured below a typical thundercloud. Also, as suggested by *Williams* (1989a), the upward and downward motion observed inside cloud seems to be not very effective in transporting negative screening charge downward and its entertainment into the cloud as required by the mechanism.

1.5.2 Precipitation Charging

To account for the cloud–scale charge separation, precipitation charging mechanism of thundercloud electrification has been proposed and evaluated by many investigators *(Levin and Ziv*,1974; *Jayaratne and Saunders*,1984; *Williams and Lhermitte*,1983). But for electrification by falling precipitation particles, the precipitation particles must reside in the location of the observed charge center inside a thundercloud. For that, the electrical forces on the precipitation particles must be comparable with the gravitational forces acting on them in order to levitate the precipitation particles. The balancing of forces demands sudden changes in the mean *Doppler velocity* of precipitation particles concurrent with nearby lightning discharges. The *Doppler radar* observation by *Williams and Lhermitte* (1983) suggested that although electric field driven levitation of precipitation particles may happen in so-called balance level but rather infrequent. Also, the observation of the first lightning before the observation of precipitation echo suggested the precipitation independent charging mechanism in cloud.

1.5.3 Inductive Charging Mechanism

For inductive charging mechanism of cloud charging, a pre-existing electric field is essential to induce polarization charges on cloud particles. In the course of a collision between two cloud particles, the smaller particles acquire positive charges while the negative charges get transferred to the larger ones. Vertical separation of smaller and larger particles due to their differential terminal velocity under gravity creates positive electrical dipole inside cloud. *Elster and Geitel* (1913) proposed this theory for colliding water drops in their terminal velocity. The inductive charging in the course of a collision between graupel and ice crystals was proposed by *Muller and Hillebrand* (1954) and supported by *Latham and Mason* (1962). But their laboratory experiment showed that charge transfer during the collision is negligible because of the short contact time between the colliding particles. Also, the conductivity of ice particles is too low for the complete charge transfer by inductive processes during typical contact time of less than 1µ*sec* (*Illingworth and Carnti*, 1984). In the region of intense electrification inside cloud, the gravitational force on cloud particles is balanced by the electric forces acting on the charged particles which may reduce the separation of larger and smaller drops *(Kamra and Vonnegut*, 1971). Many of the modeling studies shows that this mechanism alone may not be sufficient enough to explain the observed features of thunderstorm electrification (*Illingworth and Latham*,1977; *Dye et al.,* 1986). Observation of New Mexico thunderstorm by *Stolzenburg* (1998) indicated that inductive charging mechanism could play an important role in developing observed complex charge structures after some other charging mechanism has resulted in a strong electric field to build up inside cloud. Observation by *Krehbeil et al.* (1983) also suggested a significant role of inductive charging in the formation of alternating charge layers inside clouds.

1.5.4 Non-inductive charging mechanism

Among all the charging theory proposed so far, in the backdrop of extensive observation of charge distribution as well as electric field structures inside a thundercloud and numerous laboratory investigation, the non-inductive charging (NIC) mechanism of cloud electrification is most well accepted. The NIC mechanism doesn't require a pre-existing electric field. This hypothesis is solely based upon collision and growth process of ice-phased hydrometeors in the mixed phase region of cloud. Numerous laboratory investigations of the micro-scale processes of charge separation established a convincing basis for the NIC mechanism of cloud electrification, which is found to be consistent with the large scale observation of the electrical structure of thunderstorms. Most of the laboratory studies *(Reynolds et al.*,1957; *Takahashi*,1978; *Gaskell and Illingworth*,1980; *Jayaratne and Saunders*.,1984) suggested that the observed charge structure of thundercloud can be account for by considering the collision between ice crystals and graupel particles. *Reynolds et al.* (1957) reported that warmer graupels growing by accretion of supercooled droplets acquires negative charges as results of collisions with ice crystal and suggested that differential velocity between graupel pellets and ice crystal results the observed main dipole structure inside thundercloud. The influences of temperature and cloud liquid water (CLWC), especially in the mixed phase region of cloud are well recognised by most of them. *Takahashi* (1978) reported that at a temperature warmer than -10^oC, graupel particles would take positive charges while they become negatively charged at a temperature cooler than -10^oC considering a CLWC $1-2gm^{-3}$. The distribution of positive and negative charge transfer in a T-CLWC diagram was demonstrated by *Williams et al.* (1991) (Figure 1.7). They suggested that graupel particle undergoing vapour deposition charged positively while sublimating graupel acquires negative charge, supported by the laboratory evidences of *Takahashi* (1978). The process of sublimation–deposition charging mechanism may explain the main negative and upper positive charge center typically observed in a thundercloud. It was found that charge separation is substantially higher in riming processes than vapour transfer alone (*Takahashi*,1978).

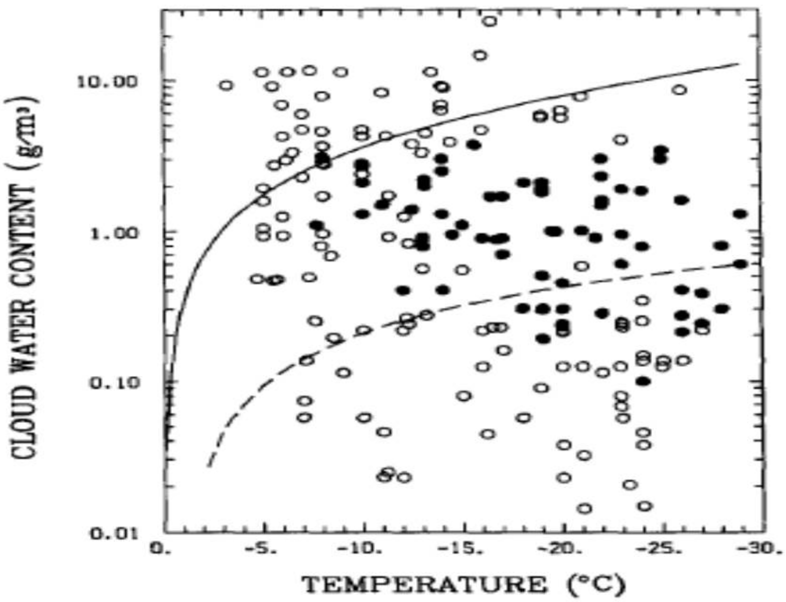

Figure 1.7: Charging of crystals through different microphysical growth states (*Takahashi*, 1978) in the mixed phase cloud. Black (white) dots denotes negative (positive) charge transfer to the rimer (graupel). (From *Williams*, 1991)

1.6 Lightning

Lightning is a visual manifestation of the release of electrical stress in the earth atmosphere. The two predominant lightning types are intra-cloud (IC) and cloud-to-ground (CG) lightning. While IC lightning links the main negative charge to the upper positive charge region, CG lightning transfer negative charges from the main negative charge region to the Earth. The typical value of lightning peak current is found to be around $40kA$, but powerful lightning reported to carry a current up to $200kA$ (*Lyu et al.* ,2015). The peak power generated by a lightning is in the order of $108 watts m^{-2}$ (*Guo and Krider*,1983) of the channel, which can raise the temperature of the channel to $30,000K$ (*Orville*,1968).

The initiation of lightning inside cloud still remains a mystery as the initiation happens deep inside the cloud and there are no physical conductors present inside cloud (*Petersen etal.*,2008). The electrical charges build up inside cloud get discharged through lightning. Initiation of lightning requires creating an elongated ionized region of length of around $10m$ or more which acts as a precursor for the formation of a hot, self-propagating lightning leader channel. The breakdown field of earth atmosphere is of the order of $10^6 V m^{-1}$. The typical measured value of electric field inside thundercloud is around 10^5 to $2 \times 10^5 V m^{-1}$. Electrical breakdown in between two parallel plane electrodes at sea levels occur at about $3 \times 10^6 V m^{-1}$. At the upper level, around $6km$ due to the reduction of pressure, breakdown field comes down to $1.6 \times 10^6 V m^{-1}$. The breakdown field again get reduced because of the elongation of the liquid hydrometeors in presence of an external electric field (*Malan and Schonland*, 1951). Corona streamers which eventually lead to the formation of stepped leader from solid and liquid hydrometeors get initiated at in-cloud field strength of at least $1.5 \times 10^5 Vm^{-1}$, at an altitude of about $3.5km$ (*Griffiths and Phelps*, 1976). Laboratory investigation of *Petersen et al.* (2008) suggested that at the low temperature region inside cloud, individual positive streamer can be initiated by ice crystals in sub-dielectric breakdown condition. Positive streamer and corona can be initiated at relatively lower field strength than the negative streamers (*Loeb*, 1966; *Dawson and Winn*,1965). The investigation by *Rison et al*. (2016) suggested that positive steamers originated in the ice crystals are primarily responsible for lightning initiation. The fast positive breakdown which is dielectric in nature consists of a number of positive streamers in a locally intense electric field region.

The relativistic runway Electron Avalanches is one of the potential candidates which observed to assist in the initiation negative CG lightning (*Chilingarian et al*., 2017). Optical observation of *bidirectional leader extension* (positive and negative) was reported by *Tran and Rakov* (2017) (Figure 1.8). The negative end observed to exhibit optical and radio-frequency electromagnetic features.

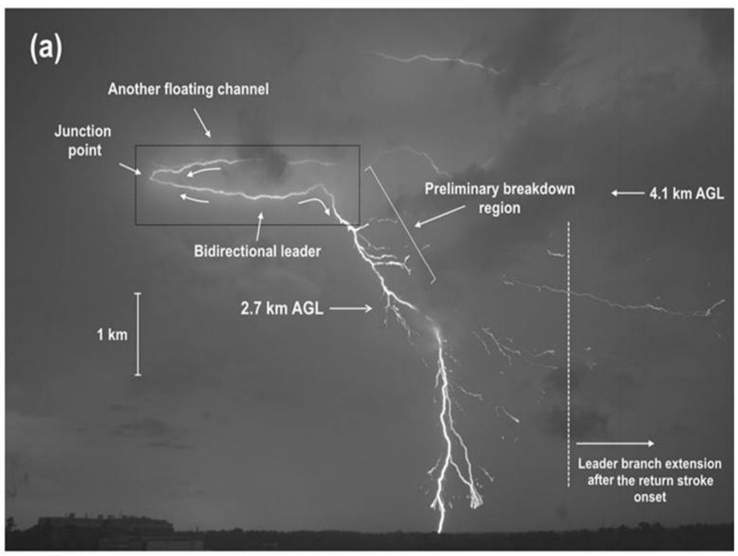

Figure 1.8: Optical observation of initiation of lightning inside cloud exhibiting bidirectional leader (From *Tran and Rakov,* 2017)

1.7 Global Electric Circuit

Assuming a surface area of $5 \times 10^{14} m^2$ of the earth surface, the total fair weather charge on the Earth will be about $5.1 \times 10^5 C$ (*Roble and Tzur*, 1986). The corresponding downward-directed surface electric field is about $130 Vm^{-1}$. Assuming a global average value of conduction current density around $3 \times 10^{-12} Ampm^{-2}$, the fair-weather current to the earth surface will have a value of about $1500 Amp$ (*Pruppacher and Klett*, 1996). This current is sufficient to neutralize the Earth in about 17 minutes in absence of any generator. *C.T.R. Wilson* proposed that the generators which keep the fair-weather current flowing are the thunderstorms and electrified shower clouds. Thunderstorms connect the highly conducting ionosphere and the Earth via poorly conducting lower and middle atmosphere. The upper positive charges of thundercloud leaked to the base of ionosphere, creating a positive potential of several hundred thousand volts with respect to the Earth's surface (*Dolezalek*, 1972). It was observed that the phase of universal time variation of thunderstorm activity over land matched the phase of the Carnegie curve of the diurnal variation of fair-weather electric field consistent with the hypothesis provided by *Wilson* (1921). The global average rate of total flashes is around $44s^{-1}$ with a maximum of $55s^{-1}$ in the northern hemisphere summer and minimum of $35s^{-1}$ in the northern hemisphere winter. *Williams and Satori* (2004) and *Williams* (2010) suggested that although lightning activity dominates the African region, the ionospheric potential measurement and the electric filed measurement over Antarctica show a dominance of South America where lighting activity peaks at 2000 UTC rather than $1400-1500$UTC when Africa is most convective.

1.8 The Interaction among the dynamics and microphysics and electrification

Cloud is the visual manifestation of air dynamics while precipitation is a realization of the interaction between dynamics and microphysical processes, while electrification is the product of both. All the processes occur simultaneously and feedback each other primarily through energy modification. It is well known that the tropical belt is the hot spot for lightning and rainfall as well. The '*Three Tropical Chimneys*' viz Africa, the Maritime Continent and the South America Continent (Figure 1.9) are the major contributor to the lightning and rainfall with varied degree of contribution to both the observable as both are having different sensitivity to the prevailing meteorological conditions (*Williams*, 2005).

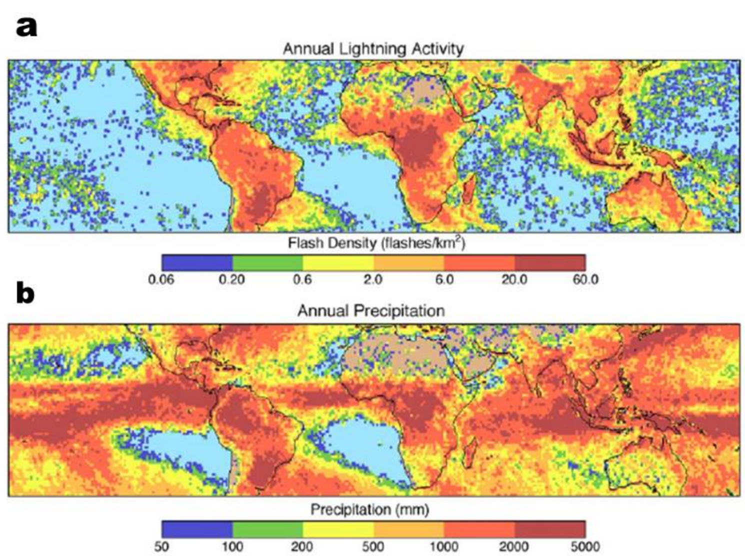

Figure 1.9: (a) Global lightning activity observed by Lightning Imaging Sensor (LIS).(b) Global rainfall observed with Special Sensor Microwave Imager.(Image is borrowed from *Williams*, 2005)

The best road map to understanding the anticipated interaction between the processes is to understand the sink and source of energy and moisture fluxes. The interaction also may be realized through redistribution of the condensate. The condensation of moisture present in the air parcels releases latent heat of condensation while depositional growth of ice particles in the mixed phase region releases latent heat of fusion. While the initial instability causes lifting of air parcels producing precipitation particles by different microphysical mechanism, the condensate loading and falling precipitation can induce downdraft which brings cold-dry air to the boundary layer (*Orvile*,1975). The drop evaporation and sublimation of ice particles to vapour phase are the major sinks of the energy inside cloud. As suggested by *Grabowski and Smolarkiewicz* (1999), cloud microphysical processes could potentially impact ocean temperature through the modification of radiation fluxes. The size of raindrops substantially influences cloud fraction and the boundary layer and hence the radiative heating and cooling and the coupling between convection and surface processes (*Grabowski*, 2000). *Li et al.*(2014) suggested that the interaction between precipitating cloud, specially the larger hydrometeors and radiation could have a larger impact on the global oceanic and atmospheric circulation. On the other hand, the influences of electrical activity in the genesis of tornadic storms were long speculated and studied historically *(Vonnegut*, 1960; *Ryan and Vonnegut*, 1970; *Armstrong and Glenn*, 2015). *Vonnegut* (1960) showed that in an updraft of radius 250m, a flash rate of 10 lightning discharges per second causes the temperature to rise by around 200^{o}C. He proposed that this intense heating can cause sustained violent updraft in a small volume of air initiating the formation of tornadic vortices. Figure 1.10 depicts a schematic representation of interaction among the prevailing dynmaical, microphysical and electrical processes inside tropical cloud.

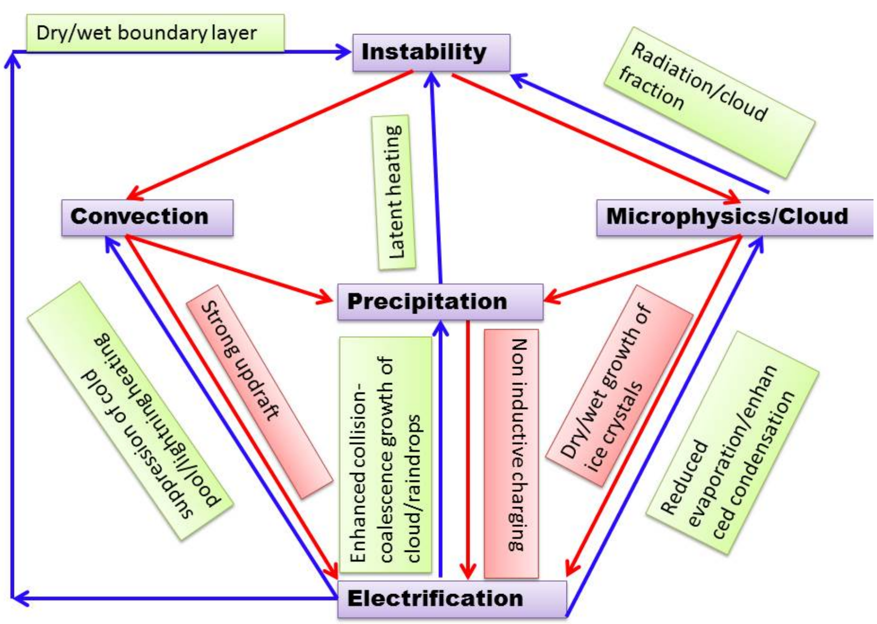

Figure 1.10: Schematic depiction of interaction among cloud dynamics, microphysical processes and electrification.

1.9 Effect of Cloud Electrification on the Microphysical Processes

Speculation about the electrical influences on precipitation formation on the Earth atmosphere is long-standing, although no quantification in the real atmospheric condition happens, may be because of the inherent complexity of microphysical processes. Back in 1879, through a set of experiment *Lord Rayleigh* observed that coalescence of two water jets is very sensitive even to the feeble electrical influences. He reported the coalescence of water drops when the jets are under the influence of feeble electricity which might encourage him to propose a mysterious connection between rain and electricity. *Davis* (1964) recognizes the importance of accurate estimation of trajectories of cloud/raindrops under the influences of hydrodynamic and electrostatic forces from the perspective of drop coalescence and charge separation in droplets inside clouds. Motivated by this, he numerically calculated the force law between two charged water drops embedded in an external electric field. The electrical force between two interacting charged drops may be represented as (*Khain et al*., 2004)

$$F_e = \frac{Q_1 Q_2}{4\pi\varepsilon_0 R^2} + \frac{1}{4\pi\varepsilon_0}\{Q_1^2 r_2)[\frac{1}{R^3} - \frac{R}{(R_2 - r_2^2)2} + Q_2^2 r_1[\frac{1}{R^3} - \frac{R}{(R_2 - r_1^2)^2} + Q_1 Q_2 r_1 r_2[\frac{1}{R^4} + \frac{1}{(R^2 - r_1^2 - r_2^2)2} - \frac{1}{(R^2 - r_1^2)^2} - \frac{1}{(R^2 - r_2^2)^2}]\} \tag{1.5}$$

Where $Q_1$and Q_2 are charges of the two drops, r_1 andr_2 are the radii of the drops, R is the distance between the center of the drops and $\varepsilon_0$is dielectric permittivity of free space. The first term of equation (1.5) represents the *Coulomb interaction*, second and third terms represent the interaction between *point charges and dipole* and the last term is for the interaction between *induced imaginary charges*. The electrical interaction increases the collision cross-section of the interacting drops.

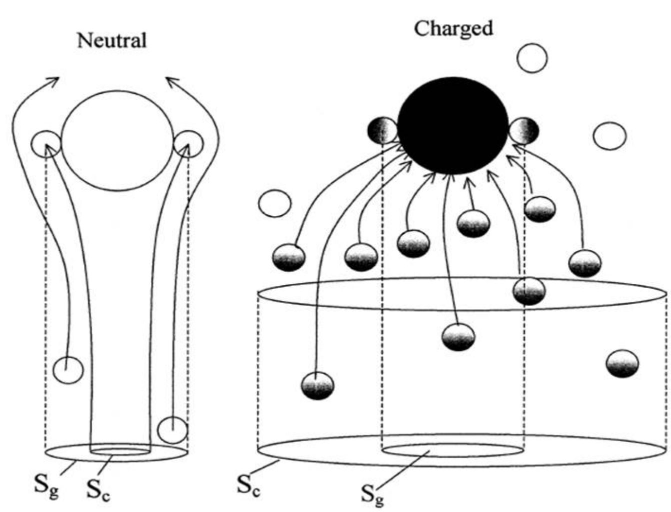

Figure 1.11: Comparison of collision cross-section of two interacting natural and charged drops. S_g indicates the geometric cross-section while S_c indicates the collision cross section (From *Khain*,2004)

The equation of motion of either of the drops can be written as (*Pruppacher and Klett*,1996)

$$m\frac{d\vec{v}}{dt} = m\vec{g}^{*} - \frac{\pi}{4}C_D N_{Re} r \eta_a(\vec{v}-\vec{u}) + \vec{F}_e \tag{1.6}$$

Where m is the mass of the drop ,v is the terminal velocity of the drop, $\vec{g}^{*}$ is the reduced gravity, C_D is the drag coefficients and N_{Re} is the *Reynolds number* with the flow field, u.

The electrical attraction between the interacting drops increase the S_g, thereby increasing the collision efficiency among the drops under the influences of hydrodynamic and electrical forces. Using the force law of *Davis* (1964), *Schlamp et al.* (1976, 1979) numerically calculated the collision efficiency between two charged cloud droplets in an external electric field (*vertically upward and downward*) and reported a significant effect of an external electric field and electric charges residing on the interacting drops on the collision efficiency of the drops (Figure 1.12a) which is also supported by the numerical calculation of *Khain et al.* (2004) (Figure 1.12b).

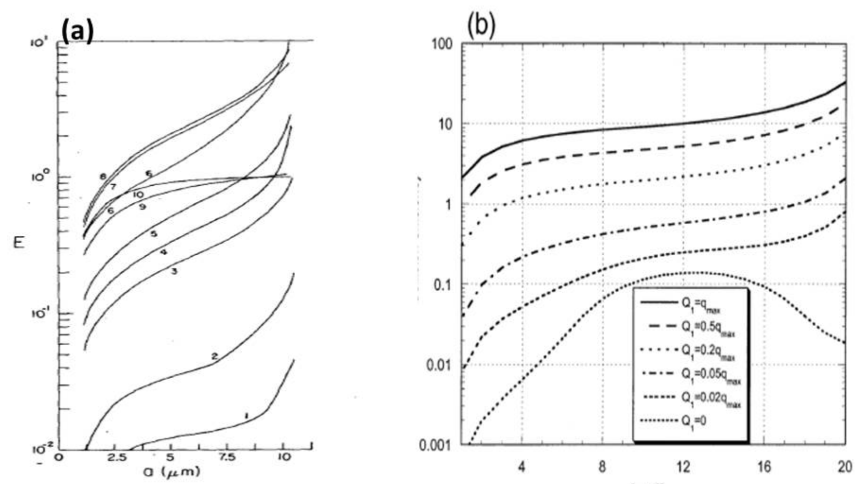

Figure 1.12: (a) Collision efficiency (E) between two interacting charged cloud drops in an external electric field. The number in the curves indicated different combinations of electric charge and fields. (From *Schlamp et al.*, 1976) (b) Same as (a), but for a 20μ*m* collector drop (From *Khain*, 2004).

Laboratory investigation of *Ochs and Czys* (1987) reported that permanent coalescence results for all impact angles upon collision of two drops if their relative charge exceeds $2 \times 10^{-12}C$ irrespective of the polarity of the charges they carry. Considering only the Coulomb interaction, the like charges on the precipitation particles will reduce the *collision/coalescence* probability of the particles. But in their investigation, *Ochs and Czys* (1987) reported permanent coalescence of two drops with same polarity for all impact angles (supported by earlier work of *Sartor*, 1960). They suggested that the coalescence may happen between the same polarity drops as the larger drops, charge carrying capacity of which is proportional to the square of the droplet radius(*Pruppacher and Klett*,1996) induce the charge of opposite kind on the other drops when they are at the closest distance of interaction (supported by *Khain et al*. 2004). They also suggested that electrical instability of the water surface may cause charge-induced coalescence of drops. With their laboratory investigation of the effect of vertical and horizontal electric field on charged and uncharged water drops *Bhalwankar and Kamra* (2007) concluded that the presence of vertical electric field can broaden the RDSD and hence enhance the growth rate of raindrops when compared to the same in the horizontal electric field. The reduction of evaporation rate for a charged water drop is also reported by *Bhalwankar et al*. (2004). A recent study by *Harrison et al.* (2015) suggested that enhanced collection efficiency caused by the charging of cloud droplets by the global circuit current flow can modify the cloud droplet size distribution and hence speed up the processes of rain formation, also supported by the investigation of *Khain et al*. (2004) (Figure 1.13).

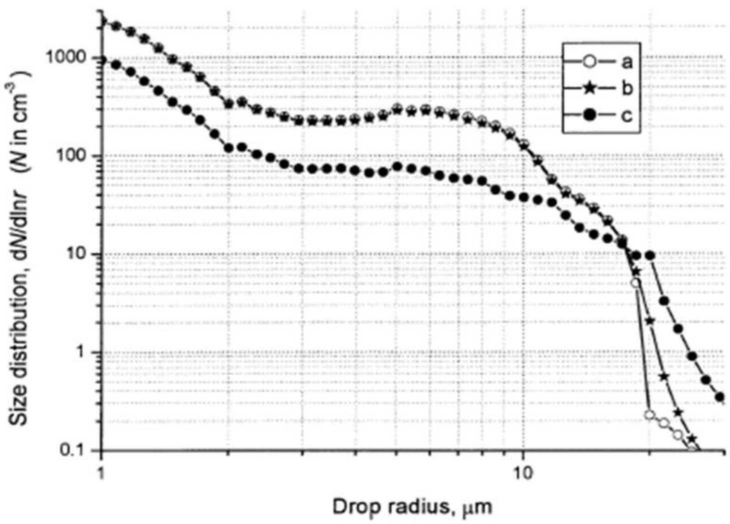

Figure 1.13: Droplet size distribution of charged (filled dots) and uncharged droplets (open dots). (From *Khain*, 2004)

Discussions above suggested that the evidences regarding the substantial electrical influences on the cloud/rain microphysics is quite compelling and is the primary motivation of the present work.

1.10 Motivation of the Thesis

"*Lightning to the global electrical circuit as rainfall to the general circulation*"... *Williams* (2005). Both the observable are intrinsically associated through the interaction of air dynamics and microphysical processes. Extensive radar observation (*Williams and Lhermitte*,1983; *Carey and Rutledge*,2000; *Bruning et al.*,2007,2010; *Calhoun et al.*,2013; *Mattos et al.*, 2016; *Mecikalski and Carey*. 2018; *Schultz et al.* ,2018) and laboratory studies (*Jayaratne* *and Saunders*, 1984; *Williams et al.*,1991; *Takahasi*, 1978 ; *Saunders and Peck*, 1998; *Saunders et al.*, 2006; *Emersic and Saunders*, 2010) presents a convincing basis regarding the role of precipitation particles on cloud electrification and subsequent lightning discharge. Discussions above present a compelling basis to anticipate a substantial influence of in-cloud electrical forces in cloud/rain microphysical processes and consequent near-surface precipitation. However, possibly due to the inherent microphysical complexity of precipitation formation and quite sophisticated interaction among the dynamics and microphysical processes, the quantification of the same in real atmospheric condition has not been done yet. Accurate understanding and characterization of cloud/microphysical processes is very important from the perspective of quantitative estimation of precipitation from observation (*Iguchi et al.*, 2009; *Islam et al.* 2012). Observations from the Tropical Rainfall Measuring Mission (TRMM) suggested that in the latitude belt of 35^oN- 35^oS, 60 % of the total rainfall over land is contributed by the strongly electrified clouds (*Liu et al*. 2010; *MacGorman et al*., 2008 ; *Williams et al.* 2010). In observation of Mediterranean winter thunderstorm, *Price And Federmesser* (2006) reported that approximately 83% of the mean rainfall variability could be explained by monitoring only the lightning activity. Understanding and quantification of in-cloud electrical influence (if there is any) on this fraction of cloud system which is lacking till now will be beneficial to the meteorologist and hydrologist alike. Availability of good quality data from sophisticated observational instruments compelled me to look for the same. Also, weather /climate models are known to underestimate the frequency of heavy precipitation events (*Goswami and Goswami*, 2016). Numerical simulation of heavy precipitation events (associated with lightning) demonstrated significant underestimation of accumulated rains towards the higher bin sizes (*Giannaros et al*. 2015; *Dafies et al*., 2018). One anticipated cause of this long-standing issue may be the absence of electrical effect on rain microphysical processes in the cloud module of weather/climate models. Motivated by this scenario and the availability of sophisticated microphysical schemes in the cloud module of the state of the art numerical cloud resolving model encourages the work presented in this thesis.

Chapter 2

Data-sets and Techniques used

Chapter 2

2 Date-sets and Techniques used

2.1 Introduction

The hypothesis proposed in the previous chapter has been tested using data from the observational platform and numerical weather prediction (NWP) model. An experiment also has been designed to test the freezing properties of water drop under the influence of electrical force which, has been discussed in details in *chapter 6* of the thesis. The details of the observational data sets used in this thesis have been presented in this chapter, followed by the detail description of the numerical experiment in the *chapter 5*.

2.2 The Observational Data sets

Some of the observational data used in the thesis have been made over the *High Altitude Cloud Physics Laboratory* (HACPL) situated over Mahabaleshwar, (India; 17.92 N, 73.66 E). The HACPL is located in the Western Ghat of peninsular India at an altitude of 1.3*km* from mean sea level with a complex topography (Figure 2.1). Some of the electrical properties of cloud reported in the thesis have been observed over Pune, India.

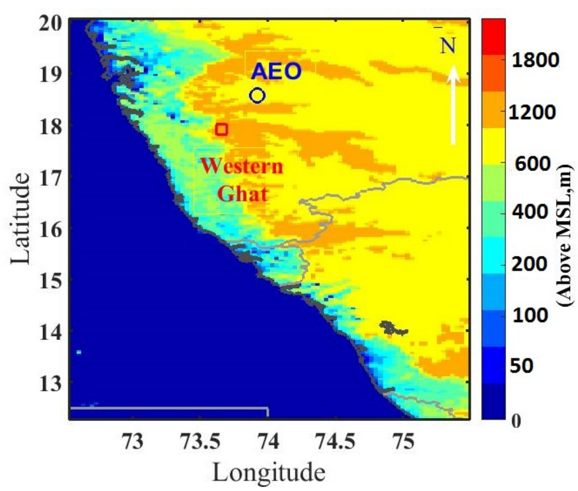

Figure 2.1: Topographical map of the Western Ghat. The red square indicate the High Altitude Cloud Physics Laboratory (HACPL)and the blue circle indicates the Atmospheric Electricity Observatory (AEO).

2.2.1 Micro rain radar (MRR)

To study the microphysical characteristics of precipitation formation, the Raindrop Size Distribution (RDSD) can be considered as a potential target of interest as RDSD reflects the prevailing microphysical and dynamical processes (*Testik and Barros*, 2007; *Konwar et al*., 2014). Vertically pointing microrain radar install at the HACPL, Mahabaleshwar, (India; 17.92 N, 73.66 E) has been used to derive information on the RDSD at higher altitude. MRR is a Doppler radar operating at a wavelength of $1.25cm$. The MRR measures the vertical profiles of different microphysical parameters like number density $N(D), (m^{-3}mm^{-1})$ in a diameter range from 0.4 to 4.9 mm, fall velocity of raindrops, $V(ms^{-1})$, radar reflectivity factor $Z(dBZ)$, Rain Liquid Water Content,$W(gm^{-3})$ and rain rate R in(mmh^{-1}) from the recorded Doppler spectra (*Peters et al*.,2005). Using the Doppler spectra $\eta(f)$, the spectral volume backscattering cross-section $(m^{-1}s)$ at the Doppler shift $f(S^{-1})$, the following rain integral parameters can be retrieved

1. Drop size distribution, $N(D)(m^{-4})$
2. Radar reflectivity factor (mm^6m^{-3})

$$Z = \int_0^\infty D^6 N(D) d(D) \tag{2.1}$$

$D(mm)$is the raindrop diameter

3. Rain Liquid water content (gmm^{-3})

$$W = 10^{-3}\rho_w \frac{\pi}{6} \int_{D_{min}}^{D_{max}} D^3 N(D) d(D) \tag{2.2}$$

ρ_w is the density of water in gmm^{-3}. D_{max} and $D_{min}$are the maximum and minimum drop diameters respectively measured by the disdrometer for a given RDSD.

4. Rain rate $(mmhr^{-1})$

$$R = 10^{-3}\rho_w \frac{\pi}{6} \int_{D_{min}}^{D_{max}} v(D) D^3 N(D) d(D) \tag{2.3}$$

$v(D)$is the fall velocity (m sec^{-1}) of a drop of diameter D

5. Mass-Weighted Diameter (MWD)

$$D_m = \frac{\int_{D_{min}}^{D_{max}} D^4 N(D) d(D)}{\int_{D_{min}}^{D_{max}} D^3 N(D) d(D)} \tag{2.4}$$

The basic equation to derive RDSD from the Doppler spectra is

$$N(D,z)\Delta D = \frac{\eta(D,z)}{\sigma(D)}\Delta D \tag{2.5}$$

Where $N(D,z)$ is the spectral drop number density (m^{-4}) at the measuring height z, $\eta(D,z)$ is spectral volume scattering cross-section as a function of drop diameter D, and $\sigma(D)$ is *single-particle backscattering cross-section*.

The vertical resolution of the MRR observations used in the present study is 300 meters. The operating frequency of the MRR is 24.1 GHz which corresponds to1.25 cm wavelength. The electromagnetic wave at 24.1GHz is attenuated by heavy rainfall. The rain attenuation coefficient κ_r at altitude $z_1$is defined as

$$\kappa_r(z_1) = \int_{D_{min}}^{D_{max}} \sigma_e(D)N(D,z_1)d(D) \tag{2.6}$$

Here, $\sigma_e(D)$ is single particles extinction cross-section, D_{max} andD_{min} are the maximum and minimum drop diameters for a given RDSD. To avoid the attenuation problem caused by heavy rainfall, it is ensured that rain intensity does not exceed 10 mm hr^{-1} at a higher altitude as well as at the surface during the period of observations reported in this thesis. Also, as the MRR doesn't distinguish between ice and liquid phase hydrometeors, the present observation by MRR is restricted below the melting layer, around 4.6 km mean sea level (MSL) height above the HACPL.

In order to validate the MRR measurement, the MRR-measured rain parameters are compared with in situ Joss-Waldvogel Disdrometer (JWD) measured ones. The lowest measuring altitude of the MRR is 300meters above the JWD for all the rain events considered here. Figure 2.2 shows a comparison of one-hour of time series of rainfall rate measured by the two instruments. There is a very good agreement between both instruments in measuring the rain rate with correlation coefficient r= 0.90 with p-value <0.0001.

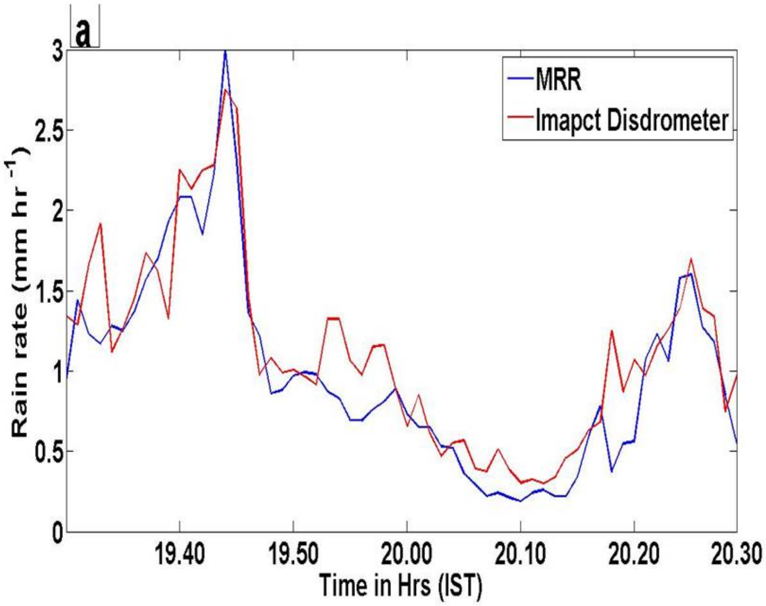

Figure 2.2: Comparison of rain rate between Microrain Radar data and in situ Impact disdrometer data for 14 November 2014 at the High Altitude Cloud Physics Laboratory (HACPL)site(correlation $r = 0.90$).The lowest measuring height of the MRR is 300 m above the ground.

2.3 Disdrometer

2.3.1 Joss Waldvogel Disdrometer (JWD)

The JWD is one of the several ground-based instruments being used for measurement and validation of precipitation. JWD is used for measurement of rain rate (R) , Raindrop size distribution (RDSD) and radar reflectivity factor(z). The JWD sensor transforms the mechanical momentum of an impacting raindrop into an electrical pulse. The amplitude of the recorded pulse is roughly proportional to the mechanical momentum produced by the raindrop. The output information is voltage amplitude, which is a measure for the size of the impacting drop. The output voltageV_L and the drop diameter D is related by the equation

$$V_L = k.D^n \tag{2.7}$$

Where $k(= 0.02586)$and n $(= 3.1$ to $4.3)$ are calibration constant. A pulse height analyzer is used to classify V_L which corresponds to the impacting drop to n_i classes. The RDSD at the discrete instant t (seconds) can be calculated by using the formula (*Montopoli et al.*, 2008)

$$N_m(D_i,t) = \frac{n_i(t)}{A.dt.v_i.dD_i} \tag{2.8}$$

Where, $N_m(D_i,t)$ is the number of raindrop per unit volume in the channel c_i at the discrete time t in units per millimeter per cubic meter, m indicate a measured quantity, D_i (mm) is the central raindrop diameter of the channel c_i, $n_i(t)$ is the number of raindrops counted in the i th channel at time t. A is the area of the sensor in m^2, v_i is the terminal velocity of the raindrop in $msec^{-1}$ and dD_i is the width of i th bin in millimeters.

JWD measures raindrops in 20 channels ranging from diameter 0.3 to 5.5*mm (Joss and Waldvogel*,1967)with sampling resolution time of 30 seconds. One limitation of JW disdrometer is it miscounts the number concentration in the diameter bin of less than 1*mm*. When two or more drops simultaneously reach the surface cross-section of the JWD, it miscounts the raindrops. Another limitation of JWD is, it can't measures the terminal velocity of raindrops.

2.3.2 Particle Size and Velocity (PARSIVEL) disdrometer

The PARSIVEL disdrometer is a laser-based optical system for measurement of all types of precipitation. The instrument consists of a laser emitter at one end which produces a horizontal beam of light of wavelength 650 nanometre along with a receiver at the other end. Precipitation particles passing through the laser beam block off a portion of the beam which corresponds to their diameters. The resultant reduced voltage at the receiver is the measure of the particle size. Measuring the blocking off time of the laser beam by the precipitation particle, the particle's fall speed can be determined. Liquid precipitation is measured in the size ranging from $0.2-8$ mm while solid precipitation is measured in the size ranging from $0.2-25$ mm (*Löffler-Mang and Joss*,2000). The precipitation particles are categorized as rain; drizzle; drizzle with rain; rain, drizzle with snow; snow; snow grains; soft hail and hail. Figure 2.3 depicts a comparison of rain intensity from the JWD and PERSIVEL disdrometer for a rain event observed on *10th of July, 2013* over the HACPL. Both the instrument recorded comparable intensity of rain during the event.

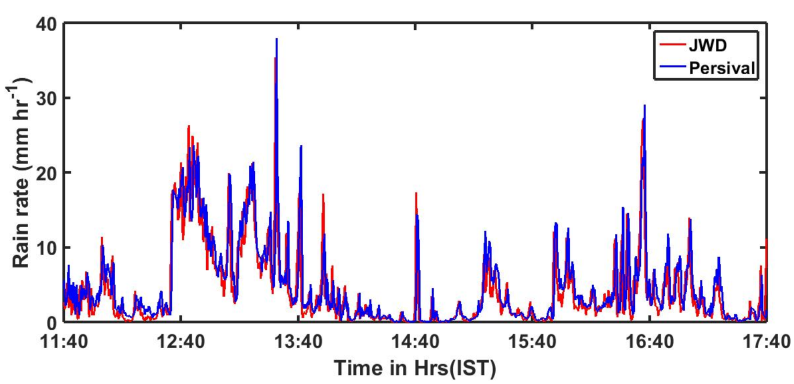

Figure 2.3: Comparison between JW disdrometer and PERSIVEL disdrometer for a rain event observed on 10th of July, 2013 over the HACPL.

2.4 Electric Field Mill

The vertical component of atmospheric electric field at the Earth's surface is measured with a field mill located at the *Atmospheric Electricity Laboratory (*AEO*)* , Pune. A schematic diagram of the filed mill is shown in Figure 2.4. The filed mill consists of two stators which are periodically exposed to and shielded from the atmospheric electric filed with a rotor fixed on the shaft of an AC synchronous motor of 1400 rpm and 12 W power. The diameter of the rotor is 12 cm and it is made of non-magnetic stainless steel. The rotor is grounded using a mercury cup at the other end of motor. Two stators are also made of the same material and of same diameter as the rotor. The stators which are connected to the inverting terminals of two operational amplifiers are separated from each other by a distance of 0.5 cm with Teflon bushes. The magnitude of the charge induced on the stators is directly proportional to the intensity of the atmospheric electric field. The two amplifiers signals are 180^o out of phase with each other. The two signals, after amplification, are fed to a demodulator for combination into a single wave. The reference signal for the demodulator is generated with a circular plate with sectors cut of the same shape as that of rotor and fixed at the other end of motor. This circular plate rotates through an opto-separator and generates a square wave of same frequency as that of input signals and in-phase with one of the two input signals. The reference square wave is used to switch the gates of demodulator on and off synchronously with the electric field to determine the polarity of electric field. Figure 2.5 shows the time evolution of surface-measured electric field during a thunderstorm observed over Pune on 3rd June, 2008.

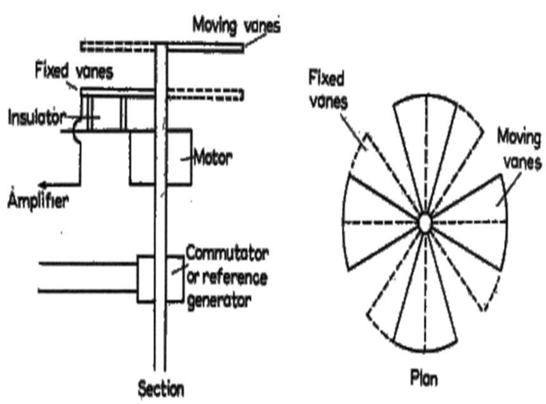

Figure 2.4: A schematic diagram of the Electric field-mill

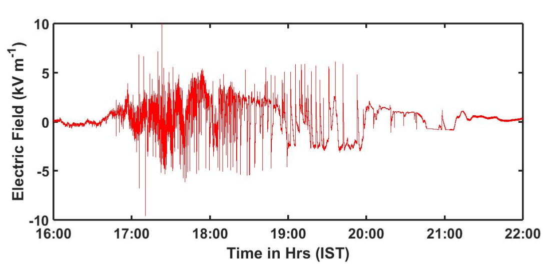

Figure 2.5: The evolution of surface-measured electric field during a thunderstorm observed over Pune on 3rd June, 2008

2.5 Maharashtra Lightning Location Network (MLLN)

The MLLN has been operational since 2014 with 20 sensors (Earth Network, USA) covering the geographical area of Indian State of Maharashtra which are separated by 150-200 km from each other located all over the state. Figure 2.6 shows the location of the sensor near to the HACPL.

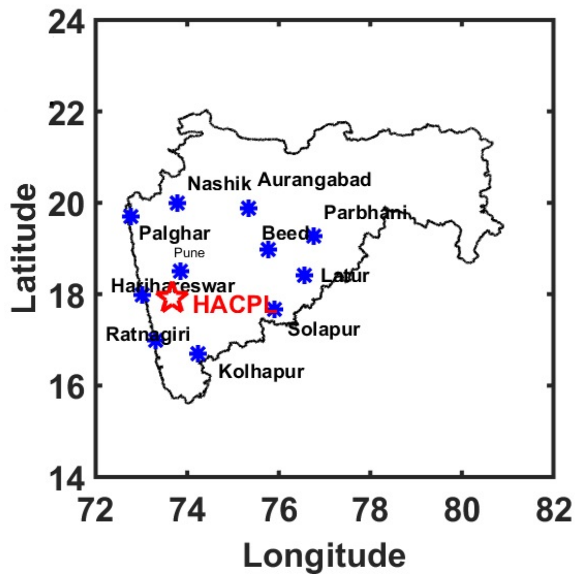

Figure 2.6: Map of MLLN sensors. The blue stars indicate sensor locations and the HACPL is indicated by the red star.

The MLLN operates in the frequency of1 KHz (VLF) and 12 MHz (HF). The VLF is used for long range detection of Cloud-to-Ground (CG) discharges while middle frequencies (1 kHz to 1 MHz) are used for locating return strokes. The frequencies range of 1 MHz to 12 MHz is used to detect and locate in-cloud (IC) pulses. The sensors record whole waveforms of each flash and send them back, in compressed data packets, to the central server. The waveforms are used for locating the flashes and differentiating between IC and CG strokes. Lightning emits electromagnetic (em) energy in all directions. The antennas in the sensors detect the waveform associated with the em signal it receives and sends it to the central lightning detection server through the Internet. The arrival times are calculated by correlating the waveforms from all the sensors that detect the strokes of a flash. The waveforms, arrival time and signal amplitude can be used to determine the peak current of the stroke and its exact spatial location along with the altitude of initiation point of the discharge. Lightning strokes are then clustered into a flash if they are within 700 milliseconds and 10 kilometers. A flash that contains at least one return stroke is classified as a CG lightning. The detection efficiency of the CG lightning is $90-95\%$ while IC discharges are detected with an efficiency of around $50-70\%$.

2.5.1 Microwave Radiometer (MWR)

The Cloud Liquid Water Content (CLWC), an important diagnostic of cloud has obtained from a 35 channel ground-based microwave radiometer (MWR) collocated with the JWD at the HACPL. The MWR measures passive radiation at microwave wavelengths associated with the emission of water vapour (from $22-30$ GHz) and oxygen molecules (from $51-59$GHz). As microwave emission from raindrops peaks at 19.35 GHz and microwave brightness temperature depends on the size, shape and number density of hydrometeors, in the case of a precipitating cloud, the contribution from the raindrops will not be substantial enough in the measuring channels. During heavy precipitation, accumulation of liquid water on the radome through which radiation passes before reaching the receiver of the MWR (*Rose et al.*, 2005) may cause erroneous estimation of the CLWC. To minimize the influence of liquid accumulation, the radome is built with a hydrophobic material and fitted with a super-blower.

2.6 Automatic Weather Station (AWS)

Surface wind and rainfall for a few event presented in the thesis rain have been collected from an Automatic Weather Station (Dynalab Weathertech-WL 1002) co-located with the disdrometer and the MRR at the HACPL site. The sampling resolution of the AWS is 1 minute.

For evaluation and quantification of the possible electrical influence in the rain microphysical processes following diagnostic techniques are adopted

1. Quantification of the effect of in-cloud electrical forces on the raindrop size distribution (RDSD) for a set of stratiform rain event observed over the HACPL using MRR and ground-based disdrometer data.

2. Quantification of the effect of a nearby lightning discharges in the near surface rain intensity using ground-based and remote sensing instruments.

3. Numerical simulation of strongly and weakly electrified rain events using weather research and forecasting (WRF) model and comparison of simulated output with observation /reanalysis data set.

4. A cloud chamber experiment to study the freezing characteristics of super-cooled water droplets in the presence of charge and electric field.

Chapter 3

Quantification of the Effect of in-cloud Electrical Forces on Raindrop Size Distribution (RDSD) in Stratiform Tropical Clouds

Chapter 3

3 Quantification of the Effect of in-cloud Electrical Forces on Raindrop Size Distribution (RDSD) in Stratiform Tropical Clouds

3.1 Introduction

A substantial contribution to the total rainfall in tropics (around 40%) comes from stratiform precipitation (*Schumacher and Houze*,2003) characterized by weak vertical air motion. The stratifrom precipitation exhibits distinct microphysical and dynamical characteristics from the convective counterpart (*Houze*, 1997). Cloud microphysical processes such as collision,coalescence, breakup, evaporation, condensation, raindrop clustering, and mixing can influence the evolution of the raindrop size distribution (RDSD) (*Testik and Barros*, 2007) and precipitation formation. Apart from these microphysical properties, ambient aerosol and cloud condensation nuclei concentrations are known to substantially influence the RDSD and precipitation formation (*Khain et al.* 1999; *Rosenfeld*, 2000; *Rosenfeld et al*. 2002). As the RDSD reflects the ambient microphysical processes, the information about the shape of the RDSD of raindrops can be very useful for understanding the dominant microphysical processes that transform the cloud water droplets into raindrops and their growth mechanisms for a particular type of cloud. The accurate understanding of RDSD is also important in pursuit of minimization of the uncertainty in the estimation of rainfall amount by ground-based and space-borne radars. Furthermore, the prediction of precipitation in the numerical weather prediction (NWP) models greatly relies on the approximation of the raindrop size spectra. The NWP model commonly assumes distribution functions in the microphysical schemes that are sensitive to the particle sizes (*Curic et a*l., 2010; *Islam et al*.,2012). This is particularly crucial for convective rain because of highly variable distributions *(Gilmore et al*., 2004; *Curic and Janc*, 2011).

Discussion presented in the section 1.9 provides a compelling basis regarding the substantial influence of in-cloud electrical forces in the rain microphysical processes through enhanced collision-coalescence growth of raindrops in the warm phase of cloud. The presence of vertical electric field and surface charge on the precipitation particles known to increase the collision efficiency of cloud/ raindrops, which in turn enhances the growth rate of particles (*Schlamp et al*. 1976 ,1979; *Bhalwankar et al*., 2007). Even though laboratory experiments clearly suggest that the electrical forces could significantly affect the rain formation processes in strongly electrified clouds, there are very few attempts to quantify the effect of electrical forces on RDSD in the real atmosphere, mainly because of the difficulty in separating the effect of electrical forces from the dynamical and microphysical processes. In this chapter, quantitative attempt has been made to investigate and quantify the anticipated electrical influence on rain microphysical processes using the profile of RDSD at upper level as well as at the ground considering some stratiform rain event observed over the HACPL with distinct electrical characteristics.

3.2 The Stratifrom Rain

The stratiform rain is characterized by weak vertical air motion (*Houze*, 1997). The prevailing updraft is weaker than the convective counterpart and horizontally uniform across the stratiform region with layered structure of precipitation.The updraft in the stratifrom regime can not support high concentration of cloud liquid water (CLWC). The net vertical air motion in the mixed phase of the cloud is upward allowing the precipitation particles to grow by vapor diffusion (*Rutledge and Houze*, 1987). In the temperature regime -5^{o}C -0^{o}C, the precipitation particles grows by aggregation of ice crystals. Below the melting layer, precipitation particles evolves primarily through collision, coalescence, breakup, and evaporation. When looked through a radar with sufficiently higher vertical resolution ($< 500m$), the larger aggregates near the melting layer produces a layer or band of higher reflectivity (z) as the refractive index of melting aggregates is higher than the non-melting particles. This band of higher radar reflectivity is conventionally known as a bright band and used to characterize the stratiform precipitation.

To quantify the electrical factor in the RDSD profile, 12 stratiform rain events observed over the HACPL have been chosen. Height Time Intensities (HTI) of radar reflectivity factor (z) for all the 12 events are shown in Figure 3.1.

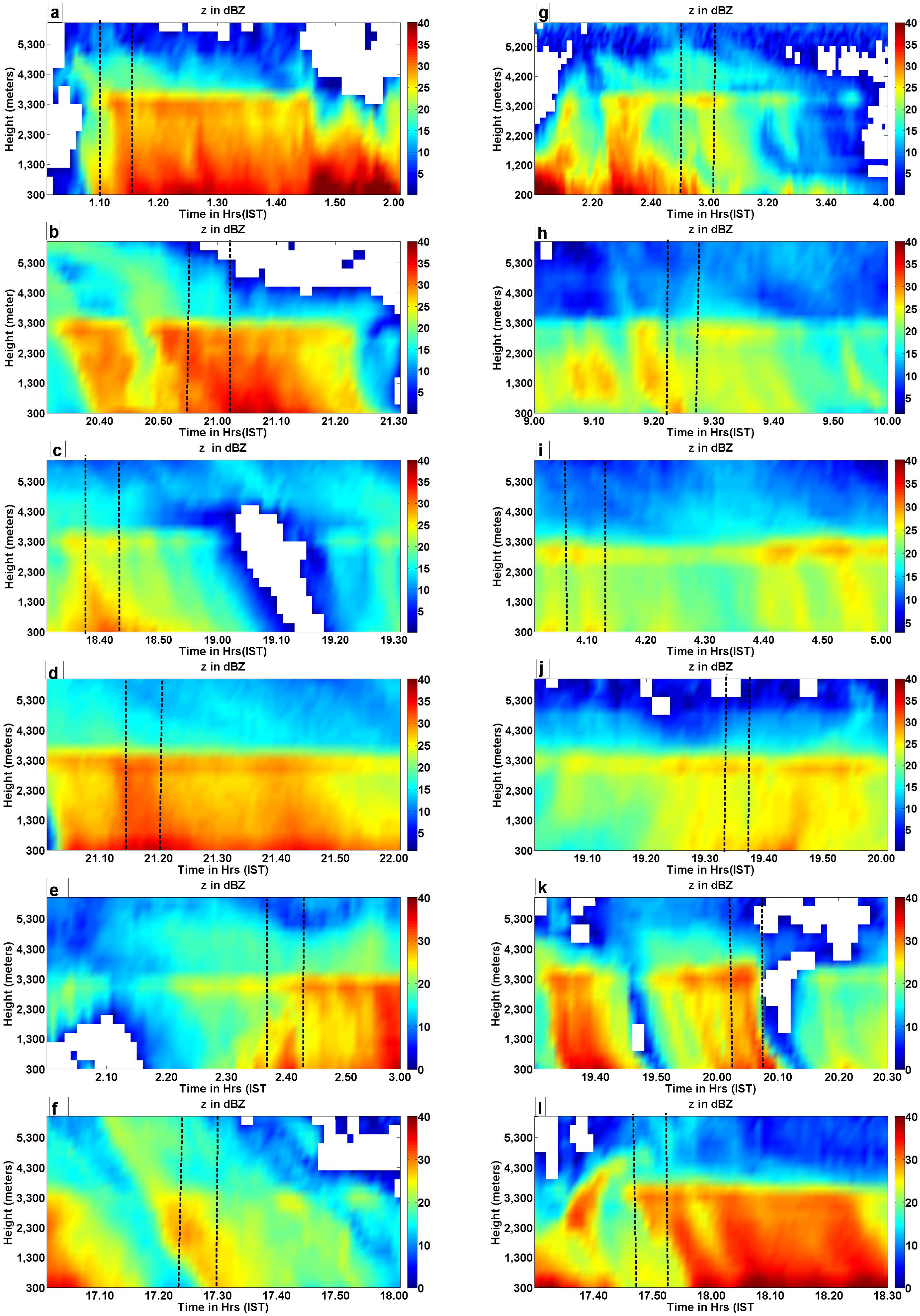

Figure 3.1: Height-Time Intensity (HTI) plot of z for strongly electrified (a-f) and weakly electrified (g-l) rain events. Heights are measured from the location of MRR. Heights are measured from the location of MRR. The dashed vertical bars indicate the data period considered for analysis

The presence of melting layer (bright band) is clearly visible for all the events at approximately 3.3 km from the surface. As the MRR is installed at an altitude of 1.3 km above the mean sea level (MSL), the effective heights of the melting layer would be around 4.6 km from the MSL.

When the precipitation particles come down below the melting level and start to melt, their fall speed increase by a factor of 5 (*Lhermitte*,1960; *Houze et al*,1997). This sudden increase of fall speed of hydrometeors produces a distinct band of Gradient of Fall Velocity (GFV) near the melting layer. The core of the maximum GFV coincides with the melting level. The presence of GFV is found to be a good indicator of the melting layer when the enhanced reflectivity factor (z) is not prominent *(Konwar et al*.,2012). Figure 3.2 depicts the GFV for all the 12 selected events.

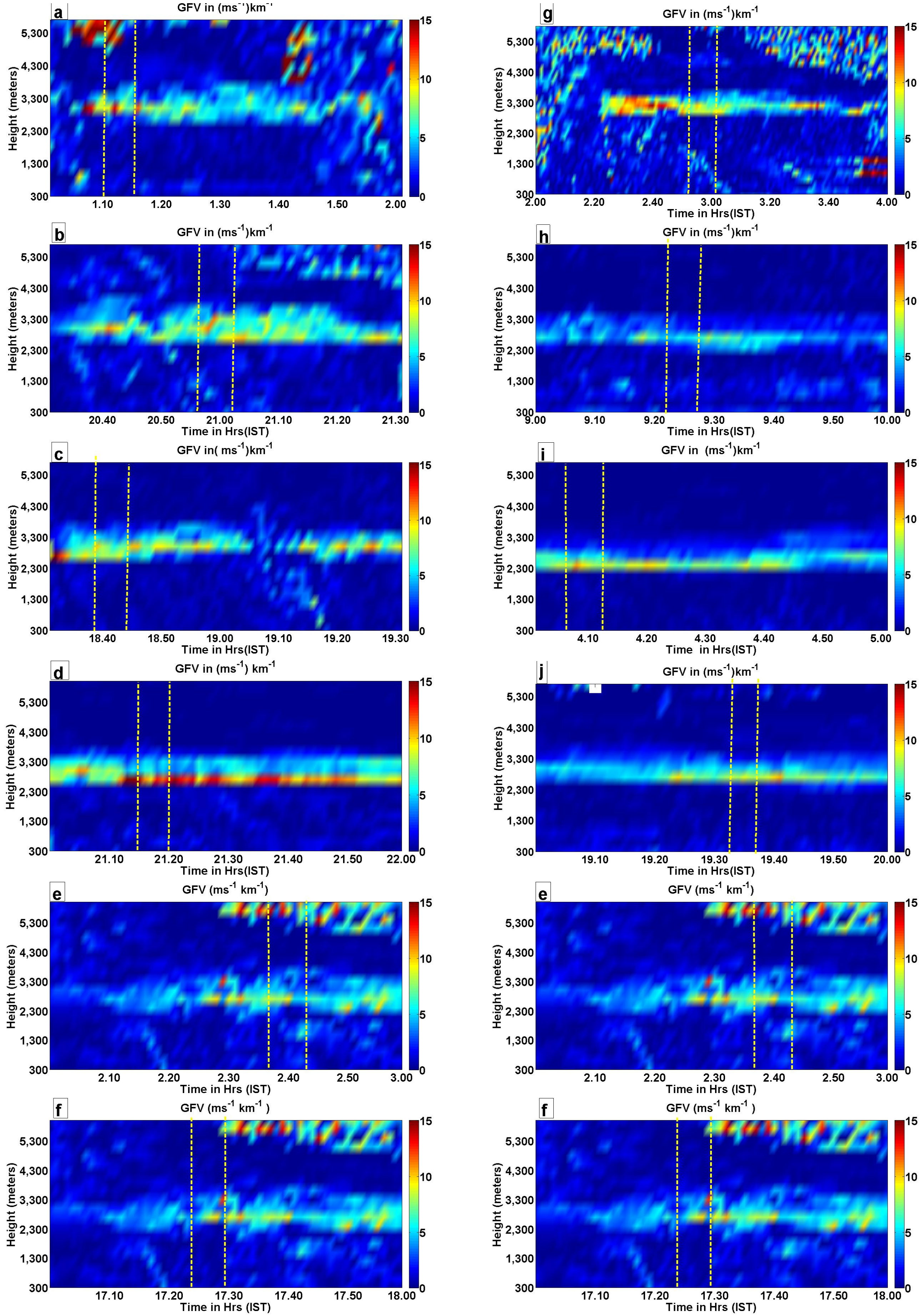

Figure 3.2: Height-time plot of Gradient of fall velocity (GFV) for strongly electrified (a-f) and weakly electrified (g-l) rain events. Heights are measured from the location of MRR. The dashed vertical bars indicate the data period considered for analysis.

In this Figure, the band of GFV is clearly visible at about 3.3 km from the surface. The Figures 3.1 & 3.2 show that although in some cases the bright band is not so prominent (faint bright band), the GFV shows a prominent band. It is also clear that the thickness and height of bright bands are not much different from each other for events considered for analysis. The presence of bright band along with the GFV near the melting layer clearly suggest that all the rain events considered here are stratiform in nature with nearly similar dynamical characteristics.

Some parameters such as bright band thickness, rain rate, mean reflectivity of the bright band, integrated 3 hour lightning count preceding the stratiform events, 0^o isotherm height from MSL, Median Volume Daimeter (MVD), Rain Liquid water Content (RLWC), intercept parameter, mean fall velocity below the bright band and availbale wind speed for all the events are given in Tables 3.1 and 3.2 respectively. All the values are averaged for the period shown by the dotted lines in Figure 3.1. As listed in, in case of strongly electrified events and weakly electrified events (defined in section 3.4) the thickness of bright band and rain rates are not much different from each other. The bright band mean reflectivity and fall velocity below the melting layer are observed to be slightly higher for the strongly electrified events compared to the weakly electrified events. Also, in Table 3.1 the times of lightning discharges and their distances from the observational site are given. In all the strongly electrified events at least one lightning strike was observed within 5 km from observation site, which ensure that the strongly electrified events were part of same cloud clusters for which we have analyzed the raindrop size distribution.

Table 3.1: Electrified stratiform rain events and some rain microphysical and dynamical parameters.(The variables are derived from MRR and surface JW disdrometer and averaged over the data period bounded by the vertical bars as shown in Figure 3.1(a-f)).

Date	Data period (IST)	Time of lightning and distance from the HACPL site	Integrated three hours lightning counts in a 100km×100 km box, including the data periods	Bright Band thickness (m)	Mean Reflectivity of the radar bright band(dBZ)	0^o isotherm height from the MSL (km)	Rain rate (mm/hr)	D_m (mm)	Intercept $N_0(mm^{-1-\mu} m^{-3})$	Mean fall velocity below the bright band (ms^{-1})	LWC (gm/m^{-3})
5-10-2012(a)	01:09:00-01:15:00	1:15:51 IST, 4.7 km	89	800	29	5.0	1.63	1.66	3.8 ×104	7.37	0.155
2-6-2013(b)	20:57:30-21:02:30	21:21:04 IST, 4 .3 km	129	600	30	NA	2.05	1.477	5.68× 104	8.77	0.10
10-9-2013(c)	18:38:30-18:43:30	18:38:19 IST,3.6 km	163	800	23	5.2	1.75	1.65	2.64× 104	7.83	0.08
5-6-2015(d	21:15:50-21:19:20	21:09:55 IST 3.7 km and 21:57:10 IST,0 km	47	800	28	4.9	1.91	2.18	4.35×103	8.3	0.07
30-5-2015(e)	02:37:40-02:42:10	2:06:02 IST at 2km,2:15:56 at 4 km	91	600	27	5.2	1.62	1.59	2.06 ×104	7.43	0.07
15-5-2015 (f)	17:11:30-17:15:30	17:18:14 ISTat4.5 km	525	600	23	5.1	1.23	1.26	3.02×105	5.54	

Table 3.2: Weakly electrified stratiform rain events and some rain microphysical and dynamical parameters. (The variables are derived from MRR and surface JW disdrometer and averaged over the data period bounded by the vertical bars as shown in Figure 3.1(g-l).

Date	Data period (IST)	Integrated three hours lightning counts in a 100km×100km box, including the data periods	Bright Band thickness (m)	Mean Reflectivity of the radar bright band(dBZ	0^o isotherm height from the MSL (km	Rain rate (mm/hr)	D_m (mm)	Intercept N_0(mm $^{-1-\mu}$ m $^{-3}$)	LWC (gm/m^{-3})	Wind speed (m/sec)	Mean fall velocity below the bright band (ms^{-1})
31-08-2014 (g)	02:56:10-02:59:400	0	800	22	NA	1.51	1.10	9.8 ×105	0.09	2.32	5.6
25-10-2014 (h)	09:23:00-09:26:00	0	800	24	NA	1.50	1.22	3.14 ×105	0.08	8.58	5.95
26-10-2014 (i)	04:07:00-04:11:00	0	600	25	NA	1.54	1.13	5.68 ×105	0.08	7.18	5.78
14-11-2014 (j)	19:33:30-19:36:30	0	800	26	4.85	1.43	1.19	5.60 ×105	0.08	4.94	6.21
02-10-2015 (k)	20:10:0-20:13:00	0	800	27.5	5.2	1.88	0.90	1.23 ×107	0.13	3.01	5.80
03-10-2015 (l)	17:45:00-17:49:00	0	800	30	5.2	2.20	0.96	4.04 ×107	0.16	3.14	5.69

3.3 Separation of Stratiform and Convective Rain Events using RDSD

The distinct microphysical processes of convective and stratiform rain results in varying RDSD parameter which may be used to distinctly classify both the rain events. In the stratiform rain, the growth of ice crystals is dominated by vapour diffusion above the melting layer. When these ice crystals drift downward, near the melting layer the ice crystal grow by aggregation and riming *(Waldvogel et al.* 1993; *Houze et al*,1997; *Sarma et al*.,2016). When these particles melt below the melting layer, they produce large raindrops, which results in a decrease of the RDSD intercept parameter N_0. On the other hand in a convective cloud, the larger vertical velocity induces the growth of precipitation particles by accretion and riming followed by collision, coalescence and break up. In the presence of high liquid water content, the precipitation particles grow in a very short span of time near the cloud base (T*okay and Short*,1996). In the approximately same range of rain rates, these distinct microphysical processes produce small to medium raindrops in convective rain events compared to stratiform rain which results in a high value of the RDSD intercept parameter N_0. This intercept parameter variation in stratiform and convective rainfall is used in Figure 3.3 to classify the convective and stratiform rain.

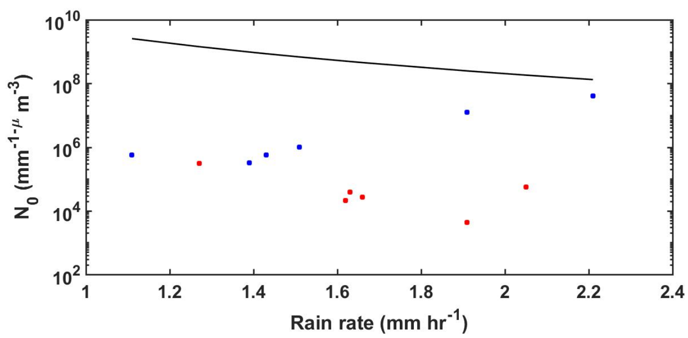

Figure 3.3: Classification of precipitation type. The red and blue squares represent the strongly electrified and the weakly electrified events respectively. The solid line represents the empirical relation (3.1).

The solid line in the Figure represents the equation

$$N_0 = 4 \times 10^9 R^{-4.3} \tag{3.1}$$

Here, N_0 is the intercept parameter (mm$^{-1-\mu}$ m^{-3}), R is the rain rate (mm hr^{-1}) from the impact disdrometer. For the present study, N_0 values are calculated using the formula (3.2) ,(*Bringi and Chandrasekar*, 2001)

$$N_0 = N_w \frac{6(\mu+4)^{(\mu+4)}}{4^4\Gamma(\mu+4)} D_m^{-\mu} \tag{3.2}$$

where Γ is the gamma function, D_0 is the Median Volume Diameter calculated as

$$D_0 = \frac{D_m(3.76+\mu)}{(4+\mu)} \tag{3.3}$$

Here, D_m is the Mass-weighted Diameter

μ, the gamma distribution shape parameter, given by the empirical relation *(Testik and Pei*,2017)

$$\mu = \frac{D_m^{-0.66}}{0.3^2} - 4 \tag{3.4}$$

N_w is the RDSD parameter given by

$$N_w = \frac{4^4}{\pi \rho_w} (\frac{10^3 W}{D_m^4}) \tag{3.5}$$

Here, $D(mm)$ is the raindrop diameter ; $N(D)$ is drop density in m^{-3}mm^{-1}; D_{max} and $D_{min}$are the maximum and minimum drop diameters respectively measured by the disdrometer for a given RDSD ; ρ_w is the density of water in gm m^{-3} and W is the RLWC in gm m^{-3} given by equation 2.2

As seen from the Figure 3.3, all the values of N_0 given by the equation (3.2) lie below the solid line which, represents the equation (3.1), clearly indicating that all the rain events considered for the present study are of stratiform nature with similar kind of microphysical and dynamical processes, although they are electrically distinguishable.

3.4 The Electrical Distinguishability

To quantify the electrical effect on the RDSD profile through comparison, it is important to have rain events with similar dynamical and microphysical characteristics, (which is ascertained by choosing the stratiform rain events) but with distinct electrical characteristics. The electrical indistinguishably of the rain events considered here are ascertained by presence or absence of lightning discharges over the HACPL. A 100 km ×100 km box was chosen, keeping the observation site in the middle. The spatial distribution of the accumulated lightning activity per 100 km^2 for 3 hours within the this box has been depicted in Figure 3.4 for all the events.

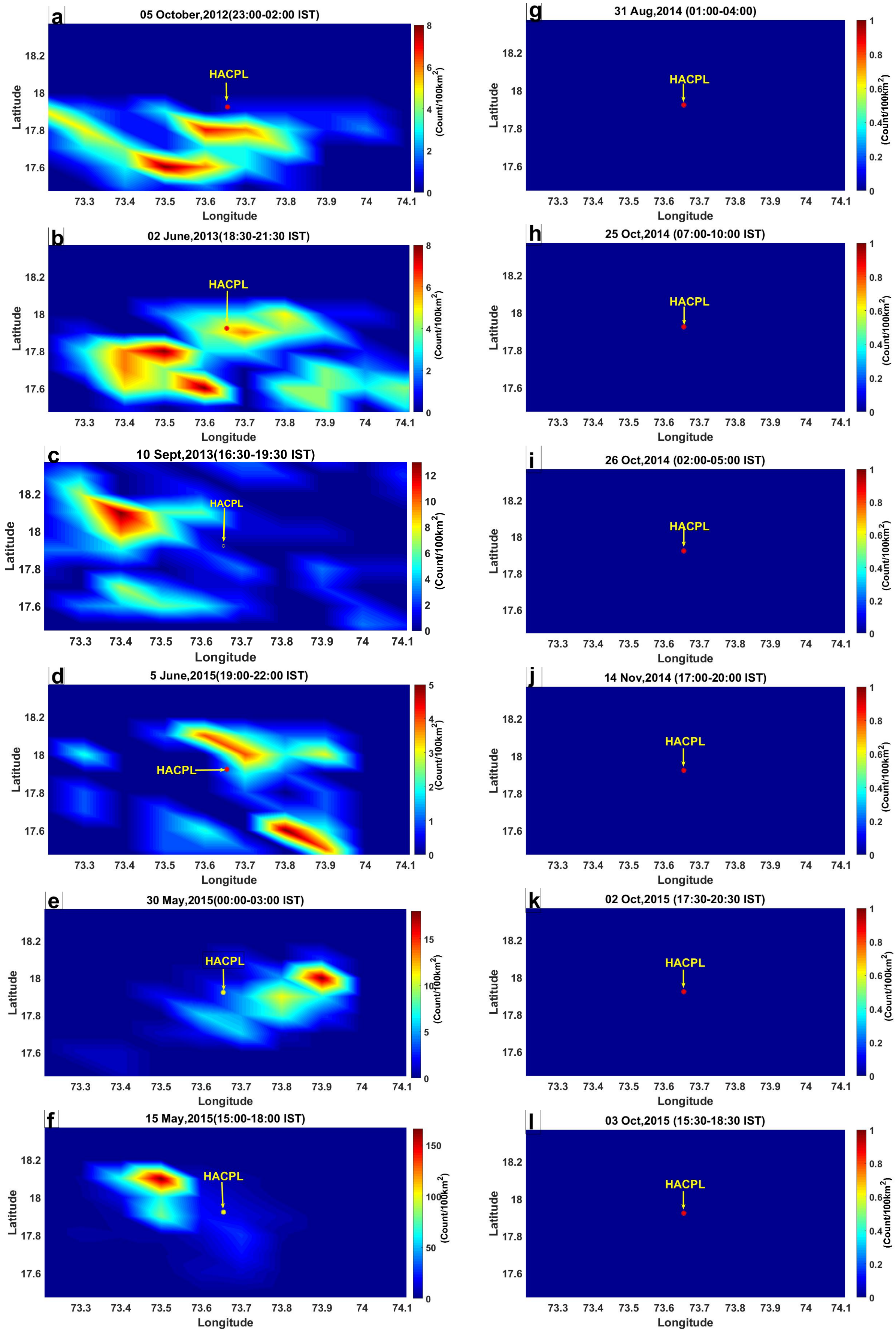

Figure 3.4: 3 hours (including the data periods) accumulated lightning flash count per 100 km^2 within a 100km×100km box. The left and right panels corresponds to the strongly and the weakly electrified events respectively. The blue colours in the right panel imply 0 counts in the mentioned spatial and temporal scales. The labeling of all the events is same as Table 3.1.

The left and right panels of Figure 3.4 corresponds to the right and left panel of Figures 3.1-3.2. The rain events presented in the left panel of Figure 3.4 shows presence of lightning activity near the HACPL, while the rain events presented in the right panels are observed to be not associated with lightning activity in the neighborhood of the HACPL. As lightning-producing clouds exhibit stronger electrical environment in terms of magnitude of electric field (400 kVm^{-1}, *Winn et al*.,1974) and charge distribution (10^9 elementary charges, *Christian et a*l.,1980; *Bateman et al*.,1999), we termed these set of events as strongly electrified (SE) events while non-lightning-producing rain events were termed as weakly electrified (WE) events.

3.5 But Why Stratiform Rain..?

The selection of stratiform rain events with approximately equal rain rate essentially ensures that the prevailing dynamical and microphysical effects on RDSD can be approximately similar for both the strongly and weakly electrified events. The strong convective events (without any discernible radar bright band) where the dynamical influence on the RDSD may be overwhelming, making the isolation of the effect of the electrification on the RDSD difficult is cautiously avoided. For that reason , the stratiform rain events are chosen, with no lightning (WE clouds) and with few lightning (SE clouds) to ensure that the dynamical properties of the chosen SE and WE clouds are not significantly different from each other.

The comparison of vertical profiles of rain rate , MVD and RDSD for both the sets of events have been presented next.

3.6 The Comparison of Vertical Profile of Rain rate and Raindrops Sizes

The vertical profiles of rain intensity for all the rain events considered for analysis has been retrieved from the MRR spectra using the equation 2.3. Figure 3.5(a) depicts the vertical profiles of rain intensity for bot SE and WE events averaged over 6 events each while Figure 3.5(b) depicts the corresponding profile of MVD.

Drops larger than the MVD in a RDSD spectrum contribute to half the total liquid water content per unit volume (*Seliga and Bringi*,1978).

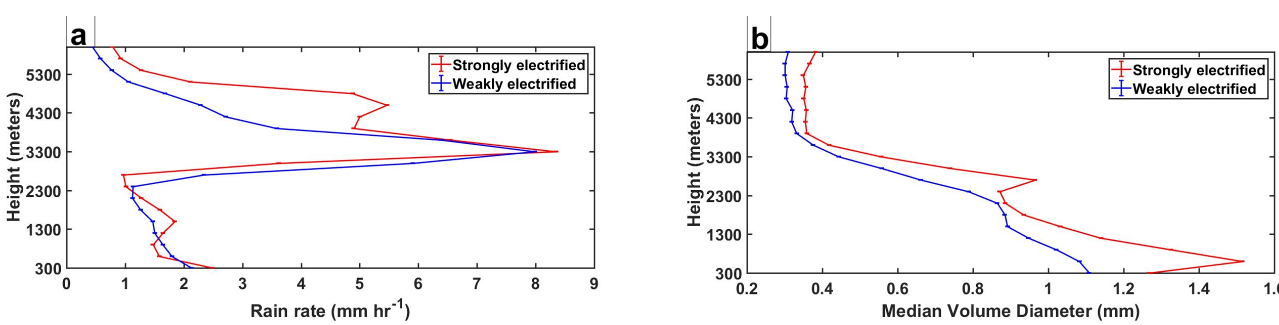

Figure 3.5: (a) Rain rate and (b) MVD averaged over 6 strongly electrified (SE) and weakly electrified (WE) stratiform rain events each.

The observed maxima in the vertical profile of rain rate below the melting layer are possibly caused by the sudden increase of fall velocity of the precipitation particles as well as by the melting of the large aggregates *(Houze* *et al*,1997). Although the vertical profile of observed rain rates of SE and WE events below melting band are nearly similar to each other, the vertical profile of MVDs for both types of events is significantly different from each other. In the strongly electrified events, the drops size shows a tendency to be in the larger size of the size range compared to the weakly electrified events.

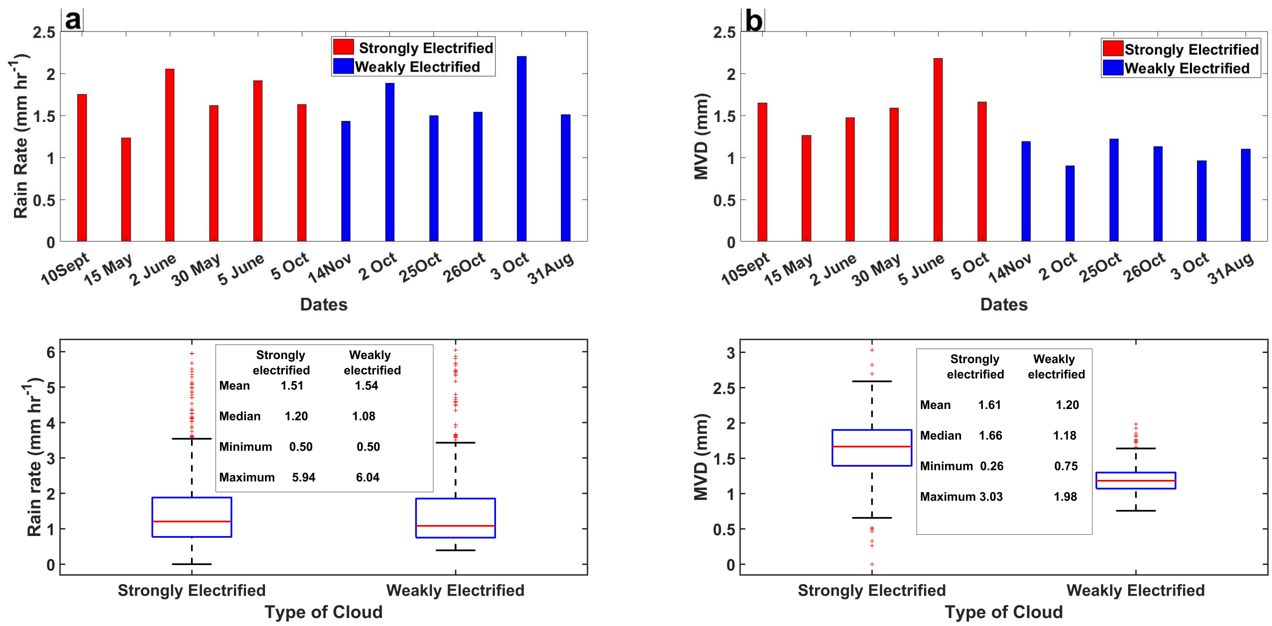

Figure 3.6: Bar graph of (a) Rain rate, (b) MVD for all the rain events of Figure 3.1 (for the time periods bounded by the vertical lines in Figure 3.1). The Figure below depicts Box and Whisker plot for rain rate and MVD plotted altogether for all the 12 events each for the entire rainy periods of each of the event. For strongly electrified events, the total number of data points are 389 and for weakly electrified events, the total number of data points are 433 (0.5< rain rates <6).

The MVD values measured with the ground-based JWD corresponding to the data periods bounded by the vertical bars in Figure 3.1 for all the 12 rain events considered here are shown in the bar graph in Figure 3.6(b) against the rain rates for the same periods in figure 3.6 (a). It is clearly evident that although the rain rates of all the 12 rain events are nearly similar, the MVDs corresponding to the strongly electrified rain events show higher values compared to weakly electrified rain events. The MVD values derived from the surface JWD at a temporal resolution of 30 seconds for the entire time period (1hour) of rainfall of each event in Figure 3.1 are shown all together in a box and whisker plot in the bottom panel of Figure 3.6. This Figure clearly shows higher mean and median values of MVD for strongly electrified events compared to the weakly electrified events, although the rain rates are having same mean and median for both categories of events.

3.7 The Insight from RDSD Comparison

The vertical profiles of MVD clearly shows presence of larger raindrops below the melting level for the SE event relative to the WE ones. This suggest substantial influence of in-cloud electrical forces in the microphysical growth of raindrops for SE stratiform rain events. How does the electrical force achieve this? Do the RDSD spectra provide any insight to answer this question?

As have already been stated above, RDSD reflects the prevailing microphysical process. The microphysical process like collision-coalescence, breakup, evaporation, condensation, raindrop clustering, and mixing can influence the RDSD. Hence, information of RDSD of can be very useful for understanding the microphysical processes that transform the cloud water droplets into raindrops and their growth mechanisms. In Figure 3.7 (a,b,c), the RDSDs, averaged over 6 cases each at heights 2400m, 1200 m, and 600 m from the MRR data respectively are shown. As the MRR doesn't distinguish between ice and liquid phase hydrometeors, the analysis has been limited below the melting layer, focused primarily on the liquid phase hydrometeors.

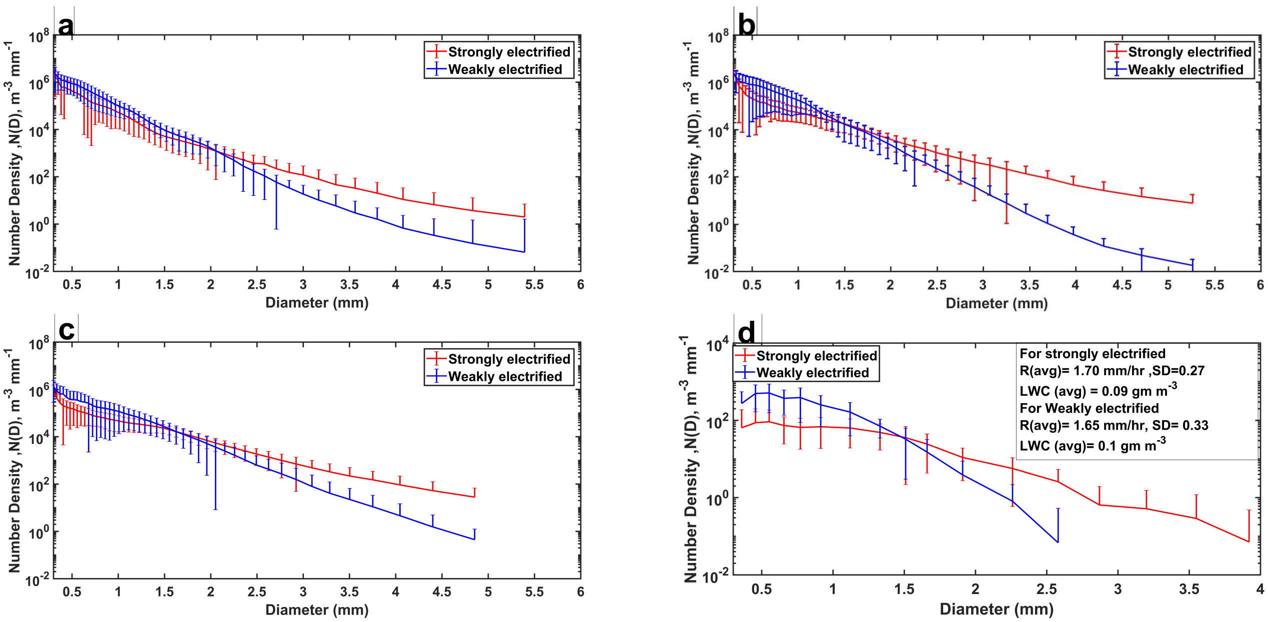

Figure 3.7: Composite raindrop size distribution (RDSD) (6 events in each composite) at selected altitudes for strongly electrified (SE) and weakly electrified (WE) clouds as observed by MRR at (a) 2400m, (b) 1200 m,(c) at 600 m,(d) at surface observed by JW disdrometer .

This Figure clearly indicate that the RDSD for SE and WE events are different from each other at all three heights. Even though the difference between the concentration of drops for SE and WE events can be seen clearly in all size ranges, the difference is substantially larger for a drop size above 2 mm. In the strongly electrified events, the number concentrations of small size drops are lower and large size drops are more numerous than weakly electrified events at all the three heights. The surface RDSD shown in Figure 3.7(d), measured by the JWD is averaged over 5 minutes for each event and again averaged over 6 SE and 6 WE events each keeping the rain rate nearly the same. The RDSDs at three different altitude as well as at the surface show that an increase in the number density of larger drops is accompanied by a compensating decrease in the number density of smaller drops. The results could indicate that due to the electric field and surface charge of raindrops, the collision-coalescence growth of raindrops in the warm phase of the cloud gets enhanced, which further modify the size distribution of raindrops.

3.8 Width of Radar Bright Band the RDSD

A significant correlation between the RDSD and strength and thickness of the radar bright band has been reported by previous observations (*A. Huggel et al.* ,1996; *Sharma et al.* 2009) . The larger mean drop diameter of raindrops are found to be associated with the larger width of the bright band and smaller mean drop diameter is associated with the weaker bright band. To strengthen the primary hypothesis of electrical influence on RDSD, we have compared the MVDs of two events, one strongly electrified ('c' in Figure 3.1; 'c' in Figure 3.2) and one weakly electrified ('g' in Figure 3.1; 'g' in Figure 3.2) with the nearly the same thickness of the bright band. The strength of the bright bands (Δz) is measured following the method of *A. Huggel et al.* (1996). An upper boundary of the bright band is determined visually for each profile so that the maximum reflectivity in the bright band is observed less than 0.4 km from the boundary. Then strength of the bright bands (Δz) is defined as the differences (in dBZ) of maximum reflectivity in a 0.4 km thick layer just below the upper boundary (z_{max}) to the minimum reflectivity in a 0.4 km thick layer adjacent to the upper layer (z_{min}).

$$\nabla z(dBZ) = z_{max}(dBZ) - z_{min}(dBZ) \tag{3.6}$$

For SE and WE events the measured strengths are found to be 2.2 dB and 3.5 dB respectively. The thicknesses of the bright band for both the events are measured to be 800 m. Figure 3.8(b) depicts the vertical profile of MVD corresponding to the rain rate profile of Figure 3.8(a) for these two events.

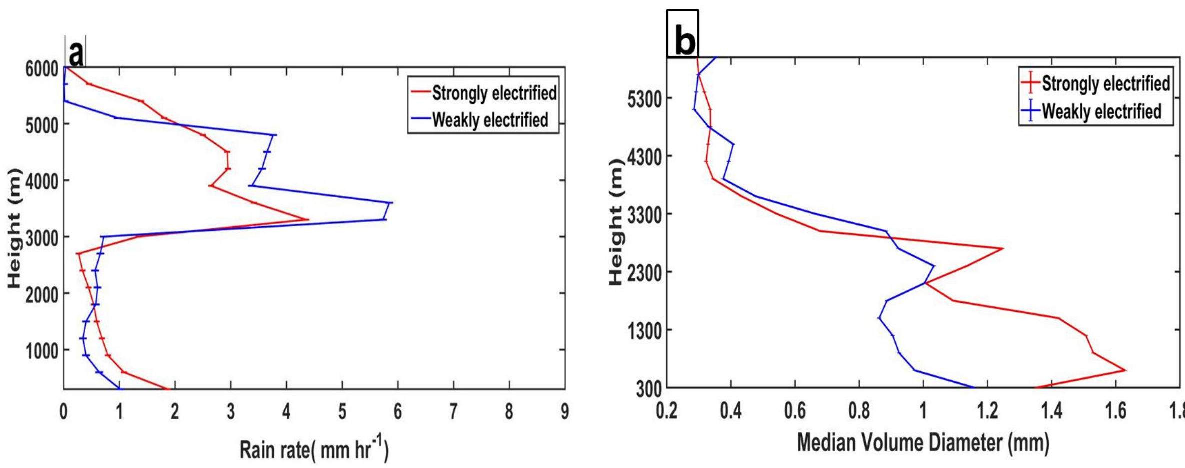

Figure 3.8: (a) Vertical profiles of Rain rate and (b) MVD under the same thickness and strength of bright band corresponding to the events in Figure 3.1(c,g)

This Figure also shows larger MVD in SE events compared to WE events below the melting level, although both the events exhibits similar bright band characteristics. The RDSD characteristics depicted in Figure 3.9(a-d) (averaged over 5 minutes each) under the same thickness and strength of the radar bright band also show a broader spectrum for SE events compared to the WE events.

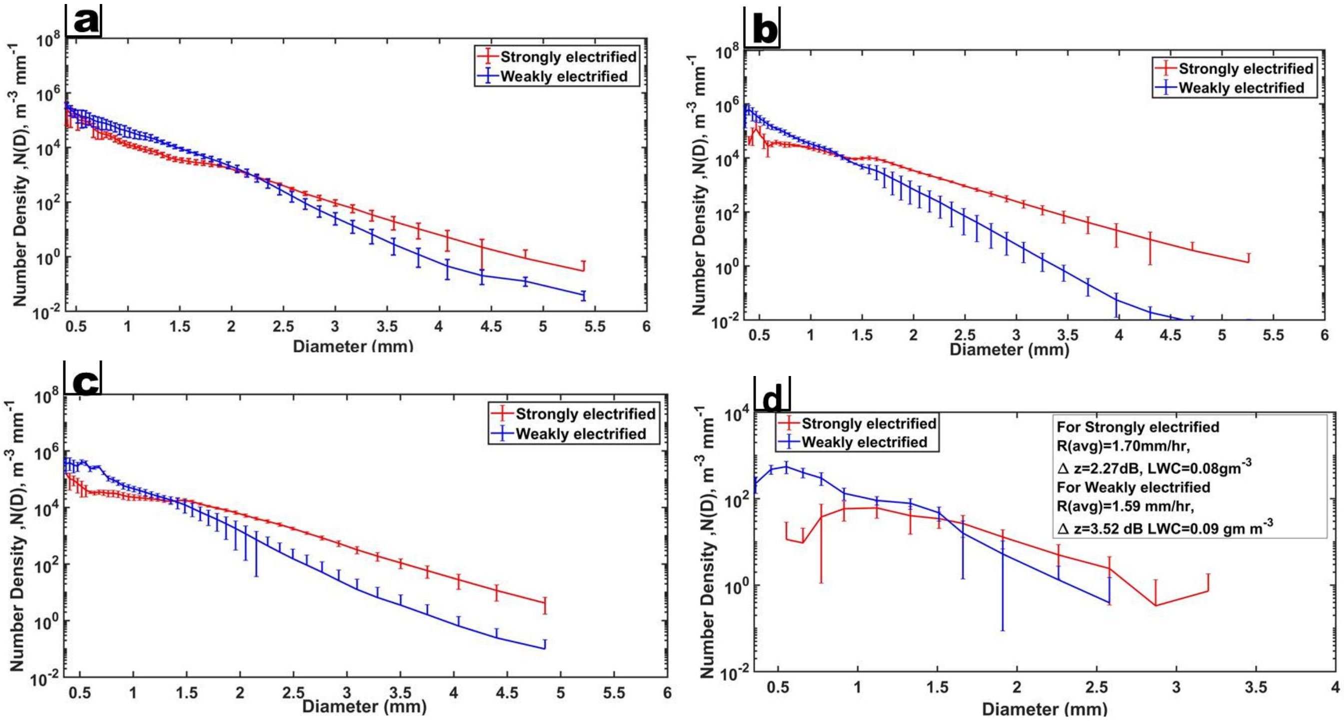

Figure 3.9: Raindrop size distribution (RDSD) at (a) 2400m, (b) 1200 m,(c) at 600 m,(d) at surface under the similar strength of bright band for strongly electrified and weakly electrified events.

This clearly suggested that some stronger mechanism is operating in the warm phase of SE cloud which helps the raindrops to overcome the break-up and evaporation and to broaden the RDSD spectrum. This mechanism is most likely the prevailing stronger in-cloud electrical forces in SE clouds. The electric forces inside SE clouds enhance the collision efficiency through coulombic (if the drops are of opposite polarity) and charge-dipole interaction (if the drops are of same polarity) of the raindrops along with the collection efficiency through effective drainage of the air film trapped in between two colliding drops.

3.9 The Relation between Surface Electric Field and Size of Raindrops

' *Electrocoalescence*', the process of electric field induced coalescence of two liquid drops has been investigated through many laboratory and numerical studies(*Schlamp et al*.,1976, 1979; *Khain et al.* 2004; *Mhatre et al*.,2015;*Wang et al*.,2018). In a cloud chamber experiment, *Yang et a*l.(2018) found that growth rate of water drops is proportional to the applied voltage. While the charge on the drops facilitate the coalescence of two colliding drops by effective drainage of the air film trapped between two colliding drops, an external electric field acts to polarize the neutral drop producing a resultant attractive force of interaction between the drops. During thunderstorms, the in-cloud electric field can reach a value up to 400 $\mathrm{kVm^{-1}}$ (*Winn et al*., 1974). Surface measurement of electric field has been done during a few thunderstorm observed over the AEO, Pune in the year 2008 with an electric field mill flushed to the ground. The simultaneous RDSD were observed with a collocated optical disdrometer. In pursuit to investigate an anticipated association between cloud electric field and raindrop size, a few rain events are selected in which intensity variation of rain is comparatively less. Figure 3.10(a-c) shows the scatter plot representation of MWD with surface electric field (both the observables are averaged over two minutes intervals during the rainy period of the storms) during three thunderstorms observed on 03 June, 1Septmeber and 31August, 2008 over the AEO.

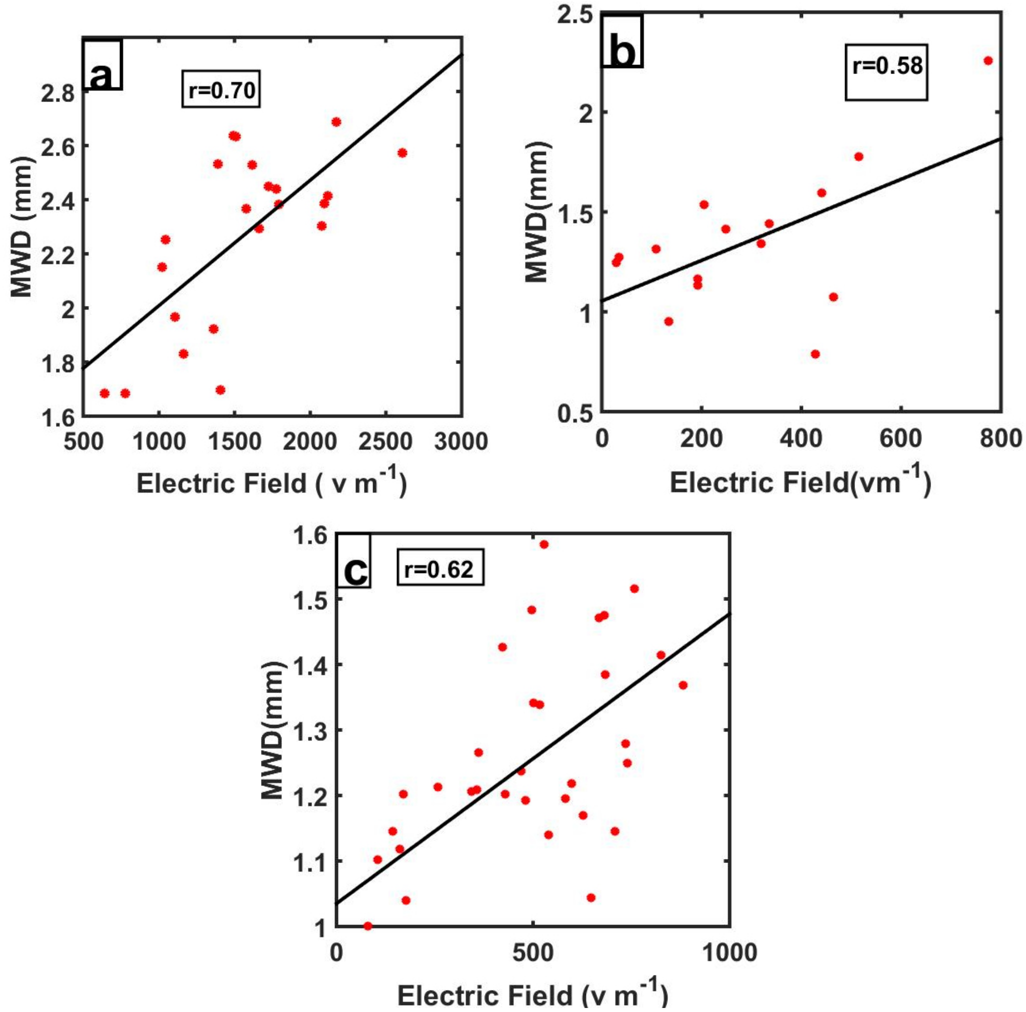

Figure 3.10: Scatter plot of Mass-weighted Diameter (MWD) of raindrop and surface Electric Field (a-c) corresponds to thunderstorms 03June, 01September and 31 August,2008 respectively over the Atmospheric Electricity Laboratory(AEO), Pune. The 'r' values indicate correlation coefficients at 95% confidence level.

It can be seen from the Figure that the raindrop size shows a positive correlation with the cloud electric field. Larger electric field is observed be associated with bigger raindrops. This supports the laboratory findings of *Yang et al.*(2018). It may be noted that this is the first direct evidence of electric field influence in the raindrop size in the Earth's atmosphere. Considering the prevailing complex and dynamic microphysical processes that operate inside a thundercloud simultaneously, the observed association (*r values*) between the two observable deemed to be significant at 95% confidence level.

3.10 The Wind and RLWC Effect

The horizontal wind speed and liquid water content are known to influence the RDSD *(Erpul et al*., 2000; *Testik and Pei* 2017). *Erpul et al.* (2000) reported larger median drop size in wind-driven rain compared to windless rain in a wind tunnel study. On the contrary, *Testik and Pei* (2017) reported a wind-induced collisional breakup of raindrops which results in a narrower RDSD. The effect of horizontal wind speed in the surface RDSD has been tested using the collocated JW disdrometer data and the AWS horizontal wind speed for all the stratiform rain events reported above considering the same data periods. Figure 3.11(a) depicts variation of MVD as a function of horizontal wind speed for both the SE and WE events.

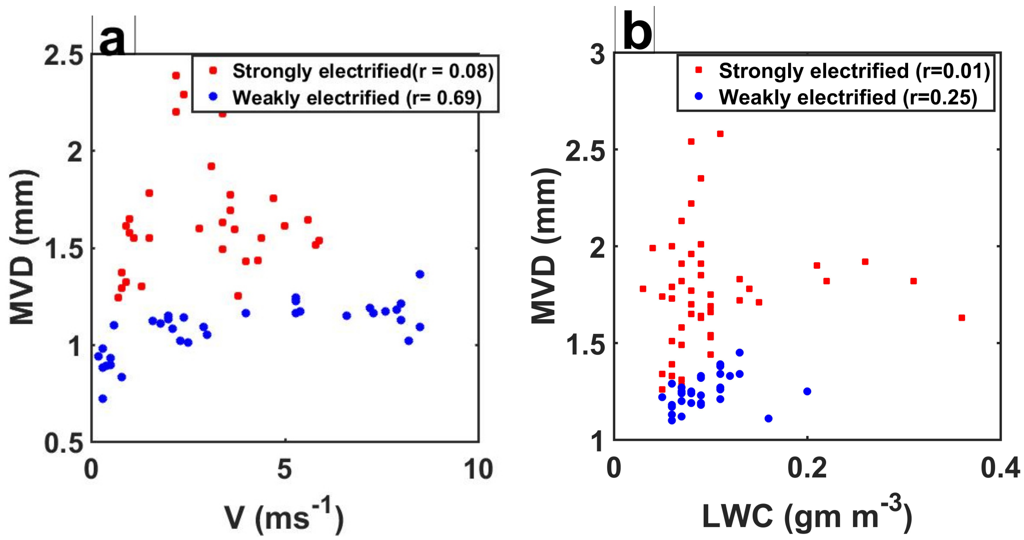

Figure 3.11: Scatter plot of MVD derived from surface based JW Disdrometer with (a) horizontal wind speed (derived from AWS), (b) with LWC (derived from JWD).

Figure 3.11(a) shows that MVD shows a reasonable correlation [r=0.69] with wind speed in WE events. However, for SE events the correlation is insignificant. *Testik and Pei* (2017) observed an increase of number of large raindrops with the increase of RLWC. Figure 3.11(b) depicts the variation of MVD with RLWC derived from surface-based JW disdrometer. While with RLWC, MVD shows a small correlation [r=0.25] for WE rain events and no significant relationship is observed for SE events. This Figure suggest that in rain events associated with stronger in-cloud electric environment, strong electrical forces among the raindrops may be playing a dominant role in determining the RDSD.

3.11 The Alternative Hypothesis

The result presented in support of the primary hypothesis strongly suggest a substantial influence of in-cloud electrical forces in the RDSD below the melting layer of stratiform SE cloud, although the observed difference in the RDSDs of the SE events and WE events can also be explained by another hypothesis based on a lightning–ice relationship (*ice factory hypothesis*). It has been shown that the more electrically active the preceding convection (and the more active the lightning activity with which it is associated), the more vigorous will be the stratiform region and greater the likelihood of lightning flashes in the stratiform region (*Williams And Boccippio*, 1993).The observation of broader RDSD in lightning-producing stratiform regions may also have a explanation in large ice concentration associated with cloud electrification. A more vigorous ice factory means larger concentrations of ice crystals which in turn drive a more vigorous aggregation process. The larger the aggregates, the larger will be the raindrops that result from the melting. However, it has been observed that the mean particle size of raindrops varies much more with precipitation intensity than the aggregation process and therefore the presence of higher ice concentration may not always results in a broader spectrum of rain RDSD (*A. Huggel et al.* ,1996) . The vertical profile of MVD plotted in extended scale in Figure 3.12(b) which corresponds to the rain rate in Figure 3.12(a) indicate that the MVDs of the raindrops are increasing significantly faster in the case of SE events compared to the WE events which evidently suggested a higher collection efficiency of drops, falling at their terminal speed below the melting level.

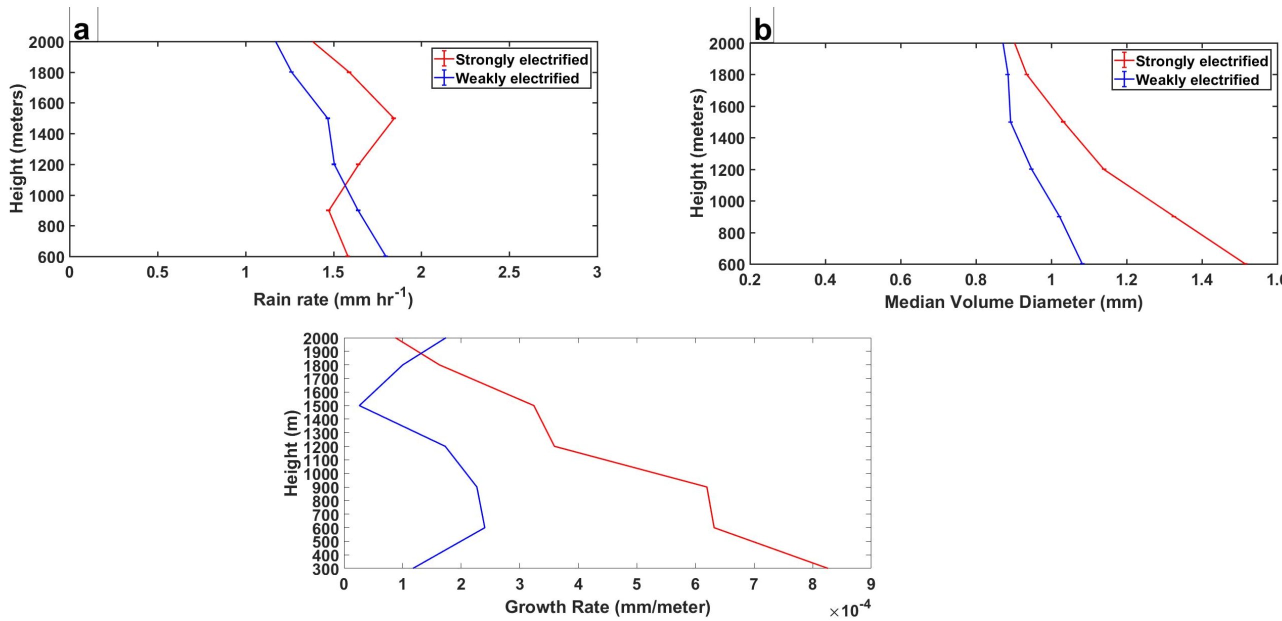

Figure 3.12: Vertical profiles of (a)rain rates and (b) MVDs in extended scale. The bottom panels depicts the Growth rate of raindrops below the melting layer averaged over six events each. Blue and red line corresponds to weakly and strongly electrified events respectively.

In the case of SE events, the vertical profiles of MVD shows a significant variability from the melting layer to the surface even though near the melting layer both types of events show approximately similar profiles of MVD.

The bottom panel of Figure 3.12 depicts the change of MVD (mm) of raindrops per unit length while they are drifting down under the influence of gravity. This Figure suggest that in case of WE events indicated by the blue curve, the drops grow (coalesce to form the bigger ones) and decay (break up and evaporate to produce smaller ones) while drifting down, maintaining certain equilibrium between growth and decay. In stratiform rain, below the melting layer, raindrops evolve by collisions, coalescence, breakup, and evaporation in sub-saturated environment (*Konwar et al*., 2014). Ultimately, the RDSD attains certain kind of equilibrium and the drops reach the ground without exhibiting significant variability (consistent with the observation of *Kollias et al*., 2002 and *Fabry et al*. ,1995). On the contrary, red curve which corresponds to the SE events indicated positive growth all along the way to the ground overcoming the break up and evaporation. Assuming that the melting of larger ice particles are resulting in the bigger raindrops, under the hydrodynamic instability the drops will break up faster than the smaller ones (in WE events) producing numerous smaller drops (Our observation indicated reduction of smaller drops on the contrary). Also, the RDSD of Figure 3.7 show that SE events have fewer smaller drops and larger concentration of bigger drops, which cannot be explained by ice factory hypothesis, because according to this hypothesis concentrations of all size drops should be higher in case of lightning producing (SE) events compared to not lightning producing (WE) events. Hence, ice factory hypothesis falls short in delineating the faster growth of raindrops in the SE stratiform rain events

3.12 Conclusions

The cloud microphysical and dynamical properties mainly determine the structure of the RDSD of rain events (*Zailiang and Srivastava* 1995, *Testik and Barros* 2007) . The discussions pertaining to the influence of in-cloud electrical forces presented in the section 1.9 clearly suggested that RDSD can be modulated effectively by electrical forces in cloud associated with stronger electric environment. A hypothesis of electrical effect on raindrop size distribution in tropical cloud has been postulated based on the convincing laboratory and numerical experiments, which has been tested with upper level RDSD infromation from MRR and surface RDSD retrieved from ground-based JW disdrometer. As the present study is carried out under almost similar dynamical and microphysical condition of rain formation, we may conclude that the significant difference in RDSDs above drop diameters of 2 mm for SE and WE events observed in this study is likely to be due to the effect of electric forces on the raindrops in strongly electrified events. This difference in drop concentration may be due to increased collision- coalescence growth of raindrops mediated by electric forces in strongly electrified environment. As raindrops fall below the melting level at the terminal fall velocities, their growth is influenced by collision break up, coalescence and evaporation. In the electrical environment of tropical clouds, the rain droplets acquire surface charge which is proportional to the square of the droplet radius and magnitude of electric field (*Pruppacher and Klett*,1996). The electrical interaction (Coulombic, charge-dipole) between charged drops increases the coalescence efficiency upon collision between the drops. The force of attraction (between opposite and same polarity drops) enhances the drainage of the air film trapped between the colliding drops which help the drops to coalesce permanently. The ambient electric field in the thundercloud which, can go up to 400 kV/cm *(Winn et al.*,1974) generated by charging processes can induce coalescence of uncharged drops or even like charged drops by the effect of polarization. The significantly increased large drop concentration in case of strongly electrified events compared to weakly electrified events in the present study strongly supports the idea that presence of vertical electric field and electric charge on raindrop modify the shape of RDSD in tropical clouds and hence can act as an influential factor in tropical precipitation formation process.

3.13 Discussions

With all the observational evidence presented in support of the hypothesis proposed, it is concluded that the electrical forces inside the cloud can modify the RDSD by influencing collision-coalescence characteristics of raindrops. In the absence of certain observational measurements which would have given a more conclusive idea about dynamical and microphysical characteristics in all of the 12 stratiform rain events considered for the present analysis, the complete rejection of the ice factory hypothesis is cautiously avoided.

One of the outstanding systematic errors in simulating the observed frequency distribution of tropical rainfall in almost all models is that the models tend to highly overestimate the frequency of very light rain events at the expense of severely underestimating heavy rainfall events (*Goswami and Goswami*, 2016). One possible reason for this persistent problem of weather and climate models may be some missing physics in the parameterization of microphysical processes in cloud modules. The effect of electrical processes on rain formation is not parameterized in most weather and climate models and could be responsible for some of the biases in simulating precipitation by such models. Our quantification of changes in RDSD spectra by the electrified environment in tropical clouds could provide a basis for the parameterization of electrical processes in rain formation in weather and climate models.

Chapter 4

Association between Lightning and Intensity of Surface Precipitation

Chapter 4

4 Association between Lightning and Intensity of Surface Precipitation

4.1 Introduction

Mesoscale Convective Systems (MCS), the genesis of which can be assigned to convective instability in the tropical atmosphere contributes a large portion of tropical precipitation (*Centron and Houze*, 2009). Observation by radar on-board the Tropical Rainfall Measuring Mission (TRMM) indicated that in the latitude belt of 35^{o}N- 35^{o}S, 60% of the total rainfall over land is contributed by thunderstorms and electrified shower cloud (ESC)(*Liu et al*.,2010). The ESC is defined as the cloud system with stronger in-cloud electrical environment but not substantial enough to produce lightning with 30 dBZ radar echo-top temperature lower than -10^{o}C over land and -17^{o}C over ocean (*Liu et al*., 2010). From TRMM observation, *Rasmussen et al*. (2016) reported that over the *La Plata* basin of South America around 95% of the accumulated rain can be attributed to the extreme convective events (with horizontal dimension greater than 1000 km^2 and 40 dBZ echo reaching 10 km maximum height) associated with MCS (that accounts for only 3% of the total events), which are likely to be electrified. Numerous observation suggested that a substantial fraction of precipitation over the tropics originates from clouds with stronger electrical environments associated with lightning.

The discussion presented in the section 1.6 strongly substantiate the evidences of electrical influence on rain microphysical processes from considerable field observation and laboratory experiments.With the radar observation of lightning-producing clouds, *Moore et al*. (1962, 1964) attributed the echo intensification concurrent with the lightning discharges and the subsequent near-surface rain intensity amplification to nearly 100-fold increase of the mass of the rain droplets caused by a mechanism known as "electrostatic precipitation" induced by a lightning discharge. The electrostatic precipitation hypothesis propose that the lightning deposit a very high space charge density of opposite polarity of the ambient charge distribution around the discharge channel and creates a very high local electric field. The newly introduced ions quickly get attached to the drops with opposite polarity and induce an accelerated growth of raindrops by collision and coalescence. They explained that some cloud droplet could acquire about 10^{-12}C of electric charge in a fraction of a second adjacent to the discharge channel. In order to test the "electrostatic precipitation" hypothesis, *Perez et al*. (2012) performed a cloud chamber experiment and reported shifting of droplet spectra towards larger sizes under the influence of electrical discharges. They observed substantial droplet growth in a short span of time after subjecting the cloud chamber to electrical discharge. This enhanced growth of droplets is expected to invariably influence the intensity of precipitation in rain events associated with lightning discharges.

On the other hand, electrification of cloud hydrometeors by lightning discharges by various physical processes is also well documented by many studies. *Heckman and Williams* (1989) explained the rearrangement of electric charges deposited by the lightning discharges inside the cloud. They suggested that space charge density deposited by leaders and return strokes alike are 3-4 orders of magnitude greater than pre-lightning values. The electrons liberated by the breakdown will get attached to oxygen molecules generating O_2^- ions which subsequently get hydrated to form $O_2^-.nH_2O$. These less mobile ions drift away from the channel at $10^{-4}ms^{-1}/voltm^{-1}$(*Longmire*, 1978) while the smaller ions have the mobility on the order of $10^{-5}ms^{-1}/voltm^{-1}$ (*Aplin*, 2000). In a recent paper, *Williams and Montanya*, (2019) discussed the distribution and polarity of electric charge around a lightning channel. They pointed out the formation of a corona sheath around the channel because of the local electric field and suggested that the precipitation particles will likely be charged with the same polarity around a channel.

Moore et al. (2001) observed a burst of radiation with energies in excess of 1 MeVconcurrent with the lightning discharge. The high energy radiation like X-ray and Gamma-rays produced by runaway electrons in the lightning discharges (*Dwyer et al.*,2012; *Marisaldi et al.*, 2014) can initiate phenomenon like terrestrial gamma-ray flashes (TGF), which are highly capable of ionizing atmospheric constituents. Recently *Abbasi et al.* (2018) reported the ground detection of gamma-ray showers originated at 3-5 km from ground level associated with downward propagating negative leader. *Bowers et al.* (2018) reported an airborne observation of a highly penetrating TGF associated with lightning in electrically active hurricane Patricia. Although the ionization resulting from these highly ionizing and penetrating radiations have not been quantified yet, it is highly plausible that the resulting ionization from these radiations could introduce a high concentration of ions inside the cloud after the electric discharge which are most likely then attached to the ambient cloud particles making them highly electrified, although the resulting increased air conductivity may act to discharge the cloud droplets as well.

The levitation of precipitation particles in the mixed phase region of the cloud produced by the balancing of gravitational and electrical forces in a pre-discharge electric field was also investigated in many previous papers (*Levin and Ziv* 1974; *Williams and Lhermitte* 1983; *Kamra,* 1985). *Piepgrass et al.* (1982) investigated the association between lightning frequency and surface rainfall considering storms with moderate lightning rate (12 flashes min^{-1}, small storms) and higher lighting rate (30 flashes min^{-1}, large storms). For the small storm, they obtain a correlation (correlation coefficient, $r = 0.79$) between rain rate and flash rate with time lag of 4 minutes while for the large storm, the best correlation ($r = 0.93$) was obtained with a time lag of 9 minutes. They attributed the variable time lag between the small and large storm to the different time intervals taken by precipitation particles to fall from an altitude of $7-9km$ (charging region inside cloud) to the ground. The higher time lag in case of the larger storm may be caused by prevailing stronger updraft, which would take the precipitation particles to higher altitudes. The observed association between lightning rate and near-surface precipitation rate also can be looked upon from the perspective of electrification of cloud through falling precipitation mechanism (*Mason, 1971; Kamra,* 1970; *Williams and Lhermitte*, 1983). *Williams and Lhermitte* (1983) showed that all the electrical energy associated with a lightning discharge could be entirely derived from the gravitational energy associated with falling precipitation, more efficiently in weakly electrified rain shower in which lightning discharge is less frequent.

Although, the association between lightning and precipitation was observed and reported by many observation, the microphysical link between them still remain illusive. Compelled by this missing link and encouraged by availability of ground-based and upper level observational data , In this chapter, an analysis of rain intensity along with corresponding surface RDSDs before and after 6 Cloud to Ground (CG) and 6 Intra-Cloud (IC) lightning discharges observed over the HACPL laboratory have been presented in pursuit of understanding the effect of air ions generated by lightning discharges on the growth rate of raindrops and consequent near-surface rain intensity in tropical convective clouds. Data collected from ground-based JW disdrometer, MRR and radiometer has been used to quantify the effect of a overhead lightning discharge in rain microphysical processes. Also, the anticipated correlation between variations in lightning rate and precipitation intensity during thunderstorms is pursued from the dual perspective of the effect of lightning on the precipitation intensity and the precipitation hypothesis of storm electrification.

4.2 Rain Gush Associated with Overhead Lightning

A total of twelve (six CG and six IC) (refer to Table 4.1 and 4.2) lightning events recorded by the MLLN within 700m of the HACPL are designated as overhead lightning and considered for investigation of rain gush associated with lightning discharges as previous observations suggested that rain intensity amplification by lightning discharges is highly localized phenomena (*Williams,* 1989). It was also ensured that not more than one lightning flash was recorded by the MLLN within 3-4 minutes of the considered lightning event in a box of $2km \times 2km$, HACPL being in the middle. This was done in order to avoid the overlapping effect of two consecutive lightning discharges took place in the same volume of cloud. Figure 4.1(a-f) depicts the time series of rain rates recorded by the surface-based JWD before and after 6 CG lightning events while (g-k) depicts the same for IC lightning events.

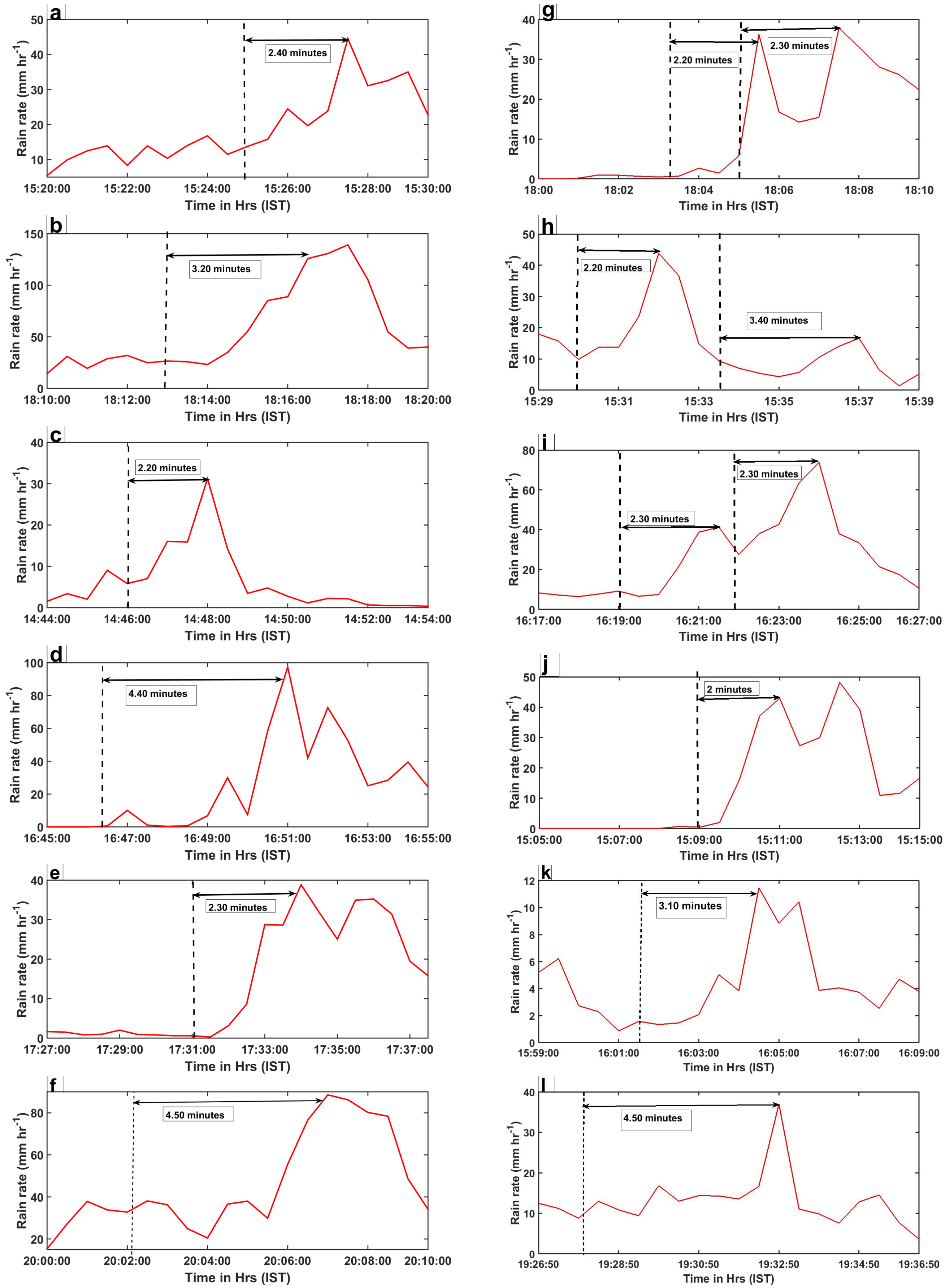

Figure 4.1: (a-f)The Rain Gushes associated with six of the Cloud to Ground (CG) lightning observed overhead of the HACPL, (g-l) Same for Intra-Cloud (IC) lightning. The vertical dashed bars represents the time of an overhead lightning.

A transient surge in rainfall intensity with an average time lag of around 2-4 minutes after the lightning is observed for all the events. The observed small time lag between the two observable clearly suggested that , the raindrops which causes the amplification in surface rain intensity after lightning possibly grows in the warm phase of the cloud induced by the electrification by lightning. The observed time lag may vary significantly depending on the magnitude and the direction of prevailing air vertical velocity. *Moore et al.* (1962) observed all the echo intensification after the lightning below the 0^o isotherm and suggested that rain gush occurs only from liquid water clouds. They observed that the average descent rate of the lightning generated echo was near about $40ms^{-1}$. Although they didn't provide any quantitative explanation for such high downdraft, they speculated such high downdraft was caused by the newly formed larger raindrops which are themselves falling at a fall speed of around $10ms^{-1}$.

Dates	Time (IST)	Type of lightning	Peak current (kA)	Peak lightning rate(per minutes) observed in a 2km×2km box	Average MVD before lightning (mm)	Average MVD during the rain gush (mm)	Average N before lightning (m^{-3})	Average N during the gush (m^{-3})	Average Rain rate before lightning (mm hr^{-1}	Average Rain rate during the gush (mm hr^{-1})	Time lag between lightning and the consequent rain gush (minutes)
05/05/2015(a)	15:25:01	CG	-25.560	5	3.59	4.60	4234.26	595	12.49	33.40	2.40
03/10/2014(b)	18:13:03	CG	-13.202	2	2.05	2.61	3565.97	2901.45	26	95.61	3.20
01/03/2016(c)	14:46:05	CG	-12.578	2	2.39	4.67	3106.04	1021.29	3.78	19.33	2.20
21/04/2015(d)	16:46:23	CG	-12.669	3	0	3.73	0	1762.06	0	64.60	4.40
14/09/2017(e)	17:31:06	CG	-61.316	1	2.33	4.04	816	3011.86	1.29	32.27	2.30
12/05/2017(f)	20:02:42	CG	-26.333	5	2.84	3.28	881.2	1104	31.62	77.58	4.50

Table 4.1: Rain gushes observed at the surface after CG lightning reported in Figure 4.1(a-f) and some microphysical parameters from surface-based JWD before and after the lightning. Note that all the lightning discharges are recorded overhead the HACPL by the MLLN.

Date	Time (IST)	Type of lightning	Peak current (kA)	Peak lightning rate(per minutes) observed in a 2km×2km box	Average MVD before lightning (mm)	Average MVD during the rain gush (mm)	Average N before lightning (m^{-3})	Average N during the gush (m^{-3})	Average Rain rate before lightning (mm hr^{-1})	Average Rain rate during the gush (mm hr^{-1})	Time lag between lightning and the consequent rain gush (minutes)
03/10/2014(a)	18:04:52	IC	11.044	2	1.30	2.32	2780.73	1171.70	1.08	26.53	2.20
08/06/2016(b)	15:30:07	IC	5.075	2	2.10	2.76	5087.78	3861.20	14.49	40.24	2.20
05/05/2015(c)	16:19:06	IC	5.195	5	2.03	3.14	2196.32	1468.04	7.75	33.86	2.30
05/05/2015(d)	15:09:37	IC	5.043	5	1.31	2.69	800	1151	0.40	37	2.0
05/05/2015(e)	16:00:43	IC	5.920	5	1.84	2.19	654.79	671.97	2.49	10.23	3.10
12/05/2017(f)	19:28:04	IC	8.660	5	2.04	2.26	4304	3377	14.6	26.82	4.50

Table 4.2: Rain gushes observed at surface after IC lightning reported in Figure 4.1(g-l) and some microphysical parameters from surface-based JWD before and after the lightning. Note that all the lightning discharges are recorded overhead the HACPL by the MLLN.

4.3 Comparison of RDSD Before and After Lightning...!

Conceivably the surface RDSD reflects the prevailing microphysical processes. Hence, the comparison of the RDSD pairs, before and after lightning might provide valuable insight to the microphysical changes caused by electric discharge. Figure 4.2 depicts the comparison of the RDSDs before and after lightning for all the events reported in Figure 4.1.

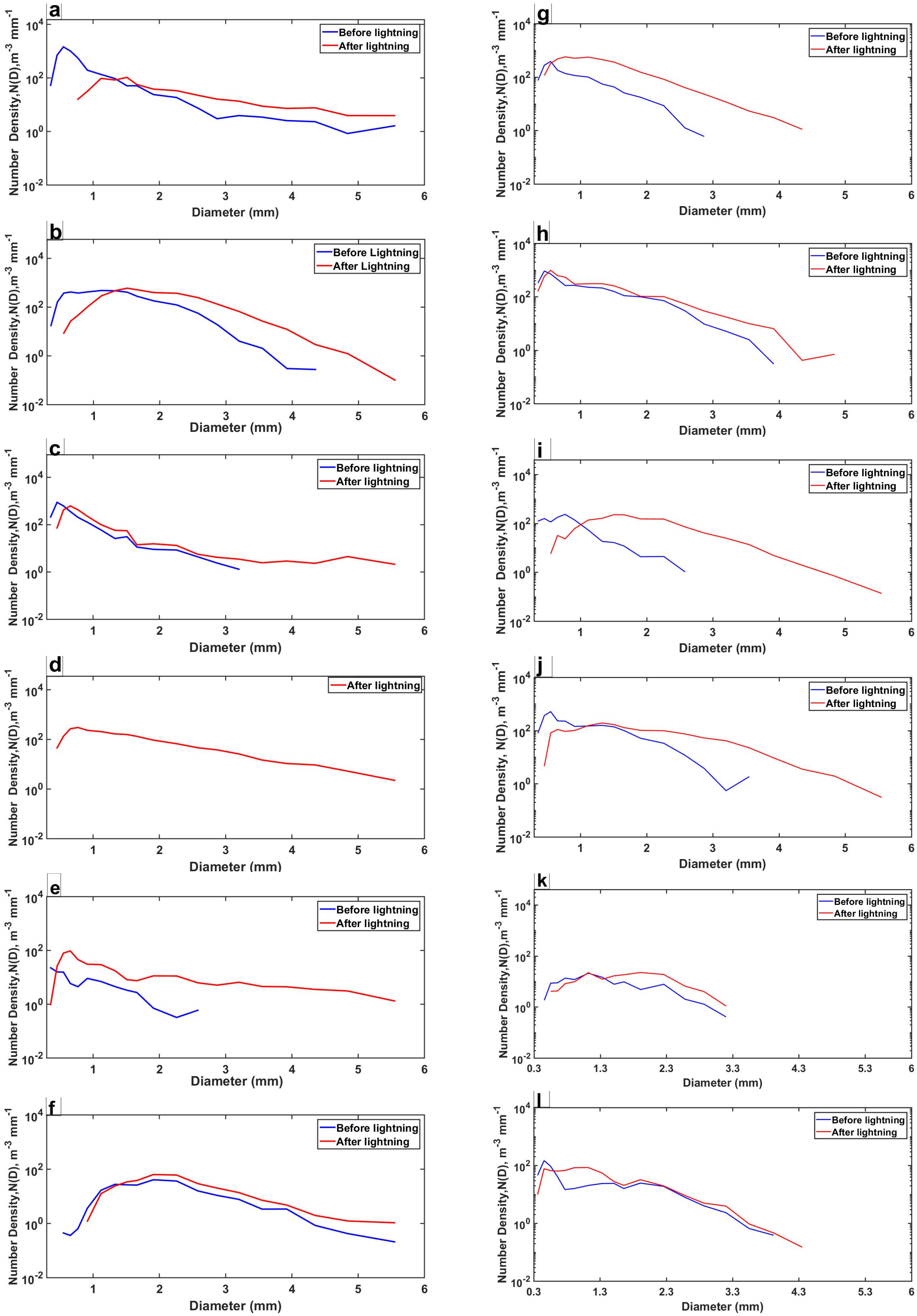

Figure 4.2: (a-f) Raindrop Size Distribution (RDSD) corresonding to the event (a-f) in Figure 4.1, (g-l) Same as (a-f) but for the events (g-l) of Figure 4.1.

It can be seen that increased rain intensity after the lightning discharges appears to be associated with substantial broadening of the corresponding RDSDs. The 'RDSD after the lightning' is averaged over the time period of the peak rain intensity (rain gush) observed after the lightning. Here, the 'time period' of rain gush is defined as the time interval during which the rain intensities have increased to at least twice that of the pre-discharge values. In most of the rain gush events reported here, this 'time period' was observed to be around 2 minutes. It is clearly evident that the number concentration of larger drops increases substantially after the lightning, indicating an enhanced collision-coalescence growth of raindrops. In case of two peaks in the rain intensity after two lightning discharges, the time period of the first peak is used for the averaging of RDSD after the lightning. As evident from the observed RDSD profiles after the lightning, this observed sudden surge of near-surface rainfall associated with the lightning can be attributed to the increased concentration of larger raindrops caused by enhanced collision-coalescence growth of raindrops. This broadening of the RDSD after the lightning is supported by the cloud chamber observation of *Perez et al.* (2012). The electrification of raindrops by air ions generated by lightning discharges enhances the collision-coalescence growth rate of raindrops and hence near-surface rain intensity after an overhead lightning in tropical convective clouds.

4.4 The Enhanced Collision-Coalescence Growth of Raindrops...!!

In the warm phase of cloud, collision and coalescence, rain embryo formation are the primary mechanisms of raindrop formation while riming/accretion form the larger graupel/hail in the cold cloud (*Cloud Physics,Rogers and Yau*,1989). As An enhanced coalescence growth of raindrops shift the RDSD towards the larger size range with consequent decrease of drops number concentration in the smaller size range as the smaller drops effectively coalesce to form the larger ones. The RDSD before & after lightning averaged over the six events each depicted in Figures 4.1 is shown in Figure 4.3 (a-b) respectively along with their corresponding Gamma-fitted RDSD described by equation

$$N(D) = N_0 D^{\mu} exp(-\lambda D) \tag{4.1}$$

Here, the RDSD parameters viz. shape parameter μ, slope parameter λ (mm^{-1}) and intercept parameter N_o (m^{-3} $\mathrm{mm}^{-(\mu+1)}$) are estimated using the moments method reported in *Konwar et al.* (2014) using the following equations

$$G = \frac{M_3^2}{M_2 M_4} \tag{4.2}$$

$$\mu = \frac{1}{(1-G)} - 4 \tag{4.3}$$

$$\lambda = \frac{M_2}{M_3}(\mu + 3) \tag{4.4}$$

$$N_0 = \frac{M_2 \Lambda^{(\mu+3)}}{\Gamma(\mu + 3)} \tag{4.5}$$

Here M_2,M_3, and M_4 are the second, third and fourth moments of the RDSD. Γ is the gamma function. In the current study, the $M234$ method was used as it has relatively less error compared with other higher and lower order methods (*Konwar et al.*, 2014). All the estimated parameters before and after lightning were documented in Table 4.3.

	IC			CG		
RDSD parameters	μ	λ	N_0	μ	λ	N_0
Before Lightning	1.48	1.93	239.4	3.3	2.94	505.31
After Lightning	2.59	1.85	228.6	4.01	2.84	616.6

Table 4.3: Mean values of Gamma RDSD parameters before and after the lightning estimated from JWD measured RDSD.μ is the shape parameter, l, slop parameter (mm^{-1}) and N$_o$, intercept parameter (m^{-3} mm$^{-(\mu+1)}$). RDSD parameters are estimated using the M234 method following *Konwar et al.* (2014).

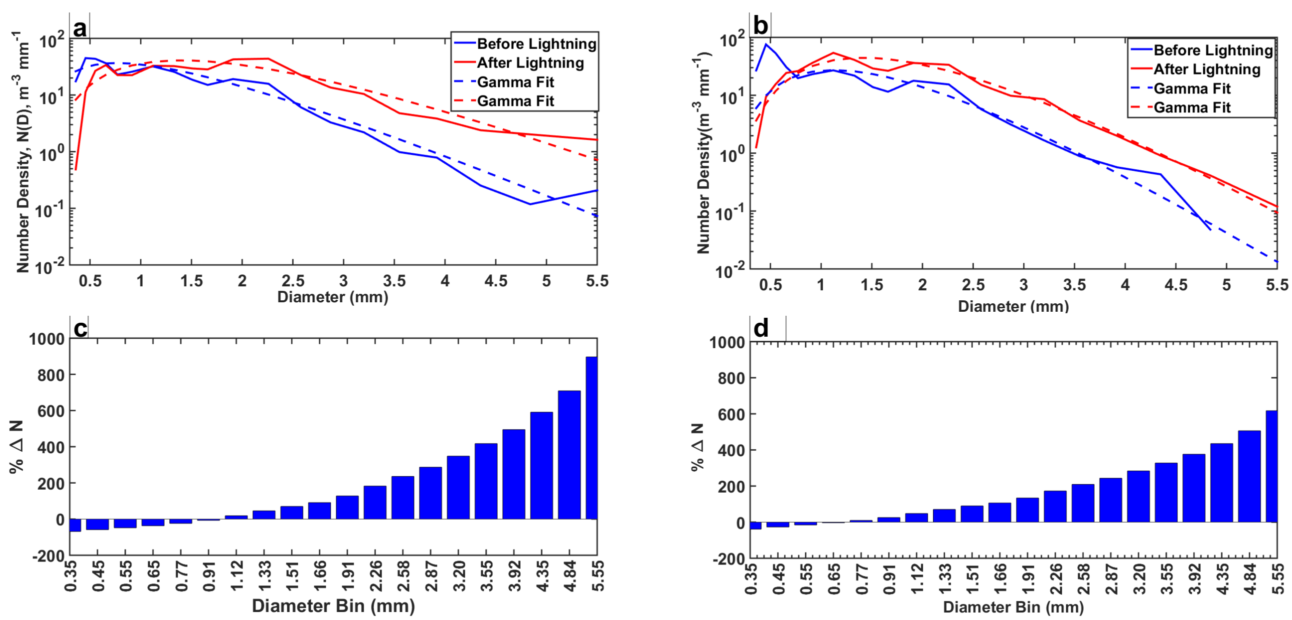

Figure 4.3: (a) RDSD averaged over all the six events reported in Figure 4.2(a-f). The solid lines and dashed lines represent JWD measured RDSD and gamma fit respectively. (b) Same as (a) but corresponding to the events reported in Figure 4.2 (g-l). (c) The relative change in N (m^{-3}) at each diameter bin after the lightning relative to before the lightning derived from the fitted RDSD shown in (a). (d) Same as (c) but corresponding to the fitted RDSD shown in (b).

Using the fitted RDSD, the relative changes in number concentration of drops, N after the lightning compared to before lightning are estimated at each size bin and shown in the bar plot diagram of Figure 4.3 (c-d). As observed from the Figure, at the lower size range (0.35-0.91 mm), N gets reduced while in the larger size range (1-5.5 mm), the number concentrations increase in each size bin after the lightning . Also, the increasing trend becomes more prominent as size increases. It is also observed that the reduction of the concentration of smaller drops is not substantial enough as expected from the electrically enhanced coalescence of smaller drops. This may be due to the fact that in the presence of larger vertical velocity, rapid condensational growth will produce numerous smaller raindrops as well. The relative changes in N in the RDSD spectrum associated with IC events found to be less compared to the CG events.

4.5 The Inverse Relationship between Size and Number

An efficient coalescence growth of raindrops will increase the size of drops at the expense of the number concentrations. Figure 4.4 (a-b) depicts the bar plot representation of MVD corresponding to the CG and IC events respectively reported in Figure 4.1 , while 4(c-d) depicts the same for N before and after lightning.

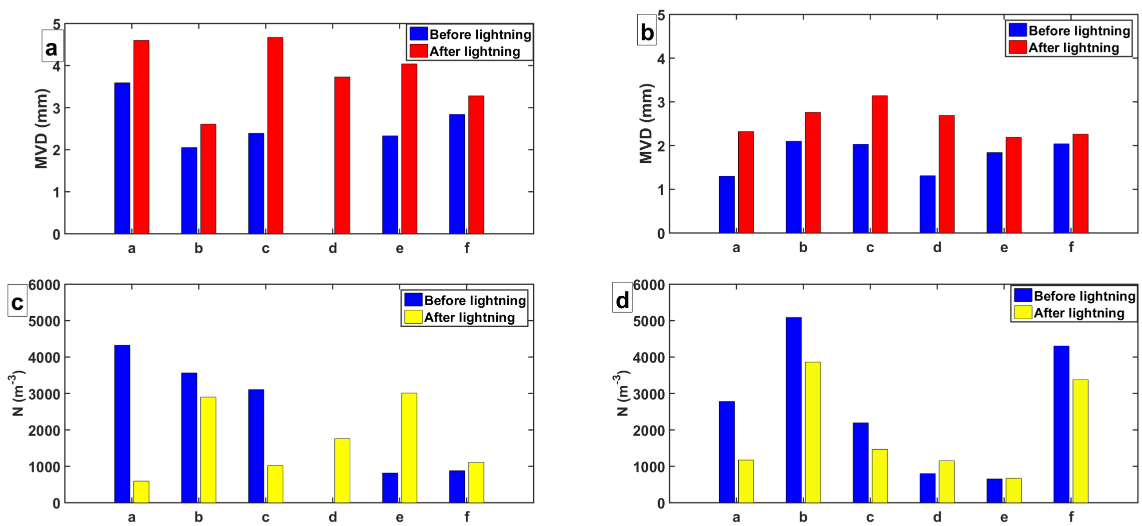

Figure 4.4: (a) Bar plot of MVD (mm) before and after lightning corresponding to the events reported in figure 4.1. (b) Same as (a) but corresponding to the events reported in figure 4.2. (c) Bar plot of total drop number concentrations (m^{-3}) of rain drops before and after lightning corresponding the events reported in figure 4.1 (d) Same as (c) but corresponding to the events reported in Figure 4.2. The blue and yellow bar represents before and after lightning respectively.

It is observed that the MVDs show larger values after the lightning in all the cases when compared to the same before the lightning. On the contrary, the total number concentration N shows a reduced value after the lightning when there was substantial rainfall before the lightning. This clearly indicates an enhanced coalescence process of drops at the lower level caused by the lightning discharge.

4.6 Microphysical modification at the Upper level

Despite having the inherent attenuation issue, MRR provides an unique opportunity to gauge the microphysical processes happening in the upper atmosphere. The MRR measurement along with the collocated surface disdrometer brings in the coherent observation of RDSD at different altitudes. A rain event recorded on 25th September 2014 over the HACPL with lower rain intensity (<10 mm hr^{-1}) and isolated lightning activity was analyzed with the MRR-derived datasets. Added precautionary measures are adopted to avoid the attenuation problem by limiting the observation below 1000m from the ground and ensuring that the rain intensity at the surface as well as at the upper level doesn't exceed 10 mm hr^{-1} during the data period. The HTI of the MRR derived radar reflectivity factor, z, is shown in Figure 4.5(a). The absence of bright band in this Figure indicates the convective nature of rain formation, where raindrops grow near the cloud base by accretion of the cloud liquid water produced by rapid condensation. A CG lightning is detected by the MLLN at 17:57:12 IST overhead the HACPL.

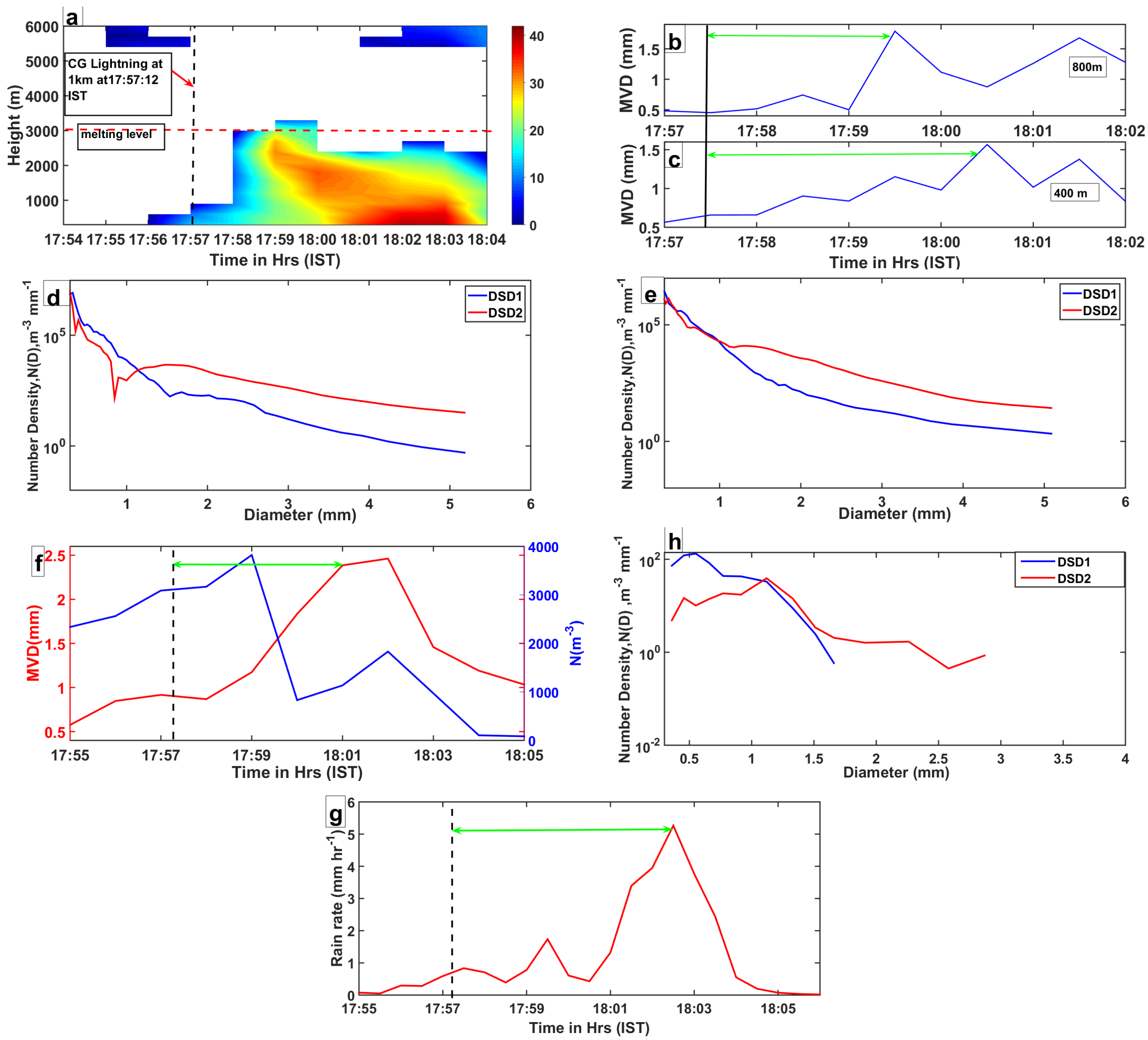

Figure 4.5: (a) Height-Time Index (HTI) of the MRR derived reflectivity. The vertical bar represents time of lightning & the horizontal red bar represents the melting level.(b-c) Time series of MVD (mm) at 800m and 400m after the lightning, (d-e) RDSD at 800m and 400m,(f) Time series of MVD and Total number concentration measured by ground-based JWD, (g) Time series of Rain rate (mm hr^{-1}) measured by ground-based JWD,(h) surface RDSD from JWD. The height is measured from the surface.

Figure 4.5(b, c) shows time series of MVD at 800m and 400m above the ground after the lightning. A transient peak of the MVD response is observed to drift downward below the melting level indicated by the dashed red horizontal line after the lightning discharge. The corresponding RDSDs at this two levels (800m and 400m MSL height) before and after the lightning have been plotted in Figure 4.5(b-c). The RDSD1 in Figure 4.5(d) is averaged over time from 17:57:00 to 17:58:00 IST and RDSD2 is averaged over 17:59:00 to 18:00:00 IST and in Figure 4.5(e) RDSD1 is averaged 17:57:00 to 17:58:00 IST and RDSD2 is averaged over 18:00:00 to 18:01:00 IST. Figures 4.5(f, g) respectively show the time series from the MVD along with the total number concentrations, N and rain rate at the surface measured by the JWD before and after the lightning. A transient peak is observed in both the MVD and the rain rate profiles with a time delay of 2.50 minutes after the discharge. The total number concentration, N shows a corresponding transient trough after the discharge indicating enhanced coalescence growth of raindrops. The JWD-measured surface RDSD shown in Figure 4.5(h) shows a substantial increase in the concentration of larger drops at the expense of smaller ones after the lightning. In Figure 4.5(h) RDSD1 is averaged from 17:55:00 to 17:57:00 IST and RDSD2 is averaged from 18:01:00 to 18:03:00 IST. These observations clearly indicate that the observed peak in the rain rate after the lightning is caused by the lightning-induced coalescence growth of raindrops.

4.7 The Effect of Ligtning Rate on Precipitation Rate (More the Thunder $\Longrightarrow$ More will be the Rain)

As it is observed that individual lightning discharges can electrically modify the RDSD as well as the rain intensity, one can anticipate a good correlation between variations in lightning rate and rainfall rate during a thunderstorm. In order to study the relation between lightning frequency on precipitation intensity, we have analyzed two thunderstorms with moderate lightning frequency over the HACPL site on the 5th of May 2015 (hereafter referred as A) and the 12 May 2017 (hereafter referred as B). A 5 km× 5 km box was created around the HACPL to record the lightning activity for both the thunderstorms. The genesis and morphology of the pre-monsoon thunderstorms over the Indian regions are governed by the synoptic conditions involving western disturbances and induced lows in the north and easterly waves in the south along with local topography, solar insolation, and advection of moisture in favorable condition (*Tyagi*, 2007). For the storm A, peak lightning rate was observed to be 8 fl. min^{-1} while the storm B exhibited peak lightning rate of 10 fl. min^{-1}. Figure 4.6 (a-b) depicts the lag-correlation analysis of rain rate and MVD and with lightning flash rate with a lag time of 3 minutes for thunderstorm A while (c-d) depicts the same for storm B with a lag time of 6 minutes..

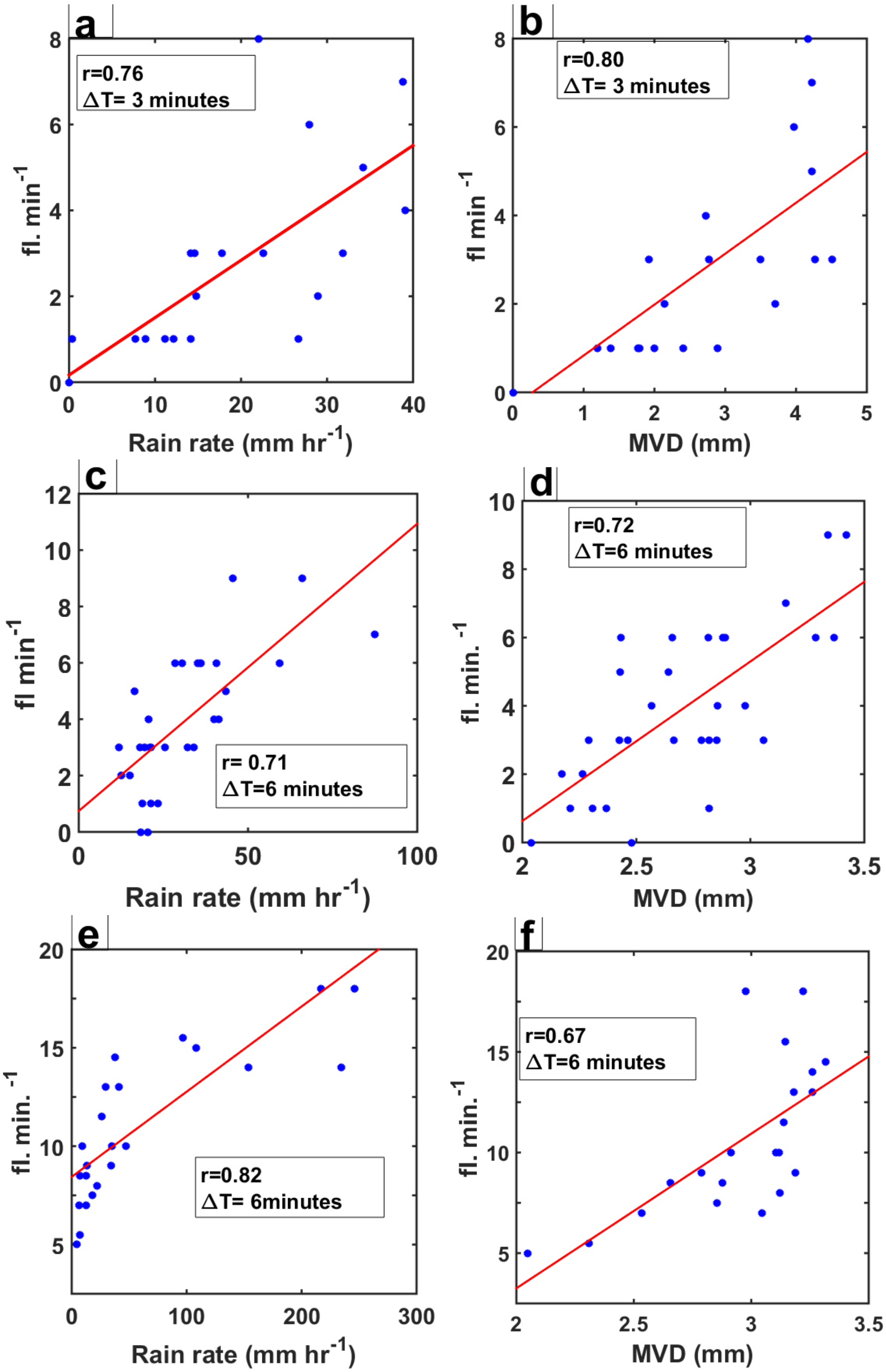

Figure 4.6: Scatter plot of rain rate (mm hr^{-1}) and MVD (mm) with lightning frequency (fl. min^{-1}). (a-b) Corresponds to the thunderstorm observed on 5 May 2015, designated as A in the text. (c-d) Corresponds to the thunderstorm observed on 12 May 2017, designated as B in the text.(e-f) Corresponds to the thunderstorms observed on 3 June 2008 observed over AEO, Pune.

For the thunderstorm A, the best correlation for the rain rate with the lightning rate was observed with correlation coefficient ,$r = 0.76$ with p-value $< 0.0001$and for MVD the best correlation was observed with correlation coefficient $r = 0.80$with p-value$< 0.0001$with 3 minutes time lag, while for the thunderstorm B the best correlation with lightning rate was observed with 6 minutes time lag for the rain rate ($r = 0.71$) and the MVD ($r = 0.72$). The variable time lag observed by *Piepgrass et al.*(1982) for small (4 minutes) and large storms (9 minutes) suggests that the time lag between lightning peak and associated rainfall peak at the surface may depend on the vertical development of the storms as well. The prevailing updraft and downdraft may substantially influence the fall velocity of the precipitation particles, thereby causing variable lag time between lightning and rainfall peak.

A stronger thunderstorm with high lightning rate (up to 24 flashes per minute) and heavy rainfall was recorded on the 3rd of June 2008 at the AEO located at Pune (18.53N, 73.80E). The electric field and rain rate during the thunderstorm was measured by collocated field mill and optical disdrometer at the AEO. Figure 4.6(e-f) shows the lag correlation analysis of rain rate and MVD with the lightning flash rate with a lag time of 6 minutes. The best correlation was observed with 6 minutes time lag for the rain rate ($r = 0.82$, p-value <0.0001) and for the MVD ($r = 0.67$, p-value <0.0001). The higher flash rate indicate that, this storm is more vertically developed than the storms A and B, although the time lag between the lightning and rain rate is similar to the storm B. This clearly indicate that the raindrops causing the intensity amplification of surface precipitation are growing below the melting layer.

4.8 But the Effect is Highly Localized...

In the endeavor to examine the anticipated time-lagged association of lightning rate and precipitation intensity, the time series of lightning flash rate counted in the mentioned 5 km$\times$ 5 km box and rain rate recorded by a JWD located at the HACPL with a 1-minute averaging time interval are plotted in Figure 4.7(a-b) for the thunderstorm ‘A’.

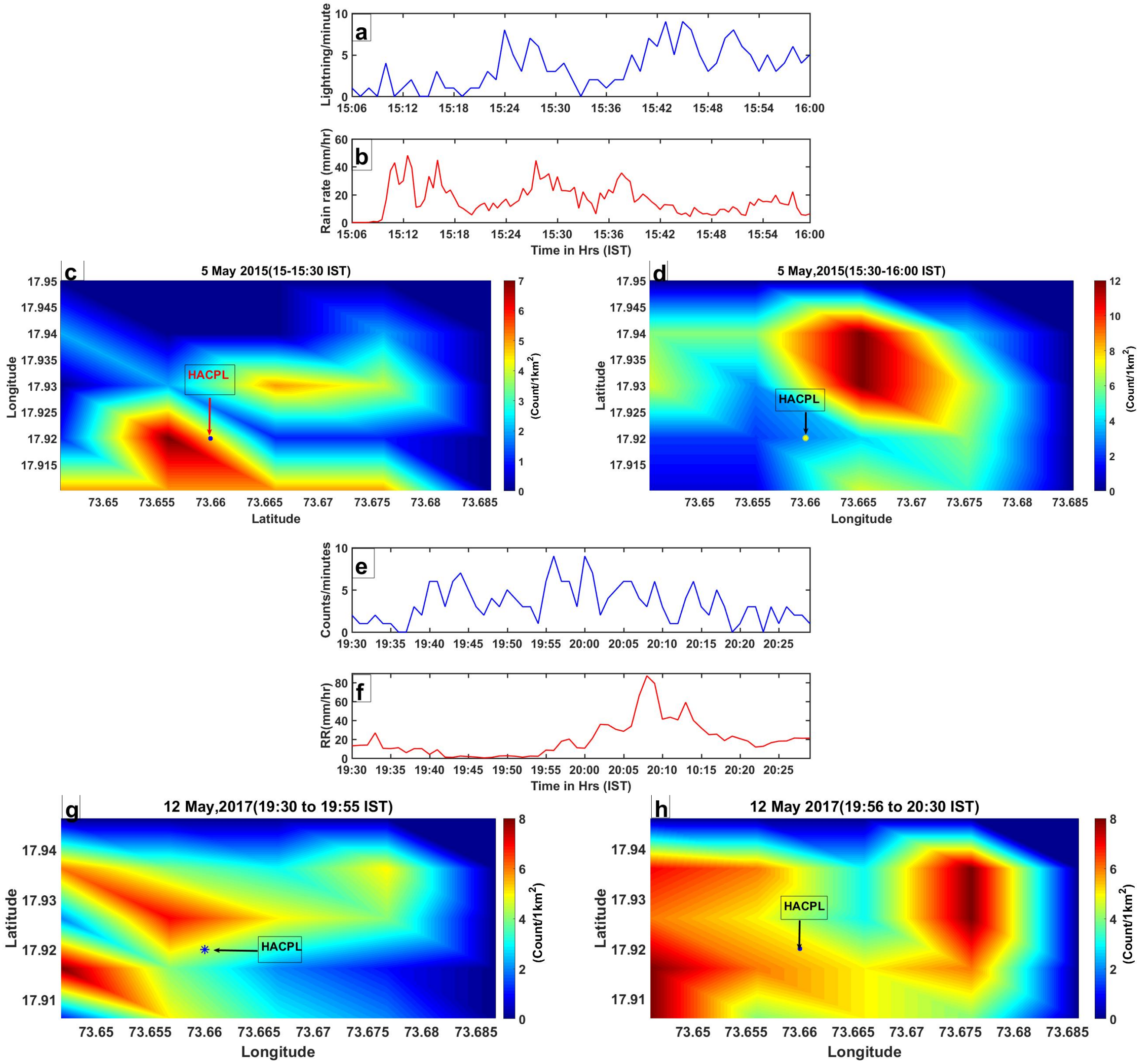

Figure 4.7: (a-b) Time evolution of lightning frequency and rain intensity, (c-d) Spatial distribution of lightning frequency in the 5km× 5km box around the HACPL from 15:00 to 15:30 IST and 15:30 to 16:00 IST respectively corresponding to the thunderstorm observed on 5 may 2015. (e-f) Time evolution of lightning frequency and rain intensity, (g-h) Spatial distribution of lightning frequency in the 5km× 5km box around the HACPL from 19:30 to 19:55 IST and 19:56 to 20:30 IST respectively corresponding to the thunderstorm observed on 12 may 2017. Please note the presence of higher lightning frequency over the HACPL in panel c and h.

A rainfall peak was observed with a time lag of about 3 minutes after a lightning frequency peak in the time interval 15:00 IST to 15:30 . Although there is another lightning frequency peak at around 15:45 IST, the anticipated lagged rainfall peak was not observed. To ascertain the cause, the spatial distribution of lightning counts was plotted in Figure 4.7(c-d). It was observed that from 15:00 to 15:30 IST, the convective core where the lightning frequency was supposed to be higher located near the HACPL. For the time period of 15:30 to 16:00 IST, the convective core was observed to migrate away from the observation site. This may be the reason for the absence of rainfall peak around 15:45 IST despite the presence of lightning frequency peak.

For the thunderstorm 'B', time series of lightning counts counted in the said box and rain rate recorded by the

JWD located at the HACPL with a 1-minute averaging time interval are plotted in figure 4.7(e-f). Although there is a lightning frequency peak at around 19:43 IST, no rain peak was observed around that time. On the other hand, two rainfall peak was recorded by the JWD at 20:01 IST and at 20:06 IST preceded by two lightning peak at 19:55 IST and 20:00 IST. From the spatial distribution of lightning flash rate in figure 4.7(g-h), it was observed that between 19:30 and 19:55 IST, the convective core was a little further away from the HACPL, while the convective activity was observed overhead the HACPL between 19:56 and 20:30 IST. This observation suggested that the effect of lightning in modification of precipitation intensity is in fact a localized phenomena as suggested by *Williams* (1989).

4.9 Convention...."The Higher the Rain Rate... Larger the Size, Larger the Number"...Really..?

The '*Electrostatic Precipitation*' hypothesis of *Moore et al.* (1962, 1964) proposed that lightning deposited a very high space charge density of opposite polarity of the ambient charge distribution around the discharge channel and creates a very high local electric field. The newly introduced ions quickly get attached to the drops with opposite polarity and induce an accelerated growth of raindrops by collision and coalescence. *Heckman and Williams* (1989) suggested that space charge density deposited by leaders and return strokes alike are 3-4 orders of magnitude greater than pre-lightning values. The electrically induce collision results in permanent coalescence of the colliding drops for every collision for all impact angles if the drops are electrically charged as suggested by *Ochs and Czys* (1987). The efficient coalescence will results in increase in the number concentration of larger drops at the expense of the smaller ones. The equation 2.3 in chapter 2 indicate that contribution to the rain intensity comes from the size as well as number concentration of raindrops. A simultaneous increase in the drop sizes as well as number concentration is observed with increase in rain intensity in convective cloud (*Tokay et al*., 2001; *Niu et al*., 2010). Figure 4.8 (a-b) depicts the scatter plot of MVD and N with rain rate for the entire time period of the thunderstorm 'A' while 4.8(c-d) depicts the same for the thunderstorm 'B'.

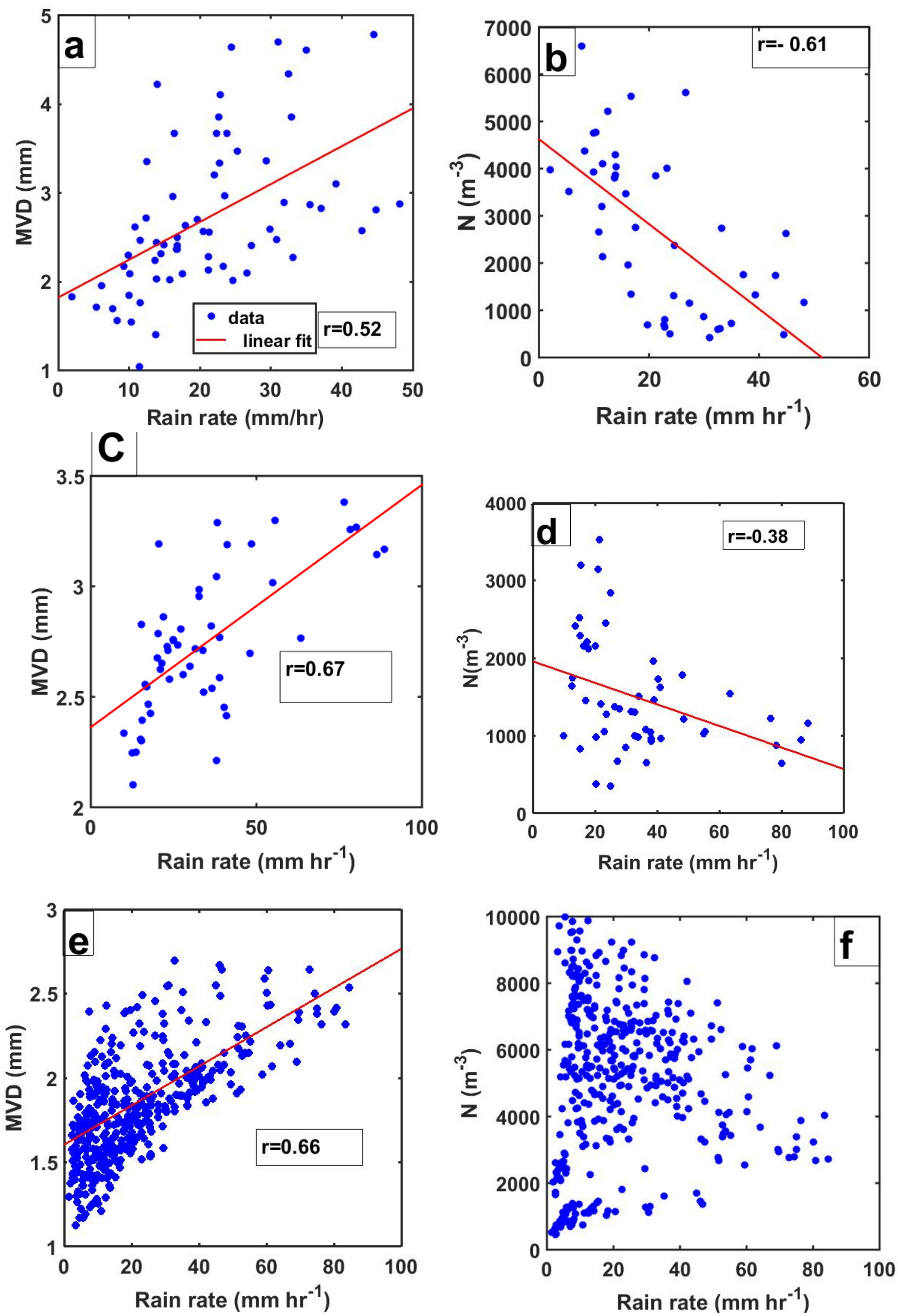

Figure 4.8: Scatter plot of MVD (mm) and N (m-3) with rain intensity (mm hr-1). (a-b) corresponds to the thunderstorm A, (c-d) corresponds to thunderstorm B (refer to the text). (e-f) Corresponds to the combined rain events observed on 6 Sept. 2014, 5 June 2015 and 24th June 2015 in the absence of lightning discharges in the vicinity of the HACPL.

It is observed that while MVD shows an increasing trend with rain rate, the total number concentration N shows decreasing trends with rain rate which implies that the larger rain intensity is caused by the electrically enhanced coalescence of smaller raindrops to form the bigger ones.

Figure 4.8(e-f) shows the composite scatter plot of MVD and N with the rain intensity for some of the rain events observed on 6 Sept. 2014, 5 June 2015 and 24th June 2015 in the absence of lightning discharges in the vicinity of the HACPL. Although the MVD shows an increasing trend with rain rate, above 2 mm the increasing trends get saturated which is consistent with the observation of *Wen et al.* (2016). The number concentration of drops, N, shows no significant trend with the rain rate. It is evident that both drop size and number concentration contribute to the larger rain intensity in the absence of appreciable electric forces inside the cloud. On the other hand, in the case of the rain events associated with lightning, where stronger electric forces are prevalent(ensured by presence of lightning), the rapid and continuous increase of MVD and depletion of N with rain intensity as observed in Figure 4.8(a-d) suggest an efficient coalescence growth of raindrops induced by electric forces.

4.10 Higher the Intensity of Lightning, Broader will be the RDSD

The MLLN records the lightning peak current flows during a discharge. The peak lightning current is associated with the total charge that get discharged during the breakdown. The total current flows below a thunderstorm, termed as Maxwell current can be expressed as sum of many field-dependent currents

$$J_M = J_E + J_C + J_L + J_P + J_D \tag{4.6}$$

Here, $J_M$is the Maxwell current, J_E is conduction current, $J_C$is the corona current, $J_L$is the lightning current, $J_P$is the precipitation current, and $J_D$is the displacement current expressed as

$$J_D = \varepsilon_0 \frac{dE}{dt} \tag{4.7}$$

Where $\varepsilon_0$is the permittivity of free space and E is electric field. The pre-discharge electric filed build up by the prevailing charging processes inside the storm is linearly related to J_L. The higher the ∇E, the higher will be the peak lightning current. The intensity of the lightning can expressed in terms of peak lightning current.

Williams et al. (1989b) also observed that the intensities of lightning echo and precipitation echo are correlated with each other, suggesting that more intense lightning is associated with more intense precipitation.Higher the peak current, more intense will be the lightning. *Mudiar et al.* (2018) have shown that raindrop sizes show a positive correlation with lightning intensity. The idea that more intense lightning will have a larger impact on the RDSD has been tested by analyzing a few RDSDs pairs with similar rain rate as a function of electric field change (∇E) during 8 overhead lightning discharges in different thunderstorms observed over the AEO. Figure 4.9(a-d) depicts the comparison of RDSD pairs with similar rain rate but associated with variable surface electric field change happened during electric breakdown. While selecting these 8 lightning events, it was ensured that no another lightning event was observed within 3-4 minutes of the reported events. This was done in order to avoid the overlapping effect of multiple discharges on the precipitation processes. The RDSDs are averaged over the time period of the subsequent rain gush corresponding to the preceding lightning discharge.

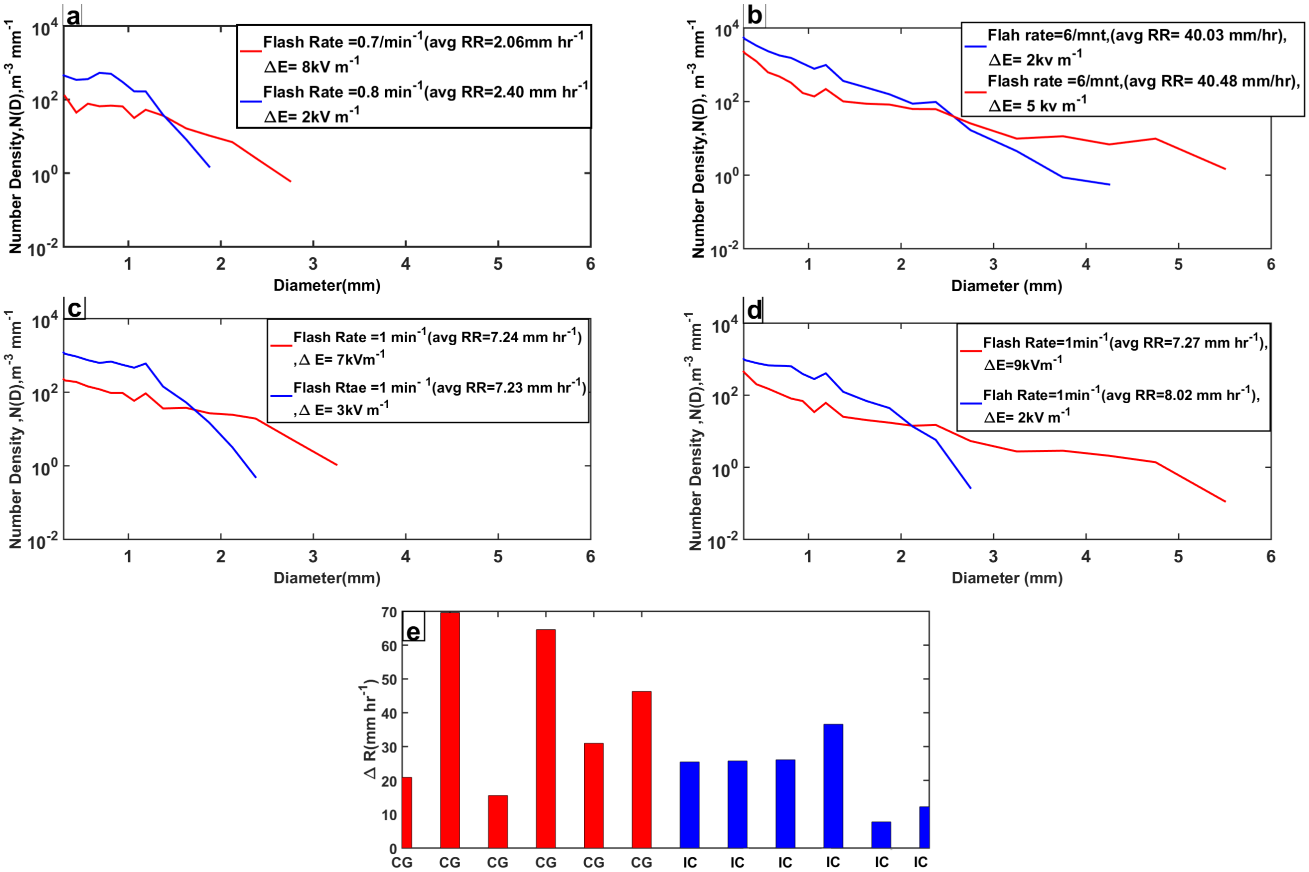

Figure 4.9: Raindrop size distribution (RDSD) corresponding to the lightning discharges with different discharge strength (magnitude of change of surface electric field, DE) observed over the AEO, Pune. The reported thunderstorms were observed on 22 May, 3-4 June, 2 and 9 September 2008. (e) Change in rain intensity (mm hr^{-1}) after lightning relative to the intensity before lightning. The red and blue bars represent the rain events reported in Figure 4.1.

Although all the RDSDs pairs correspond to different thunderstorm events, it is distinctly visible from these Figures that larger ∇E corresponds to a broader spectrum of RDSDs. Larger raindrops are associated with higher intensity of lightning. Figure 4.9(e) depicts the change in rain intensity during the rain gush reported in Figure 4.1 after the lightning relative to the intensity before lightning. It is observed that larger intensity changes in rainfall are associated with the intense CG (with higher peak current) lightning discharges confirming the idea that intense lightning is associated with more intense precipitation (*Williams et al.* 1989b). One possible reason may be the electrical enhancement of collision-coalescence growth of raindrops caused by lightning as intense lightning possibly causes higher ion concentration and hence more electrification of precipitation particles in a larger volume of cloud.

4.11 Conclusions

The primary conclusion drawn from the test of hypothesis of lightning influence on the near-surface rain intensity using the observational data sets is

"In lightning producing clouds ,the two observable lightning and precipitation intensity stay electrically connected through electrical modification of microphysical processes, although genesis of both can be assigned to the initial updraft speed."

The observations presented in this chapter suggest that lightning discharge can amplify the effect of electric force on the growth rate of raindrops below freezing level and enhance the surface precipitation intensity. The transient amplification in the near-surface rain intensity observed after an overhead lightning with average time delay of 2-4 minutes suggested that the effect is spatially and temporarily localized. The genesis of the raindrops causing the amplification of rain possibly happens in the warm phase of the cloud as the observed very short time lag suggest so. The comparison of the observed RDSD before and after lightning suggested that the amplification in the intensity of rain is possibly due to the enhanced collision-coalescence growth of raindrops caused by the electrification of raindrops by lightning discharges along with possible contribution from the melting of ice and graupel particles which participated in the pre-discharge charge separation inside the clouds. This observation also reaffirms the idea that more intense (with higher peak current) lightning are associated with more intense precipitation.

4.12 Discussion

Keeping the dynamic association between the two observable (lightning and precipitation) in consideration, the current observations encourage us to propose that precipitation intensity is coupled with lightning through electric processes. Along with the observations reported in *Mudiar et al.* (2018), the present observation suggested that the electrical forces may influence the cloud microphysical processes substantially inside strongly electrified stratiform as well as convective clouds in the Earth's atmosphere even though the degree of influence in both types of clouds is modulated by the prevailing dynamical as well as microphysical conditions.

The observed association between lightning rate and near-surface precipitation rate also can be looked upon from the perspective of electrification of cloud through falling precipitation mechanism (*Kamra*, 1971; *Mason*, 1971; *Williams and Lhermitte*, 1983). *Williams and Lhermitte* (1983) showed that all the electrical energy associated with a lightning discharge could be entirely derived from the gravitational energy associated with falling precipitation, more efficiently in weakly electrified rain shower in which lightning discharge is less frequent. The precipitation hypothesis of electrification of thunderstorm requires descent of charged precipitation particles to the mixed phase region (central dipole region) located between -10^o to -25^o C (*Latham*, 1981) which corresponds to 7-8 km MSL height over the HACPL. Assuming that the lightning discharge got initiated in this region of the cloud (*Williams*, 1989) because of the charges carried by the precipitation particles, with a fall velocity of 10-15 m sec^{-1} (*Williams*, 1989), these precipitation particles will take around 8-11 minutes to reach the MSL. As the observation site (The

HACPL) is at an altitude of 1.3km form MSL, the precipitation would be effectively taking around 7-10 minutes to reach the recording instruments. Although, the prevailing downdraft (which may be comparable or greater than the fall speed of the precipitation particles) can substantially shorten the transit time of precipitation particles between the melting layer and the ground, reducing the observed time-lag considerably. But downdraft is dominant in the lower portion of the cloud, primarily below the melting layer. Mixed phase region is primarily dominated by stronger updraft in lightning producing cloud.(*Williams*,1981, *new mexico hailstorm over Langmuir laboratory*) However, the present observation of the average time-lag of 2-4 minutes between the individual lightning and the associated rain gush suggest that the substantial fraction of precipitation particles which causes the transient amplification in the near-surface precipitation intensity may be originating in the warm phase. A substantial contribution from the melting of ice and graupel particles to the rain gush associated with individual overhead lightning discharge is highly unlikely in such short span transit time and time of rain gush.

The reported generic bias of underestimation of heavy precipitation in weather models might be due to some missing physics in the calculation of the microphysical tendency equations for collision-coalescence, collection and accretion terms (*Hazra et al*., 2017). The improvement of microphysical parameterization, particularly the tendency equations in global climate models based on observations can help to improve the simulation of heavy rainfall (*Hazra et al*., 2017). The collection efficiency of raindrops is governed by the size distribution and the fall velocity of the drops (*Bradley and Stow*, 1984). The current results suggested that prevailing electric forces can modify the RDSD, thereby influencing the collection and collision-coalescence efficiency of raindrops. Therefore, the observed RDSD and the terminal velocity can be used to calculate a modified collision kinetic energy and total surface energy of the raindrops (*Bradley and Stow*, 1984). With a new collection and collision-coalescence efficiency from the observation, the equation of growth rate of raindrops can be modified. The modified kernel of collection efficiency might be helpful for the improvement of heavy rainfall in climate models. Furthermore, the slope parameter of the Marshall-Palmer RDSD in the NWP model can be re-calculated based on the observed RDSD and modify the present formulation of the RDSD in the model. Hence the present findings could provide a compelling basis for parameterization of the electrical effects on rain formation process in weather models.

Chapter 5

The Electrical Route to Realising Intensity Simulation of Heavy Rain Events in Tropics

Chapter 5

5 The Electrical Route to Realising Intensity Simulation of Heavy Rain Events in Tropics

5.1 Introduction

The data and analysis presented in the chapter 3 and 4 strongly indicate a substantial influence of in-cloud electrical forces in rain microphysical processes through enhanced collision-coalescence growth of raindrops in strongly electrified cloud. Broadening of the raindrop size distribution is observed to be inherent to strongly electrified cloud which in turn modify the intensity of surface precipitation. Rain intensity is known to show a strong association with the drop size distribution (*Smith et al.* 2009, *Seela et al.*,2019). Larger size and higher number concentrations are observed to be associated with higher rate of convective precipitation in weakly electrified cloud (*Niu et al*., 2010) . On the other hand, in-cloud electric forces found to increase the size of the raindrops at the expense of the number concentration which suggested that rain in strongly electrified cloud will be size dominated.

The revolution in weather forecasting (*Boer et al*., 2014) has led to significant improvement of simulation of precipitation in synoptic and mesoscales by Numerical Weather Prediction (NWP) models. However, the quantitative precipitation forecast (QPF) on a smaller scale, required for hydrological forecasts remains a challenge even in the latest high resolution operational models (*Shrestha et al*., 2013; *Wang et al*., 2016; *Shahrban et al.*, 2016) with unacceptably large mean absolute error (MAE), (*Giinaros et al*., 2015).The problem of errors in the QPF appears to be related to (a) displacement of the simulated centre of the mesoscale system compared to observed, (b) simulation of the phase of the diurnal cycle of precipitation by models a few hours before observed over land (*Dirmeyer et al.*, 2012) and (c) underestimation of heavy precipitation by almost all climate models even up to resolution of 12 km (*Kendon et al.*, 2012). The major uncertainties associated with the proper estimation of precipitation are estimated to be model incorporation of complex sub-grid scale cloud processes *(Khain et al*., 2000). Using WRF model *Giinaros et al*.(2015) reported large MEA in the simulated precipitation suggesting model inability to reproduce heavy precipitation in storms associated with lightning. *Dafis et al*. (2018) reported significant bias (under estimation) in the accumulated precipitation towards the higher precipitation range ($\geq 20mm$) in the simulation of lightning producing storms. For the skillful predictions of hazards associated with increasing frequency of extreme rainfall events (*Goswami et al.*, 2006), it is important to improve the prediction of thunderstorms and extreme rainfall events with reduced errors. A simple increase in resolution of a model, however, is not enough as has been found that it has little impact on the skill of prediction (*Shrestha et al*., 2013) or produces too intense extreme events (*Kendon et al.*, 2012). It is recognized that high 'resolution' in a climate model is a necessary but not sufficient condition for simulating the variance of high-frequency fluctuations (*Goswami and Goswami*, 2016).

It is also known that an adequate 'cloud microphysics' parameterization is essential for simulation of the organization of mesoscale systems and equatorial waves (*Hazra et al*., 2017, 2020). It is well known that model accumulated precipitation is highly sensitive to the prescribed RDSD (*Gilmore et al.*, 2004; *Curic et al*.,2010, *Curic and Janc*,2011; *Morrision* ,2012; *Kovacevic and Curic*,2015). The quantification of the in-cloud electrical forces in rain microphysical processes from the chapter 3 and 4 suggeset significant electrical modification of RDSD, while the effective inclusion of electrical factor in the cloud module of NWP model still remain illusive. On the other hand, substantial fraction of tropical precipitation ($57-60\%$) originated from thunderstorms and electrified shower cloud associated with Mesoscale Convective Systems (MCS) both of which exhibits strong electrical environment *(MacGorman et al.*,2008; *Centron and Houze*, 2009; *Liu et al*., 2010). In that regard, it is important to properly represent this fraction of tropical cloud properly in the NWP model for better estimation of precipitation. However, numerical simulation of electrical forces within clouds associated with extreme rainfall events are only beginning to be addressed in NWP models (*Dafies et al*., 2018).

Encouraged by the compelling evidences of strong electrical influences in raindrop size distribution (RDSD) presented in chapter 3 and 4, in this chapter a hypothesis that a large part of underestimation of the 'intensity' of the observed precipitation may be related to modification of the RDSD by in-cloud electric fields has been tested through simulations of rainfall in several 'strongly' electrified cases and 'weakly' electrified cases observed over the HACPL in a convection-permitting NWP model.

5.2 Numerous Uncertaintny in Our Understanding of Basic Physics..!

The formation of hydrometeors and inter-interaction of them inside cloud observed to be non-linear and complicated. Substantial uncertainty still persist in our understanding of physical processes which resulted in cloud formation and subsequent precipitation. It is observed that even within a given species of hydrometeors (ice-phase), there is large variability in density and shape (*Heymfield et al*.,2004). Due to this inherent complexity of hydrometeors in real atmosphere, it become a challenge to properly represent the processes in weather models (*Morrison and Milbrandt*, 2015). Aerosol and CCN concentration *(Rosenfeld*, 2000, *Khain et al*., 2005) along with electrification of cloud (*Mudiar et al*., 2018) substantially impact the microphysical process rates inside clouds. Different microphyical parameterization schemes are employed in weather/climate models to represent the physical processes of formation and interaction of hydrometeors. Numerical Weather Prediction (NWP),cloud resolving models are considered as great tool for physics/microphysical parameterization research as it provides unique opportunity to deal with a controlled atmosphere, which I guess is quite exciting...!!

5.3 The Convection-Permitting NWP Model

Numerical Weather Prediction (NWP) is a process which assign initial conditions (***ics***) based on observation of the current atmospheric state and then integrate forward in time using numerical approximation to the laws of physics governing the atmospheric circulations including the approximate representation of cloud physics,turbulence and radiation. In coarse resolution global models, convection are represented using parameterization scheme. Consistent attempt has been made over the years to accurately represent the complex sub-grid cloud processes in NWP models. Convection Permitting Models (CPM) enhances the accuracy of representation of convective storms as they explicitly represents the storm themselves (*Clark et al.* ,2016). It has been shown that the finer horizontal grid spacing of CPM allows the simulations of cold pools, which can influence the model's synoptic-scale fluxes and trigger new convection in the neighborhood (*Marsham et al.*,2013; *Garcia-Carreras et a*l.,2013). Numerous observation suggested that CPM produces more realistic-looking precipitation field and have an improved diurnal cycle (*Weisman et al*.,2008; *Prein et al*.,2015). The Weather Research and Forecasting (WRF) model, a community weather model developed by the National Centre for Atmospheric Research (NCAR) is widely used CPM for simulation and forecasting of weather events. The WRF is fully compressible, non-hydrostatic, terrain-following 3D mesoscale model (Figure 5.1). The grid staggering used is the Arakawa C-grid with 2nd and 3rd order Runge-Kutta time integration numerical schemes.

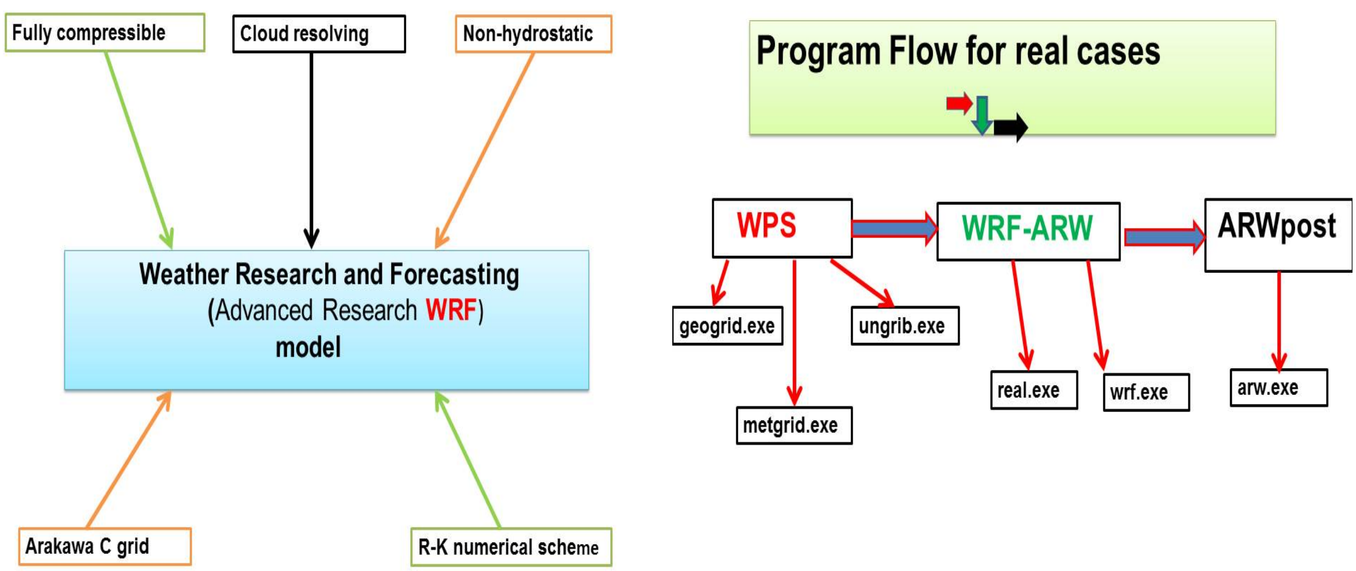

Figure 5.1: WRF model basic structures and program flow chart.

The present simulations are performed considering four nested domain d01, d02, d03, d04 with a horizontal grid spacing of 27km, 9km, 3km &1km respectively. Figure 5.2a depicts the geographical coverage of the model domain along with the topographical map (Figure 5.2b) of the innermost domain. The innermost domain d04 is centre at the HACPL, Mahabaleshwar, (India; 17.92 N, 73.66 E).

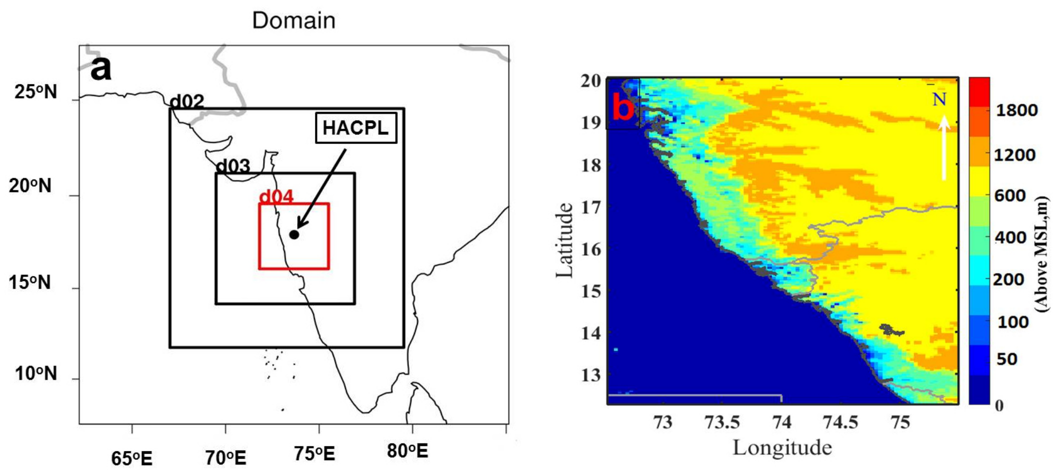

Figure 5.2: (a) Nested model domain, (b) topographical map encompassing domain d04

The initial and boundary conditions are provided from 6 hourly National Centre for Environmental Prediction (NCEP) Final operational global analysis data with $1^o \times 1^o$ horizontal resolution. The Rapid Radiative Transfer Model (RRTM) has been used for long wave (*Mlawer et al.*, 1997) while Dudhia scheme (*Dudhia*, 1989) has been used for short wave radiation. In the model, the sub-grid scale effects of convective and shallow cloud are represented by the cumulus parameterization. The current model set up was tested with Betts-Miller-Janjic (BMJ) , Kain-Fritsch (KF) and Grell-Devenyi ensemble (GD) cumulus schemes. After comparison with observation, BMJ scheme is found to give best result among all the schemes and hence used for the current simulations. The cumulus parameterization (BMJ scheme) is used in only the outer two domains (d01 & d02). The cloud-resolving 3rd and 4th domain are treated with explicit convection.

The microphysical sensitivity of the model was tested with three bulk microphysical parameterization schemes, namely the WRF Double-Moment (WDM6) (*Hong et al.*, 2010), the Thompson scheme (*Thompson et al.*, 2004) and the Morrison double moment with six classes of hydrometeors (*Morrison et al.*, 2005). Figure 5.3 depicts the comparison of simulated rainfall for all the three schemes with observed accumulated rain.

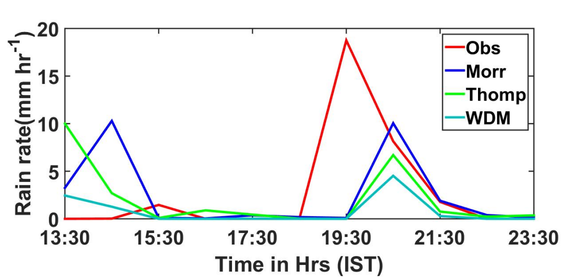

Figure 5.3: Comparison of simulated rain accumulation for all the three microphysical parameterization schemes with the observed accumulation. Observation is indicated as 'Obs', Morrison scheme as 'Morr',Thompson scheme as 'Thomp' and WDM6 as 'WDM'.

After a comparison of simulated precipitation with the observations, Morrison double moment scheme was found to be better and hence has been used for all the current simulations.

5.4 The Experiment Design

All together 13 rain events have been selected to test the WRF models fidelity in simulating rain events with distinct electrical characteristics. Out of 13 events 8 events are associated with a stronger in-cloud electrical environment and 5 events are associated with weaker electrical environments. The distinction of stronger/weaker cloud electrical environments are ascertained by the presence/absence of lightning activity in the vicinity of the observation site. The observed lightning activity recorded by the MLLN for the 10 events (The other three events are observed over Solapur, state of Maharashtra, India and discussed in section 5.8) over the HACPL has been shown in Figure 5.4

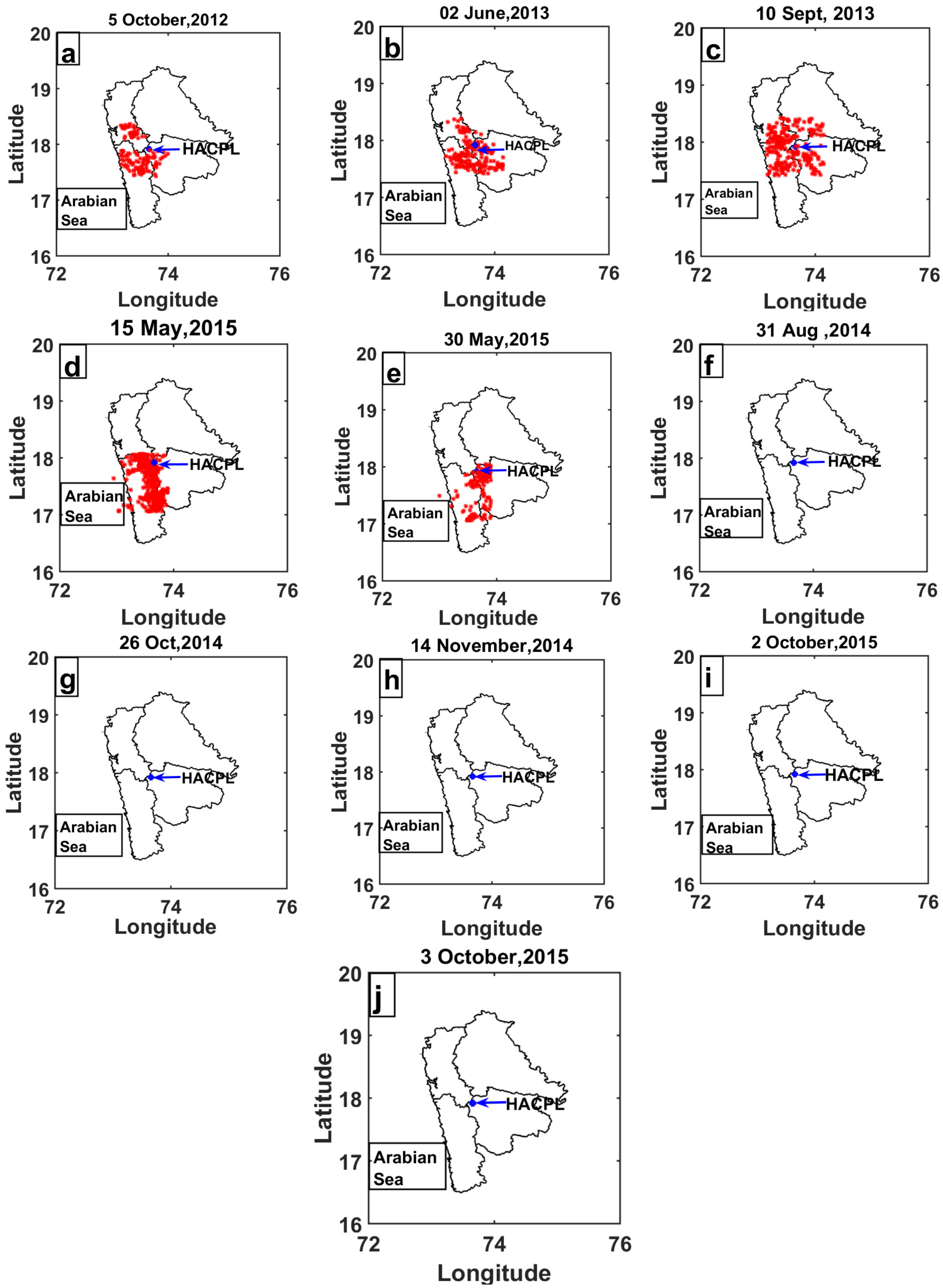

Figure 5.4: The spatial distribution of lightning observed in the model domain d04. Panels (a-e) correspond to strongly electrified (SE) events and (f-j) corresponds to weakly electrified events (WE). The labelling of all the events is same as Table 1 & 2. For events 2(a-c) distribution was derived from the World Wide Lightning Location Network (WWLLN) and for the rest from the Maharashtra Lightning Location Network (MLLN).

The spatial distributions of lightning discharges observed for the events shown in Figure 5.4(a-f) indicated that these rain events over the HACPL are associated with stronger in-cloud electric environment. On the other hand, lightning discharges are conspicuous by absence in the events shown in Figures 5.4(f-j). As lightning-producing clouds exhibit stronger electrical environment in terms of magnitude of electric field and charge distribution, the first set of cloud (a-f) is termed as 'Strongly Electrified' (SE) cloud while the other set (f-j) is termed as 'Weakly Electrified' (WE) cloud as like chapter 3.

The events observed over the HACPL are documented in the Tables 5.1 & 5.2 along with some of the available cloud properties and features derived from the Moderate Resolution Imaging Spectroradiometer (MODIS) (Terra platform) collection 6 (*Baum et al*., 2012) and European Centre for Medium-Range Weather Forecasts (ECMWF) interim reanalysis (ERA-Interim; *Dee et al*., 2011) at 0.25° × 0.25° resolution data sets.

Dates	Cloud top temperature(K)	Total accumulated rain from JWD (mm)	Total column cloud liquid water (kg m^{-2})	Daily accumulated lightning count in *d04*
5 October,2012(a)	250	21.64	0.19	98
2 June,2013(b)	-	30.16	0.08	186
10 sept.,2013(c)	-	71.5	0.04	249
15 May,2015(d)	252	6.98	0.002	898
30 May,2015(e)	-	3.74	0.03	173

Table 5.1: Some Cloud and Electrical properties of the Strongly Electrified (SE) events.The lightning counts for the events (a-c) are derived from WWLLN and for (d-e) from MLLN with higher detection efficiency. The total column cloud liquid water was derived from the Era-interim data sets while cloud top temperature was derived from MODIS terra data sets. The labeling for the events is same as Figure 4.4

Dates	Cloud top temperature(K)	Total accumulated rain from JWD (mm)	Total column cloud liquid water (kg m^{-2})	Daily accumulated lightning count in *d04*
31Aug,2014(f)	250	116	0.75	0
26Oct.,2014(g)	-	5.4	0.06	0
14Nov.,2014(h)	-	13.41	0.01	0
2 Oct.,2015(i)	-	22.7	0.01	0
3 Oct.,2015(j)	270	70	0.004	0

Table 5.2: Some Cloud and Electrical properties of the Weakly Electrified (WE) events. The lightning counts for the events (a-e) derived from MLLN. The total column cloud liquid water was derived from the Era-interim datasets while cloud top temperature was derived from MODIS terra datasets. The labelling for the events is same as Figure 4.4

The experiments were carried out as discussed below

A set of control (CTL) experiments were carried out for both the SE and WE of events with WRF-ARW model with the standard physics packages using the same model set up and the simulated precipitation field and RDSD were validated against available observed variables.

In the WRF-ARW, the precipitation is calculated using a Marshall-Palmar formulation of RDSD with a specified slope parameter, λ. We find that λ, used in the default physics scheme is inadequate to represent precipitation in the SE events. Hence in a second set of experiment, the default minimum value of the RDSD slope parameter, λ in the physics module has been replaced with a new λ as obtained from observation, averaged over all the five SE events observed over the HACPL. The influence of λ on the simulated precipitation has been discussed in the supporting text in details. A new set of simulations was carried out for the same SE events using the same model setup with the modified physics.

For the rain events recorded in the afternoon or late afternoon hours, the model was initialized with the NCEP FNL 00:00:00 UTC *ic*s, while for the late night or early morning events, initialization was done using the 12:00:00 UTC ***ics***. The details of the model design have been summarized in Table 5.3.

		Name of Experiments		
Physical Processes	Control (CTL) run	Modification of limit of l in Morrison scheme	Modification of aerosol number concentration	Modification of aerosol number concentration + Modification of l
Convective process	Betts-Miller-Janjic (BMJ)	BMJ	BMJ	BMJ
Microphysics process	Default Morrison Scheme (Morr) following Morrison et al.,2005.	Modified Morrison (Morr(M)). The default minimum value of l in the physics module has been replaced with a new l, averaged over all the five SE events observed over the HACPL	Default Morrison Scheme (Morr) + change in aerosol number concentration in Mode 1(0.05 µm)	Modified Morrison (Morr(M)) + change in aerosol number concentration in Mode 1(0.05 µm)
	Model Initialization	For the events (b-d) documented in the Table 1, (a,c,d,e) in Table 2 and the events (a-b) in Figure 6, the model was initialized with 00:00:00 UTC NCEP ICs while for the events (a & e) in Table 1, (b) in Table 2 and event (c) in Figure 6 , model was initialized with 12:00:00 UTC IC.		

Table 5.3: The WRF Model Experiment Design. Other physical processes (short and long wave radiation scheme) are kept same for both sets of sensitivity experiment.

For comparison with observations, data from surface-based JW disdrometer (JWD) located at the HACPL and Solapur were used which record the RDSD and rain intensity (*Joss and Waldvogel*, 1967). The hourly accumulated rain was extracted from the JWD record and considered for validation of simulated hourly precipitation. The recorded distribution was also used to calculate the RDSD parameters from the gamma distribution fitted to RDSD. Data recorded by an optical disdrometer installed at Pune (18.52^{o}N, 73.85^{o}E) was also used to study the geographical variability of the RDSD. Aerosol distribution was observed over the HACPL with a Scanning Mobility Particle Sizer (SMPS) while CCN was measured with a collocated Cloud Condensation Nuclei Counter (CCNC) (*Singla et al.*,2019).

5.5 Let's See How WRF Model Respond to the SE Events

The reported underestimation of simulated rain intensity for the rain events that are associated with lightning discharges suggested model's inability to reproduce heavy precipitation amount towards higher rain bins. The 5 SE events obsrved over the HACPL have been simulated using the same physics and cumulus schemes. As we have not addressed the spatial displacement of the simulated center of mesoscale convection relative to the observation, the simulated precipitation is verified in all the grid points within a 25km $\times$ 25 km box, centered at the HACPL. The grid point that shows the closest value of precipitation rate to the observed one is considered as model simulated precipitation and compared with the observation. Figure 5.5 (a-e) shows the simulated rain rate for the events reported in Figure 5.4(a-e) along with the observed rain rate measured by surface-based JW disdrometer.

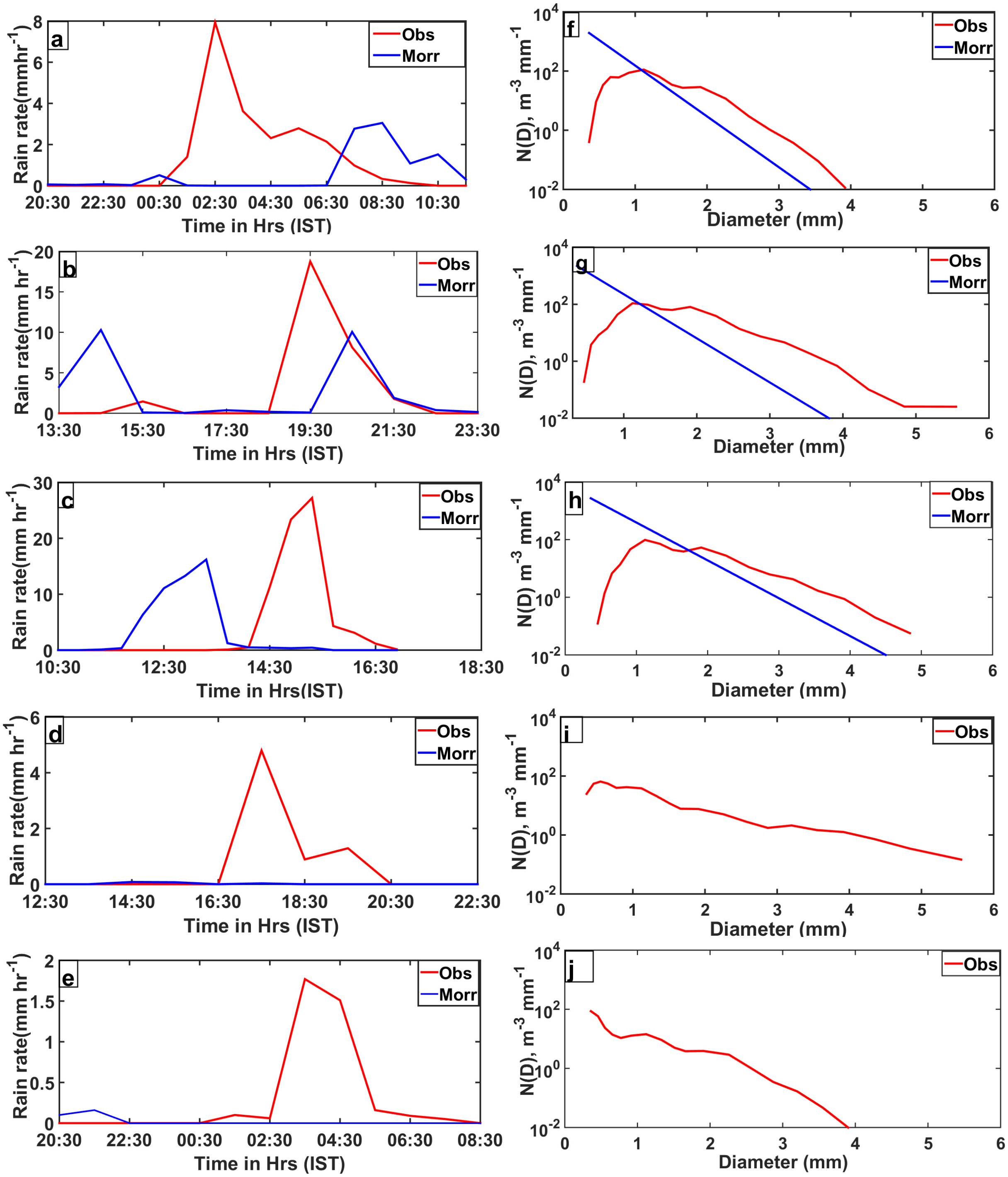

Figure 5.5: Comparison of simulated rain rate (a-e) and simulated RDSD (f-j) with the observation for the strongly electrified (SE) events observed over the HACPL. N(D) is the number density of drops. The legends in the figure 'Obs' indicated observation while 'Morr' indicated Morrison double moment scheme.

Apart from the shift in timing of the peak rainfall, significant underestimation of the observed precipitation intensity can be seen in the simulations for the events shown in Figure 4.5(a-c) while for events shown in 4.5(d-e), model failed to simulate any rain during the event duration. The underestimation of rain intensity is found to be consistent with the earlier reported dry bias in the simulation of heavy precipitation associated with lightning activity (*Giinaros et al*.,2015; *Dafis et al*., 2018). In some cases, the model predicted the rainfall 3-4 hours advance while in others the rainfall was delayed by 1-2 hours. This phase difference in the diurnal cycle of the simulated peak and observed peak in precipitation is well recognized (*Jeong et al*., 2011; *Diro et al*., 2012 ; *Walther et al*., 2013; *Gao et al*., 2018).

Possible Cause of Underestimation

The model simulated rainfall was found to be very sensitive to the assumed RDSD (*Gilmore et al., 2004, Morrision, 2012, Abel and Boutle*,2012, *Freeman et al*.,2019). The prognostic variables like mixing ratios and number concentrations of different species of hydrometeors are expressed as a function of RDSD parameters.To have a first hand knowledge of the current underestimation in intensity of rainfall, the model simulated RDSD is compared with the observed ones (derived from surface-based JW disdrometer) as depicted in Figure 5.5 (f-j). The observed RDSD was averaged over the entire duration of rainfall for each event. The simulated RDSD was calculated using the model predicted rain mixing ratio averaged over the rain period. The double moment microphysics scheme predicts the mass mixing ratios and number concentration of hydrometers assuming gamma particle size distribution (Equation 4.1). With $\mu = 0$ for rain (*Morrison et al*., 2008), the size distribution of raindrops will take the form of exponential functions (*Marshall-Palmer* distribution)

$$N(D) = N_0 exp(-\lambda D) \tag{5.1}$$

λ & N_0 can be derived from the model predicted rain number concentration N and rain mixing ratio q using the equations

$$\lambda = (\frac{\pi \rho_r N}{q\rho})^{1/3} \tag{5.2}$$

Where ρ_r is the density of raindrops (1000 kg m^{-3}) and ρ is the air density.

$$N_0 = N\lambda \tag{5.3}$$

Consistent with the underestimation of observed rainfall intensity by the model in the events shown in Figure 5.5(a-c), the simulated RDSD in Figure 5.5(f-h) shows substantial underestimation in the number concentration of larger raindrops compared to the observation. As the model was unable to reproduce rainfall at the surface for the SE events shown in Figure 5.5(d-e), the RDSD corresponding to these events only depicts the observed distributions (Figure 5.5(i-j)). The overestimation of the smaller-size raindrops may be caused by the inherent deficiency of assumed Marshall-Palmer distribution (*Gao et al*., 2018). It was observed that the underestimation in drops number concentration increases as drop size increases. The model's inability to reproduce the larger raindrops in the RDSD spectrum possibly due to absence of electric factor in the cloud module of model physics scheme, as the chapter 3 and 4 clearly indicate that in-cloud electric force produces larger rain drops through enhanced collision-coalescence growth.

5.6 What about the Weakly Electrified Events...

The in-cloud electric environments in WE events are comparatively weaker than the SE events. The gravity induced coalescence growth of raindrops prevails in the warm phase of the cloud while cold microphysics lime vapor deposition, riming and aggregation prevails above the freezing level (*Houze et al.*,1997). The five WE events reported in Table 5.2 have been simulated using the same physics and cumulus scheme. Figure 5.6 (a-e) depicts the comparison of the simulated precipitation intensity with the observed ones derived from surface-based JW disdrometer.

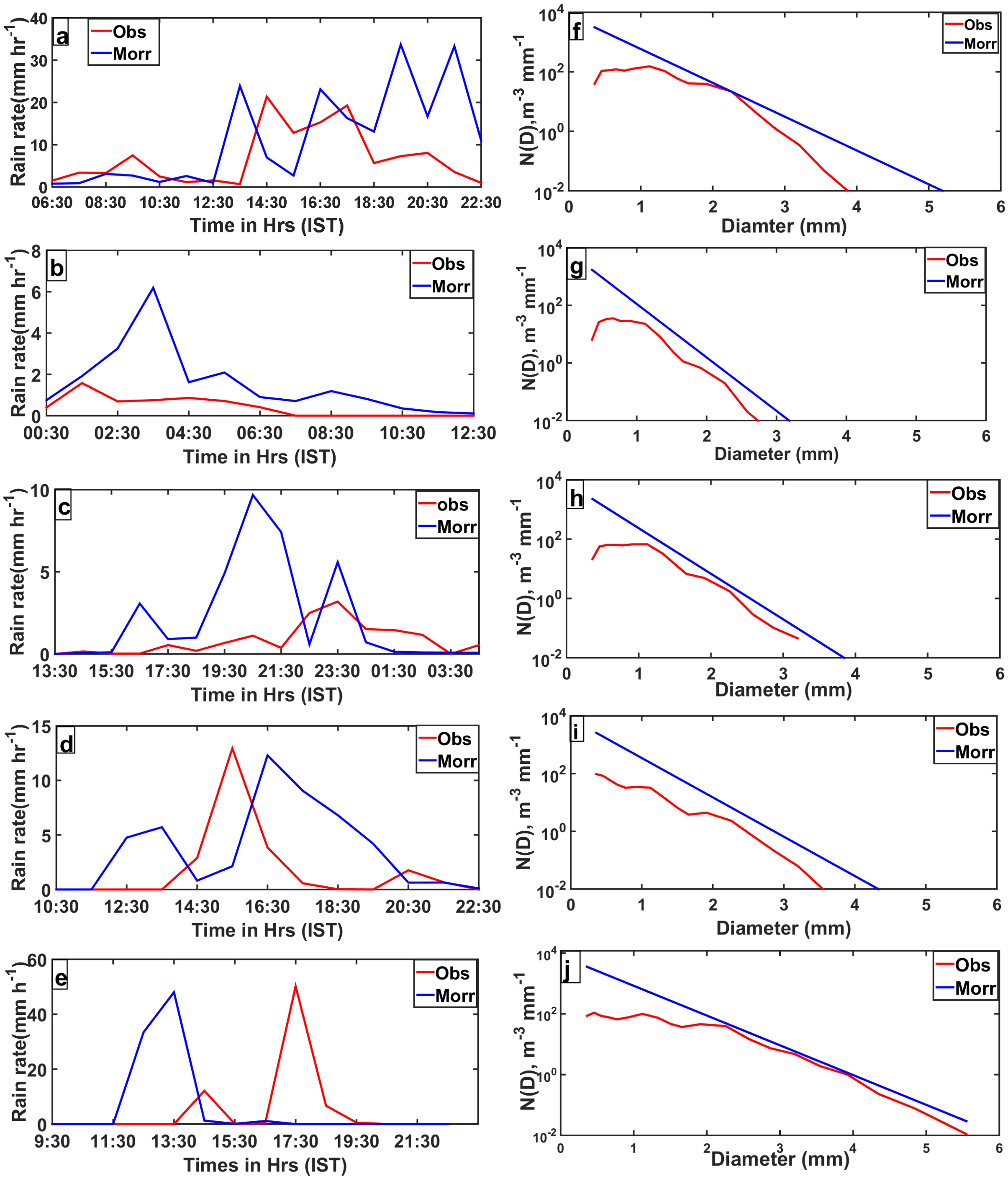

Figure 5.6: As in Figure 5.5 but for weakly electrified (WE) events

It is interesting to note that there is no underestimation of observed rainfall by the model in the WE cases. Apart from the generic problem of timing of peak rainfall simulation, the model in fact slightly overestimated the precipitation intensity as compared with the observation in three out of five events as shown in Figure 5.6(a-c). This wet bias in the WE events was found to be in contrast with the reported dry bias in SE events. The temporal spread in the simulated rain was found to be consistent with the observation. For some of the events, the phase shift in the precipitation peak was found to be 1-4 hours.

The right panels of Figure 5.6(f-j) depict the comparison of the simulated RDSD with the observed ones. Both the sets of RDSD are averaged over the entire rain duration recorded by the model and JWD. The observed RDSD for the WE events primarily found to be of exponential in nature and comparable with the simulated ones in almost all the events, as shown in Figure 5.6(f-j). It is also observed that in both types of events (SE and WE) , the model overestimated the number concentration of smaller size drops. In the case of WE events for higher rain intensity, the tail of the distribution was extended towards the larger drop size in the JWD measured RDSD, while in contrast, broadening of the RDSD towards the larger size range was observed irrespective of the rain intensity for SE events.

5.7 Then How to Improve The Simulation of Rainfall Intensity in SE Events..??

The discussions presented in the section 5.5 and 5. 6 indicate that WRF model can reproduce the precipitation intensity as well as the RDSD with reasonable fidelity for the WE events, while for the SE cases intensity of rainfall is underestimated consistent with significant underestimation of larger drops indicating a potential limitation in the RDSD parameterization in the Morrison microphysics used in the WRF-ARW model. This limitation possibly comes from the fact that, Morrison microphysics scheme does not take into account the electric factor present inside a SE cloud. But chapter 3 and 4 suggest a substantial influence of in-cloud electric forces in broadening of RDSD.

So Let's Bring in The Electric Factor to the Physics Module of WRF...!!

The numerical simulation of electrical field within clouds associated with extreme rainfall events are only beginning to be addressed in NWP models (*Mansell et al.,*20*10; Dafies et al*., 2018). *Dementyeva et al*.(2015) reported direct simulation of electric field using WRF model solving the 3D Poisson equation considering the charge distribution of graupel and ice particles

$$\nabla\varphi(x,y,z,t) = -\frac{1}{\varepsilon_0}(\rho_g(x,y,z,t) + \rho_i(x,y,z,t)) \tag{5.4}$$

where, $\varphi$is the electric potential,ρ_g and ρ_i are the respective charge density of graupel and ice particles.

However, direct feedback from the electric field to the microphysics module is still lacking in almost all NWP weathre/climate models. Two indirect approach can be adopted to bring in the electric factor to the model physics based on the work of *Mudiar et al.* (2018).

(a) The reported generic bias of underestimation of heavy precipitation in weather models might be due to absence of electric factor in the calculation of the microphysical tendency equations for collision-coalescence, collection and accretion terms (*Hazra et al.*, 2017). The improvement of microphysical parameterization incorporating the electric factor, particularly the tendency equations in global climate models based on observations can help to improve the simulation of heavy rainfall (*Hazra et al*., 2017). The collection efficiency of raindrops is governed by the size distribution and the fall velocity of the drops (*Bradley and Stow*, 1984). The results and discussions presented in chapters 3 and 4 suggested that prevailing electric forces can modify the RDSD, thereby influencing the collection and collision-coalescence efficiency of raindrops. Therefore, the observed RDSD and the terminal velocity can be used to calculate a modified collision kinetic energy and total surface energy of the raindrops (*Bradley and Stow*, 1984). With a new collection and collision-coalescence efficiency from the observation, the equation of growth rate of raindrops can be modified. The modified kernel of collection efficiency might be helpful for the improvement of heavy rainfall in weather/climate models.

(b) From the discussions of section 5.5 and 5.6, it is clear that the inability of the model to simulate the intensity of precipitation in the SE cases is related to its bias in simulating the larger drops in the RDSD. The fact that the slope of the RDSD, λ in the WE cases match well with that of observations, indicates that the model specification of 'slope' for SE cases is inadequate. Modeling studies (*Gilmore et al*., 2004; *Curic et al*., 2010; *Morrison*, 2012) indicating that the simulated precipitation is sensitive to the prescribed RDSD parameters viz. μ, λ and N_o as they are explicitly depends on the prevailing microphysical processes (*Konwar et al*., 2014). In NWP models, rain microphysics is characterized by an assumed RDSD. Different microphysical processes which control the evolution of cloud and precipitation like evaporation, accretion, droplet growth are related by the assumed RDSD *(Zhang et al*.,2006). Some microphysical schemes assumed an exponential distribution *(Lin et al*., 1983; *Seifert and Beheng*, 2006; *Morrison and Gettelman*, 2008; *Thompson et al*., 2008) while others assumes a gamma distribution *(Ferrier*,1994; *Morrison et al*. ,2005). Microphysical process rates which depends on the prescribed particle size such as evaporation, accretion, precipitation rate (bigger drops tends to fall faster) can be controlled through prescribing the value of RDSD slope parameters λ. In that regard accurate characterisation of the RDSD parameters, particularly λ is very important *(Abel & Boutle*, 2012). The value of λ characterizes the truncation of the RDSD along the diameter, e.g., smaller value of λ implies extension of the tail to larger value of diameter indicating the presence of larger drops *(Konwar et al.* 2014). As observation convincingly suggested presence of high concentration of larger drops for SE events, proper characterization and representation of λ in the NWP model is deemed to be critical for accurate estimation of precipitation. By virtue of microphysical modification of λ through enhanced collision-coalescence growth of raindrops in presence of stronger in-cloud electric forces (*Mudiar et al*., 2018), the characteristic value of λ for the SE events is expected to be distinct from the WE one. Hence, the electric factor can be brought in to the model physics through modification of the default value of λ in the Morrison scheme by introducing a new value of λobserved for the SE rain events.

But How the Value of λ get Modified inisde the SE Clouds..? Let's see from Observation..!

The findings reported in *Mudiar et al.* (2018) indicate a substantial modification of RDSD by in-cloud electrical forces. The observed broadening of the RDSD in SE events reduces the value of λ for the distribution when compared to the same for the WE events. The RDSD achieve this broadening through enhanced collision–coalescence growth of raindrops below the melting layer mediated by in-cloud electrical forces as suggested by *Mudiar et al.* (2018). Figure 5.7(a) depicts the bar plot representation of λ for all the events reported in Figure 5.4

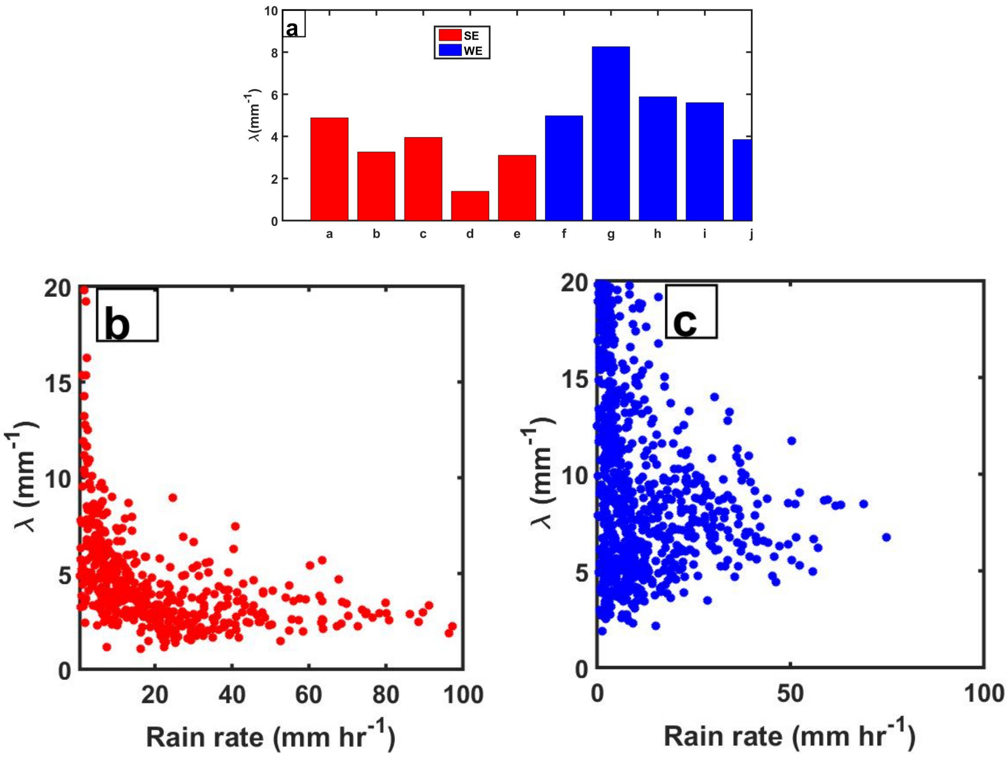

Figure 5.7: (a) Bar plot representation of λ value for all the SE and WE events reported in Table 1-2. Scatter plot of slope parameter λ with rain intensity (b) strongly electrified (SE), (c) weakly electrified (WE) rain events observed over the HACPL. The values of λ are estimated using the method of moments reported in *Konwar et al*.,(2014).

The values of λ are estimated using the method of moments reported in *Konwar et al*.,(2014). It is clearly seen that values of λ are distinguishable between the SE and WE events with substantially lower values for the SE events. Figure 5.7(b-c) depicts the observed relation between rain intensity and λ for some more SE and WE events observed over the HACPL. This Figures show that for same rain intensity, SE events are associated with much lower value of λ than the WE ones which clearly suggested that broader RDSD spectrum dominates the SE events.

The observed difference in λ between the both set of events can be attributed to the prevailing stronger in-cloud electrical environment in SE clouds. This attribution is based on the backdrop of extensive laboratory (*Bhalwankar and Kamra*., 2007; *Perez et al*., 2012; *Harrison et al*., 2015, *Y. Yang et al*.,2018), numerical (*Schlamp et al*., 1976, 1979; *Khain et al*., 2004) and observational *(Mudiar et al*.,2018; *Harrison et al*., 2020) evidence regarding the substantial electrical influence in the microphysical properties of cloud/rain drops size distribution. It has been shown that stratiform clouds with stronger electrical environment are inherently associated with broader RDSD (*Mudiar et al*., 2018) with smaller value of λ.

In order to further investigate the effect of lightning in modification of the value of λ, we have selected some isolated lightning events recorded by the MLLN within 700 m of the HACPL. While selecting these lightning events, it was ensured that no other lightning events were recorded by the MLLN within 3-4 minutes of the selected event. Figure 5.8(a-d) depicts time evolution of values of λ before and after seven selected lightning events.

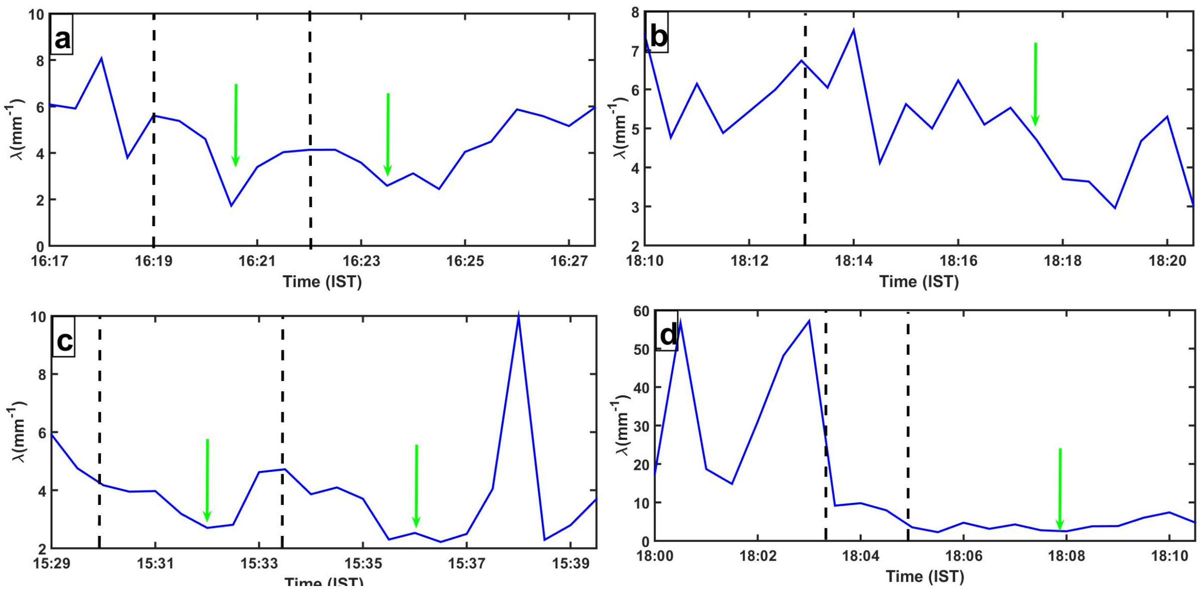

Figure 5.8: Time evolution of λ before and after some isolated lightning event recorded within 700m of the HACPL. The vertical dashed bar indicate the time of lightning recorded by the Maharashtra Lightning Location Network (MLLN). The green downward arrow indicates the trough in λ after the lightning. It may be noted here that, the observed dip in the values of λ were inherently associated with a transient amplification in rate intensity.

The interesting observation is that 2-3 minutes after the lightning, λ exhibits a transient dip indicated by the downward arrow. It may be noted here that the dip in the value of λ observed to be inherently associated with a transient amplification in rain intensity as well. It has also been observed that surface RDSD broadens with a 2-3 minutes time lag after an overhead lightning which suggested that lightning could enhance the growth of raindrops in the warm phase of cloud (as discussed in the chapter 4) through deposition of ions inside the cloud (*Heckman and Williams*, 1989; *Williams and Montanya*, 2019). We hypothesize that the broadening of RDSD by electrification of cloud droplets by lightning may be a possible cause of lower value of λ, observed after an overhead lightning. However, we also recognize that the robustness of this decrease in λ following lightning needs to be established with more number of observations.

The evidence presented above strongly indicates that the electrical field within the clouds plays a critical role in broadening the RDSD and in increasing the rainfall. Laboratory experiments mentioned above strongly support this conclusion where the role of dynamics on RDSD could be controlled. A counter argument in the case of observations is that the SE cases are largely associated with strong convective events where dynamics broadens the RDSD and lightning is a result, not the cause. Our view is that indeed the initiation of electrification and lightning could be due to dynamics. However, once electrified, they would broaden the RDSD further (weaken λ) and lead to further increase in rainfall. The question, therefore, is not whether but by how much λ is decreased by the electrical effects? In order to make an estimate of this influence of electrical fields of λ, we investigate the influence of in-cloud electric environment in the modification of λ for the SE event by analyzing a few thunderstorms observed over the AEO. Four thunderstorms were observed over the AEO on 3 June; 31 August; 1 September and 9 September 2008. For all the four storms, the surface electric field was recorded with a surface-based field mill located at the AEO. The simultaneous RDSDs for all the storms were measured with a collocated optical disdrometer. While for the storm observed on 3 June exhibits a peak lightning frequency of 24 flashes min^{-1}, the other three storms are smaller storms with a peak lightning rate of 3-8 flashes min^{-1}. It has been observed that, although the strength of the surface-measured electric field is the summation of fields due to charges in the primary charge centre and space charge in the sub-cloud layer, the variation of the field at the surface remained coupled with the charging processes in the main negative charge centre located in the temperature regime ranging -10^{o}C to -25^{o}C inside a strongly electrified cloud *(Standler and Winn*,1979; *Soula and Chauzy*,1991). Figure 5.9(a-d) depicts the scatter plot representation of the surface measured-electric field and λ for all the four storms.

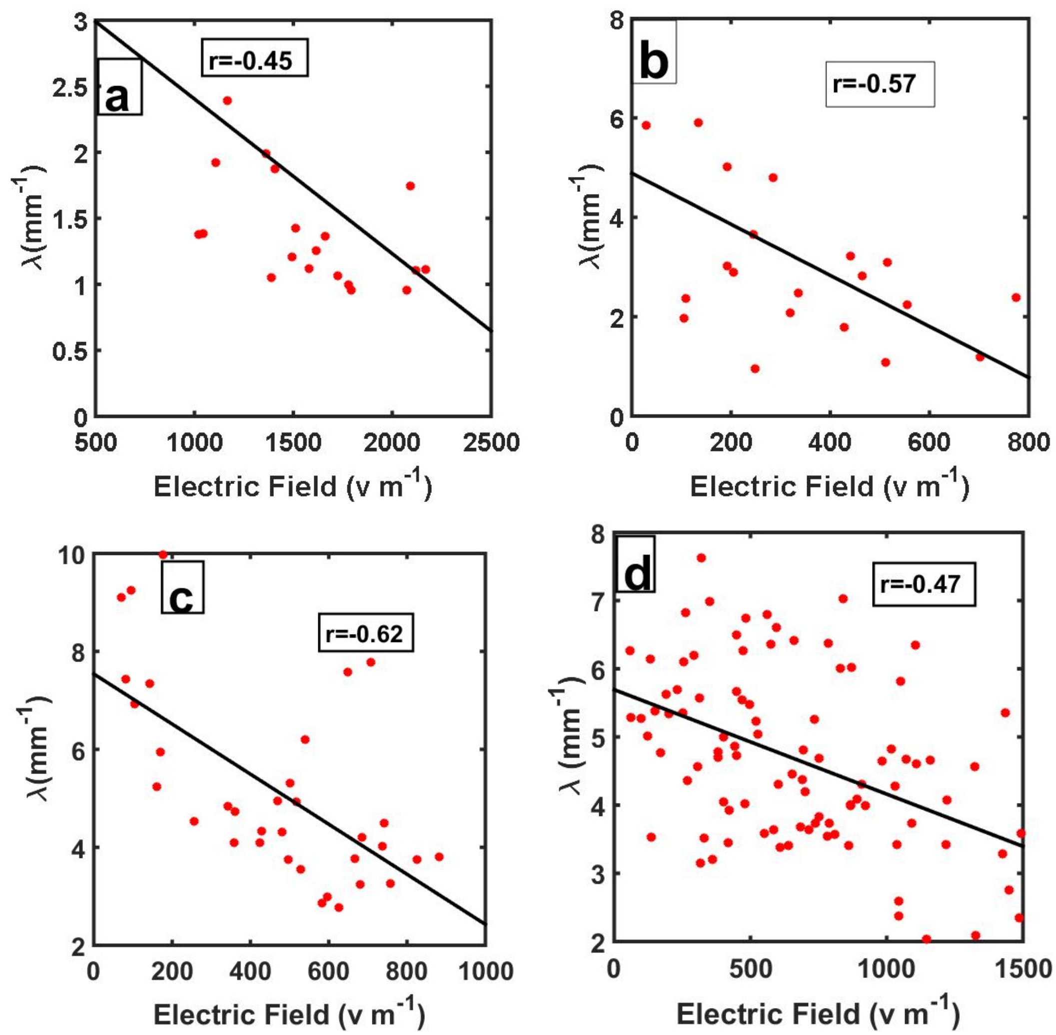

Figure 5.9: Scatter plot of slope parameter, λ with surface measured electric field (a) 3 June, 2008, (b) 31 August, (c) 1 Sept., (d) 9 Sept., 2008. All the events are observed over the Atmospheric Electricity Laboratory, (AEO) Pune. 'r' indicate correlation coefficient with p-value <0.0001.

The two observables have been averaged over every two minutes interval during the rainy periods. For all the storm, λ exhibits a decreasing trend with the increasing magnitude of electric field. This decrease in value of λ is caused by the broadening of the corresponding RDSD. In a cloud chamber experiment, *Y. Yang et al.*,(2018) observed broadening of particle size distribution after applying an electric field. They observed that with higher applied electric field, the size of single water drop increases and propose that presence of electric field can enhance the collision-coalescence processes between water drops. Same observation has been reported by Mudiar et al.,

(2018) in their observation of SE stratiform rain events. The collective evidence from laboratory experiments and observational analysis confirmed the significant influence of in-cloud electric fields on the microphysical properties (primarily the collision-coalescence process) of SE clouds and hence on the electrical modification of λ. It is noted that the correlations between λ and the electric field are highly significant but not perfect. This may be due to the role of dynamics on λ. The correlations in the Figure indicate that a 20-40% decrease in the value of λ may be attributed to electrical effect. This may be considered an important quantification of broadening of RDSD by electric field.

Table 5.4 depicts the values of μ,λ and N_0derived from surface-based JW disdrometer for all the SE events documneted in Table 5.1 while Table 5.5 depicts the same for some more the SE events observed over the HACPL . Table 5.6 depicts the same for all the WE rain events documneted in Table 5.2 along with some more events obeserved over the HACPL.

Date	μ	$\lambda(mm^{-1})$	N_0(m-3 mm- (μ+1)	mean λ	S. D. of λ
5 October,2012(a)	5.1	4.88	6.2×10^3		
2 June,2013(b)	3.44	3.26	1.8×10^3		
10 sept.,2013(c)	5.2	3.95	2.9×10^3	3.31	1.28
15 May,2015(d)	0.45	1.39	70		
30 May,2015(e)	2.1	3.10	390		

Table 5.4: The RDSD parameters for the five events reported in Table 1 obtained from surface-based JW disdrometer for the SE events over the HACPL. μ is the shape parameter, l slope parameter (mm-1) and No intercept parameter (m-3 mm- (μ+1)). RDSD parameters are estimated using the M234 method following Konwar et al. (2014). Labelling of the events is same as Table1.

Date	μ	$\lambda(mm^{-1})$	N_0(m-3 mm- (μ+1)	mean λ	S. D. of λ
25 Sept.,2014	2.12	3.18	684		
3 October,2014	5.5	3.73	2.2×103		
4 October,2014	3.88	4.45	3.1×10^3		
10 March,2015	2.87	3.3	652		
21 April, 2015	1.63	1.85	200		
5 May,2015	1.72	1.95	236		
9 May,2015	0.32	1.51	152		
13 May,2015	2.58	3.17	1.0×10^3		
16 May,2015	3.22	2.62	704		
5June,2015	2.24	3.06	1.09×10^3	3.02	0.79
16 Sept.,2015	4.60	3.79	4.2×10^3		
4 October,2015	3.91	3.65	3.41×10^3		
4 June, 2016	3.30	3.06	1.13×10^3		
8 June,2016	2.98	3.02	1.19×10^3		
12 May,2017	3.7	2.59	370		
13 May,2017	3.19	2.10	132		
23 May,2017	2.47	2.60	565		
30 May,2017	1.94	3.05	2.62×10^3		
7 Sept.,2017	3.62	3.77	2.87×10^3		
10Sept.,2017	4.76	3.55	2.04×10^3		
14 Sept.,2017	2.03	2.24	654		
26 Sept.,2017	6.2	4.40	4.32×10^3		

Table 5.5: The RDSD parameters for some of additional SE events (other than the events documented in the Table 5.4) from surface-based JW Disdrometer for SE events over the HACPL.

Date	μ	$\lambda(mm^{-1})$	N_0(m-3 mm- (μ+1)	mean λ	S. D. of λ
31 Aug.,2014(f)	4.5	4.98	1.5×10^4		
26 Oct.,2014(g)	5.88	8.26	9.3×10^4		
14Nov.,2014(h)	3.61	5.88	1.5×10^4		
2Oct.,2015(i)	5.53	5.60	2.49×10^4		
3Oct.,2015(j)	4.13	3.85	2.99×10^3		
6 Sept.,2014	8.03	8.50	9.6×10^5		
5 June,2015	2.27	3.00	1.28×10^3		
14 June,2015	6.05	6.17	7.7×10^4		
23 June,2015	7.65	6.45	6.61×10^4		
24 June,2015	3.97	4.14	4.8×10^3	5.58	1.58
11Oct,2015	3.82	3.56	2.12×10^3		
25June,2016	6.29	8.10	5.41×10^5		
21 Sept.,2016	3.18	5.34	3.45×10^4		
3Oct.,2016	6.88	6.90	2.08×10^5		
11 June,2017	2.63	4.02	5.0×10^3		
26June,2017	5.13	5.23	1.7×10^4		
18Sept.,2017	4.76	6.23	8.4×10^4		
9 Oct.,2017	4.82	5.02	1.3×10^4		
15Oct.,2017	6.06	4.80	7.8×10^3		

Table 5.6: The RDSD parameters from the surface-based JW Disdrometer for a few WE events over the HACPL. Labeling of the events is same as Table 2

The collective effect of electric field and lightning on the RDSD modification in the SE events may explain the observed difference in the values of λ observed in Figure 5.7(b-c). An appropriately modified Morrison scheme for the SE cases and re-simulation of the SE cases with the modified scheme is presented next.

In this endeavor to bring in the electric factor to the model physics, the default minimum value of the λ in the physics module (Morrison scheme) has been replaced with a new λ (refer to Table 5.4) averaged over all the five SE events as obtained from observation over the Indian subcontinent. As indicated in the physics module of WRF (Morrison), earlier attempt has been made to increase the minimum value of λ for rain in the WRF version 3.2, although as would be seen from the current study, use of a universal λ may be responsible for the observed discrepancy between simulated and observed rainfall in the case of the SE and WE events. The modified simulated precipitation is shown in green colors in Figures 5.10(a-e) indicated as ‘Morr(M)’ along with the default Morrison indicated as ‘Morr’ together with the observed (‘Obs’) .

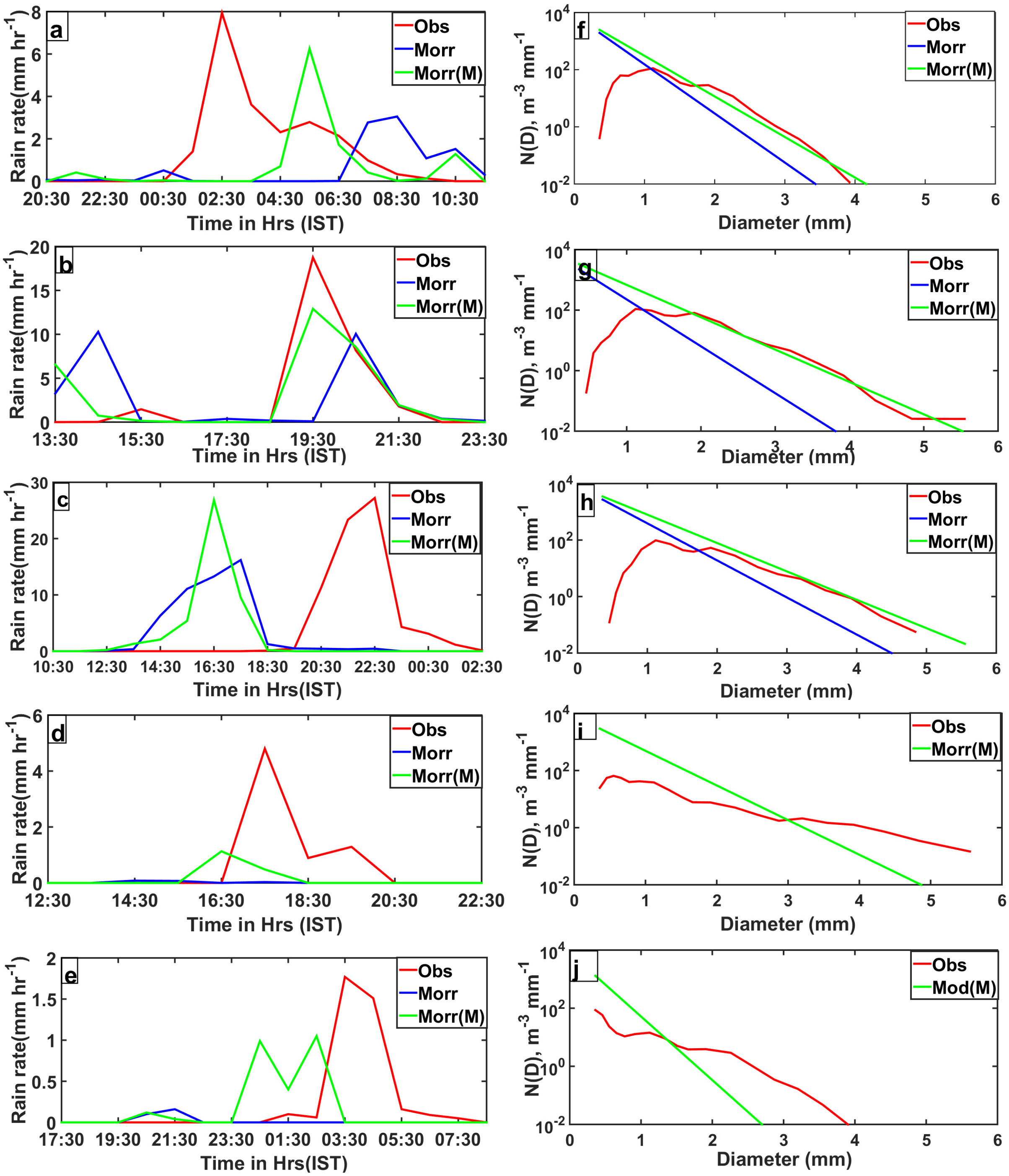

Figure 5.10: As in Figure 5. 5 but with modified Morrison scheme. The legends ‘Obs’ indicated observation, ‘Morr’ indicated Morrison scheme and ‘Morr(M)’ indicated modified Morrison scheme.

Substantial improvement was observed in rain intensity with the incorporation of electrically modified λ in all the events. For the events shown in Figure 5.10 (d-e), for which the default Morrison scheme was unable to reproduce any rain for the simulated period, the model with the Morr(M) reproduces substantial amount of rain albeit with some underestimation still remaining. The right panels of Figure 5.10 depict the simulated RDSD with the modified scheme along with the default and the observed ones. Substantial improvement in number concentrations of larger raindrops can be observed with the Morr(M) (Figure 5.10(f-h)). While for the events shown in Figure 5.10(i-j), the simulated RDSD show some improvement consistent with the larger amount of simulated rainfall, with underestimation of larger raindrops still persisting. The overestimation of the number concentration of the smaller size drops still persists. The overall improvement in the accumulated rain and RDSD indicate considerable sensitivity of simulated precipitation to λ and establishes the benefit of electrically modified slope parameter, λ. So this section demonstrate that the simulated precipitation exhibits significant improvement for the SE events if the electrically modified RDSD parameters adequately included in the model physics.

5.8 The HTI of simulated radar reflectivity (dBZ)

In WRF-ARW, the equivalent reflectivity factor, Z_e ($m^6 m^{-3}$) computed from the forecast mixing ratios assuming Rayleigh scattering by spherical particles of constant density *(Stoelinga*, 2005). The $Z_e$which is expressed as the sixth moment of size distribution is calculated from

$$Z_e = \Gamma(7) N_0 \lambda^{-7} \tag{5.5}$$

The size distribution of the particles is assumed to be of exponential form as equation (5.1), where N_0 is considered as constant value of 8×10^6, 2×10^7 and 4×10^6 m^{-4} for rain, snow and graupel respectively *(Min et al.*, 2015). Z_e is multiplied by 1018 and expressed in common units mm^6 m^{-3}. The Z_e, associated with each hydrometeor mixing ratio is calculated at each model grid points and summed together to get a total equivalent reflectivity factor given by

$$Z_e(dBZ) = 10 log_{10}[Z_e(mm^6 m^{-3}] \tag{5.6}$$

The simulated radar reflectivity (dBZ) is identified as an important prognostic variable which allows the detailed study of structures, evolution, and motion of storms *(Min et al.*, 2015). The major advantage of the simulated reflectivity field is, it can be readily compared in real time with the observed reflectivity products. Figure 5.11(a-e) depicts the model derived (HTI) of dBZ for the SE events shown in Figures 5.5 with Morrison and modified Morrison schemes.

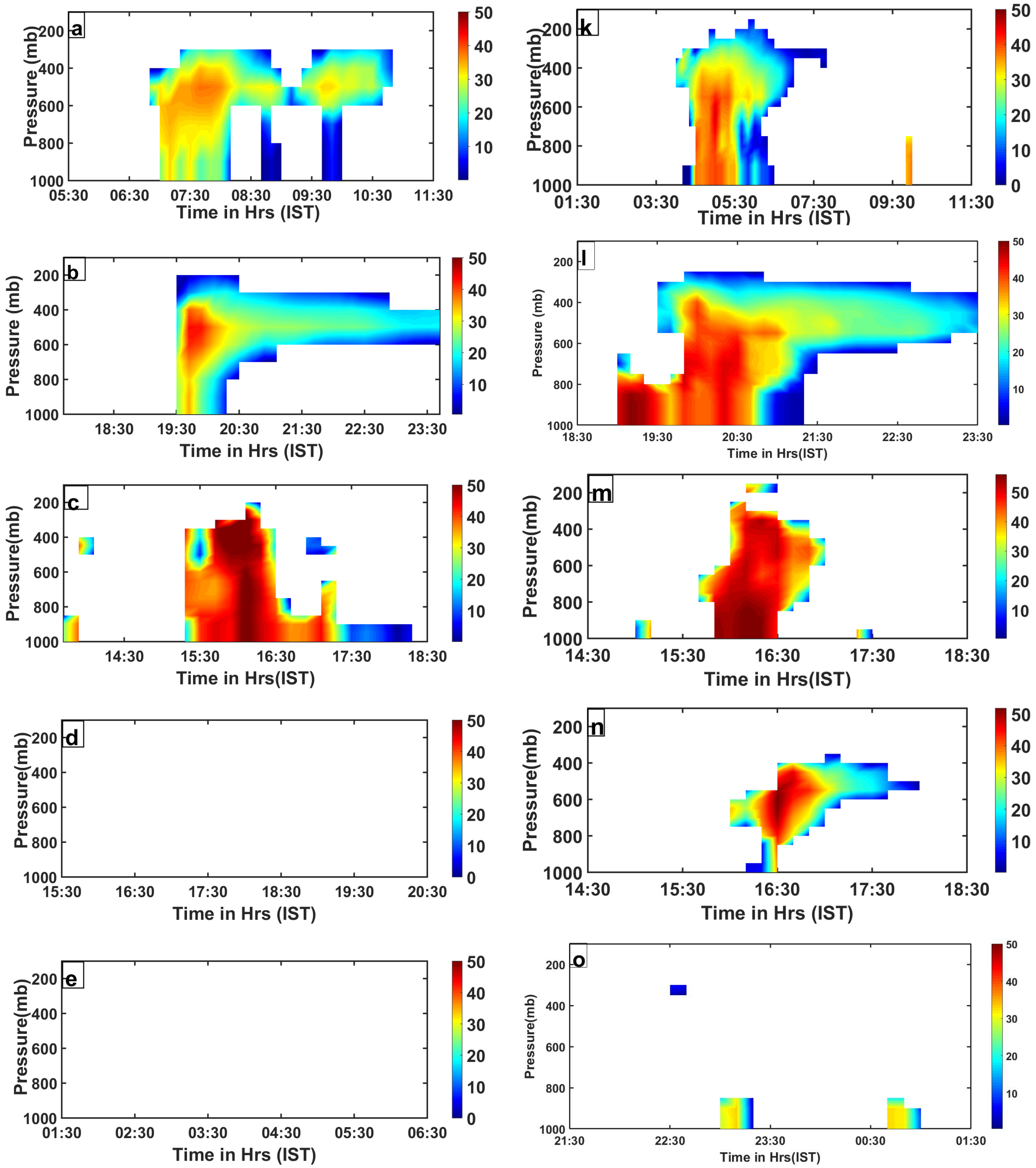

Figure 5.11: (a-e) Height Time Index (HTI) of simulated reflectivity (dBZ) for the SE event with default Morrison scheme. (k-o) same as (a-e),but with Morr(M).

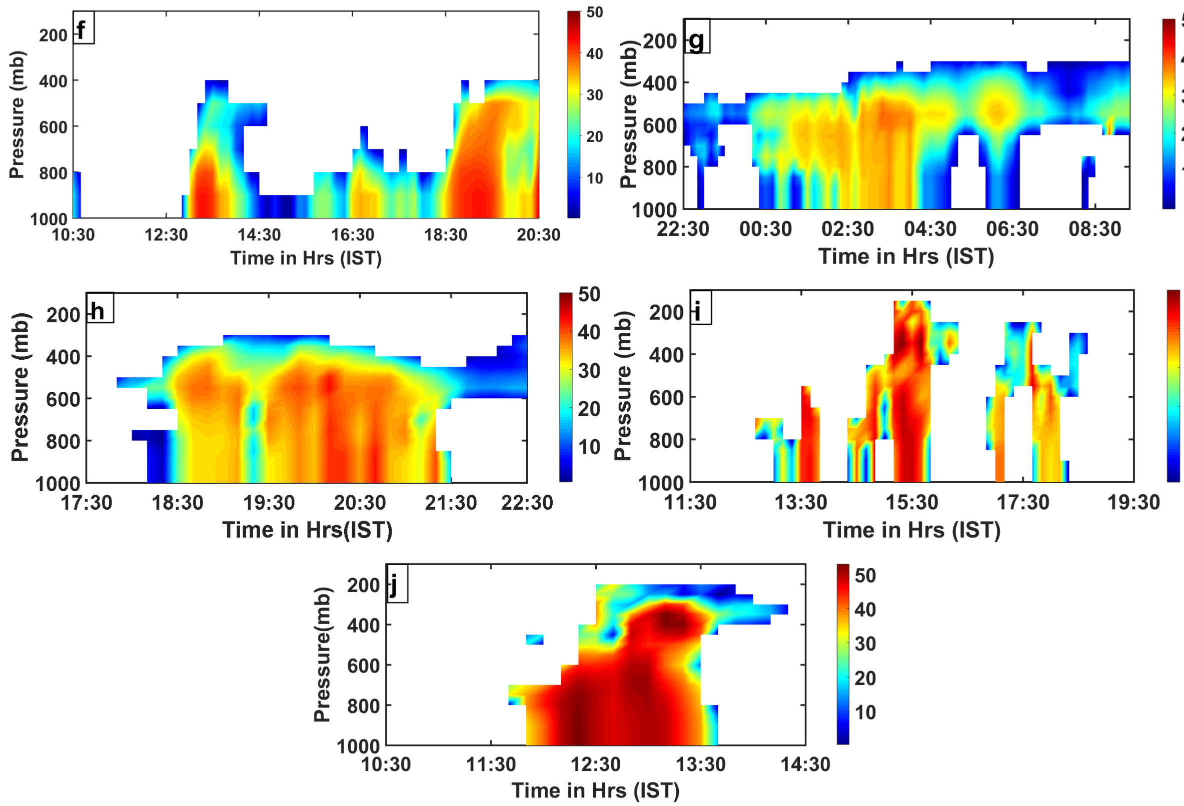

Figure 5.12: Same as Figure 5.11, but for the WE events. Labels are same as in Figure 5.4

While higher dBZ value around 500mb can be observed for the events shown in Figure 5.11(a-c), indicating the presence of a higher concentration of graupel and snow, the near-surface dBZ values are relatively weaker compared to the upper levels consistent with the findings of *Min et al.* (2015). The figure 5.11(a-b) shows bright band signature around 500 mb indicating stratiform nature of precipitation, while for the events shown in Figure 5.11(d-e), the model does not simulate any measurable reflectivity (dBZ) at any altitude.

The HTI of dBZ depicted in the figure 5.11(k-o) with Morr(M) exhibits higher near-surface value compared to the default Morrison scheme indicating higher precipitation intensity near the ground. For the event shown in Figure 5.11(o), the model simulated the dBZ only in the warm phase of cloud.

Figure 5.12(f-j) depicts the HTI of dBZ for the WE events, showing uniform values across the vertical levels. For the events 5.12(g-h), the stratiform rain signature was observed with an elevated melting layer at an altitude of 500 mb which corresponds to the altitude of 5.7 km from the MSL while radiosonde profiles indicated the presence of 0^o isotherm near around 4.8 km from the MSL over the HACPL.

5.9 Geographical Variability of λ

Recognizing the inherent spatio-temporal as well climatic variability of λ caused by distinct microphysical processes *(Konwar et al.*, 2014), the value of λ has been evaluated over different geographic location as well in distinct climatic regime for both SE and WE events. For SE, along with the HACPL, the values of λ were evaluated at

Pune and Solapur, using surface-based disdrometer data. While HACPL is at a higher elevation and in windward side of Western Ghat during the summer monsoon, Pune and Solapur are located in the leeward side of WG with MSL height of 560m and 458m respectively. The observations over Solapur were made in a ground campaign conducted during the Cloud-Aerosol Interaction and Precipitation Enhancement Experiment (CAIPEEX) (*Kulkarni et al.*, 2012). Despite variation in measuring instrument, geographical location and climatic regime, λ was found to be in a similar range for the SE events as seen from Tables 5.4, 5.5, 5.7, & 5.8.

Date	μ	$\lambda(mm^{-1})$	N_0(m^{-3} mm-$^{(\mu+1)}$	mean λ	S. D. of λ
22May ,2008	-0.71	1.41	6.62×10^3		
3 June,2008	-1.40	1.23	1.7×10^4		
31 Aug, 2008	0.71	3.38	7.5×10^4	2.32	0.94
1 Sept, 2008	-0.20	2.20	1.1×10^4		
2 sept,2008	-0.18	2.28	3.35×10^4		
9 sept.,2008	0.88	3.45	8.62×10^4		

Table 5.7: The RDSD parameters obtained from the surface-based Optical disdrometer for strongly electrified events over Pune.

Date	μ	$\lambda(mm^{-1})$	N_0(m^{-3} mm-$^{(\mu+1)}$	mean λ	S. D. of λ
	4.6	3.32	1.49×10^3		
	3.37	3.42	1.50×10^3		
	2.95	3.42	1.52×10^3		
	5.71	2.32	916	3.21	0.91
	4.15	3.74	3.32×10^3		
	2.36	1.75	133		
	4.63	4.54	5.7×10^3		

Table 5.8: The RDSD parameters obtained from the surface-based JW Disdrometer for strongly electrified events over Solapur.

Three of the SE events observed over Solapur documented in Table 5.8 have been simulated using the same model set up (apart from the domain configuration) as over the HACPL. This is done in order to ascertain the robustness of the primary hypothesis presented here in distinct geographical and meteorological regimes. The pre-monsoon thunderstorm over this region is predominantly air-mass thunderstorms caused by local heating. Figure 5.13 depicts the comparison of simulated rain rate and RDSD with the observations.

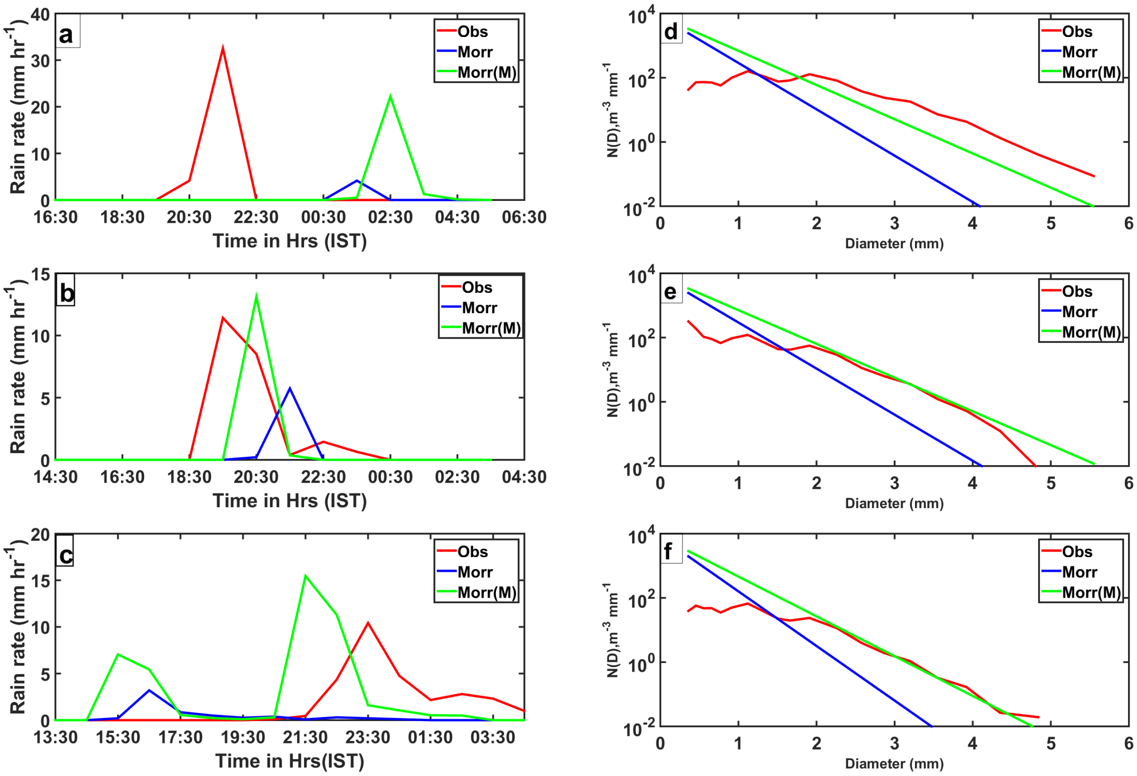

Figure 5.13: Comparison of simulated precipitation (a-c) and corresponding RDSD (d-f) with the observation for the SE events observed over Solapur documented in Table 5.13. The legends 'Obs' indicated observation, 'Morr' indicated Morrison scheme and 'Morr(M)' indicated modified Morrison scheme.

Here, the modified simulated precipitation (Morr(M)) corresponds to the same value of λ as over the HACPL. The substantial improvement in the precipitation field as well as in the RDSD with the modified physics over the HACPL as well as over Solapur, a region of significantly lower climatological mean rainfall added confidence to our conclusion that the effect of electrically enhanced coalescence growth of raindrops in precipitation formation inside SE cloud is valid irrespective of geographical locations.

5.10 The Vertical Evolution of Simulated Hydrometeors

Lightning-producing clouds are invariably associated with large concentration of ice phased hydromenetors in the mixed phase region of cloud. The melting of larger graupel particles (e.g. *Palucki et al.* 2011; *Mattos et al.* 2016) could have a substantial contribution to the surface rainfall. However, quantification of the same is lacking. The uncertainty in the accurate prediction of ice phase hydrometeors (ice, graupel, and snow) produces major uncertainty in the simulation fields. However, through a WRF simulation of convective storm, *Morrison et al.*, (2009) find that accurate prediction of number concentration of rain has more impact on the simulated fields than the prediction of number concentration of snow and graupel.

The vertical profiles of simulated hydrometeors for the two sets of events (SE and WE) observed over the HACPL and selected for the testing of our primary hypothesis have been presented in Figure 5.14

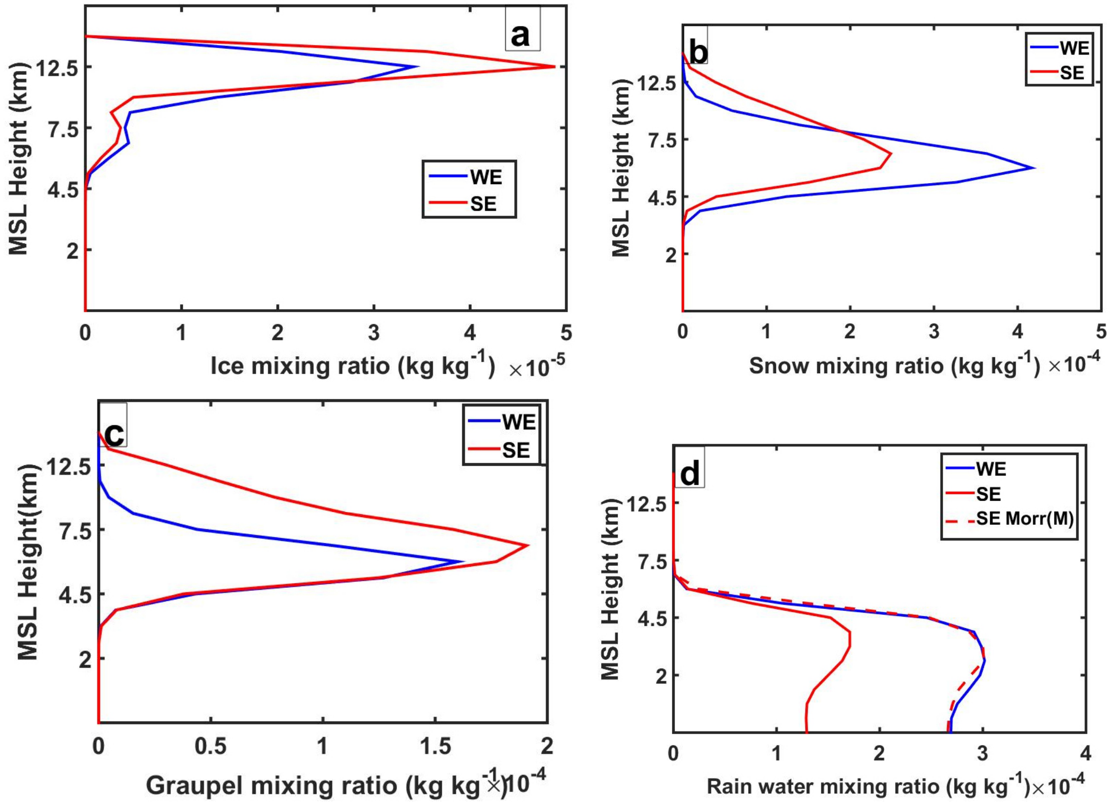

Figure 5.14: Area and time-averaged vertical distribution of simulated (a) Ice mixing ratio (kg kg^{-1}), (b) Snow mixing ratio (kg kg^{-1}), (c) Graupel mixing ratio (kg kg^{-1}) (d) Rain mixing ratio (kg kg^{-1}) for the events observed over the HACPL. The blue and red curves correspond to the WE and SE events, respectively. Each profile has been averaged over 5 events each.

Higher cloud ice ($\sim 5 \times 10^{-5}$ kg kg^{-1} for SE and 3.3×10^{-5} kg kg^{-1} for WE) and graupel mixing ratio($\sim 1.8 \times 10^{-4}$ kg kg^{-1} for SE and 1.6×10^{-5} kg kg^{-1} for WE) (Figure 5.14a & 5.14c) are as expected for the lightning-producing clouds required by the non-inductive charging mechanism of cloud electrification. In case WE events, it is also found that graupel resides at lower altitude in the mixed phase region of cloud compared to the SE events (*Mattos et a*l., 2016) suggesting the presence of larger size graupel particles above the melting layer in WE events relative to the SE ones, where they are more numerous. The underestimation in rain intensity in SE events despite having higher graupel and ice mass than the WE events suggest that the underestimation in the observed rain intensity may be caused by some missing microphysical processes influenced by electric forces, which broaden the RDSD and hence enhance the growth rate of raindrops.

5.11 Let's Look How Aerosol Concentration Impact the Simulated Rain Intensity

The discussion above clearly indicated that simulated rain intensity get substantially improved if the model physics is perturbed with the electrically modified RDSD slope parameter λ. One factor that could add a certain amount of uncertainty to our primary conclusion is the precipitation modification by aerosol concentrations. Numerous in-depth studies reported significant modification of accumulated precipitation by ambient aerosol concentration, although the relationship between the two observables is quite non-linear (*Khain et al*. 1999; *Rosenfeld*, 2000; *Rosenfeld* *et al*. 2002; *Rosenfeld and Woodley*, 2003; *Andreae et al*., 2004; *Khain et al*., 2005). To get more confidence in our primary hypothesis of electrical enhancement of precipitation intensity, I further investigated the response of precipitation to the number concentration of aerosol, which can act as Cloud Condensation Nuclei (CCN) over the HACPL. Aerosol distribution was measured over the HACPL with Scanning Mobility Particle Sizer (SMPS) while CCN was measured with a collocated Cloud Condensation Nuclei Counter (CCNC) (*Singla et al*., 2019). The measured aerosol concentration shows little higher value for SE (157 cm^{-3}) events compared to that of WE (137 cm^{-3}), both exhibiting peak around 0.05 µm (*Aitken mode*) (Figure 5.15a) while the measured CCN number concentration over the HACPL indicated no discernible difference between the SE and WE events (Figure 5.15b).

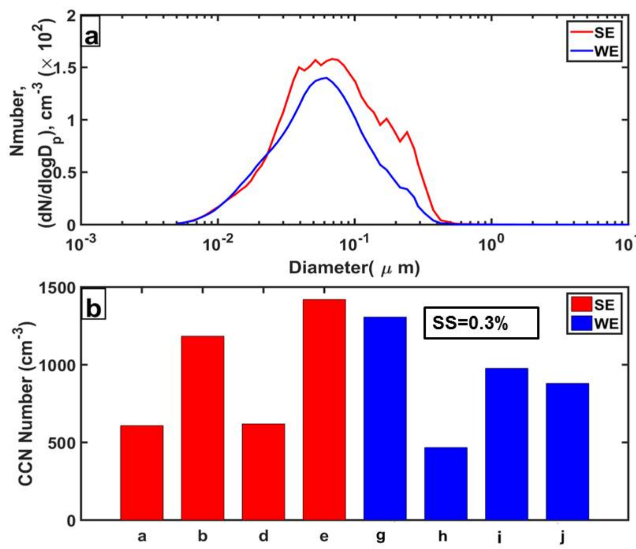

Figure 5.15: (a) Log-normal distribution of aerosol concentration over the HACPL for the SE and WE events tabulated in Tables 1& 2, (b)Bar representation of total CCN number concentration for SE and WE events at 0.3% supersaturation.

To test the sensitivity of simulated precipitation intensity to the aerosol concentration, we have run a simulation for the SE event (b) reported in the Table 5.4 as first experiment with modification of the default total concentration of aerosol in the size bin of 0.05 µm (*Mode1*) in Morrison scheme. When the model physics is perturbed by adding the difference between the mean concentration of aerosol and the one observed for SE events (around 6% of mean), it is observed that increase of aerosol concentration alone does not substantially change the simulated intensity of precipitation, although adds a little to the total accumulation (Figure 5.16a). However, when the aerosol perturbation is added with Morr(M) (The second experiment), simulated intensity shows a discernible improvement while the peak rainfall is delayed by an hour.

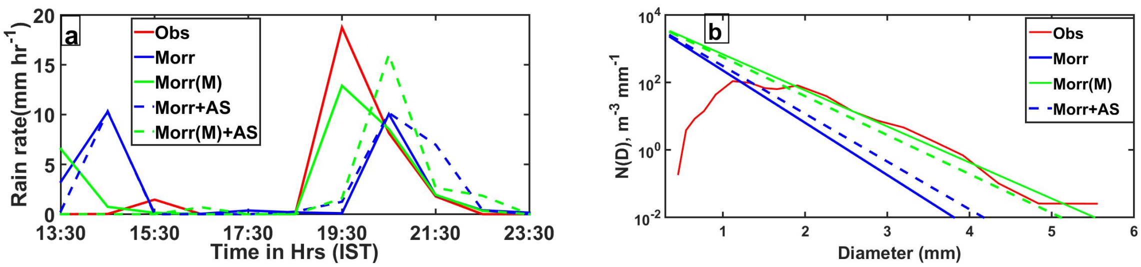

Figure 5.16: . (a) Comparison of simulated and observed rain intensity with aerosol modification. (b) Comparison of RDSD. The simulation with aerosol modification alone is indicated as 'Morr+AS' while simulation with both aerosol and λ modification is indicated as 'Morr(M)+AS' while 'Morr' indicated Morrison scheme and 'Morr(M)' indicated modified Morrison scheme.

This delaying is expected as a higher concentration of aerosol would reduce the drop sizes inhibiting collision-coalescence growth of drops in the warm phase, thereby suppressing the warm rain by the first aerosol indirect effect (*Twomey et al.*, 1984, *Hazra et al.*, 2013). The RDSDs shown in Figure 5.16(b) also do not indicate a significant change in the number concentration of larger drops by aerosol modification only, although the modification achieved through electrically modified λ is quite significant.

Results of this experiment established the robustness of the primary conclusion of electrical modification of simulated precipitation intensity.

5.12 Sensitivity of Simulated Precipitation Intensity to the Perturbed Initial Condition (*ic*):

The simulations presented in the study are short-range predictions and as such sensitive to ***ic***. The coarse resolution analysis (NCEP-FNL) interpolated to the finer model domain may introduce some uncertainty in the ***ic*** over the finer resolution model domain. The simulated field like precipitation is reported to be quite sensitive to the ***ic*** (*Jankov at el.* 2007; *Etherton and Santos*,2008). In the current study, the model was initialized with the coarse resolution ($1^o \times 1^o$) NCEP 6 hourly ***ic*** which was interpolated to the finer model domain. To ascertain that the uncertainty in the ***ics*** produced because of the interpolation of coarse resolution data to the finer scales doesn't introduce any major uncertainty in the interpretation of the primary results of the study, we have performed an ensemble of simulation with 10 ensemble components for the SE event (b) documented in the Table 5.1 using the default Morrison and Modified Morrison scheme. The ensemble members were generated by adding slight perturbation to the temperature field in NCEP ***ics*** of in the range of ± 0.05 K, determined based on the standard deviation of hourly mean vertical profiles. The model was initialized with the ***ic*** of 00:00:00 UTC for the entire 10 components. The result is depicted in Figure 5.17. The mean of the 10 component was depicted in the black colour as 'Ens. Mean' .

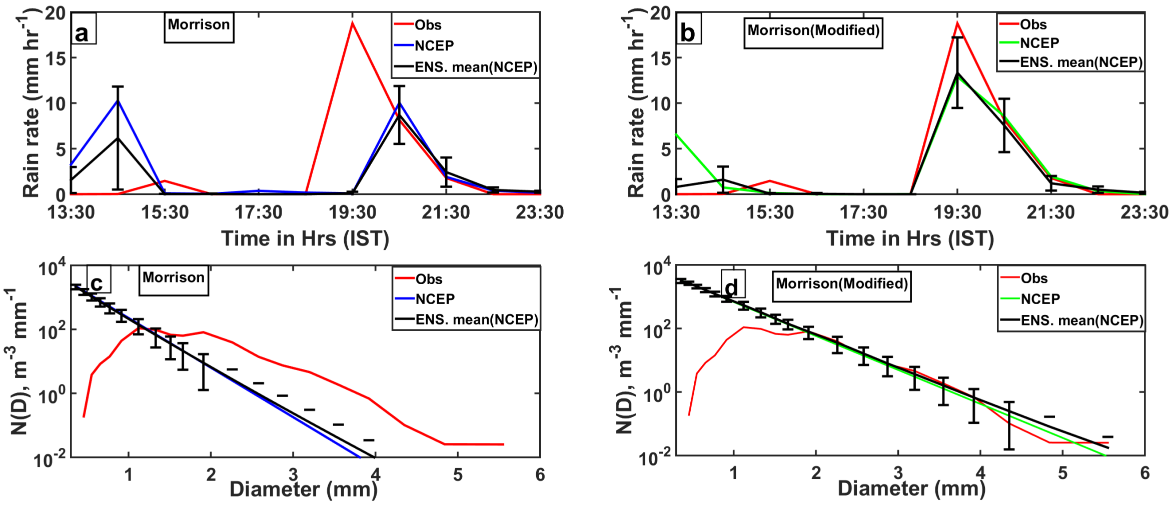

Figure 5.17: Inter-comparison among observation and simulation with NCEP Initial Condition (***ic***) as well with ensemble mean of 10 member ensemble generated by perturbing the temperature field of NCEP ***ic***, labelled as Obs, NCEP, ENS. Mean (NCEP) respectively. (a-b) precipitation intensity, (c-d) RDSD. The vertical bars indicate the respective standard deviation.

It is observed that the rain intensity as well the RDSD don't show significant sensitivity to the perturbed ***ics*** while the sensitivity to the electrically modified λ found to be highly significant establishing the robustness of the primary hypothesis presented in this chapter.

5.13 Conclusions

The problem of underestimation of heavier precipitation by weather/climate models is long standing. In quest of better estimation of precipitation for the benefit of meteorological as well as hydrological applications and encouraged by compelling evidences from laboratory as well as field experiments on substantial influences of electrical forces on cloud/rain microphysical processes, this chapter demonstrate that modeling the RDSD correctly in an NWP model is critical in simulating and predicting the rainfall intensity in cloud associated with stronger in-cloud electrical environments. The results presented here clearly suggested that the underestimations of heavy rainfall associated with SE events may be caused by the model's inability to properly reproduce the larger raindrops which get substantially improved with the inclusion of electrically modulated RDSD slope parameter λ. The improvement in rain intensity with the inclusion of characteristics slope parameter for SE events suggested a substantial influences of electrical forces (possibly in the warm phase of the cloud by virtue of enhanced collision-coalescence growth of raindrops) on the rain formation processes inside lightning-producing clouds.

Although, the results and discussion presented in this chapter originated from primarily a sensitivity experiment subject to knowledge of the observed RDSD, substantial improvement in the simulated precipitation with the electrically modulated RDSD parameters provides a promising pathway for parameterizing the electrical forces in weather/climate models. The optimism is based on the recent findings (*Mudiar et al.*, 2018) that quantify the modification of RDSD by electrical forces in stratiform as well as convective rain events. With the parameterization of the electrical effect in the physics module of NWP model, the reported dry bias associated with heavy precipitation events in the weather/climate models is likely to be minimized and increase the skill of the models in predicting intensity of quantitative precipitation.

Chapter 6

The Laboratory Investigation of Electrical Influence on the Freezing of water drops in Perspective of Cloud Physics

Chapter 6

6 The Laboratory Investigation of Electrical Influence on the Freezing of water drops in Perspective of Cloud Physics

6.1 Introduction

The chapters 3,4 and 5 are focused on the effect of in-cloud electrical forces in the rain microphysical processes primarily through collision-coalescence process in the warm phase of cloud. However, the electrification of cloud is inherently associated with cold rain microphysics in the mixed-phase region of cloud. It is well known that ice phase hydrometeors play a major role in cloud electrification through non-inductive charging mechanism *(Stolzenburg*, 1998; *Takahasi*,1978; *Bruning et al*.,2007; 2010) and also modify the surface precipitation through cold rain microphysics. But few studies are available concerning the growth behavior of ice-phased hydrometeors in the mixed-phased region of cloud once the clouds become strongly electrified. *How the in-cloud electric field is going to effect the growth or decay of the ice particles ?* Also, to understand the Earth's climate system, the underlying cloud microphysical processes (both warm and clod) must be understood. The chapters 3-5 are limited below the melting level as no observational data regarding cloud microphysical processes are available above the freezing layer during the course of study. Also, complex growth processes and inter-changeable habitat of the frozen hydrometeors makes it difficult to study their growth behavior in natural clouds. However, laboratory investigations provides a unique opportunity to understand the underlying micro scale processes of a macro system like clouds. It is well known that the formation of ice crystal in Earth's atmosphere is often catalyzed by different factors through different mechanism. The primary processes are homogeneous and heterogeneous ice nucleation processes. Homgenous nucleation occurs at a temperature below ~ -37^{o}C,without the assistance of any ice nuclei particles (*Pruppacher and Klett,1996),* whereas the heterogeneous nucleation occcurs at different mode of nucleation processes which can initiate the formation of ice crystals at a temperature warmer than -37^{o}C. Numerous laboratory investigation has been carried out to study the effect of electrical influences in water droplets break up, evaporation, oscillation and coalescence *(Lord*,1879; *Taylor*, 1966; *Ausman and Brook*, 1967; *Richards and Dawson*, 1971*; Kamra and Ahire, 1989, Bhalwankar et al*., 2004,2017; *Bhalwankar and Kamra,* 2007). As for example, *Taylor*,(1966) observed that electric field can induce disintegration of water drops . *Kamra and Ahire, (1989)* observed that an external electric field can change the shape of a water drop falling in its terminal velocity. *Bhalwankar et al*. (2004) observed that rate of evaporation of charged drops is less than uncharged drops of same size. It has been also observed that presence of charge on surface of a water drops reduces the equilibrium saturation vapor pressure stabilizing the drop at subsaturated environments *(Lapshin et al*., 2002; *Nielesn et al*., 2011)

The uncertainty in the accurate prediction of ice phase hydrometeors (ice, graupel, and snow) produces major uncertainty in the simulation fields (*Morrison et al*., 2009). But as mentioned, few laboratory studies investigating the effect of electrical force in ice crystals are available in literature. *Pruppacher and Klett*, (1978) reported that inside strongly electrified cloud, the number concentration of ice crystals is found to be several order of magnitude greater than measured ice nuclei and suggested that some secondary crystal generation mechanism must operate inside the cloud. In a cloud chamber investigation, *Pruppacher* (1963) observed enhanced ice-nucleation in presence of electrostatically charged surfaces and external electric field. He proposed that electrical relief of the surface of solid substrate (and not the crystallochemical relief) is inducing the heterogeneous ice nucleation in presence of electric force. *Abbas and Latham* (1968) reported electro-freezing of a water drop in a temperature range -5 to -20^oC if the drops are disrupted by an external electric field. They suggested that the electro-freezing is associated with the movements of triple-phase boundary and cause of freezing was attributed to the emanation of a filament structure from the drops which contain molecular aggregates that act a freezing nuclei. *Schaefer* (1968) and *Salt* (1961) suggested that ice nucleation of super-cooled water drops may takes place through impurities produced by electric discharge. *Mandal and Pradeep Kumar* (2002) observed ice nucleation in a cold room experiment through corona discharge and suggested that the nucleation was possibly caused by large number of ions produced during the discharge. They didn't detect any nucleation by application of only high electric field. In a cloud chamber experiment, *Anderson et al.* (1980) observed that ice particles which preferentially form on ions have the greater chance of growing to a larger size. A wind tunnel experiment of electro-freezing by *Dawson and Cardell* (1973) suggest no substantial influence of vertical electric field in the enhancement of freezing of super-cooled water drops in the temperature range $-8^oC$to -15^oC.The *Cosmics Leaving Outdoor Droplets* (CLOUD) experiment in CERN uses a spherical cloud chamber to study the effect of inter galactic cosmic ray in nucleation of super-cooled droplets in the Earth's atmosphere.

Although there are some evidences of electro-crystallizaition with application of an external electric field, it has been observed that the drops are subject to electrical or mechanical disturbances. The possibility of electro-crystallization without disturbing the drops has not been investigated much. A proper understanding of this aspect is important as the freezing of super-cooled droplets at higher temperature will generate significant amount of latent heat which may in-turn impact the dynamics of the thunderclouds. A proper understanding of the freezing characteristics along with the crystal habitat will help to reduce the uncertainty associated with ice hydrometeors in weather/climate models.To investigate the effect of an external electric field in electro-crystallization along with the shape and size of crystals, a cloud chamber experiment has been designed. In this chapter, the fabrication of the cloud chamber, experimental procedures and some preliminary results will be presented.

6.2 The Desgine and Fabrication of the Cloud Chamber

A chamber has been designed and fabricated with internal dimension 1ft.$\times$1ft. with aluminum wall inside the chamber. A compressor has been used to cool the inside of the chamber to -25^oC from room temperature. Figure 6.1(a-b) shows the front and side view of the cloud chamber.

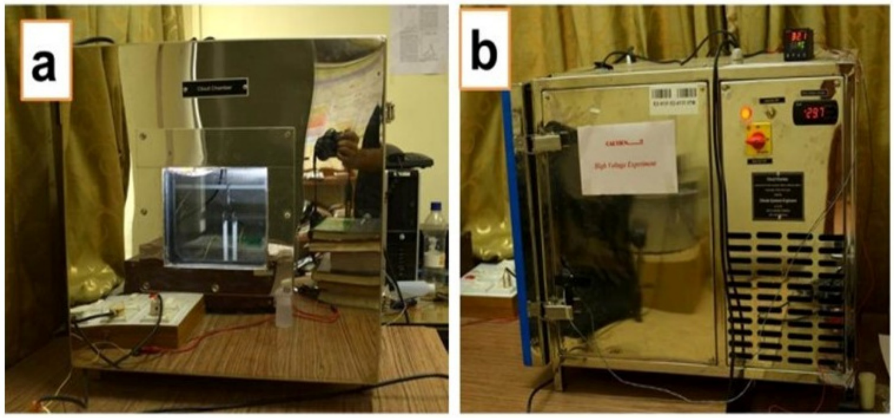

Figure 6.1: (a) Front (b) Side view of the cloud chamber

Arrangement has been made to access and view the inside of the chamber through a front door with LED lighting inside the chamber.

6.3 The Experiment

In the first experiment, drops of pure water (conductivity~0.056 μsemen cm^{-1}) with approximate size of 1 mm kept suspended in a Nylon wire. The experimental set up has been depicted in Figure 6.2. The chamber was allowed to cool from the room temperature to $-25^{o}C$. A platinum resistance thermometer (PT-100) was installed near the drops to detect the freezing of the drop. When the phase change happens, latent heat of fusion is released by the drops. A temperature controller connected to local computer through a data logger is used to record the temperature rise at the freezing point. Figure 6.3 depicts a typical cooling curve record by the temperature controller. The freezing point can be clearly seen as the rise of temperature. The relative humidity and aerosol concentration inside the chamber was kept as the ambient air at the beginning of the experiment. More than 100 samples are collected in this setup.

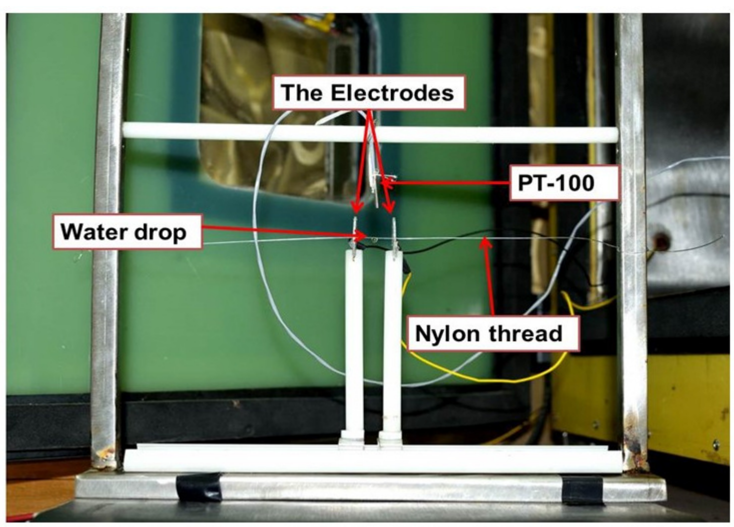

Figure 6.2: Exerimental set up

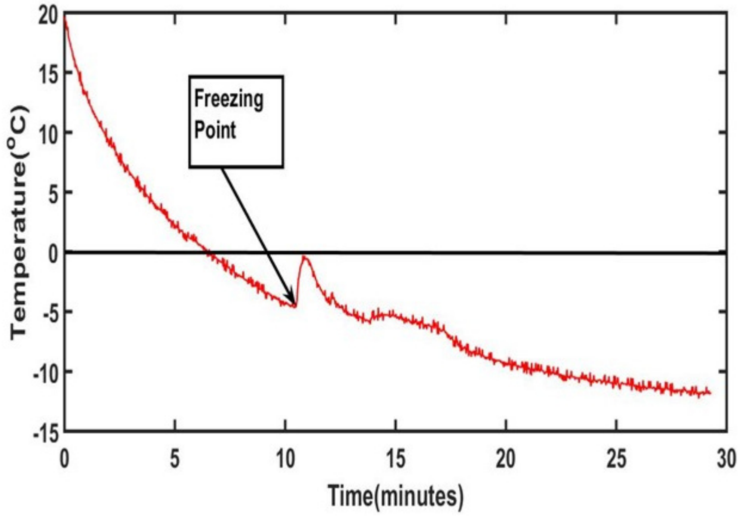

Figure 6.3: A typical cooling curve recorded by the temeprature controller kept near the drop.

In the second experiment, the water drops are kept suspended in the Nylon thread as the first one. The drops are now subjected to a dc voltage in the range of $1-5$kv cm^{-1} using a dc power supply. Two plate electrodes are used for the application of an electric field. It has been also ensured that no electric discharge takes place during the experiment as electric discharge near the drop may create mechanical disturbance. In this set up, more than 50 samples are collected.

6.4 Results and Discussion

Figure 6.4(a) shows bar representation of frequency distribution of the freezing temperature when the drop is allowed to freeze without any electrical influence. The drops are observed to freeze in the temperature ranging -4^{o}C to -16^{o}C. Approximately 36% drops are observed to freeze between $-14^oC$to -16^oC.

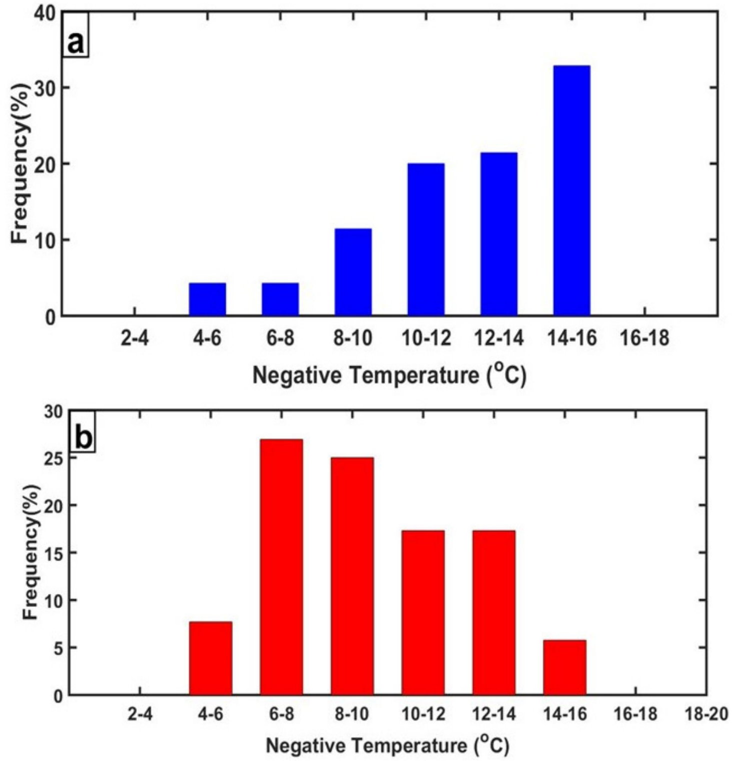

Figure 6.4: Frequency distribution of freezing temperature of disilled water drops.(a) No electric field is applied during the experiment. (b) The drops are subjected to electric field of magnitude ranging 2.5-5 kv cm^{-1}.

Figure 6.4(b) depicts the frequency distribution of the freezing temperature when the drops are subjected to an electric field of magnitude ranging $2.5-5kvcm^{-1}$. A shift in the distribution towards warmer temperature is evident from the Figure. When the drops are subjected to an electric field, most of the drops freeze between negative $6-10^{o}C$. But as this result is derived only from around 50 experiment, the most likely freezing temperature may vary with more number of samples.

Visual observation suggested that for a few of the drops, crystallization starts at the surface, while for others, crystallization process observed to initiate at the center of the drops. The mode of freezing will be investigated with high-speed camera photography in future experiments. It may be noted here that, although all the experiments have been performed using distilled water drops, the surrounding environment of the cloud chamber remain largely uncontrolled. This may be one possible reason for large variability in the observed freezing temperature in the both set of experiments.

The cause of the shift in freezing temperature in the presence of electric field could not be ascertained at present. *Pruppacher* (1963) suggested that the movement of a deformed super-cooled water drops on a solid surface can cause freezing in presence of an electric field. The present experiments have been carried out in absence of any water-oil interface unlike *Pruppacher* (1963). During the freezing process no deformation and movement of the drops are observed. *Loeb* (1963) suggested that presence of a super-cooled solid surface (*In this case, the Nylon thread*) which can efficiently absorb the latent heat of fusion can facilitate the freezing of the drops. He also suggests the essential requirement of free space for volume expansion during freezing. *Loeb* (1963) also suggested that an intense electric field can draw out fine filaments from the drops, which can initiate the freezing .

In future experiment, the role of ions in the nucleation of super-cooled water drops will be investigated.

Chapter 7

Conclusion

Chapter 7

7 Conclusion

7.1 Summary

The primary objective of this thesis as defined in the introductory chapter was to quantify the in-cloud electric effect in cloud/rain microphysical processes in tropical cloud. In that endeavor, observations of electrically distinguished tropical clouds has been made and data sets are analyzed to in order to bring out the electrical contribution from other microphysical processes. Sensitivity experiments has been performed using WRF model in order to validate numerical weather model's fidelity in simulating weather events with distinguishable electrical characteristics. Encouraged by promising evidence of substantial electrical influence in cloud/rain microphysical processes from observational data , attempts have also been made to bring in the electric influence to cloud physics module of WRF model. The major findings of this thesis are enlisted below

The quantification of electrical effect in stratiform cloud

- The vertical profile of raindrop size shifted towards larger size below the melting layer for SE stratiform tropical cloud when compared to the WE ones for the same rain intensity.
- The RDSD at different altitude exhibits broadening towards larger size bins for SE stratiform cloud compared to the WE ones with similar rain intensity below the melting level. A compensating reduction of smaller drops is observed to invariably associated with the broadening. This broadening of RDSD is attributed to the electrically enhanced collision-coalescence growth of raindrops facilitated by surface charge and in-cloud electric field.
- Observation of the surface RDSD suggested significantly higher concentration of larger raindrops in SE stratiform rain events compared to WE events.
- Substantially higher concentration of larger raindrops is observed in the RDSD spectrum for SE stratiform rain events relative to WE stratiform rain events when compared under the same width of radar bright band, which suggest a prevalence growth of raindrop through electrically enhanced collision-coalescence mechanism in SE stratiform rain events.
- Significantly higher growth rate of raindrops in their terminal speed below the melting layer is observed as a consequence of electrically enhanced collision-coalescence in SE stratiform rain events.
- The MVD shows no significant relationship with surface wind speed and rain liquid water content for the SE events.

- A transient increase in raindrop size is observed to associated with a preceding lightning. The size of raindrop shows a positive linear relationship with the change in surface electric field during a lightning. Stronger the discharge, larger the drop.

- A significant correlation has been observed between the surface measured electric field and raindrop size during storms suggesting that electric field could enhance the growth of raindrops inducing efficient collision and coalescence between the raindrops falling under gravity..

- As the SE clouds distinguished by the presence of lightning which invariably remain associated with larger and numerous graupel particles in the mixed phase region of cloud, the effect of graupel melting in broadening of RDSD needs to be examined.

- **The Electrical association between rain intensity and lightning**

- In the investigation of anticipated association between lightning and rain intensity, a transient amplification in intensity of surface rain is found to be associated with an overhead lightning discharge with an average time lag of 2-4 minutes.

- The investigation of the RDSD before and after lightning reveal broadening of the distribution towards larger size bins. An associated reduction in the number concentration of smaller raindrops was observed which suggest an enhanced collision-coalescence growth of raindrops. This enhanced growth of raindrops is attributed to the electrification of raindrops by lightning discharge in the neighborhood cloud volume through ion deposition.

- The very short time lag of 2-4 minutes between the lightning and the amplification of surface rain suggested that the growth of raindrops that causes the observed transient amplification of rain intensity at the surface primarily takes place in the warm phase of cloud indicating that collision-coalescence growth is the primary mechanism through which lightning can amplify the surface rain.

The association between lightning rate and surface rain rate

- An analysis of three lightning-producing-storms revels significant correlation [$r(ave) = 0.75$, $pvalue = 0.001$] between lightning rate and surface rain rate, where surface rain rate is observed to lag the lightning rate by 3-6 minutes. Both the observable show lagged association only when lightning activity is present overhead the rain gauge. This indicate highly localized characteristics of lightning-induced rain amplification. The results of this analysis indicate that lightning-induced atmospheric ions and prevailing electrical forces significantly modulate the RDSD as well as the surface rain intensity. The smaller time lag between lightning rate and surface rain rate also suggested that the genesis of lightning induced rain amplification can be attributed to the warm phase of cloud.

- The raindrop size (MWD) is observed to show positive correlation with the lightning rate while the drop number concentration is observed to show negative correlation in lightning-producing clouds. This indicate an enhanced collision-coalescence growth of raindrops induced by lightning induced electrification of precipitation particles.

- It is also observed that, in non-lightning-producing clouds, raindrop size and number concentration proportionally contribute to the rain intensity, a finding consistent with previous observations in distinct climatic regimes. The increasing trend of MWD with rain rate in non-lightning-producing cloud observed to get saturated at diameter above 2 mm, while no significant trend was observed for drop number concentration with rain rate.

- It is also observed that higher lightning intensity (in terms of peak current and change of surface-measured electric field during the discharge) associated with a broader RDSD. The more intense lightning is associated with more intense precipitation at the surface which reaffirm the idea of strong association between electrification of cloud and precipitation intensity.

The numerical simulation of SE and WE tropical clouds

- The numerical simulation of SE rain events using WRF model with Morrison physics scheme indicate that the model substantially underestimate the intensity of observed rain while in contrast the observed and simulated rain intensity are found to be comparable to each other.

- In some cases, the model predicted the rainfall 3-4 hours advance while in others the rainfall was delayed by 1-2 hours. This phase difference in the diurnal cycle of the simulated peak and observed peak in precipitation is found to be consistent with previous simulation studies.

- The comparison of observed and simulated RDSD indicated that model significantly underestimate the number concentration of large raindrops in the RDSD spectrum for the SE events while for WE events both the distributions are found to be comparable, although some overestimation of smaller size drops are noted for both kind of events.

- From the comparison of simulated and observed rain intensity along with the RDSD, it is inferred that the underestimation of rain intensity in the SE events is possibly due to the absence of electric effect in the physics module of WRF as the chapter 3 and 4 indicate a substantial electrical influence in rain microphysical processes inside SE clouds.

- A transient dip in the RDSD slope parameter at the surface found to remain associated with an overhead lightning discharge. It is hypothesized that this reduction in the value of slope parameters may be caused by broadening of the corresponding RDSD induced of lightning.

- Simultaneous measurements of RDSD slope parameter and surface electric field suggest that lower values of slope parameters are remain associated with higher magnitude of cloud electric field measured at the surface.

- In endeavor to parameterize the electric effect in the Morrison microphysics scheme, the default minimum value of model prescribed RDSD slope parameter for rain in SE events has been modified with the observed RDSD slope parameter as observation suggest the RDSD slope parameter get substantially modified by the in-cloud electric forces. Substantial improvement in rain intensity has been observed with the modified physics. The diurnal cycle as well show some improvement. The modified sachem found to reproduce the RDSD spectrum reasonably well. This improvement suggested that the missing physics causing the underestimation in SE rain events is the electric effect.

- The comparison of simulated vertical profiles of hydrometeors for both kind of events reveals presence of higher concentration ice and gruapel in SE events in the mixed phase region. This result is quite expected as the electrification in SE events takes place through non-inductive charging mechanism where the ice phase hydrometeors primarily ice particles and larger graupels interact with each other in the process of charge separation.

- The effect of ambient aerosol size distribution in the simulated rain intensity also has been investigated by perturbing the model prescribed aerosol size distribution with the observed distribution. It has been found that aerosol size distribution alone does not improve the simulated precipitation as much as the modification of slope parameter. But when both the aerosol size distribution as well as the slope parameter were modified, substantial improvement was observed in the simulated precipitation in SE rain event.

- The conventional hypothesis of rain intensity modification by melting of large graupel particles in SE events has been also tested and found that the melting of graupel particles may not contribute much to the observed bias.

- A simulation experiment with 10 ensemble components has been performed by perturbing the NCEP ICs to establish the robustness of the primary hypothesis of electrical modification of rain intensity considering one of the SE events. The results indicate that rain intensity and the RDSD does not show significant sensitivity to the perturbed ics

The Lab experiment

- A frequency distribution of freezing temperature of a water drop in absence of any electrical field indicate that most of the drops (sample size of 100 droops) freezes between -12^oC to -15^o C consistent with previous laboratory studies.

- A collection of around 50 sample point in presence of an electric field of magnitude 5kv cm^{-1}suggested that the distribution of freezing temperature shifted to much lower range, i.e. -5^oC to -10^o C.

- The cause of electrically induced freezing needs to investigate in future experiments.

7.2 Future Scope

The work presented in this thesis exclusively focused in the effect of in-cloud electric forces in the collision-coalescence growth of raindrops, which primarily takes place in the warm phase of the cloud. But as suggested by numerous observations (*Williams and Lhermitte*, 1983; *Williams et al.*, l989; *Mattos et al.*, 2016, *Bruning et al.*,2007; *Bruning et al.*,2010) the precipitation from SE clouds are dominated by cold rain microphysics as interaction of ice phase hydrometeors particularly ice crystal and graupel particles are essential for storm electrification. The ice factory hypothesis as discussed in the *chapter 3* may be a substantial contributor to the total rainfall in SE clouds. On the other hand, a few observational evidences are also available regarding the alignment and crystals growth in the mixed phase region of cloud by pre-discharge electric field. In the absence of any observation in the mixed phase microphysical process in lightning producing storms, this thesis is limited to the warm phase rain only. But in future, the work may be extended to the mixed phase microphysical process to study the effect of electric force in the growth of ice phased hydrometeors.

Another important aspect of cloud microphysical processes is the condensation growth of cloud drops. The *kohler theory* suggested that, the condenstaional growth of cloud drops are primarily dominated by the curvature effect (surface tension) and solute effect both of which changes the saturation vapor pressure. A few laboratory studies suggested that presence of electric charge in the drop surface may change the surface tension of the drops substantially. It is also known that presence of charge in surface of cloud droplets and electric field can substantially influence condensational or diffusional growth of droplets by reducing the equilibrium saturation vapor pressure *(Lapshin et al.*, 2002; *Nielesn et al.*, 2011). Hence, it is will be interesting to investigate the effect of in-cloud electric force in the condensational growth of cloud droplet in clouds associated with stronger in-cloud electric environment.

As discussed in the Chapter 1, the prevailing cloud microphysical processes can also influence dynamics of the cloud (*Grabowski*, 2000). The presence of larger raindrops in SE cloud suggested that evaporation rate in the sub-saturated region of cloud will get reduced. This in turn may suppress the cold pool, thereby invigorating the storms (*Morrison et al.*,2008; *Tao and Li*, 2016). This aspect of electrical invigoration of storms need to be explored in future.

7.3 Concluding remarks

This thesis has been designed and written in an endeavor to solve a long standing problem (From the time of *Lord Rayleigh*,1879) in atmospheric sciences i. e. effect of in-cloud electric forces in rain formation processes the Earth atmosphere, in the backdrop of ample laboratory and numerical evidences. The quantification of the same has been achieved with observational data sets which revealed an substantial influence of in-cloud electric forces in rain microphysical processes. A method has been also proposed to bring in the electric effect through modification of model prescribed RDSD slope parameter to the numerical weather prediction model and found to be quite effective. The thesis raise a hope as well as some promise and concludes that with the parameterization of the electrical effect in the physics module of numerical weather prediction model, the longstanding problem of dry bias associated with heavy precipitation events in the weather/climate models is likely to be minimized and will increase the skill of the models in predicting the intensity of quantitative precipitation.

References

References

Abbas, M. and Latham, J. The Electrofreezing of Supercooled Water Drops. *Journal of the Meteorological Society of Japan. Ser. II*, 47(2):65–74, 1969. ISSN 0026-1165. doi: 10.2151/jmsj1965.47.2$_6$5.

Abbasi, R. U., Abu-Zayyad, T., Allen, M., Barcikowski, E., Belz, J. W., Bergman, D. R., Blake, S. A., Byrne, M., Cady, R., Cheon, B. G., Chiba, J., Chikawa, M., Fujii, T., Fukushima, M., Furlich, G., Goto, T., Hanlon, W., Hayashi, Y., Hayashida, N., Hibino, K., Honda, K., Ikeda, D., Inoue, N., Ishii, T., Ito, H., Ivanov, D., Jeong, S., Jui, C. C., Kadota, K., Kakimoto, F., Kalashev, O., Kasahara, K., Kawai, H., Kawakami, S., Kawata, K., Kido, E., Kim, H. B., Kim, J. H., Kim, J. H., Kishigami, S. S., Krehbiel, P. R., Kuzmin, V., Kwon, Y. J., Lan, J., LeVon, R., Lundquist, J. P., Machida, K., Martens, K., Matuyama, T., Matthews, J. N., Minamino, M., Mukai, K., Myers, I., Nagataki, S., Nakamura, R., Nakamura, T., Nonaka, T., Ogio, S., Ohnishi, M., Ohoka, H., Oki, K., Okuda, T., Ono, M., Onogi, R., Oshima, A., Ozawa, S., Park, I. H., Pshirkov, M. S., Remington, J., Rison, W., Rodeheffer, D., Rodriguez, D. C., Rubtsov, G., Ryu, D., Sagawa, H., Saito, K., Sakaki, N., Sakurai, N., Seki, T., Sekino, K., Shah, P. D., Shibata, F., Shibata, T., Shimodaira, H., Shin, B. K., Shin, H. S., Smith, J. D., Sokolsky, P., Springer, R. W., Stokes, B. T., Stroman, T. A., Takai, H., Takeda, M., Takeishi, R., Taketa, A., Takita, M., Tameda, Y., Tanaka, H., Tanaka, K., Tanaka, M., Thomas, R. J., Thomas, S. B., Thomson, G. B., Tinyakov, P., Tkachev, I., Tokuno, H., Tomida, T., Troitsky, S., Tsunesada, Y., Uchihori, Y., Udo, S., Urban, F., Vasiloff, G., Wong, T., Yamamoto, M., Yamane, R., Yamaoka, H., Yamazaki, K., Yang, J., Yashiro, K., Yoneda, Y., Yoshida, S., Yoshii, H., and Zundel, Z. Gamma Ray Showers Observed at Ground Level in Coincidence With Downward Lightning Leaders. *Journal of Geophysical Research: Atmospheres*, 123(13):6864–6879, 2018. ISSN 21698996. doi: 10.1029/2017JD027931.

Abel, S. J. and Boutle, I. A. An improved representation of the raindrop size distribution for single-moment microphysics schemes. *Quarterly Journal of the Royal Meteorological Society*, 138(669):2151–2162, 2012. ISSN 00359009. doi: 10.1002/qj.1949.

A.Huggel, W.Schmid, A. W. Raindrop Size Distributions and the Radar Bright Band. *Journal of Applied Meteorology*, 35, 1996.

Anderson, R. J., Miller, R. C., Kassner, J. L., and Hagen, D. E. A Study of Homogeneous Condensation-Freezing Nucleation of Small Water Droplets in an Expansion Cloud Chamber. *Journal of the Atmospheric Sciences*, 37(11): 2508–2520, 1980. ISSN 0022-4928. doi: 10.1175/1520-0469(1980)037<2508:asohcf>2.0.co;2.

Andreae, M. O., D. Rosenfeld, P. Artaxo, A. A. Costa, G. P. Frank, K. M. Longo and Silva-Dias, M. A. F. Smoking rainclouds over the Amazon. *Science*, 303:1337–1342, 2004.

Aplin, K. L. *Instrumentation for atmospheric ion measurements*. PhD thesis, University of Reading, 2000.

Armstrong, R. and Glenn, J. Electrical Role for Severe Storm Tornadogenesis (and Modification). *Journal of Climatology & Weather Forecasting*, 03(03), 2015. doi: 10.4172/2332-2594.1000139.

Ausman, E. L. and Brook, M. Distortion and disintegration of water drops in strong electric fields. *Journal of Geophysical Research*, 72(24):6131–6135, 1967. doi: 10.1029/jz072i024p06131.

Bateman, M. G., Marshall, T. C., Stolzenburg, M., and Rust, W. D. Precipitation charge and size measurements inside a New Mexico mountain thunderstorm. *Journal of Geophysical Research Atmospheres*, 104(D8):9643–9653, 1999. ISSN 01480227. doi: 10.1029/1998JD200118.

Baum, B. A., Menzel, W. P., Frey, R. A., Tobin, D. C., Holz, R. E., Ackerman, S. A., Heidinger, A. K., and Yang, P. MODIS cloud-top property refinements for collection 6. *Journal of Applied Meteorology and Climatology*, 51(6): 1145–1163, 2012. ISSN 15588424. doi: 10.1175/JAMC-D-11-0203.1.

Bhalwankar, R. V. and Kamra, A. K. A wind tunnel investigation of the deformation of water drops in the vertical and horizontal electric fields. *Journal of Geophysical Research Atmospheres*, 112(10), 2007. ISSN 01480227. doi: 10.1029/2006JD007863.

Bhalwankar, R., Deshpande, C. G., and Kamra, A. K. Breakup modes of the drops suspended in a vertical wind tunnel in presence of the horizontal electric field. *Journal of Geophysical Research*, 122(3):1838–1849, 2017. ISSN 21562202. doi: 10.1002/2016JD025805.

Bhalwankar, R. V., Sathe, A. B., and Kamra, A. K. The evaporation of the charged and uncharged water drops suspended in a wind tunnel. *Proceedings of the Indian Academy of Sciences, Earth and Planetary Sciences*, 113(2): 129–138, 2004. ISSN 02534126. doi: 10.1007/BF02709783.

Boers, N., Bookhagen, B., Barbosa, H. M., Marwan, N., Kurths, J., and Marengo, J. A. Prediction of extreme floods in the eastern Central Andes based on a complex networks approach. *Nature Communications*, 5, 2014. ISSN 20411723. doi: 10.1038/ncomms6199.

Bowers, G. S., Smith, D. M., Kelley, N. A., Martinez-McKinney, G. F., Cummer, S. A., Dwyer, J. R., Heckman, S., Holzworth, R. H., Marks, F., Reasor, P., Gamache, J., Dunion, J., Richards, T., and Rassoul, H. K. A Terrestrial Gamma-Ray Flash inside the Eyewall of Hurricane Patricia. *Journal of Geophysical Research: Atmospheres*, 123 (10):4977–4987, 2018. ISSN 21698996. doi: 10.1029/2017JD027771.

Bradley, S. G. and Stow, C. D. Comments on âCollision, Coalescence and Breakup of Raindrops. Parts I and IIâ. *Journal of the Atmospheric Sciences*, 41(4):701–703, 1984. ISSN 0022-4928. doi: 10.1175/1520-0469(1984)041<0701:cocabo>2.0.co;2.

Bringi V. N., and V. Chandrasekar, . P. D. W. R. P. and University, A. C. *Polarimetric Doppler Weather Radar: Principles and Applications*. 2001.

Bruning, E. C., Rust, W. D., Schuur, T. J., MacGorman, D. R., Krehbiel, P. R., and Rison, W. Electrical and polarimetric radar observations of a multicell storm in TELEX. *Monthly Weather Review*, 135(7):2525–2544, 2007. ISSN 00270644. doi: 10.1175/MWR3421.1.

Bruning, E. C., Rust, W. D., Macgorman, D. R., Biggerstaff, M. I., and Schuur, T. J. Formation of charge structures in a supercell. *Monthly Weather Review*, 138(10):3740–3761, 2010. ISSN 00270644. doi: 10.1175/2010MWR3160.1.

Calhoun, K. M., Macgorman, D. R., Ziegler, C. L., and Biggerstaff, M. I. Evolution of lightning activity and storm charge relative to dual-doppler analysis of a high-precipitation supercell storm. *Monthly Weather Review*, 141(7): 2199–2223, 2013. ISSN 00270644. doi: 10.1175/MWR-D-12-00258.1.

Carey, L. D. and Rutledge, S. A. The relationship between precipitation and lightning in tropical island convection: A C-band polarimetric radar study. *Monthly Weather Review*, 128(8 PART 1):2687–2710, 2000. ISSN 00270644. doi: 10.1175/1520-0493(2000)128<2687:trbpal>2.0.co;2.

Cetrone, J. and Houze, R. A. Anvil clouds of tropical mesoscale convective systems in monsoon regions. *Quarterly Journal of the Royal Meteorological Society*, 135(639):305–317, 2009. ISSN 00359009. doi: 10.1002/qj.389.

Chalmers, J. A. *Atmospheric Electricity*. Pergamon Press, New york, 1967.

Chilingarian, A., Chilingaryan, S., Karapetyan, T., Kozliner, L., Khanikyants, Y., Hovsepyan, G., Pokhsraryan, D., and Soghomonyan, S. On the initiation of lightning in thunderclouds. *Scientific Reports*, 7(1), 2017. ISSN 20452322. doi: 10.1038/s41598-017-01288-0.

Christian, H., Holmes, C. R., Bullock, J. W., Gaskell, W., Illingworth, A. J., and Latham, J. Airborne and groundâbased studies of thunderstorms in the vicinity of Langmuir Laboratory. *Quarterly Journal of the Royal Meteorological Society*, 106(447):159–174, 1980. ISSN 1477870X. doi: 10.1002/qj.49710644711.

Clark, P., Roberts, N., Lean, H., Ballard, S. P., and Charlton-Perez, C. Convection-permitting models: A step-change in rainfall forecasting. *Meteorological Applications*, 23(2):165–181, 2016. ISSN 14698080. doi: 10.1002/met.1538.

Ćurić, M. and Janc, D. Comparison of modeled and observed accumulated convective precipitation in mountainous and flat land areas. *Journal of Hydrometeorology*, 12(2):245–261, 2011. ISSN 1525755X. doi: 10.1175/2010JHM1259.1.

Ćurić, M., Janc, D., and Veljović, K. Dependence of accumulated precipitation on cloud drop size distribution. *Theoretical and Applied Climatology*, 102(3):471–481, 2010. ISSN 14344483. doi: 10.1007/s00704-010-0332-5.

Dafis, S., Fierro, A., Giannaros, T. M., Kotroni, V., Lagouvardos, K., and Mansell, E. Performance Evaluation of an Explicit Lightning Forecasting System. *Journal of Geophysical Research: Atmospheres*, 123(10):5130–5148, 2018a. ISSN 21698996. doi: 10.1029/2017JD027930.

Dafis, S., Fierro, A., Giannaros, T. M., Kotroni, V., Lagouvardos, K., and Mansell, E. Performance Evaluation of an Explicit Lightning Forecasting System. *Journal of Geophysical Research: Atmospheres*, 123(10):5130–5148, 2018b. ISSN 21698996. doi: 10.1029/2017JD027930.

Davis, M. H. Two charged spherical conductors in a uniform electric field: Forces and field strength. *Quarterly Journal of Mechanics and Applied Mathematics*, 17(4):499–511, 1964. ISSN 00335614. doi: 10.1093/qjmam/17.4.499.

Dawson, G. A. and Cardell, G. R. Electrofreezing of supercooled waterdrops. *Journal of Geophysical Research*, 78 (36):8864–8866, 1973. doi: 10.1029/jc078i036p08864.

Dawson, G. A. and Winn, W. P. A model for streamer propagation. *Zeitschrift für Physik*, 183(2):159–171, 1965. ISSN 14346001. doi: 10.1007/BF01380792.

Dee, D. P., Uppala, S. M., Simmons, A. J., Berrisford, P., Poli, P., Kobayashi, S., Andrae, U., Balmaseda, M. A., Balsamo, G., Bauer, P., Bechtold, P., Beljaars, A. C., van de Berg, L., Bidlot, J., Bormann, N., Delsol, C., Dragani, R., Fuentes, M., Geer, A. J., Haimberger, L., Healy, S. B., Hersbach, H., Hólm, E. V., Isaksen, L., Kållberg, P., Köhler, M., Matricardi, M., Mcnally, A. P., Monge-Sanz, B. M., Morcrette, J. J., Park, B. K., Peubey, C., de Rosnay, P., Tavolato, C., Thépaut, J. N., and Vitart, F. The ERA-Interim reanalysis: Configuration and performance of the data assimilation system. *Quarterly Journal of the Royal Meteorological Society*, 137(656):553–597, 2011. ISSN 00359009. doi: 10.1002/qj.828.

Dementyeva, S., Ilin, N., and Mareev, E. Calculation of the lightning potential index and electric field in numerical weather prediction models. *Atmos. Ocean. Phys.*, 2015.

Dirmeyer, P. A., Cash, B. A., Kinter, J. L., Jung, T., Marx, L., Satoh, M., Stan, C., Tomita, H., Towers, P., Wedi, N., Achuthavarier, D., Adams, J. M., Altshuler, E. L., Huang, B., Jin, E. K., and Manganello, J. Simulating the diurnal cycle of rainfall in global climate models: Resolution versus parameterization. *Climate Dynamics*, 39(1-2):399–418, 2012. ISSN 09307575. doi: 10.1007/s00382-011-1127-9.

Diro, G. T., Rauscher, S. A., Giorgi, F., and Tompkins, A. M. Sensitivity of seasonal climate and diurnal precipitation over Central America to land and sea surface schemes in RegCM4. *Climate Research*, 52(1):31–48, 2012. ISSN 0936577X. doi: 10.3354/cr01049.

Dolezalek, H. Discussion of the fundamental problem of atmospheric electricity. *Pure and Applied Geophysics PAGEOPH*, 100(1):8–43, 1972. ISSN 00334553. doi: 10.1007/BF00880224.

Dudhia, J. Numerical study of convection observed during the Winter Monsoon Experiment using a mesoscale two-dimensional model. *Journal of the Atmospheric Sciences*, 46(20):3077–3107, 1989. ISSN 00224928. doi: 10.1175/1520-0469(1989)046<3077:NSOCOD>2.0.CO;2.

Dwyer, J. R., Smith, D. M., and Cummer, S. A. High-energy atmospheric physics: Terrestrial gamma-ray flashes and related phenomena. *Space Science Reviews*, 173(1-4):133–196, 2012. ISSN 00386308. doi: 10.1007/s11214-012-9894-0.

Dye, J. E. Early electrification and precipitation development in a small, isolated Montana cumulonimbus. *Journal of Geophysical Research*, 91(D1):1231–1247, 1986. ISSN 01480227. doi: 10.1029/JD091iD01p01231.

Elster, J. and Geitel, H. Zur influenz theorie der Niederschlogs - electrizitat. *Physica D*, Z-14, 1913.

Emersic, C. and Saunders, C. P. Further laboratory investigations into the Relative Diffusional Growth Rate theory of thunderstorm electrification. *Atmospheric Research*, 98(2-4):327–340, 2010. ISSN 01698095. doi: 10.1016/j.atmosres.2010.07.011.

Erpul G, D. Gabriels, D. J. The effect of wind on size and energy of small simulated raindrops: a wind tunnel study. *International Agrophysics*, 2000.

et al. Bony, S. Clouds, circulation and climate sensitivity. *Nat. Geosci.*, 8:261– 268, 2015.

Etherton, B. and Santos, P. Sensitivity of WRF forecasts for South Florida to initial conditions. *Weather and Forecasting*, 23(4):725–740, 2008. ISSN 08828156. doi: 10.1175/2007WAF2006115.1.

Fabry, F. and Zawadzki, I. Long-term radar observations of the melting layer of precipitation and their interpretation. *Journal of the Atmospheric Sciences*, 52(7):838–851, 1995. ISSN 00224928. doi: 10.1175/1520-0469(1995)052<0838:LTROOT>2.0.CO;2.

Ferrier, B. S. A double-moment multiple-phase four-class bulk ice scheme. Part I: description. *Journal of the Atmospheric Sciences*, 51(2):249–280, 1994. ISSN 00224928.

Franklin, B. A letter of Benjamin Franklin, Esq; to Mr. Peter Collinson, F. R. S. concerning an electrical kite. *Philos. Trans*, 47:Philos. Trans, 1751.

Freeman, S. W., Igel, A. L., and van den Heever, S. C. Relative sensitivities of simulated rainfall to fixed shape parameters and collection efficiencies. *Quarterly Journal of the Royal Meteorological Society*, 145(722):2181–2201, 2019. ISSN 1477870X. doi: 10.1002/qj.3550.

Gao, W., Liu, L., Li, J., and Lu, C. The Microphysical Properties of Convective Precipitation Over the Tibetan Plateau by a Subkilometer Resolution Cloud-Resolving Simulation. *Journal of Geophysical Research: Atmospheres*, 123 (6):3212–3227, 2018. ISSN 21698996. doi: 10.1002/2017JD027812.

Garcia-Carreras, L., Marsham, J. H., Parker, D. J., Bain, C. L., Milton, S., Saci, A., Salah-Ferroudj, M., Ouchene, B., and Washington, R. The impact of convective cold pool outflows on model biases in the Sahara. *Geophysical Research Letters*, 40(8):1647–1652, 2013. ISSN 00948276. doi: 10.1002/grl.50239.

Gaskell, W. and Illingworth, A. J. Charge transfer accompanying individual collisions between ice particles and its role in thunderstorm electrification. *Quarterly Journal of the Royal Meteorological Society*, 106(450):841–854, 1980. ISSN 1477870X. doi: 10.1002/qj.49710645013.

Giannaros, T. M., Kotroni, V., and Lagouvardos, K. Predicting lightning activity in Greece with the Weather Research and Forecasting (WRF) model. *Atmospheric Research*, 156:1–13, 2015. ISSN 01698095. doi: 10.1016/j.atmosres.2014.12.009.

Gilmore, M. S., Straka, J. M., and Rasmussen, E. N. Precipitation and evolution sensitivity in simulated deep convective storms: Comparisons between liquid-only and simple ice and liquid phase microphysics. *Monthly Weather Review*, 132(8):1897–1916, 2004. ISSN 00270644. doi: 10.1175/1520-0493(2004)132<1897:PAESIS>2.0.CO;2.

Goswami, B. N., Venugopal, V., Sangupta, D., Madhusoodanan, M. S., and Xavier, P. K. Increasing trend of extreme rain events over India in a warming environment. *Science*, 314(5804):1442–1445, 2006. ISSN 00368075. doi: 10.1126/science.1132027.

Goswami B.B., B. A Road Map for Improving Dry-Bias in Simulating the South Asian Monsoon Precipitation by Climate Models. *Climate Dynamics*, 2016.

Grabowski, W. W. Cloud microphysics and the tropical climate: Cloud-resolving model perspective. *Journal of Climate*, 13(13):2306–2322, 2000. ISSN 08948755. doi: 10.1175/1520-0442(2000)013<2306:CMATTC>2.0.CO;2.

Grabowski, W. W. and Smolarkiewicz, P. A Cloud Resolving Convection Parameterization for modeling the tropical convecting atmosphere. *Physica D*, 133:171–178, 1999.

Grenet, G. Essai d'explication de la charge electrique des nuages d'orages. *Extrait Ann. Geophys.*, 3, 1947.

Griffiths, R. F. and Phelps, C. T. A model of lightning initiation arising from positive corona streamer development. *J. Geophys. Res.*, 31, 1976.

Gu, G. and Zhang, C. Cloud components of the Intertropical Convergence Zone. *J. Geophys. Res.*, 107(D21), 2002.

Guo, C., & Krider, E. P. The optical power radiated by lightning return strokes. *Journal of Geophysical Research*, pages 8621–8622, 1983. doi: https://doi.org/10.1029/JC088iC13p08621.

Harrison, R. G., Nicoll, K. A., and Ambaum, M. H. On the microphysical effects of observed cloud edge charging. *Quarterly Journal of the Royal Meteorological Society*, 141(692):2690–2699, 2015. ISSN 1477870X. doi: 10.1002/qj.2554.

Harrison, R. G., Nicoll, K., Ambaum, M., Marlton, G., Aplin, K., and Lockwood, M. Precipitation modification by ionization. *phys. Rev. Lett.*, 2020.

Hazra, A., Goswami, B. N., and Chen, J. P. Role of interactions between aerosol radiative effect, dynamics, and cloud microphysics on transitions of monsoon intraseasonal oscillations. *Journal of the Atmospheric Sciences*, 70 (7):2073–2087, 2013a. ISSN 00224928. doi: 10.1175/JAS-D-12-0179.1.

Hazra, A., Goswami, B. N., and Chen, J. P. Role of interactions between aerosol radiative effect, dynamics, and cloud microphysics on transitions of monsoon intraseasonal oscillations. *Journal of the Atmospheric Sciences*, 70 (7):2073–2087, 2013b. ISSN 00224928. doi: 10.1175/JAS-D-12-0179.1.

Hazra, A., Chaudhari, H. S., Saha, S. K., Pokhrel, S., and Goswami, B. N. Progress Towards Achieving the Challenge of Indian Summer Monsoon Climate Simulation in a Coupled Ocean-Atmosphere Model. *Journal of Advances in Modeling Earth Systems*, 9(6):2268–2290, 2017. ISSN 19422466. doi: 10.1002/2017MS000966.

Hazra, A., Chaudhari, H. S., Saha, S. K., Pokhrel, S., Dutta, U., and Goswami, B. N. Role of cloud microphysics in improved simulation of the Asian monsoon quasi-biweekly mode (QBM). *Climate Dynamics*, 54(1-2):599–614, 2020. ISSN 14320894. doi: 10.1007/s00382-019-05015-5.

Heckman, S. J. and Williams, E. R. Corona envelopes and lightning currents. *Journal of Geophysical Research*, 94 (D11), 1989. ISSN 01480227. doi: 10.1029/jd094id11p13287.

Heymsfield, A. J., Bansemer, A., Schmitt, C., Twohy, C., and Poellot, M. R. Effective ice particle densities derived from aircraft data. *Journal of the Atmospheric Sciences*, 61(9):982–1003, 2004. ISSN 00224928. doi: 10.1175/1520-0469(2004)061<0982:EIPDDF>2.0.CO;2.

Hobbs, P. V. *Ice Physics*. Oxford Press, 837 pp edition, 1974.

Hong, S.-Y., Lim, K.-S. S., Lee, Y.-H., Ha, J.-C., Kim, H.-W., Ham, S.-J., and Dudhia, J. Evaluation of the WRF Double-Moment 6-Class Microphysics Scheme for Precipitating Convection. *Advances in Meteorology*, 2010:1–10, 2010. ISSN 1687-9309. doi: 10.1155/2010/707253.

Houghton, J. G. On precipitation mechanisms and their artificial modification. *J. Appl. Meteor.*, 7:851–859, 1968.

Houze Jr., R. a. Stratiform precipitation in the tropics: A meteorological paradox? *Bull. Amer. Meterol. Soc.*, 78(10): 2179–2196, 1997.

Iguchi, T., Kozu, T., Kwiatkowski, J., Meneghini, R., Awaka, J., and Okamoto, K. Uncertainties in the rain profiling algorithm for the trmm precipitation radar. *Journal of the Meteorological Society of Japan*, 87 A:1–30, 2009. ISSN 00261165. doi: 10.2151/jmsj.87A.1.

Illingworth, A. J. and Caranti, J. M. Ice Conductivity Restraints on the Inductive Theory of Thunderstorm Electrification. pages 196–201, 1984.

Illingworth , A. J. and Latham, J. Calculation of electric field growth, field structure and charge distribution in thunderstorms. *Q. J. R. Meteorol. Soc*, 103, 1977.

Islam, T., Rico-Ramirez, M. A., Han, D., Srivastava, P. K., and Ishak, A. M. Performance evaluation of the TRMM precipitation estimation using ground-based radars from the GPM validation network. *Journal of Atmospheric and Solar-Terrestrial Physics*, 77:194–208, 2012. ISSN 13646826. doi: 10.1016/j.jastp.2012.01.001.

Jankov, I., Gallus, W. A., Segal, M., and Koch, S. E. Influence of initial conditions on the WRF-ARW Model QPF response to physical parameterization changes. *Weather and Forecasting*, 22(3):501–519, 2007. ISSN 08828156. doi: 10.1175/WAF998.1.

Jayaratne, E. R. and Saunders, C. P. The ' rain gush', lightning, and the lower positive charge center in thunderstorms. *Journal of Geophysical Research*, 89(D7), 1984. ISSN 01480227. doi: 10.1029/jd089id07p11816.

Jeong, J. H., Walther, A., Nikulin, G., Chen, D., and Jones, C. Diurnal cycle of precipitation amount and frequency in Sweden: Observation versus model simulation. *Tellus, Series A: Dynamic Meteorology and Oceanography*, 63(4): 664–674, 2011. ISSN 02806495. doi: 10.1111/j.1600-0870.2011.00517.x.

Joss, J. & Waldvogel, A. Ein Spektrograph für Niederschlagstropfen mit automatischer Auswertung. *Pure and Applied Geophysics PAGEOPH*, 68:240–246, 1967.

Kamra, A. K. Modification of some microphysical properties in the highly electrified regions of thundercloud. *Archives for Meteorology, Geophysics, and Bioclimatology Series A*, 34(1):37–50, 1985. ISSN 14365065. doi: 10.1007/BF02267394.

Kamra, A. K. and Ahire, D. V. Wind-tunnel studies of the shape of charged and uncharged water drops in the absence or presence of an electric field. *Atmospheric Research*, 23(2):117–134, 1989. ISSN 01698095. doi: 10.1016/0169-8095(89)90003-3.

Kamra, A. K. and Vonnegut, B. A Laboratory Investigation of the Effect of Particle Collisions on the Generation of Electric Fields in Thunderstorms. *Journal of the Atmospheric Sciences*, 28(4):640–644, 1971. ISSN 0022-4928. doi: 10.1175/1520-0469(1971)028<0640:aliote>2.0.co;2.

KAMRA AK. Effect of Electric Field on Charge Separation By the Falling Precipitation Mechanism in Thunderclouds. *Journal of the Atmospheric Sciences*, 27(8):1182–1185, 1970. ISSN 00224928. doi: 10.1175/1520-0469(1971)028<0819:cooefo>2.0.co;2.

Kendon, E. J., Roberts, N. M., Senior, C. A., and Roberts, M. J. Realism of rainfall in a very high-resolution regional climate model. *Journal of Climate*, 25(17):5791–5806, 2012. ISSN 08948755. doi: 10.1175/JCLI-D-11-00562.1.

Khain, A., Pokrovsky, A., and Sednev, I. Some effects of cloud-aerosol interaction on cloud microphysics structure and precipitation formation: Numerical experiments with a spectral microphysics cloud ensemble model. *Atmospheric Research*, 52(3):195–220, 1999. ISSN 01698095. doi: 10.1016/S0169-8095(99)00027-7.

Khain, A., Ovtchinnikov, M., Pinsky, M., Pokrovsky, A., and Krugliak, H. Notes on the state-of-the-art numerical modeling of cloud microphysics. *Atmospheric Research*, 55(3-4):159–224, 2000. ISSN 01698095. doi: 10.1016/S0169-8095(00)00064-8.

Khain, A., Arkhipov, V., Pinsky, M., Feldman, Y., and Ryabov, Y. Rain enhancement and fog elimination by seeding with charged droplets. Part I: Theory and numerical simulations. *Journal of Applied Meteorology*, 43(10):1513–1529, 2004. ISSN 08948763. doi: 10.1175/JAM2131.1.

Khain, A., Rosenfeld, D., and Pokrovsky, A. Aerosol impact on the dynamics and microphysics of deep convective clouds. *Quarterly Journal of the Royal Meteorological Society*, 131(611):2639–2663, 2005. ISSN 00359009. doi: 10.1256/qj.04.62.

Kollias, P., B. A. Albrecht, and F. Marks, J. Why Mie? Accurateobservations of vertical air velocities and raindrops using a cloud radar. *Bull. Am. Meteorol. Soc*, 83:1471 – 1483, 2002. doi: doi:10.2151/jmsj.84A.

Konwar, M., Maheskumar, R. S., Das, S. K., and Morwal, S. B. Nature of light rain during presence and absence of bright band. *Journal of Earth System Science*, 121(4):947–961, 2012. ISSN 02534126. doi: 10.1007/s12040-012-0202-x.

Konwar, M., Das, S. K., Deshpande, S. M., Chakravarty, K., and Goswami, B. N. Microphysics of clouds and rain over the Western Ghat. *Journal of Geophysical Research*, 119(10):6140–6159, 2014. ISSN 21562202. doi: 10.1002/2014JD021606.

Kovačević, N. and Ćurić, M. Precipitation sensitivity to the mean radius of drop spectra: Comparison of single-and double-moment bulk microphysical schemes. *Atmosphere*, 6(4):451–473, 2015. ISSN 20734433. doi: 10.3390/atmos6040451.

Krehbiel, P. R., Brook, M., Lhermitte, R. L., and Lennon, C. L. Lightning charge structure in thunderstorms. *Proc. Conf. on Atmos. Elec.*, pages 408–411, 1983.

Krehbiel, P. R., M. Brook and McCrory, R. A. An analysis of the charge structure of lighting discharges to ground. *J. Geophys. Res*, 84:2432–2456, 1979.

Kulkarni, J. R., Maheskumar, R. S., Morwal, S. B., Padma Kumari, B., Konwar, M., Deshpande, C. G., Joshi, R. R., Bhalwankar, R. V., Pandithurai, G., Safai, P. D., Narkhedkar, S. G., Dani, K. K., Nath, A., Nair, S., Sapre, V. V., Puranik, P. V., Kandalgaonkar, S. S., Mujumdar, V. R., Khaladkar, R. M., Vijayakumar, R., Prabha, T. V., and Goswami, B. N. The cloud aerosol interaction and precipitation enhancement experiment (CAIPEEX): Overview and preliminary results. *Current Science*, 102(3):413–425, 2012. ISSN 00113891.

Lapshin, V. B., Yablokov, M. Y., and Palej, A. A. Vapor pressure over a charged drop. *Zhurnal Fizicheskoj Khimii*, 76 (10):1901–1904, 2002. ISSN 00444537.

LATHAM, J. The electrification of thunderstorms. *Quarterly Journal of the Royal Meteorological Society*, 107(452): 277–298, 1981. ISSN 00359009. doi: 10.1256/smsqj.45201.

Latham, J. and Mason, B. J. Electric charging of hail pellets in a polarizing electric field. *Proc. R. Soc. Lond*, A 266, 1962.

Lau, K.-M. and Wu, H. T. Warm rain processes over tropical oceans and climate implications. *Geophys. Res. Lett.*, 30(24), 2003.

Levin, Z. and Ziv, A. The electrification of thunderclouds and the rain gush. *Journal of Geophysical Research*, 79(18): 2699–2704, 1974. ISSN 0148-0227. doi: 10.1029/jc079i018p02699.

Lhermitte, R. The use of a special pulse Doppler radar in measurement of particles fall velocities. *Proc. Eighth Wea. Radar Conf., Boston, Amer. Meteor. Soc*, 1960.

Li, J. L., Lee, W. L., Waliser, D. E., Neelin, J. D., Stachnik, J. P., and Lee, T. Cloud-precipitation-radiation-dynamics interaction in global climate models: A snow and radiation interaction sensitivity experiment. *Journal of Geophysical Research*, 119(7):3809–3824, 2014. ISSN 21562202. doi: 10.1002/2013JD021038.

Lin, Y. L., Farley, R. D., and Orville, H. D. Bulk parameterization of the snow field in a cloud model. *Journal of Climate & Applied Meteorology*, 22(6):1065–1092, 1983. doi: 10.1175/1520-0450(1983)022<1065:BPOTSF>2.0.CO;2.

Liu, C., Williams, E. R., Zipser, E. J., and Burns, G. Diurnal variations of global thunderstorms and electrified shower clouds and their contribution to the global electrical circuit. *Journal of the Atmospheric Sciences*, 67(2):309–323, 2010. ISSN 00224928. doi: 10.1175/2009JAS3248.1.

Loeb, L. B. A tentative explanation of the electrical field effect on the freezing of supercooled water drops. *Journal of Geophysical Research*, 68(15):4475–4476, 1963. ISSN 0148-0227. doi: 10.1029/jz068i015p04475.

Loeb, L. B. The mechanisms of stepped and dart leaders in cloud-to-ground lightning strokes. *Journal of Geophysical Research*, 71(20):4711–4721, 1966. ISSN 0148-0227. doi: 10.1029/jz071i020p04711.

Löffler-Mang, M. and Joss, J. An optical disdrometer for measuring size and velocity of hydrometeors. *Journal of Atmospheric and Oceanic Technology*, 17(2):130–139, 2000. ISSN 07390572. doi: 10.1175/1520-0426(2000)017<0130:AODFMS>2.0.CO;2.

Lohmann, U. and Diehl, K. Sensitivity studies of the importance of dust ice nuclei for the indirect aerosol effect on stratiform mixedâphase clouds. *J. Atmos. Sci.*, 63(3):968–982, 2006.

Lohmann, U. and Feichter, J. Global indirect aerosol effects: A review. *Atmos. Chem. Phys.*, 5:715–737, 2005.

Longmire, C. L. On the Electromagnetic Pulse Produced by Nuclear Explosions. *IEEE Transactions on Electromagnetic Compatibility*, EMC-20(1):3–13, 1978. ISSN 1558187X. doi: 10.1109/TEMC.1978.303688.

Lord, R. The Influence of Electricity on Colliding Water Drops. *Proc. Roy. Soc. London*, 28:406–409, 1879.

Lyu, F., Cummer, S. A., and McTague, L. Insights into high peak current in-cloud lightning events during thunderstorms. *Geophysical Research Letters*, 42(16):6836–6843, 2015. ISSN 19448007. doi: 10.1002/2015GL065047.

MacGorman, D. R., David Rust, W., Schuur, T. J., Biggerstaff, M. I., Straka, J. M., Ziegler, C. L., Mansell, E. R., Bruning, E. C., Kuhlman, K. M., Lund, N. R., Biermann, N. S., Payne, C., Carey, L. D., Krehbiel, P. R., Rison, W., Eack, K. B., and Beasley, W. H. TELEX The Thunderstorm Electrification and Lightning Experiment. *Bulletin of the American Meteorological Society*, 89(7):997–1013, 2008. ISSN 00030007. doi: 10.1175/2007BAMS2352.1.

Malan, D. J. and Schonland, B. F. J. The distribution of electricity in thunderclouds. *Proceedings of the Royal Society of London. Series A. Mathematical and Physical Sciences*, 209(1097):158–177, 1951. ISSN 0080-4630. doi: 10.1098/rspa.1951.0195.

Mandal, G. and Pradeep Kumar, P. A laboratory study of ice nucleation due to electrical discharge. *Atmospheric Research*, 61(2):115–123, 2002. ISSN 01698095. doi: 10.1016/S0169-8095(01)00129-6.

Mansell, E. R., Ziegler, C. L., , and Bruning, E. C. Simulated electrification of a small thunderstorm with twoâmoment bulk microphysics. *J. Atmos. Sci.*, 2010.

Mapes, B. E. Gregarious tropical convection. *J. Atmos. Sci.*, 50:2026–2037, 1993.

Marisaldi, M., Fuschino, F., Tavani, M., Dietrich, S., Price, C., Galli, M., Pittori, C., Verrecchia, F., Mereghetti, S., Cattaneo, P. W., Colafrancesco, S., Argan, A., Labanti, C., Longo, F., Del Monte, E., Barbiellini, G., Giuliani, A., Bulgarelli, A., Campana, R., Chen, A., Gianotti, F., Giommi, P., Lazzarotto, F., Morselli, A., Rapisarda, M., Rappoldi, A., Trifoglio, M., Trois, A., and Vercellone, S. Properties of terrestrial gamma ray flashes detected by AGILE MCAL below 30 MeV. *Journal of Geophysical Research A: Space Physics*, 119(2):1337–1355, 2014. ISSN 21699402. doi: 10.1002/2013JA019301.

Marshall, T. C. and Winn, W. P. Measurements of charged precipitation in a New Mexico thunderstorm: lower positive charge centers. *Journal of Geophysical Research*, 87(C9):7141–7157, 1982. ISSN 01480227. doi: 10.1029/JC087iC09p07141.

Marsham, J. H., Dixon, N. S., Garcia-Carreras, L., Lister, G. M., Parker, D. J., Knippertz, P., and Birch, C. E. The role of moist convection in the West African monsoon system: Insights from continental-scale convection-permitting simulations. *Geophysical Research Letters*, 40(9):1843–1849, 2013. ISSN 00948276. doi: 10.1002/grl.50347.

Mason, B. J. *The Physics of Cloud*. Oxford, Londo, 1971.

Mattos, E. V., Machado, L. A., Williams, E. R., and Albrecht, R. I. Polarimetric radar characteristics of storms with and without lightning activity. *Journal of Geophysical Research*, 121(23):14,201–14,220, 2016. ISSN 21562202. doi: 10.1002/2016JD025142.

Mecikalski, R. M. and Carey, L. D. Radar Reflectivity and Altitude Distributions of Lightning Flashes as a Function of Three Main Storm Types. *Journal of Geophysical Research: Atmospheres*, 123(22):12,814–12,828, 2018. ISSN 21698996. doi: 10.1029/2018JD029238.

Mhatre, S., Deshmukh, S., and Thaokar, R. M. Electrocoalescence of a drop pair. *Physics of Fluids*, 27(9), 2015. ISSN 10897666. doi: 10.1063/1.4931592.

Min, K. H., Choo, S., Lee, D., and Lee, G. Evaluation of WRF cloud microphysics schemes using radar observations. *Weather and Forecasting*, 30(6):1571–1589, 2015. ISSN 15200434. doi: 10.1175/WAF-D-14-00095.1.

Mlawer, E. J., Taubman, S. J., Brown, P. D., Iacono, M. J., and Clough, S. A. Radiative transfer for inhomogeneous atmospheres: RRTM, a validated correlated-k model for the longwave. *Journal of Geophysical Research D: Atmospheres*, 102(14):16663–16682, 1997. ISSN 01480227. doi: 10.1029/97jd00237.

Mo, Q., Helsdon, J. H., and Winn, W. P. Aircraft observations of the creation of lower positive charges in thunderstorms. *Journal of Geophysical Research Atmospheres*, 107(22):ACL 4–1–ACL 4–15, 2002. ISSN 01480227. doi: 10.1029/2002JD002099.

Montopoli M, Marzano FS, V. G. Analysis and synthesis of raindrop size distribution time series from disdrometer data. *IEEE Transactions on Geoscience and Remote Sensing*, pages 466–478, 2008.

Moore, C. B. An Assessment of Thunderstorm Electrification Mechanisms. *Electrical Processes in Atmospheres*, pages 333–352, 1976. doi: 10.1007/978-3-642-85294-7$_5$0.

Moore, C. B., Vonnegut, B., Machado, J. A., and Survilas, H. J. Radar observations of rain gushes following overhead lightning strokes. *Journal of Geophysical Research*, 67(1):207–220, 1962. doi: 10.1029/jz067i001p00207.

Moore, C. B., Vonnegut, B., Vrablik, E. A., and McCaig, D. A. Gushes of Rain and Hail After Lightning. *Journal of the Atmospheric Sciences*, 21(6):646–665, 1964. ISSN 0022-4928. doi: 10.1175/1520-0469(1964)021<0646:gorama>2.0.co;2.

Moore, C. B., Eack, K. B., Aulich, G. D., and Rison, W. Energetic radiation associated with lightning stepped-leaders. *Geophysical Research Letters*, 28(11):2141–2144, 2001. ISSN 00948276. doi: 10.1029/2001GL013140.

Morrison, H. and Gettelman, A. A new two-moment bulk stratiform cloud microphysics scheme in the community atmosphere model, version 3 (CAM3). Part I: Description and numerical tests. *Journal of Climate*, 21(15):3642–3659, 2008. ISSN 08948755. doi: 10.1175/2008JCLI2105.1.

Morrison, H. and Milbrandt, J. A. Parameterization of cloud microphysics based on the prediction of bulk ice particle properties. Part I: Scheme description and idealized tests. *Journal of the Atmospheric Sciences*, 72(1):287–311, 2015. ISSN 15200469. doi: 10.1175/JAS-D-14-0065.1.

Morrison, H., Curry, J. A., and Khvorostyanov, V. A New Double-Moment Microphysics Parameterization for Application in Cloud and Climate Models . Part I : Description. *Journal of the Atmospheric Sciences*, 62(6):1665–1677, 2005.

Morrison, H., Thompson, G., and Tatarskii, V. Impact of cloud microphysics on the development of trailing stratiform precipitation in a simulated squall line: Comparison of one- and two-moment schemes. *Monthly Weather Review*, 137(3):991–1007, 2009. ISSN 00270644. doi: 10.1175/2008MWR2556.1.

Morrison, H., Tessendorf, S. A., Ikeda, K., and Thompson, G. Sensitivity of a simulated midlatitude squall line to parameterization of raindrop breakup. *Monthly Weather Review*, 140(8):2437–2460, 2012. ISSN 00270644. doi: 10.1175/MWR-D-11-00283.1.

Mudiar, D., Pawar, S. D., Hazra, A., Konwar, M., Gopalakrishnan, V., Srivastava, M. K., and Goswami, B. N. Quantification of Observed Electrical Effect on the Raindrop Size Distribution in Tropical Clouds. *Journal of Geophysical Research: Atmospheres*, 123(9):4527–4544, 2018. ISSN 21698996. doi: 10.1029/2017JD028205.

Muller-Hillebrand, D. Charge generation in Thunderstorms by collision of ice crystals with graupel, falling through a vertical electric field. *Tellus*, 6(4):367–381, 1954. ISSN 0040-2826. doi: 10.3402/tellusa.v6i4.8757.

Nielsen, J. K., Maus, C., Rzesanke, D., and Leisner, T. Charge induced stability of water droplets in subsaturated environment. *Atmospheric Chemistry and Physics Discussions*, 10(11):25743–25757, 2010. doi: 10.5194/acpd-10-25743-2010.

Niu, S., Jia, X., Sang, J., Liu, X., Lu, C., and Liu, Y. Distributions of raindrop sizes and fall velocities in a semiarid plateau climate: Convective versus stratiform rains. *Journal of Applied Meteorology and Climatology*, 49(4):632–645, 2010. ISSN 15588424. doi: 10.1175/2009JAMC2208.1.

Ochs, H. T. and Czys, R. R. Charge effects on the coalescence of water drops in free fall. *Nature*, 327(6123):606–608, 1987. ISSN 00280836. doi: 10.1038/327606a0.

Orville, H. D., Kopp, F. J., and Myers, C. G. The dynamics and thermodynamics of precipitation loading. *Pure and Applied Geophysics PAGEOPH*, 113(1):983–1004, 1975. ISSN 00334553. doi: 10.1007/BF01592970.

Orville, R. E. A High-Speed Time-Resolved Spectroscopic Study of the Lightning Return Stroke: Part II. A Quantitative Analysis. *Journal of the Atmospheric Sciences*, 25(5):839–851, 1968. ISSN 0022-4928. doi: 10.1175/1520-0469(1968)025<0839:ahstrs>2.0.co;2.

Palucki, J. L., Biggerstaff, M. I., MacGorman, D. R., and Schuur, T. Comparison between low-flash and non-lightning-producing convective areas within a mature mesoscale convective system. *Weather and Forecasting*, 26(4):468–486, 2011. ISSN 08828156. doi: 10.1175/WAF-D-10-05012.1.

Pérez Hortal, A. A., García, S. E., and Caranti, G. M. Droplet charging by high voltage discharges and its influence on precipitation enhancement. *Atmospheric Research*, 108:115–121, 2012. ISSN 01698095. doi: 10.1016/j.atmosres.2012.02.006.

Peters, G., B. Fischer, H. Münster, M. Clemens and Wagner, A. Profiles of raindrop size distributions by micro rain radars. *J. Appl. Meteorol*, 44:1930–1949, 2005.

Petersen, D., Bailey, M., Beasley, W. H., and Hallett, J. A brief review of the problem of lightning initiation and a hypothesis of initial lightning leader formation. *Journal of Geophysical Research Atmospheres*, 113(17), 2008. ISSN 01480227. doi: 10.1029/2007JD009036.

Piepgrass, M. V., Krider, E. P., and Moore, C. B. Lightning and surface rainfall during Florida thunderstorms. *Journal of Geophysical Research*, 87(C13):11193, 1982. ISSN 0148-0227. doi: 10.1029/jc087ic13p11193.

Pinsky, M., A. P. Khain and Shapiro, M. Collision efficiency of drops in a wide range of Reynolds numbers: Effects of pressure on spectrum evolution. *J. Atmos.Sci.*, 58:742–764, 2011.

Prein, A. F., Langhans, W., Fosser, G., Ferrone, A., Ban, N., Goergen, K., Keller, M., Tölle, M., Gutjahr, O., Feser, F., Brisson, E., Kollet, S., Schmidli, J., Van Lipzig, N. P., and Leung, R. A review on regional convection-permitting climate modeling: Demonstrations, prospects, and challenges. *Reviews of Geophysics*, 53(2):323–361, 2015. ISSN 19449208. doi: 10.1002/2014RG000475.

Price, C. and Federmesser, B. Lightning-rainfall relationships in Mediterranean winter thunderstorms. *Geophysical Research Letters*, 33(7), 2006. ISSN 00948276. doi: 10.1029/2005GL024794.

Pruppacher, H. The effect of an external electric field on the supercooling of water drops. *Journal of Geophysical Research*, 68(15):4463–4474, 1963.

Pruppacher H.R., J. K. *Microphysics of Clouds and Precipitation(second edition)*. 1996.

Rasmussen, K. L., Chaplin, M. M., Zuluaga, M. D., and Houze, R. A. Contribution of extreme convective storms to rainfall in South America. *Journal of Hydrometeorology*, 17(1):353–367, 2016. ISSN 15257541. doi: 10.1175/JHM-D-15-0067.1.

Reynolds, S. E., Brook, M., and Gourley, M. F. Thunderstorm Charge Separation. *Journal of Meteorology*, 14(5): 426–436, 1957. ISSN 0095-9634. doi: 10.1175/1520-0469(1957)014<0426:tcs>2.0.co;2.

RICHARDS CN and DAWSON GA. Hydrodynamic instability of water drops falling at terminal velocity in vertical electric fields. *J Geophys Res*, 76(15):3445–3455, 1971. doi: 10.1029/jc076i015p03445.

Rison, W., Krehbiel, P. R., Stock, M. G., Edens, H. E., Shao, X. M., Thomas, R. J., Stanley, M. A., and Zhang, Y. Observations of narrow bipolar events reveal how lightning is initiated in thunderstorms. *Nature Communications*, 7, 2016. ISSN 20411723. doi: 10.1038/ncomms10721.

Roble,R.G., and Tzur, I. *The earth s Electrical Environments*. Natl. Acad. Sci. press, Washington D.C, 1986.

Rogers R. R. and M. K. Yau. A short course in cloud physics. 1989.

Rose, T., Crewell, S., Löhnert, U., and Simmer, C. A network suitable microwave radiometer for operational monitoring of the cloudy atmosphere. *Atmospheric Research*, 75(3):183–200, 2005. ISSN 01698095. doi: 10.1016/j.atmosres.2004.12.005.

Rosenfeld, D. and Woodley, W. L. Closing the 50-year circle: from cloud seeding to space and back to climate change through precipitation physics. *Cloud Systems, Hurricanes, and the Tropical Rainfall Measuring Mission (TRMM)*, (January 2003):234, 2003.

Rosenfeld, D. TRMM observed first direct evidence of smoke from forest fires inhibiting rainfall. *Geophysical Research Letters*, 26(20):3105–3108, 1999. ISSN 00948276. doi: 10.1029/1999GL006066.

Rosenfeld, D. Suppression of rain and snow by urban and industrial air pollution. *Science*, 287(5459):1793–1796, 2000. ISSN 00368075. doi: 10.1126/science.287.5459.1793.

Rosenfeld, D., Lahav, R., Khain, A., and Pinsky, M. The role of sea spray in cleansing air pollution over ocean via cloud processes. *Science*, 297(5587):1667–1670, 2002. ISSN 00368075. doi: 10.1126/science.1073869.

Rutledge, S. A. and Houze, R. A. A Diagnostic Modelling Study of the Trailing Stratiform Region of a Midlatitude Squall Line, 1987. ISSN 0022-4928.

Rutledge, S. A., and Jr., R. A. H. A diagnostic modeling study of the trailing stratiform region of a midlatitude squall line. . *J. Atmos. Sci.*, 44:2640–2656, 1987.

Ryan, R. T. and Vonnegut, B. Miniature whirlwinds produced in the laboratory by high-voltage electrical discharges. *Science*, 168(3937):1349–1351, 1970. ISSN 00368075. doi: 10.1126/science.168.3937.1349.

Salt, R. W. Effect of electrostatic field on freezing of supercooled water and insects. *Science*, 133(3451):458–459, 1961. ISSN 00368075. doi: 10.1126/science.133.3451.458.

Sarma, A. C., Deshamukhya, A., Narayana Rao, T., and Sharma, S. A study of raindrop size distribution during stratiform rain and development of its parameterization scheme in the framework of multi-parameter observations. *Meteorological Applications*, 23(2):254–268, 2016. ISSN 14698080. doi: 10.1002/met.1551.

Sartor, J. D. Some electrostatic cloud-droplet collision efficiencies. *Journal of Geophysical Research*, 65(7):1953–1957, 1960. ISSN 0148-0227. doi: 10.1029/jz065i007p01953.

Saunders, C. P. and Peck, S. L. Laboratory studies of the influence of the rime accretion rate on charge transfer during crystal/graupel collisions. *Journal of Geophysical Research Atmospheres*, 103(D12):13949–13956, 1998. ISSN 01480227. doi: 10.1029/97JD02644.

Saunders, C. P., Bax-Norman, H., Emersic, C., Avila, E. E., and Castellano, N. E. Laboratory studies of the effect of cloud conditions on graupel/crystal charge transfer in thunderstorm electrification. *Quarterly Journal of the Royal Meteorological Society*, 132(621):2653–2673, 2006. ISSN 00359009. doi: 10.1256/qj.05.218.

Schaefer, V. J. The Generation of Large Numbers of Ice Crystals in an Electric Field. *Journal of Applied Meteorology*, 7(3):452–455, 1968. ISSN 0021-8952. doi: 10.1175/1520-0450(1968)007<0452:tgolno>2.0.co;2.

Schlamp, R. J., Grover, S. N., Pruppacher, H. R., and Hamielec, A. E. Numerical Investigation of the Effect of Electric Charges and Vertical External Electric Fields on the Collision Efficiency of Cloud Drops. *Journal of the Atmospheric Sciences*, 33(9):1747–1755, 1976. ISSN 00224928. doi: 10.1175/1520-0469(1976)033<1747:ANIOTE>2.0.CO;2.

Schlamp, R. J., Grover, S. N., Pruppacher, H. R., and Hamielec, A. E. A Numerical Investigation of the Effect of Electric Charges and Vertical External Electric Fields an the Collision Efficiency of Cloud Drops: Part II. *Journal of the Atmospheric Sciences*, 36(2):339–349, 1979. ISSN 0022-4928. doi: 10.1175/1520-0469(1979)036<0339:aniote>2.0.co;2.

Schonland, B. F. J. The interchange of electricity between thunderclouds and the Earth. *Proceedings of the Royal Society of London. Series A, Containing Papers of a Mathematical and Physical Character*, 118(779):252–262, 1928. ISSN 0950-1207. doi: 10.1098/rspa.1928.0049.

Schultz, C. J., Lang, T. J., Bruning, E. C., Calhoun, K. M., Harkema, S., and Curtis, N. Characteristics of Lightning Within Electrified Snowfall Events Using Lightning Mapping Arrays. *Journal of Geophysical Research: Atmospheres*, 123(4):2347–2367, 2018. ISSN 21698996. doi: 10.1002/2017JD027821.

Schumacher, C. and Houze, R. A. Stratiform rain in the tropics as seen by the TRMM precipitation radar. *Journal of Climate*, 16(11):1739–1756, 2003. ISSN 08948755. doi: 10.1175/1520-0442(2003)016<1739:SRITTA>2.0.CO;2.

Seela, B. K., Janapati, J., Lin, P. L., Wang, P. K., and Lee, M. T. Raindrop Size Distribution Characteristics of Summer and Winter Season Rainfall Over North Taiwan. *Journal of Geophysical Research: Atmospheres*, 123(20):11,602–11,624, 2018. ISSN 21698996. doi: 10.1029/2018JD028307.

Seifert, A. and Beheng, K. D. A two-moment cloud microphysics parameterization for mixed-phase clouds. Part 1: Model description. *Meteorology and atmospheric physics*, 92(1):45–66, 2006. URL http://dx.doi.org/10.1007/s00703-005-0112-4.

Seliga, T. A. and Bringi, V. N. Differential reflectivity and differential phase shift: Applications in radar meteorology, 1978. ISSN 1944799X.

Shahrban, M., Walker, J. P., Wang, Q. J., Seed, A., and Steinle, P. An evaluation of numerical weather prediction based rainfall forecasts. *Hydrological Sciences Journal*, 61(15):2704–2717, 2016. ISSN 21503435. doi: 10.1080/02626667.2016.1170131.

Sharma, S., Konwar, M., Sarma, D. K., Kalapureddy, M. C., and Jain, A. R. Characteristics of rain integral parameters during tropical convective, transition, and stratiform rain at Gadanki and its application in rain retrieval. *Journal of Applied Meteorology and Climatology*, 48(6):1245–1266, 2009. ISSN 15588424. doi: 10.1175/2008JAMC1948.1.

Shrestha, D. L., Robertson, D. E., Wang, Q. J., Pagano, T. C., and Hapuarachchi, H. A. Evaluation of numerical weather prediction model precipitation forecasts for short-term streamflow forecasting purpose. *Hydrology and Earth System Sciences*, 17(5):1913–1931, 2013. ISSN 10275606. doi: 10.5194/hess-17-1913-2013.

Simpson, G. C. and Scrase, F. J. The distribution of electricity in thunderclouds. *Proceedings of the Royal Society of London. Series A. Mathematical and Physical Sciences*, 209(1097):158–177, 1937. ISSN 0080-4630. doi: 10.1098/rspa.1951.0195.

Singla, V., Mukherjee, S., Kashikar, A. S., Safai, P. D., and Pandithurai, G. Black carbon: source apportionment and its implications on CCN activity over a rural region in Western Ghats, India. *Environmental Science and Pollution Research*, 26(7):7071–7081, 2019. ISSN 16147499. doi: 10.1007/s11356-019-04162-w.

Smith, J. A., Hui, E., Steiner, M., Baeck, M. L., Krajewski, W. F., and Ntelekos, A. A. Variability of rainfall rate and raindrop size distributions in heavy rain. *Water Resources Research*, 45(4), 2009. ISSN 00431397. doi: 10.1029/2008WR006840.

Soula, S. and Chauzy, S. Multilevel measurement of the electric field underneath a thundercloud 2. dynamical evolution of ground space charge. *, J. Geophys. Res.*, 1991.

Standler, R. B. and Winn, W. P. Effects of coronae on electric field beneath thunderstorms. *Q. J. R. Meteorol. Soc.*, 1979.

Stoelinga, M. T. Simulated equivalent reflectivity factor as currently formulated in RIP: Description and possible improvements. *Technical Report*, pages 1–5, 2005. URL http://www.atmos.washington.edu/ stoeling/RIP_sim_ref.pdf.

Stolzenburg, M., Rust, W. D., and Marshall, T. C. Electrical structure in thunderstorm convective regions 2. Isolated storms. *Journal of Geophysical Research Atmospheres*, 103(D12):14079–14096, 1998. ISSN 01480227. doi: 10.1029/97JD03547.

Takahashi, T. Riming Electrification as a Charge Generation Mechanism in Thunderstorms. *Journal of the Atmospheric Sciences*, 35(8):1536–1548, 1978. ISSN 0022-4928. doi: 10.1175/1520-0469(1978)035<1536:reaacg>2.0.co;2.

Tao, W. K., Chen, J. P., Li, Z., Wang, C., and Zhang, C. Impact of aerosols on convective clouds and precipitation. *Reviews of Geophysics*, 50(2), 2012. ISSN 87551209. doi: 10.1029/2011RG000369.

Taylor, G. Disintegration of pairs of water drops in an electric field. *Proceedings of the Royal Society of London. Series A. Mathematical and Physical Sciences*, 295(1440):84–97, 1966. ISSN 0080-4630. doi: 10.1098/rspa.1966.0227.

Testik, F. Y. and Barros, A. P. Toward elucidating the microstructure of warm rainfall: A survey. *Reviews of Geophysics*, 45(2), 2007. ISSN 87551209. doi: 10.1029/2005RG000182.

Testik, F. Y. and Pei, B. Wind effects on the shape of raindrop size distribution. *Journal of Hydrometeorology*, 18(5): 1285–1303, 2017. ISSN 15257541. doi: 10.1175/JHM-D-16-0211.1.

Thompson, G., Rasmussen, R. M., and Manning, K. Explicit forecasts of winter precipitation using an improved bulk microphysics scheme. Part I: Description and sensitivity analysis. *Monthly Weather Review*, 132:519–542, 2004. ISSN 0027-0644.

Thompson, G., Field, P. R., Rasmussen, R. M., and Hall, W. D. Explicit forecasts of winter precipitation using an improved bulk microphysics scheme. Part II: Implementation of a new snow parameterization . *Monthly Weather Review*, 136:5095–5115, 2008.

Tokay, A., Kruger, A., and Krajewski, W. F. Comparison of drop size distribution measurements by impact and optical disdrometers. *Journal of Applied Meteorology*, 40(11):2083–2097, 2001. ISSN 08948763. doi: 10.1175/1520-0450(2001)040<2083:CODSDM>2.0.CO;2.

Tokay, A. and Short, D. A. Evidence from tropical raindrop spectra of the origin of rain from stratiform versus convective clouds. *Journal of Applied Meteorology*, 35(3):355–371, 1996. ISSN 08948763. doi: 10.1175/1520-0450(1996)035<0355:EFTRSO>2.0.CO;2.

Tran, M. D. and Rakov, V. A. A study of the ground-attachment process in natural lightning with emphasis on its breakthrough phase. *Scientific Reports*, 7(1), 2017. ISSN 20452322. doi: 10.1038/s41598-017-14842-7.

TWOMEY, S. A., PIEPGRASS, M., and WOLFE, T. L. An assessment of the impact of pollution on global cloud albedo. *Tellus B*, 36 B(5):356–366, 1984. ISSN 16000889. doi: 10.1111/j.1600-0889.1984.tb00254.x.

Tyagi, A. Thunderstorm climatology over Indian region. *Mausam*, 2(April):189–212, 2007.

Vonnegut, B. Possible mechanism for the formation of thunderstorm electricity. *Bull. Am Meteorol. Soc.*, 34:378–381, 1953.

Vonnegut, B. Proceedings International Conference on Atmospheric Electricity, Geophys. Res. Pap. No. 42, Air Force Cambridge Research Centre, Bedford, Mass. page p 169, 1955.

Vonnegut, B., Moore, C. B., Semonin, R. G., Bullock, J. W., Staggs, D. W., and Bradley, W. E. Effect of atmospheric space charge on initial electrification of cumulus clouds. *Journal of Geophysical Research*, 67(10):3909–3922, 1962. doi: 10.1029/jz067i010p03909.

Vonnegut, B. Electrical theory of tornadoes. *Journal of Geophysical Research*, 65(1):203–212, 1960. ISSN 0148-0227. doi: 10.1029/jz065i001p00203.

Waldvogel A, Henrich W, M. L. New insight into the coupling between snow spectra and rain drop size distribution. *26th International Conference on Radar Meteorology, Norman, OK, American Meteorological Society*, 1993.

Walther, A., Jeong, J. H., Nikulin, G., Jones, C., and Chen, D. Evaluation of the warm season diurnal cycle of precipitation over Sweden simulated by the Rossby Centre regional climate model RCA3. *Atmospheric Research*, 119:131–139, 2013. ISSN 01698095. doi: 10.1016/j.atmosres.2011.10.012.

Wang, G., Yang, J., Wang, D., and Liu, L. A quantitative comparison of precipitation forecasts between the storm-scale numerical weather prediction model and auto-nowcast system in Jiangsu, China. *Atmospheric Research*, 181:1–11, 2016. ISSN 01698095. doi: 10.1016/j.atmosres.2016.06.004.

Wang, Z., Dong, K., Tian, L., Wang, J., and Tu, J. Numerical study on coalescence behavior of suspended drop pair in viscous liquid under uniform electric field. *AIP Advances*, 8(8), 2018. ISSN 21583226. doi: 10.1063/1.5045747. URL `http://dx.doi.org/10.1063/1.5045747`.

Weisman, M. L., Davis, C., Wang, W., Manning, K. W., and Klemp, J. B. Experiences with 0-36-h explicit convective forecasts with the WRF-ARW model. *Weather and Forecasting*, 23(3):407–437, 2008. ISSN 08828156. doi: 10.1175/2007WAF2007005.1.

Wen, L., Zhao, K., Zhang, G., Xue, M., Zhou, B., Liu, S., and Chen, X. Statistical characteristics of raindrop size distributions observed in East China during the asian summer monsoon season using 2-D video disdrometer and micro rain radar data. *Journal of Geophysical Research*, 121(5):2265–2282, 2016. ISSN 21562202. doi: 10.1002/2015JD024160.

Williams, E. R. New mexico hailstorm over Langmuir laboratory. *Mon. Wea. Rev.*, 1981.

Williams, E. R. The tripole structure of thunderstorms. *Journal of Geophysical Research*, 94(D11), 1989. ISSN 01480227. doi: 10.1029/jd094id11p13151.

Williams, E. R. The electrification of severe storms. *Meteorol. Monogr*, pages 527–561, 2001.

Williams, E. R. Lightning and climate: A review. *Atmospheric Research*, 76(1-4):272–287, 2005. ISSN 01698095. doi: 10.1016/j.atmosres.2004.11.014.

Williams, E. R. and Lhermitte, R. M. Radar tests of the precipitation hypothesis for thunderstorm electrification. *Journal of Geophysical Research*, 88(C15):10984–10992, 1983. ISSN 01480227. doi: 10.1029/JC088iC15p10984.

Williams, E. R. and Montanya, J. A closer look at lightning reveals needle-like structures. *nature*, volume-568, 2019.

Williams, E. R. and Sátori, G. Lightning, thermodynamic and hydrological comparison of the two tropical continental chimneys. *Journal of Atmospheric and Solar-Terrestrial Physics*, 66(13-14 SPEC. ISS.):1213–1231, 2004. ISSN 13646826. doi: 10.1016/j.jastp.2004.05.015.

Williams, E. R., Geotis, S. G., and Bhattacharya, A. B. A radar study of the plasma and geometry of lightning. *Journal of the Atmospheric Sciences*, 46(9):1173–1185, 1989a. ISSN 00224928. doi: 10.1175/1520-0469(1989)046<1173:ARSOTP>2.0.CO;2.

Williams, E. R., Weber, M. E., and Orville, R. E. The relationship between lightning type and convective state of thunderclouds. *Journal of Geophysical Research*, 94(D11), 1989b. ISSN 01480227. doi: 10.1029/jd094id11p13213.

Williams, E. R., Zhang, R., and Rydock, J. Mixed-phase microphysics and cloud electrification. *Journal of the Atmospheric Sciences*, 48(19):2195–2203, 1991. ISSN 00224928. doi: 10.1175/1520-0469(1991)048<2195:MPMACE>2.0.CO;2.

Williams, E. R., Lyons, W. A., Hobara, Y., Mushtak, V. C., Asencio, N., Boldi, R., Bór, J., Cummer, S. A., Greenberg, E., Hayakaw, M., Holzworth, R. H., Kotroni, V., Li, J., Morales, C., Nelson, T. E., Price, C., Russell, B., Sato, M., Sátori, G., Shirahata, K., Takahashio, Y., and Yamashitao, K. Ground-based detection of sprites and their parent lightning flashes over Africa during the 2006 AMMA campaign. *Quarterly Journal of the Royal Meteorological Society*, 136(SUPPL. 1):257–271, 2010. ISSN 00359009. doi: 10.1002/qj.489.

Williams, E. R. C.T.R. Wilson versus G.C. Simpson: Fifty years of controversy in atmospheric electricity. *Atmospheric Research*, 91(2-4):259–271, 2009. ISSN 01698095. doi: 10.1016/j.atmosres.2008.03.024.

Williams, E. R., B. D. J. Dependence of cloud microphysics and electrification on mesoscale vertical air motion in stratiform precipitation. *International Conference on Radar Meteorology,American Meteorological Society*, 1993.

Wilson, C. T. R. Investigations on Lightning Discharges and on the Electric Field of Thunderstorms. 1 . *Monthly Weather Review*, 49(4):241–241, 1921. ISSN 0027-0644. doi: 10.1175/1520-0493(1921)49<241a:ioldao>2.0.co;2.

Wilson, C. T. R. A theory of thundercloud electricity. *Proceedings of the Royal Society of London. Series A. Mathematical and Physical Sciences*, 236(1206):297–317, 1956. ISSN 0080-4630. doi: 10.1098/rspa.1956.0137.

Winn, W. P., Schwede, G. W., and Moore, C. B. Measurements of electric fields in thunderclouds. *Journal of Geophysical Research*, 79(12):1761–1767, 1974. ISSN 0148-0227. doi: 10.1029/jc079i012p01761.

Wormell, T. W. Vertical electric currents below thunderstorms and showers. *Proceedings of the Royal Society of London. Series A, Containing Papers of a Mathematical and Physical Character*, 127(806):567–590, 1930. ISSN 0950-1207. doi: 10.1098/rspa.1930.0077.

Wormell, T. W. Atmospheric electricity; some recent trends and problems. *Quarterly Journal of the Royal Meteorological Society*, 79(339):3–38, 1953. ISSN 1477870X. doi: 10.1002/qj.49707933903.

Xu, K. and Emanuel, K. Is the tropical atmosphere conditionally unstable. *Mon. Weather Rev.*, (117):1471–1479, 1989.

Yang, Y., Tan, X., Liu, D., Lu, X., Zhao, C., Lu, J., and Pan, Y. Corona Discharge-Induced Rain and Snow Formation in Air. *IEEE Transactions on Plasma Science*, 46(5):1786–1792, 2018. ISSN 00933813. doi: 10.1109/TPS.2018.2820200.

Yin, Y., Levin, Z., Reisin, T. G., and Tzivion, S. The effects of giant cloud condensation nuclei on the development of precipitation in convective clouds - A numerical study. *Atmospheric Research*, 53(1-3):91–116, 2000. ISSN 01698095. doi: 10.1016/S0169-8095(99)00046-0.

Zailiang Hu and Srivastava, R. C. Evolution of raindrop size distribution by coalescence, breakup, and evaporation: theory and observations, 1995. ISSN 00224928.

Zhang, G., Sun, J., and Brandes, E. A. Improving parameterization of rain microphysics with disdrometer and radar observations. *Journal of the Atmospheric Sciences*, 63(4):1273–1290, 2006. ISSN 00224928. doi: 10.1175/JAS3680.1.

Appendices

List of Publications

1. **Mudiar, D.**, S. D Pawar, Anupam Hazra,, Konwar, M., Gopalakrishnan, V., Srivastava, M. K., & Goswami, B. N. (2018), Quantification of observed electrical effect on the raindrop size distribution in tropical clouds. Journal of Geophysical Research: Atmospheres, 123 https://doi.org/10.1029/2017JD028205 [Chapter 3]

2. **Mudiar D.**, S. D. Pawar, Anupam Hazra, V. Gopalakrishnana, D. M. Lal, Kaustav Chakravarty, M. K. Srivastava, B. N. Goswami and E. R. Williams, Lightning and Precipitation: The Electrical Modification of Observed Raindrop Size Distributions (under revision, Atmospheric Research) [Chapter 4]

3. **Mudiar D.** , Anupam Hazra, S. D. Pawar, Rama Krishna Karumuri, Mahen Konwar , Subrata Mukherjee, M. K. Srivastava, E. R. Williams and B. N. Goswami, Role of Electrical Effects in Intensifying Rainfall rates in the Tropics (under review)(pre-print available at https://arxiv.org/abs/2004.08888 [Chapter 5]

4. **Mudiar D**., S. D. Pawar, Anupam Hazra, D. M. Lal, M. K. Srivastava, Effect of Electric field on the freezing temperature of pure water drops: A cloud chamber Experiment (To be submitted)[Chapter 6]

Publications

JGR Atmospheres

Impact factor: 3.82
2019 Journal Citation Reports (Clarivate Analytics)
Online ISSN: 2169-8996

JGR: Atmospheres publishes original research articles that advance and improve the understanding of atmospheric properties and processes, including the interaction of the atmosphere with other components of the Earth system, as well as their roles in climate variability and change.

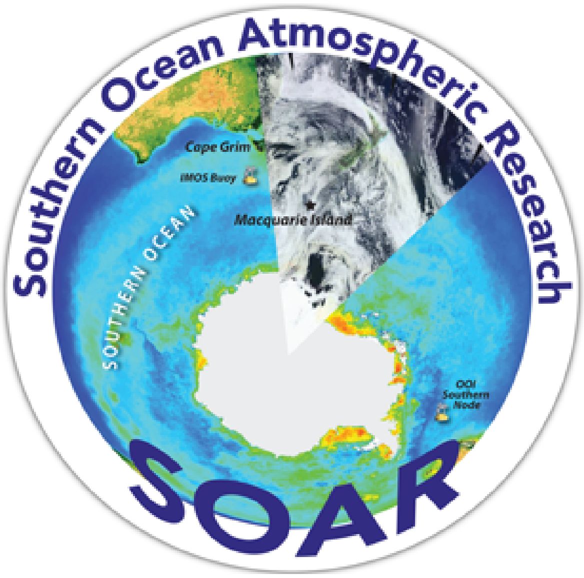

CALL FOR PAPERS
Southern Ocean clouds, aerosols, precipitation and radiation

Browse Articles

Recently Published | Accepted Articles | Most Cited | Most Read

Free Access

Issue Information

First Published: 1 September 2020

Abstract | PDF | Request permissions

AGU100 ADVANCING EARTH AND SPACE SCIENCE

JGR

Journal of Geophysical Research: Atmospheres

RESEARCH ARTICLE

10.1029/2017JD028205

Key Points:
- Drop size distribution of six strongly electrified and six weakly electrified stratiform rain events have been studied
- Drop size distributions at all heights for strongly electrified events and weakly electrified events are significantly different from each other
- The electric field and surface charge of raindrops can affect the collision-coalescence processes and breakup characteristics of raindrops

Correspondence to:
S. D. Pawar,
pawar@tropmet.res.in

Citation:
Mudiar, D., Pawar, S. D., Hazra, A., Konwar, M., Gopalakrishnan, V., Srivastava, M. K., & Goswami, B. N. (2018). Quantification of observed electrical effect on the raindrop size distribution in tropical clouds. *Journal of Geophysical Research: Atmospheres*, *123*. https://doi.org/10.1029/2017JD028205

Received 20 DEC 2017
Accepted 28 MAR 2018
Accepted article online 9 APR 2018

Quantification of Observed Electrical Effect on the Raindrop Size Distribution in Tropical Clouds

Dipjyoti Mudiar[1,2], S. D. Pawar[1], Anupam Hazra[1], Mahen Konwar[1], V. Gopalakrishnan[1], M. K. Srivastava[2], and B. N. Goswami[3]

[1]Indian Institute of Tropical Meteorology, Pune, India, [2]Department of Geophysics, Banaras Hindu University, Varanasi, India, [3]Department of Physics, Cotton University, Guwahati, India

Abstract In the backdrop of extensive laboratory and theoretical evidence of broadening of the drop size distribution (DSD) of raindrops in the presence of electric field, quantification of the same in observed tropical clouds is lacking. Here this is quantified using the DSD measured by a microrain radar at 2,400-, 1,200-, and 600-m heights from the surface in six strongly electrified and six weakly electrified stratiform rain events together with the DSD of raindrops at the surface measured by a disdrometer for the same cases. The presence/absence of lightning is used to distinguish between strongly and weakly electrified events. The vertical profile of Median Volume Diameter below the melting layer and DSDs at all three heights for strongly electrified events and weakly electrified events are significantly different from each other, consistent with previous laboratory and numerical studies (Rayleigh, 1879; Davis, 1964; Moore et al., 1964, https://doi.org/10.1175/1520-0469(1964)021<0646:GORAMA>2.0.CO;2). Our results indicate that the electric field and surface charge of raindrops can affect the collision-coalescence process and breakup characteristics of raindrops. Our study suggests that the parameterization of electrical processes in weather/climate models can possibly improve the simulation of tropical rainfall in numerical models as well as a proper representation of DSD will improve the estimation of tropical rainfall in airborne measurements.

1. Introduction

The global atmospheric circulation is mainly maintained by tropical convection, which transports moisture and heat vertically as well as laterally in the atmosphere. Tropical clouds feedback to the circulation through radiative and latent heating effects. The microphysical and dynamical properties of clouds determine their role in the global radiative budget and the water cycle. Many studies have shown that deep tropical convection is more likely associated with lightning activity (Kodama et al., 2006; Morita et al., 2006). Virts and Houze (2015) studied the characteristics of mesoscale convective systems (MCSs) in regions affected by the Madden-Julian Oscillation and found that during all Madden-Julian Oscillation phases, lightning frequency decreases with distance from the center of the MCS; however, during suppressed periods, the area of enhanced lightning extends to the surroundings from the convective core. Many studies of electrical properties of MCSs have found that the stratiform regions of MCSs can be highly electrified (MacGorman et al., 2008; Williams et al., 2010). Using electric field soundings, Marshall and Rust (1993) and Stolzenburg et al. (1994) showed that the charge in the stratiform region tends to occur in four to six layers, which can extend up to 100 km horizontally. Some studies suggest that the advection of charge from the convective region and some local charge generation mechanisms will be the main cause of intense charge observed in the stratiform regions of MCSs (Stolzenburg et al., 1994, 1998; Williams & Boccippio, 1993).

Many microphysical processes such as coalescence, breakup, evaporation, condensation, raindrop clustering, and mixing can influence the evolution of the raindrop size distribution (DSD; Testik & Barros, 2007). The information about the shape of the DSD of raindrops can be very useful for understanding the microphysical processes that transform the cloud water droplets into raindrops and their growth mechanisms. The DSD of raindrops can play a crucial role in the estimation of rainfall by radars because the characteristics of raindrop spectra, represented by DSD, are generally used to develop rainfall retrieval algorithms (Islam et al., 2012b). Studies by Iguchi et al. (2009) and Islam et al. (2012a) have shown that one of the main causes of rainfall retrieval uncertainty using precipitation radars aboard the Tropical Rain Measuring Mission is the incorrect representation of global DSD characteristics. Furthermore, the prediction of precipitation in the numerical weather prediction models greatly relies on the approximation of the raindrop size spectra. The numerical weather prediction model commonly assumes distribution functions in the microphysical schemes that are sensitive to the particle sizes (Curic et al., 2010; Islam et al., 2012b). This is particularly crucial for convective rain because of highly variable distributions (Gilmore et al., 2004; Curic & Janc, 2011).

Numerous studies have shown that the electric fields inside thundercloud and lightning discharges can influence the microphysical and dynamical properties of thundercloud (Ausman & Brook, 1967; Bhalwankar et al., 2004; Kamra & Ahire, 1989; Kamra et al., 1991; Rasmussen et al., 1985; Richards & Dawson, 1971; Taylor, 1964). In a set of experiments, Rayleigh (1879) observed that coalescence of water jets is extraordinarily sensitive even to the feeble electrical influence and concluded that the observed coalescence behavior is sensitive to the electrical condition of the particles. He observed that a water jet shows coherent behavior in the influence of an electrical field in contrast to the usual behavior of having separated drops at the summit of the jet. As a bipolar molecule, water shows strong electrical characteristics in the presence of surface charge and ambient atmospheric electric field. Charge and electric fields influence different microphysical processes like condensational or diffusional growth of water droplets (Lapshin et al., 2002; Nielsen et al., 2011), collision and coalescence process, and evaporation (Bhalwankar et al., 2004; Schlamp et al., 1979, 1976), which in turn may influence the DSD inside cloud and can thereby modulate the DSD of precipitation at surface. For example, studies by Bhalwankar et al. (2004) and Bhalwankar and Kamra (2007) have shown that the shape, growth, breakup, and evaporation characteristics of water drops are strongly influenced if the drops are charged or they are falling through electric fields. Davis (1964) calculated the force between two charged water drops in an external electric field considering two drops as charged spherical conductors embedded in an external electric field. The electrostatic forces between the drops can influence the trajectories of the drops under the action of both hydrodynamic and electrostatic forces, resulting in a change in collision efficiency of the drops. Following the work of Davis (1964), Schlamp et al. (1976, 1979) numerically calculated the collision efficiency of charged cloud drops in positive and negative (vertically upward and downward respectively) external electric fields for different sizes of collector drops and found that collision efficiency increases significantly. The increased collision will induce the collection efficiency of the falling raindrops. Moore et al. (1964) proposed a mechanism of electrostatic precipitation as a result of enhanced coalescence of charged particles after the lightning discharge and thereby explained the phenomenon of rain gush observed after the electric discharge. Bhalwankar and Kamra (2007) studied the effect of vertical and horizontal electric fields on charged and uncharged water drops in the laboratory and concluded that the presence of vertical electric field can broaden the rain DSD and hence enhance the growth rate of raindrops when compared to the same in the horizontal electric field. Lapshin et al. (2002) proposed the enhanced condensational growth of polar molecules in highly ionized environments by the charge-dipole mechanism. This charge-dipole mechanism of induced growth of polar molecules can be attributed to the stabilization of water droplets in presence of surface charge in a subsaturated environment compared to uncharged droplet (Nielsen et al., 2011). These studies clearly suggest that although dynamics and microphysics of storm cloud may be the cause of initial electrical activity, the electrical forces within clouds in turn could modulate the microphysics thereby modulating the dynamics of the thunderstorm.

Here we have analyzed the DSD in six lightning-producing and six non–lightning-producing stratiform rain events. Electric fields inside a strongly electrified cloud, which produces lightning, can go up to 400 kV/m (Winn et al., 1974). The stratiform clouds, which are not producing lightning, can also have some charge since it contains large ice concentrations. However, the electric fields and charges inside lightning-producing clouds and non–lightning-producing clouds will be significantly different from each other. Therefore, we have termed lightning-producing rain events as "strongly electrified rain events" and non–lightning-producing events have termed as "weakly electrified events." From all previous laboratory and numerical studies, it is very reasonable to expect a modified rain DSD in a strongly electrified cloud compared to a weakly electrified one. Inside a strongly electrified cloud like a thunderstorm, the charge densities could go up to 10^9 elementary charges (Bateman et al., 1999; Christian et al., 1980). A hydrometeor of size 0.5 mm carrying this amount of elementary charge can attain surface charge density of 2.5×10^{-4} C/m^2 (Nielsen et al., 2011), which can increase both the collision-coalescence and condensational growth by a very significant amount and hence modify the DSD and precipitation rate. Because of increased collision efficiency, the Median Volume Diameter (MVD) of raindrops is expected to show large values in strongly electrified clouds, as shown by Moore et al. (1964). Even though laboratory experiments clearly suggest that the strongly electrical forces could significantly affect the rain formation processes in strongly electrified clouds, there are very few attempts to quantify the effect of electrical forces on DSD in the real atmosphere, mainly

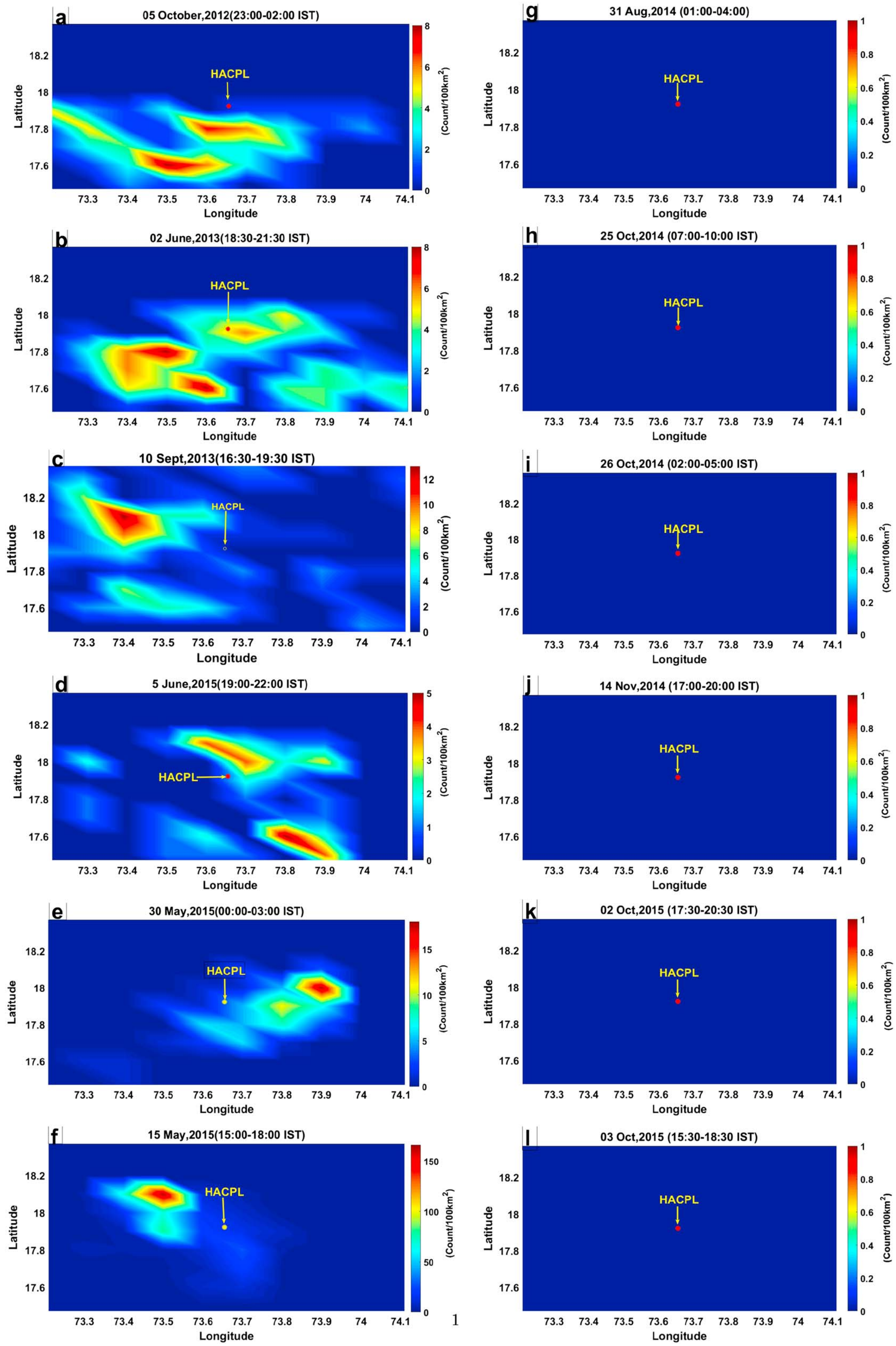

Figure 1. Three-hour (including the data periods) accumulated lightning flash count per 100 km^2 within a 100 km × 100 km box. The left and right panels respectively corresponds to the strongly (a–f) and the weakly (g–l) electrified events. The blue colors in the right panel imply 0 count in the mentioned spatial and temporal scales. The labeling of all the events is same as Tables 1 and 2.

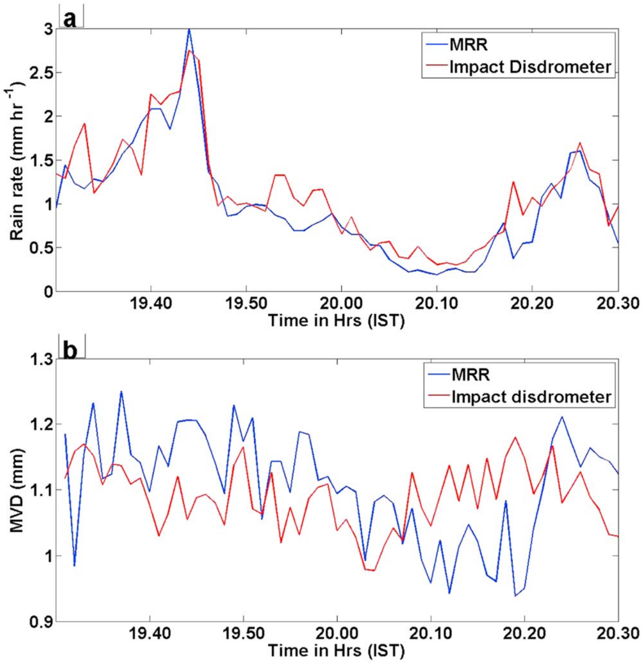

Figure 2. Comparison between micro rain radar data and in situ JW disdrometer data for 14 November 2014 at the High Altitude Cloud Physics Laboratory site. (a) Rain rate (correlation r = 0.90). (b) Median volume diameter (correlation r = 0.73).

because of the difficulty in separating the effect of electrical forces from different dynamical and microphysical processes. As the stratiform rain is characterized by weak vertical air motion (Houze, 1997), and we have chosen all the rain events with approximately similar rain rate, therefore, the selection of stratiform rain events with approximately equal rain rate essentially ensures that the prevailing dynamical and microphysical effects on rain DSD can be approximately similar for both strongly electrified and weakly electrified events. We avoid strong convective events (without any discernible radar bright band) where the dynamical influence on the DSD may be overwhelming, making it difficult to isolate the effect of the electrification. For that, we chose stratiform rain events, with no lightning (weakly electrified clouds) and with few lightning (strongly electrified clouds) to ensure that the dynamical properties of strongly electrified and weakly electrified clouds are not significantly different from each other. The vertical profiles of the DSDs of 12 stratiform rain events have been studied at the three respective heights (2,400-, 1,200-, and 600-m heights from the surface) together with the DSD of raindrops at surface measured by a microrain radar (MRR) and a disdrometer respectively for the same cases to get a quantitative idea about the electrical effect on microphysical process of rain formation in tropical clouds.

2. Data and Methods

Here we have chosen six cases of stratiform rains events, where lightning was observed within 5 km from the High Altitude Cloud Physics Laboratory (HACPL), Pune, and within an hour of the data periods chosen for analysis and termed them as "strongly electrified events." Also, we have chosen six cases of stratiform rain where no lightning was observed in a 100 km × 100 km box, the observation site being in the middle and within a time period of 3 hr (including the data periods chosen for analysis). We have termed these six cases as "weakly electrified events." Figure 1 shows the accumulated lightning activity per 100 km^2 for 3 hr within the 100 km × 100 km box. As shown in this figure in the strongly electrified events in each case, the convective cloud was present near to the observation site, which ensures that cloud overhead of the observation site was strongly electrified (which is also confirmed by the lightning observed over observation site). Whereas, in the weakly electrified events in each case, not a single lightning discharge was observed nearby as can be seen from the right panels of Figure 1. Previous studies suggested that the advection of charge from the convective core(s) could be the cause of high electric fields observed in stratiform clouds (Marshall & Rust, 1993; Rutledge & MacGorman, 1988; Rutledge et al., 1990; Stolzenburg et al., 1994). However, local charge generation mechanism such as melting-charging (Shepherd et al., 1996) and collisions of ice crystals with aggregates (Williams, 2018) could also cause the electrification of stratiform clouds. The absence of any lightning discharges in the neighborhood of HACPL as seen from the Figures 1g–1l has ensured that these six stratiform events are weakly electrified. It is observed that for all the strongly electrified stratiform rain events, the observation site does not fall in the main convective core implying the fact that the observed electrical activities in stratiform clouds over the HACPL are caused by the advection of charges from the surrounding regions. It should be noted here that the lightning data for Figures 1a–1c extracted from the World Wide Lightning Location Network with detection efficiency of 25%–30% and for Figures 1d–1l extracted from Maharashtra Lightning Location Network (MLLN) (V. S. Pawar et al., 2017) with detection efficiency about 90% are used to separate these strongly electrified from weakly electrified events. MLLN became operational in February 2014.

To calculate the DSD at the respective heights, vertically pointing MRR data are used. The radar is installed at the HACPL situated at Mahabaleshwar (India; 17.92°N,73.66°E) at an altitude of 1.3 km from mean sea level (MSL). It measures the vertical profiles of number density, $N(D)$ (m^{-3} · mm^{-1}), in the diameters ranging between 0.4 and 4.9 mm; the fall velocity of hydrometeor, V (m/s); the radar reflectivity factor, z (dBZ); the rain liquid water content, LWC (g/m^3); and the rain rate, R (mm/hr). The vertical resolution of the MRR observations

10.1029/2017JD028205

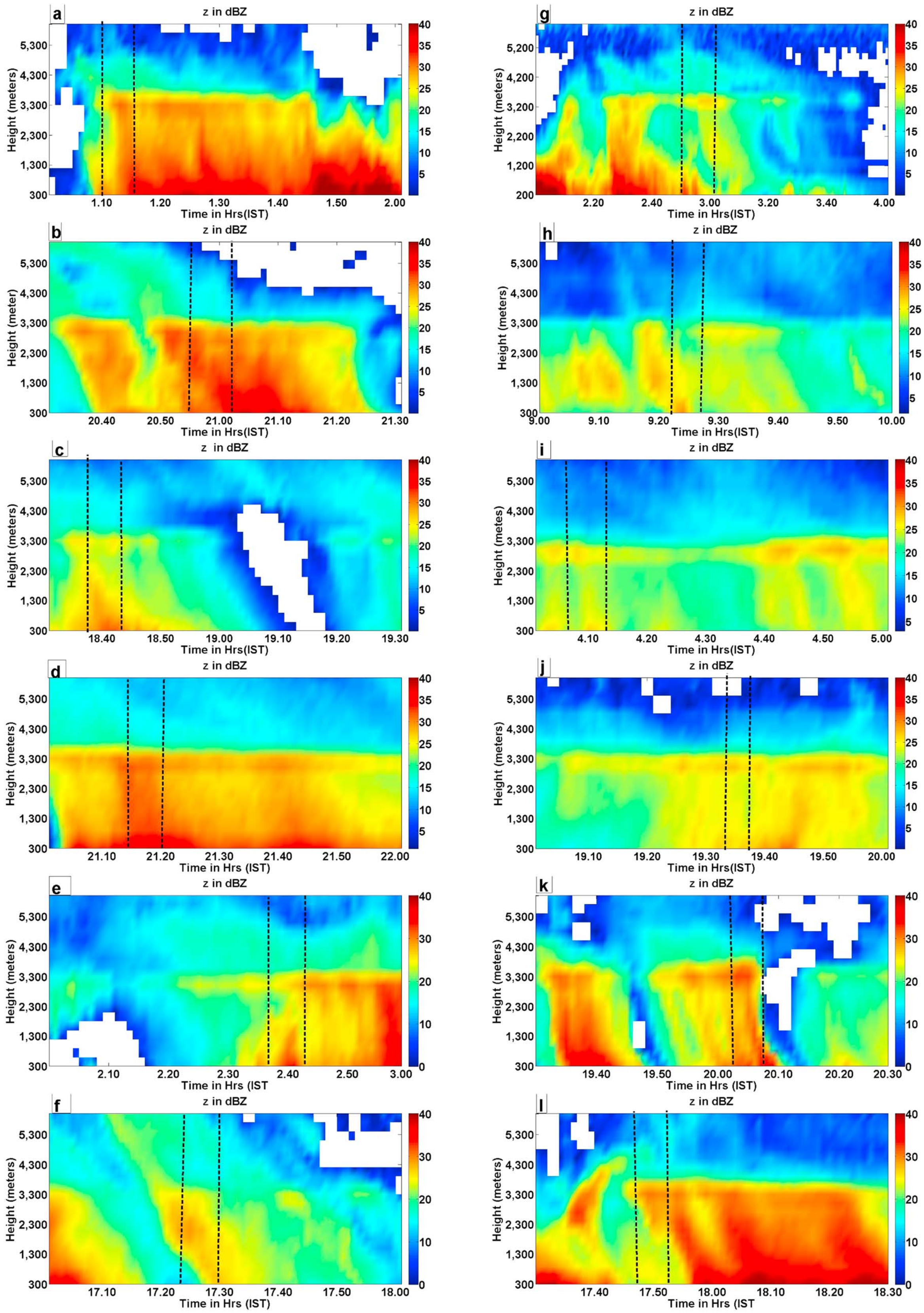

Figure 3. Height-time plot of *z* for strongly electrified (a–f) and weakly electrified (g–l) rain events. Heights are measured from the location of MRR. The dashed vertical bars indicate the data period considered for analysis.

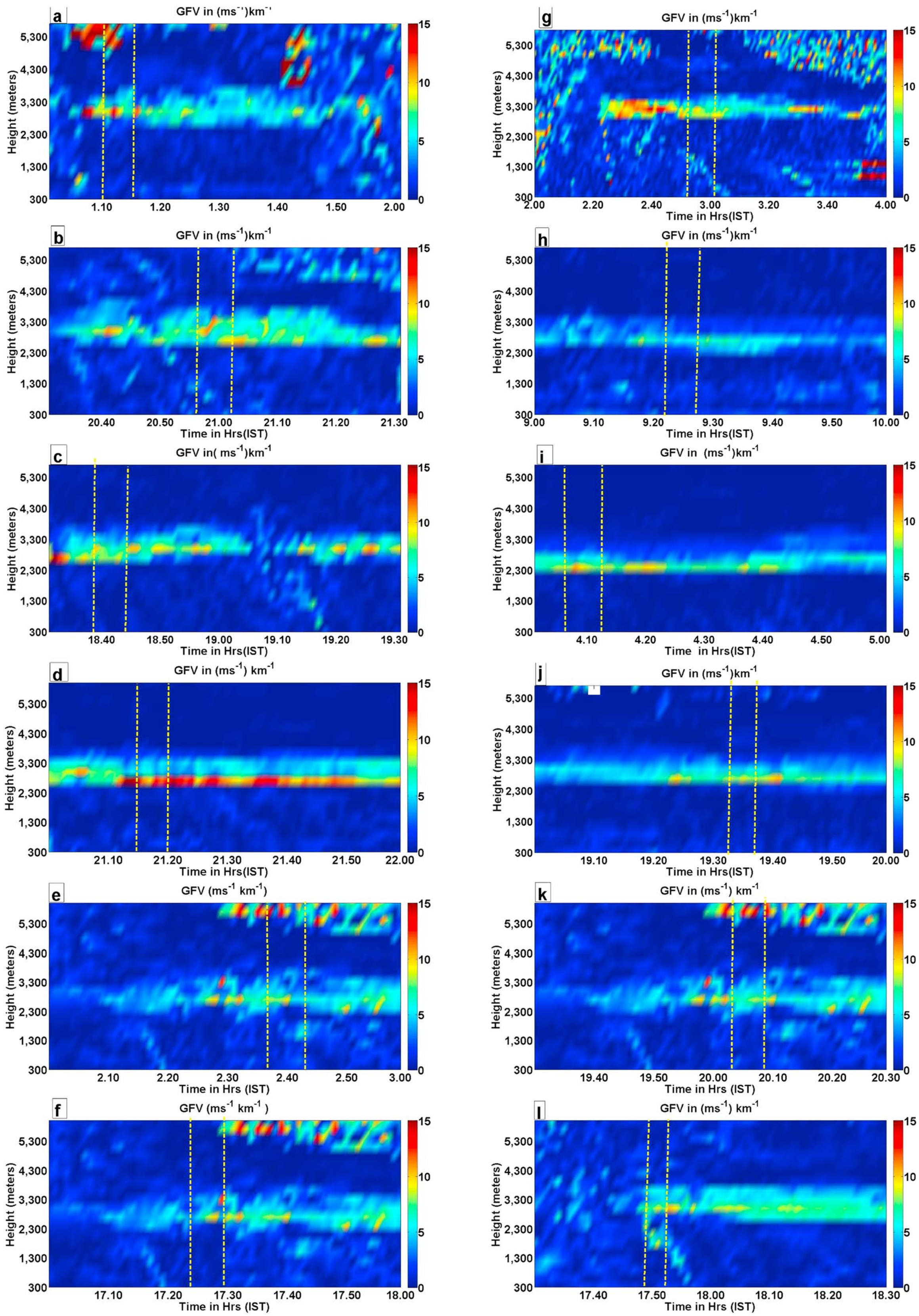

Figure 4. Height-time plot of gradient of fall velocity for strongly electrified (a–f) and weakly electrified (g–l) rain events. Heights are measured from the location of MRR. The dashed vertical bars indicate the data period considered for analysis.

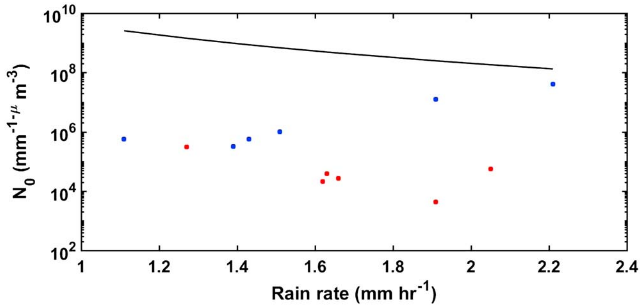

Figure 5. Classification of precipitation type. The red and blue squares represent the strongly electrified and the weakly electrified events, respectively. The solid line represents the empirical relation (1).

used in the present study is 300 m. It operates at 24.1 GHz, which corresponds to 1.25-cm wavelength (Peters et al., 2005). The detailed retrieval method of different microphysical parameters by MRR is discussed by Peters et al. (2005). Since the electromagnetic wave at 24.1 GHz is attenuated by heavy rainfall, we restricted our present study by MRR to low rainfall rate ($0.1 \leq R \leq 10$ mm/hr), similar to the criteria used in Konwar et al. (2014). For all the events considered for the present study, the melting layers are observed near 3.3 km above the surface. Hence, we considered MRR data below the melting layers, as above the melting layer, the hydrometeors may be in the ice or mixed phase state. The present study is mainly focused on the liquid phase hydrometeors below the melting level as MRR does not distinguish between ice and liquid phase hydrometeors.

Data from a ground-based JWD (Joss Waldvogel Disdrometer), which measures raindrops in 20 channels ranging from diameter 0.3 to 5.5 mm, were utilized to measure the DSD at the surface (Joss & Waldvogel, 1967). The sampling resolution time of the JWD was 30 s. Ground-based laser optical Particle Size and Velocity (PARSIVEL) disdrometer is also used to measure the raindrop size during lightning discharges. It detects precipitation particles in the diameter range from 0.3 to 30 mm (Löffler-Mang & Joss, 2000). Surface wind data for all the rain events are collected from an automatic weather station (Dynalab Weathertech-WL 1002) co-located with the disdrometer and the MRR at the HACPL site. The sampling resolution of the AWS is 1 min.

The surface electric field is measured at the Atmospheric Electricity Observatory (AEO) at Pune (India). The electric field is measured with a field mill kept in a pit with its sensor flush with the ground. The details of the instruments are given in S. D. Pawar et al. (2017)

In order to validate the MRR measurement, the MRR-measured rain parameters are compared with in situ JWD measured ones. The lowest measuring altitude of the MRR is 300 m above the JWD for all the rain events considered here. Figure 2 shows a comparison of 1 hr of time series of rainfall rate and corresponding MVD measured by the two instruments. There is a very good agreement between both instruments in measuring the rain rate with correlation coefficient $r = 0.90$ with p-value <0.0001. In addition, the high-frequency variations of the MVD measured by these two instruments are comparable to each other($r = 0.73$ with p-value <0.0001).

From MRR observations, the convective and stratiform rain events are separated on the basis of the presence or absence of the radar bright band and a prominent band of gradient of fall velocity (GFV) of raindrops in the vicinity of the melting level (Konwar et al., 2012). Houze (1997) reported a clear distinction between active convection and stratiform (older convection) in terms of upward vertical velocity, net mass transport, and the presence of a radar bright band around the melting level. In the stratiform region, the net vertical velocity below the melting level is downward, while at upper level the net vertical velocity is upward, which allows the precipitation particles to grow by vapor diffusion. The melting and evaporation of precipitation particles result in a net cooling below the melting layer.

3. Results

The evolutions of electrical, microphysical, and dynamic characteristics occur almost simultaneously in a cloud and their interactions feedback on each other. Therefore, to study the electrical effect on DSD, it is necessary to have clouds with significantly different electrical properties but similar dynamical and microphysical properties. As explained by Houze (1997), the stratiform region of precipitation is characterized by a horizontally uniform, weak vertical air motion (<1 m/s) producing a layered structure of precipitation. In the absence of high LWC, collision, coalescence, breakup, and evaporation are the dominant microphysical processes in the stratiform rain events below the melting level (Konwar et al., 2012, 2014). We have chosen 12 such stratiform rain events to ensure that the dynamical properties are not much different from each other.

Height time intensities of radar reflectivity factor (z) are plotted in Figure 3 for strongly electrified and weakly electrified cases. As seen in this figure, the presence of melting layer (bright band) is clearly

Table 1
Strongly Electrified Stratiform Rain Events and Some Rain Microphysical and Dynamical Parameters

Date	Data period (IST)	Time of lightning and distance from the HACPL site	Integrated 3-hr lightning counts in a 100 km × 100 km box, including the data periods	Bright band thickness (m)	Mean reflectivity of the radar bright band (dBZ)	0° isotherm height from the MSL (km)	Rain rate (mm/hr)	D_m (mm)	Intercept N_0 ($\mathrm{mm}^{-1-\mu} \cdot \mathrm{m}^{-3}$)	LWC ($\mathrm{g/m^3}$)	Wind speed (m/s)	Mean fall velocity below the bright band (m/s)
5-10-2012(a)	01:09:00–01:15:00	1:15:51 IST, 4.7 km	89	800	29	5.2	1.63	1.66	3.8×10^4	0.155	3.15	7.37
2-6-2013(b)	20:57:30–21:02:30	21:21:04 IST, 4.3 km	129	600	30	NA	2.05	1.477	5.68×10^4	0.10	3.30	8.77
10-9-2013(c)	18:38:30–18:43:30	18:38:19 IST,3.6 km	163	800	23	5.2	1.75	1.65	2.64×10^4	0.08	1.15	7.83
5-6-2015(d)	21:15:50–21:19:20	21:09:55 IST 3.7 km and 21:57:10 IST,0 km	47	800	28	4.9	1.91	2.18	4.35×10^3	0.07	2.66	8.3
30-5-2015(e)	02:37:40–02:42:10	2:06:02 IST at 2 km, 2:15:56 at 4 km	91	600	27	5.0	1.62	1.59	2.06×10^4	0.07	5.22	7.43
15-5-2015 (f)	17:11:30–17:15:30	17:18:14 ISTat4.5 km	525	600	23	5.1	1.23	1.26	3.02×10^5		1.19	5.54

Note. The variables are derived from MRR and surface Joss Waldvogel Disdrometer and averaged over the data period bounded by the vertical bars as shown in Figure 3). The lightning counts for the events (a–c) are derived from WWLLN and (d–f) from MLLN. The 100 km × 100 km box is created keeping the HACPL site in the middle. The 0° isotherm heights are derived from the radiosonde soundings.

visible for both strongly electrified and weakly electrified rain events. The heights of the melting levels for strongly electrified and weakly electrified cases are observed at approximately 3.3 km from the surface. It may be noted here that as the MRR is installed at an altitude of 1.3 km above the MSL, the effective heights of the melting layer would be around 4.6 km from the MSL. In the stratiform rain, when the ice particles come down below the melting level and start to melt, their fall speed increase by a factor of 5 (Houze, 1997; Lhermitte, 1960). This sudden increase of fall speed of hydrometeors produces a distinct band of GFV near the melting layer. The core of the maximum GFV coincides with the melting level. The presence of GFV is found to be a good indicator of the melting layer when the enhanced reflectivity factor (*z*) is not prominent (Konwar et al., 2012). Figure 4 depicts the height time intensities of GFV for strongly electrified and weakly electrified events corresponding to the rain events of Figure 3. In this figure, the band of GFV is also clearly visible at about 3.3 km from the surface. Figures 3 and 4 show that although in some cases the bright band is not so prominent (faint bright band), the GFV shows a prominent band. It is also clear that the thickness and height of bright bands are not much different from each other for both the strongly and weakly electrified events.

Assuming a gamma raindrop size distribution, Tokay and Short (1996) and Testik and Pei (2017) made a classification of convective and stratiform rain from the empirical relationship of DSD intercept parameter (N_0) and rain rate (R) measured by surface-based disdrometer. The distinct microphysical processes of convective and stratiform rain result in varying rain DSD parameter, which may be used to distinctly classify both the rain events. In the stratiform rain, the growth of ice crystals is dominated by vapor diffusion above the melting layer. When these ice crystals drift downward, near the melting layer, the ice crystals grow by aggregation and riming (Houze, 1997; Sarma et al., 2016; Waldvogel et al., 1993). When these particles melt below the melting layer, they produce large raindrops, which results in a decrease of the DSD intercept parameter N_0. On the other hand, in a convective cloud, the larger vertical velocity induces the growth of precipitation particles by accretion and riming followed by collision, coalescence, and breakup. In the presence of high LWC, the precipitation particles grow in a very short span of time near the cloud base (Tokay & Short, 1996). In the approximately similar range of rain rates, these distinct microphysical processes produce small to medium raindrops in convective rain compared to stratiform rain, which results in a high value of the DSD intercept parameter N_0.

This intercept parameter variation in stratiform and convective rainfall is used in Figure 5 to classify the convective and stratiform rain. In this figure, the solid line represents the empirical relation (1) from Tokay and Short (1996)

$$\boldsymbol{N_0 = 4 \times 10^9 R^{-4.3}} \tag{1}$$

where N_0 is the intercept parameter ($\mathrm{mm}^{-1-\mu} \cdot \mathrm{m}^{-3}$) and R is the rain rate (mm/hr) measured by the impact disdrometer. For the present study, N_0 values are calculated using the formula (2) (Bringi & Chandrasekar, 2001)

$$\boldsymbol{N_0 = N_w \frac{6(\mu+4)^{\mu+4}}{4^4 \Gamma(\mu+4)} D_m^{-\mu}} \tag{2}$$

where r is the gamma function and D_m is the MVD given by

Table 2
Weakly Electrified Rain Events and Some Rain Microphysical and Dynamical Parameters

Date	Data period (IST)	Integrated 3-hr lightning counts in a 100 km × 100 km box, including the data periods	Bright band thickness (m)	Mean reflectivity of the radar bright band (dBZ)	0° isotherm height from the MSL (km)	Rain rate (mm/hr)	D_m (mm)	Intercept N_0 ($mm^{-1-\mu} \cdot m^{-3}$)	LWC (g/m^3)	Wind speed (m/s)	Mean fall velocity below the bright band (m/s)
31-8-2014 (g)	02:56:10–02:59:40	0	800	22	NA	1.51	1.10	9.8×10^5	0.09	2.32	5.6
25-10-2014 (h)	09:23:00–09:26:00	0	800	24	NA	1.50	1.22	3.14×10^5	0.08	8.58	5.95
26-10-2014 (i)	04:07:00–04:11:00	0	600	25	NA	1.54	1.13	5.68×10^5	0.08	7.18	5.78
14-11-2014 (j)	19:33:30–19:36:30	0	800	26	4.85	1.43	1.19	5.60×10^5	0.08	4.94	6.21
02-10-2015 (k)	20:10:0–20:13:00	0	800	27.5	5.2	1.88	0.90	1.23×10^7	0.13	3.01	5.80
03-10-2015 (l)	17:45:00–17:49:00	0	600	30	5.2	2.20	0.96	4.04×10^7	0.16	3.14	5.69

Note. The variables are derived from MRR and surface Joss Waldvogel Disdrometer and averaged over the data period bounded by the vertical bars as shown in Figure 3. The lightning counts for the events (g–l) are derived from MLLN. The 100 km × 100 km box is created keeping the HACPL site in the middle. The 0° isotherm heights are derived from the radiosonde soundings.

$$D_m = \frac{\int_{D_{min}}^{D_{max}} D^4 N(D) d(D)}{\int_{D_{min}}^{D_{max}} D^3 N(D) d(D)} \tag{3}$$

μ is the gamma distribution shape parameter, given by the empirical relation (Testik & Pei, 2017)

$$\mu = \frac{D_m^{-0.66}}{0.3^2} - 4 \tag{4}$$

N_w is the DSD parameter given by

$$N_w = \frac{4^4}{\pi \rho_w} \left(\frac{10^3 W}{D_m^4} \right) \tag{5}$$

Here D (mm) is the raindrop diameter; $N(D)$ is drop density in $m^{-3} \cdot mm^{-1}$; D_{max} and D_{min} are the maximum and minimum drop diameters, respectively, measured by the disdrometer for a given DSD; ρ_w is the density of water in g/m^3; and W is the LWC in g/m^3 given by

$$W = 10^{-3} \frac{\pi}{6} \rho_w \int_{D_{min}}^{D_{max}} D^3 N(D) d(D) \tag{6}$$

As seen from the Figure 5, all the values of N_0 given by the formula (2) lie below the solid line, which represents the formula (1), clearly indicating that all the rain events considered for the present study are of stratiform nature with similar kind of microphysical and dynamical processes.

Some parameters such as bright band thickness, rain rates mean reflectivity of the bright band, integrated 3-hr lightning counts including the stratiform events, and 0° isotherm heights from MSL, MVDs, LWCs, intercept parameters, mean fall velocity below the bright band, and wind speed for strongly electrified and weakly electrified cases are given in Tables 1 and 2**,** respectively. All the values are averaged for the period shown by the dotted lines in Figure 3. As listed in case of strongly electrified events and weakly electrified events, the thickness of bright band and rain rates are not much different from each other. The bright band mean reflectivity and fall velocity below the melting layer are observed to be slightly higher for the strongly electrified events compared to weakly electrified events Also, in Table 1**,** the times of lightning discharges and their distances from the observational site are given. In all the strongly electrified events at least one lightning strike was observed within 5 km from observation site, which ensure that the strongly electrified events were part of same cloud clusters for which we have analyzed the DSD.

The vertical profiles of MVDs are calculated from the MRR data for both strongly electrified and weakly electrified events, averaged over six events each and plotted against the height as shown in Figure 6b corresponding to the rain rate profile of Figure 6a. The rain rate profiles are derived from the MRR measured DSD using the equation.

$$R = 10^{-3} \frac{\pi}{6} \rho_w \int_{D_{min}}^{D_{max}} v(D) D^3 N(D) d(D) \tag{7}$$

where R is the rain rate (mm/hr) and v (D) is the fall velocity (m/s) of a drop of diameter D. The observed maxima in the vertical profile of rain rate below the melting layer are possibly caused by the sudden increase of fall velocity of the precipitation particles as well as by the melting of the large aggregates (Houze, 1997).

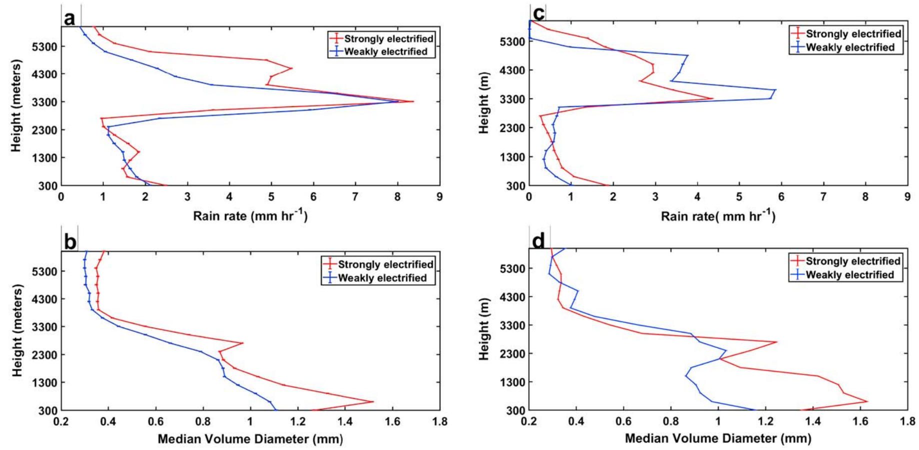

Figure 6. (a) Rain rate and (b) MVD averaged over six strongly electrified and weakly electrified stratiform rain events each. (c and d) The same but under the same thickness of radar bright band corresponding to the events in Figures 3c and 3g. The horizontal bars represent the respective standard deviation of the rain rates and MVD. Heights are measured from the location of MRR.

Although the vertical profile of observed rain rates of strongly electrified and weakly electrified events below melting band is nearly similar to each other, the vertical profile of MVDs for both types of events is significantly different from each other. In the strongly electrified events, the drop size shows a tendency to be in the larger size of the size range compared to the weakly electrified events. The MVD values measured with the ground-based JWD corresponding to the data periods bounded by the vertical bars in Figure 3 for all the 12 rain events considered here are shown in the bar graph in Figure 7b against the rain rates for the same periods in Figure 7a. It is clearly evident that although the rain rates of all the 12 rain events are nearly similar, the MVDs corresponding to the strongly electrified rain events show higher values compared to weakly electrified rain events. The MVD values derived from the surface JWD at a temporal resolution of 30 s for the entire time period (1 hr) of rainfall of each event in Figure 3 are shown all together in a box and whisker plot in Figure 8. This figure clearly shows higher mean and median values of MVD for strongly electrified events compared to the weakly electrified events, although the rain rates are having same mean and median for both categories of events.

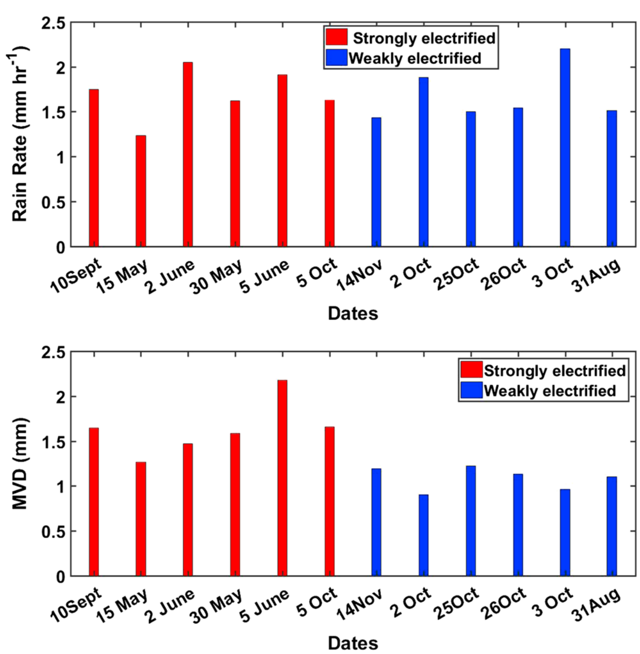

Figure 7. Bar graph of (a) rain rates and (b) MVDs for all the rain events of Figure 3.

Previous studies show a significant correlation between the DSD and strength and thickness of the radar bright band. Huggel et al. (1996) found a good correlation between the strength of the bright band and the slope and intercept parameters of the Marshall-Palmer rain DSD. Sharma et al. (2009) have shown that larger mean drop diameter is associated with the larger width of the bright band and smaller mean drop diameter is associated with the weaker bright band. To strengthen our argument that the differences in MVDs in strongly electrified and weakly electrified events are due to electric forces present in the strongly electrified cloud and not due to difference in dynamic properties, we have compared the MVDs of two events, one strongly electrified (Figures 3c and 4c) and one weakly electrified (Figures 3g and 4g) with the nearly the same thickness of the bright band. The strength of the bright bands (Δz) is measured following the method of Huggel et al. (1996). An upper boundary of the bright band is determined visually for each profile so that the maximum reflectivity in the bright band is observed less than 0.4 km from the boundary. Then strength of the bright bands (Δz) is defined as the differences (in dBZ) of maximum reflectivity in a 0.4-km-thick layer just below the upper boundary (z_{max}) and the minimum reflectivity in a 0.4-km-thick layer adjacent to the upper layer (z_{min}).

10.1029/2017JD028205

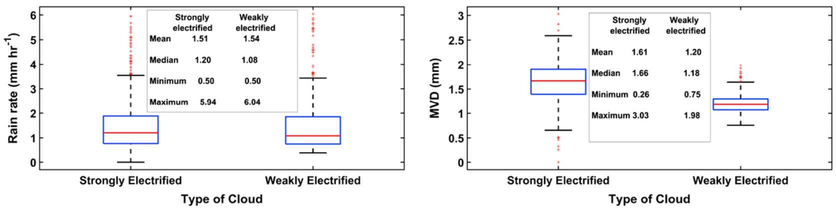

Figure 8. The box and whisker plot for rain rate and MVD plotted altogether for all the 6 events each. For strongly electrified events, the total number of data points is 389 and for weakly electrified events, the total number of data points is 433 ($0.5 <$ rain rates <6).

$$\Delta z(\mathrm{dBZ}) = z\max(\mathrm{dBZ}) - z\min(\mathrm{dBZ}) \quad (8)$$

For strongly electrified and weakly electrified events the measured strengths are found to be 2.2 and 3.5 dB, respectively. The thicknesses of the bright band for both the events are measured to be 800 m. Please note that the bright band is a property of the radar data and the measured thickness of the bright band depends upon the vertical resolution of the radar (Houze, 1997). In Figure 6d we have plotted the vertical profile of MVD corresponding to the rain rate profile of Figure 6c for these two events. This figure also shows larger MVD in strongly electrified events compared to weakly electrified events below the melting level. In the melting level the mixed-phase cloud hydrometeors (e.g., snow and graupel) change the state and start to convert to rainwater through melting, and below the melting level, further rain formation processes (e.g., collision, coalescence, formation of rain embryos, rain autoconversion, and breakup of drops) can dominate the DSD. The enhanced collision-coalescence process of raindrops in the strongly electrified cloud will effectively increase the size of raindrops below the melting level. Figures 6b and 6d clearly show the sharp increase in median diameter of the raindrops of strongly electrified and weakly electrified events at melting band height. The strongly electrified events show larger median diameter compared to weakly electrified events below the melting level with the difference in median diameter being highest just below the melting band. How does the electrical force achieve this? Do the DSD spectra provide any insight to answer this question?

In Figures 9a–9c, we have plotted the DSDs, averaged over six cases each at heights 2,400, 1,200, and 600 m from the MRR data, respectively. As shown in these figures the DSDs for strongly electrified and weakly electrified events are different from each other at all three heights. Even though the difference between the concentration of drops for strongly electrified and weakly electrified events can be seen clearly in all size ranges, the difference is substantially larger for a drop size above 2 mm. In the strongly electrified events, the number concentrations of small size drops are lower and large size drops are more numerous than weakly electrified events at all the three heights. We note from these three figures that an increase in the number density of larger drops is accompanied by a compensating decrease in the number density of smaller drops. The results could indicate that due to the electric field and surface charge of raindrops, the collision-coalescence growth process gets enhanced, which further modify the size distribution of raindrops. Figures 9e–9g depict the DSDs at the same heights as in Figures 9a–9c but under the same thickness and strength of the radar bright band. Although, both the events have the same strength and thickness of the BB, and nearly the same rain rate, the DSD profiles of the strongly electrified events have shown a broader spectrum compared to the weakly electrified events.

In Figure 9d we have plotted the surface DSD from JWD data averaged over 5 min for each event and again averaged over six strongly electrified and weakly electrified events each keeping the rain rate nearly the same. Figure 9h depicts the surface DSDs for strongly electrified and weakly electrified events averaged over 5 min each, under the same thickness and strength of the bright band. These figures also show a clear difference between DSDs of strongly electrified and weakly electrified events consistent with changes in DSD at higher levels.

Erpul et al. (2000) and Testik and Pei (2017) have shown that the horizontal wind speed and LWC can influence the rain DSD. Erpul et al. (2000) reported larger median drop size in wind-driven rain compared to windless rain in a wind tunnel study. On the contrary, Testik and Pei (2017) reported a wind-induced collisional breakup of raindrops, which results in a narrower DSD. We have plotted the MVDs calculated from the impact disdrometer data against the horizontal wind speed from the AWS located in the HACPL site for strongly electrified and weakly electrified rain events for the same data periods used in this study (Figure 10a). Testik and

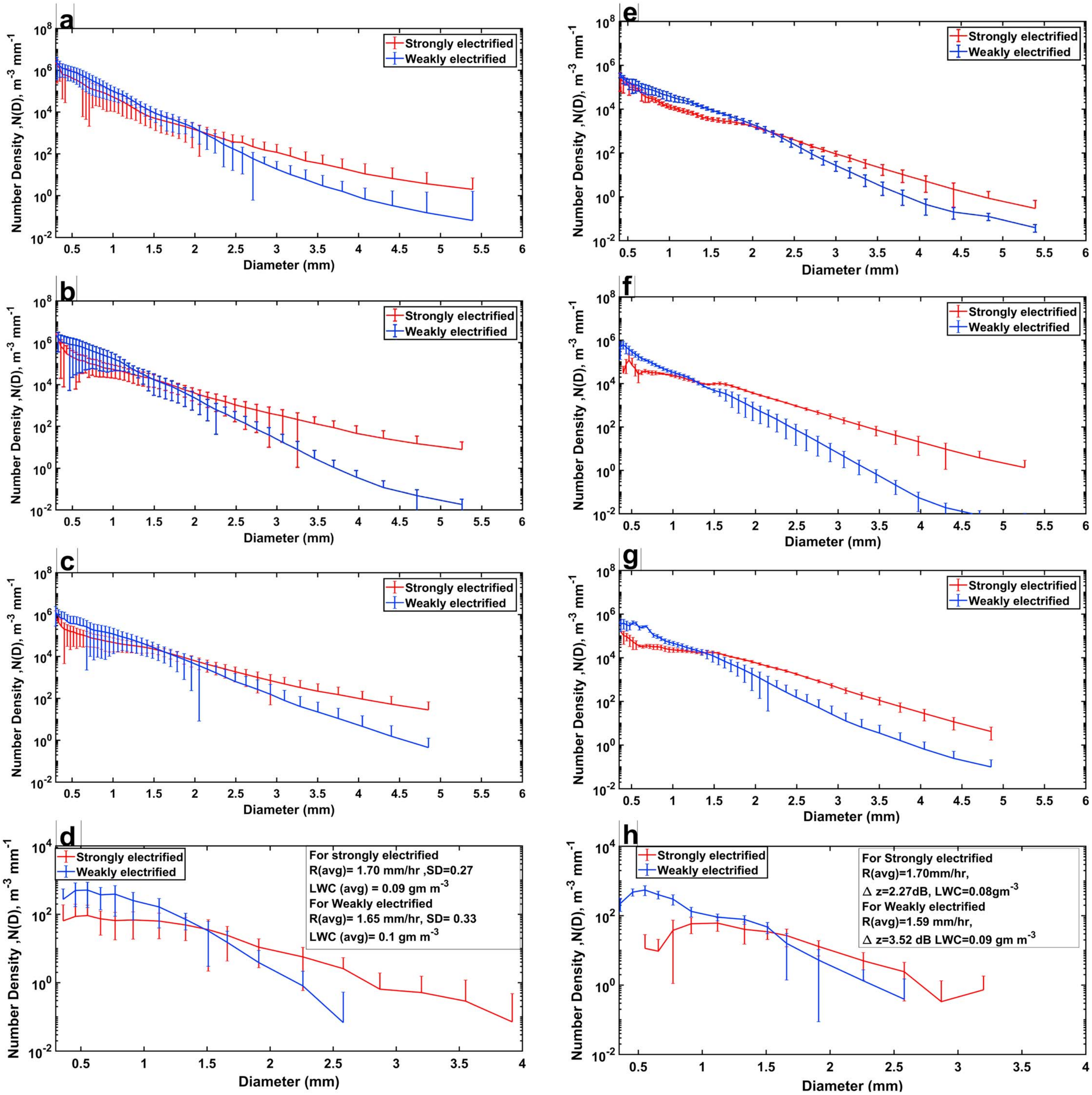

Figure 9. Composite raindrop size distribution (six events in each composite) at selected altitudes for strongly electrified and weakly electrified clouds as observed by MRR at (a) 2,400 m, (b) 1,200 m, (c) 600 m, and (d) at surface observed by JW disdrometer. The right panel depicts the altitude evolution of DSD under the similar strength of bright band for strongly electrified and weakly electrified events (Figures 1c and 1g) observed by MRR at (e) 2,400 m, (f) 1,200 m, (g) 600 m, and (h) at surface observed by JWD. The vertical bars represent the standard deviations of the respective DSDs. Heights are measured from the location of MRR.

Pei (2017) observed an increase of number of large raindrops with the increase of LWC. For the present study, we have derived the LWC and MVD using formulas (6) and (3), respectively, from the disdrometer measured DSD for all the rain events and plotted the results in Figure 10b. These figures show that MVD shows a

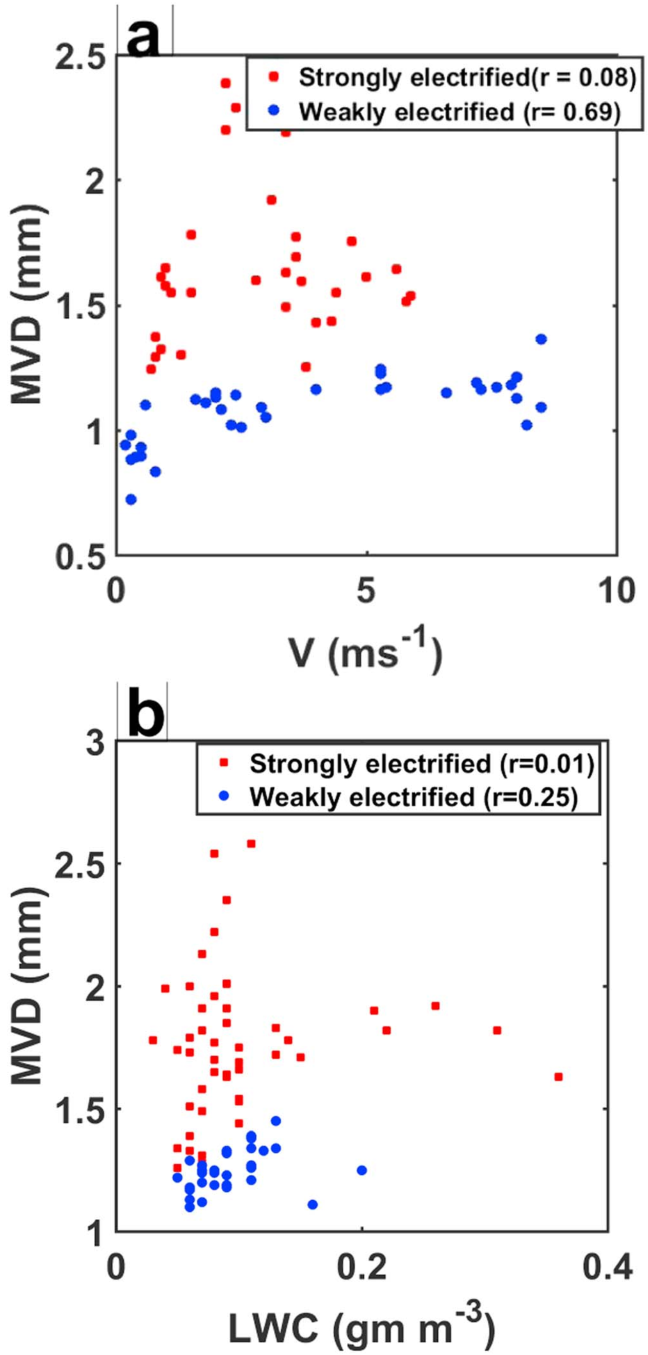

Figure 10. Scatter plot of MVDs derived from surface based JW disdrometer with (a) wind speed (derived from AWS) and (b) with LWC (derived from JWD).

reasonable correlation (r = 0.69) with wind speed in weakly electrified events. However, for strongly electrified events, the correlation is insignificant. While with LWC, MVD shows a small correlation (r = 0.25) for weakly electrified rain events and no significant relationship is observed for strongly electrified events. These figures clearly suggest that in strongly electrified events, strong electrical forces among the raindrops may be playing a dominant role in determining the rain DSD.

4. Discussion

Studies by Hu and Srivastava (1995) and Testik and Barros (2007) have shown that the cloud microphysical and dynamical properties mainly determine the structure of the DSD of rain events. However, studies like Kamra (1985) show a modified DSD in the region of intense electrification in a thundercloud as a result of the accumulation of precipitation particle whose fall velocity under the influence of gravitational and electrical forces becomes equal and opposite to the updraft speed in that particular region. As can be seen from Figures 1, the 6 rain events where lightning was observed overhead of observation site will surely have significantly larger electric forces inside clouds compared to other six events where lightning was not observed. As the present study is carried out under almost similar dynamical and microphysical condition of rain formation, we may conclude that the significant difference in DSDs above drop diameters of 2 mm for strongly electrified and weakly electrified events observed in our study is likely to be due to the effect of electric forces on the raindrops in strongly electrified events. Our study strongly demonstrates that the electrical forces inside cloud can modify the DSD of raindrops. As shown in Figure 9 the DSDs of strongly electrified events show clear deviation from weakly electrified events. In the case of strongly electrified events, the concentration of larger drops (larger than about 2 mm) is significantly more than the concentration of the same size drops in weakly electrified events. Furthermore, the concentrations of smaller drops in the strongly electrified events are less than weakly electrified rain events. This difference in drop concentration may be due to increased collision and coalescence because of electric forces in strongly electrified environment. Theoretical studies by Davis (1964) and Schlamp et al. (1976, 1979) have shown that the strong electric fields inside cloud and charges on drops can increase the collision efficiency by many times. As raindrops fall below the melting level at the terminal fall velocities, their growth is influenced by collision breakup, coalescence, and evaporation. In the electrical environment of tropical clouds, the rain droplets acquire surface charge, which is proportional to the square of the droplet radius and magnitude of electric field inside the cloud (Pruppacher & Klett, 1996). The Coulomb interaction between charged drops increases the coalescence efficiency upon collision between the drops. Ochs III and Czys (1987) have shown that permanent coalescence results for all impact angles upon collision of two drops if their relative charge exceeds 2×10^{-12} C, while in the absence of charge, there exists a critical impact angle of 43°, which divides the region of coalescence and noncoalescence. The Coulomb interaction enhances the drainage of the air film trapped between the colliding drops, which help the drops to coalesce permanently. The ambient electric field in the thundercloud, which can go up to 400 kV/cm (Winn et al., 1974) generated by charging processes, can induce coalescence of uncharged drops or even like charged drops by the effect of polarization. The observed increased growth rate in case of strongly electrified events can be attributed to the increased coalescence efficiency due to electric fields and surface charge on raindrops inside clouds. Furthermore, the DSDs in the strongly electrified events

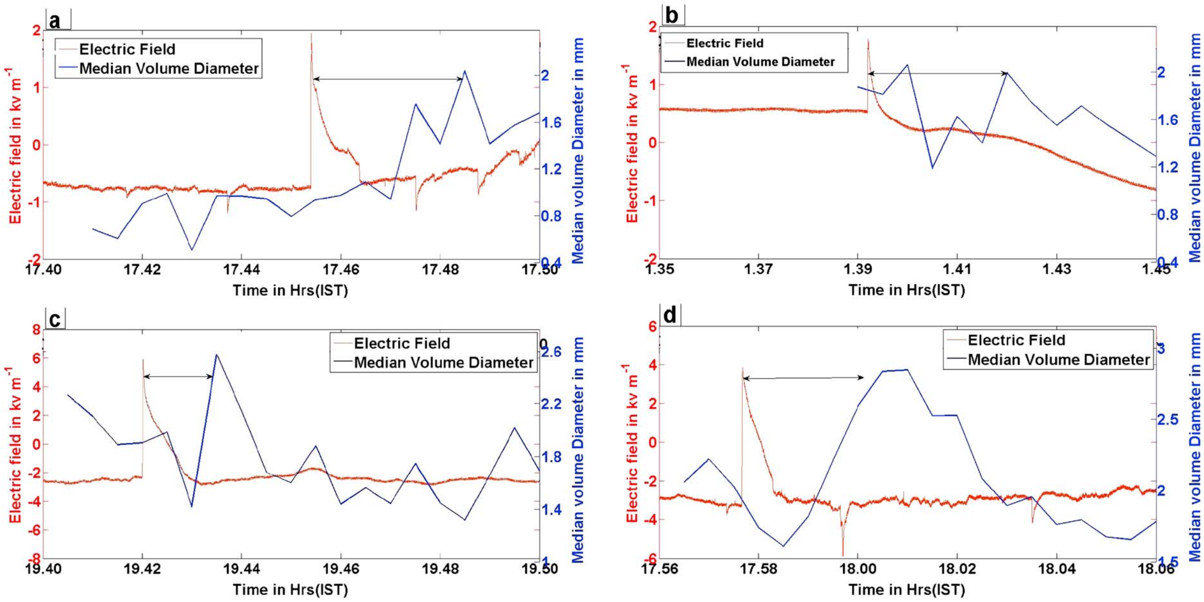

Figure 11. Relationship between lightning discharge and MVD. These events are observed over Atmospheric Electricity Observatory at Pune (India) in the year of 2008.

show a broader spectrum compared to weakly electrified events. Konwar et al. (2012, 2014) have shown that the breakup characteristic of raindrops is one of the dominant factors in determining the shape of DSD curve. Bhalwankar and Kamra (2007) have shown that the electric field inside a cloud can influence breakup characteristics of raindrops. In the wind tunnel experiments, they have shown that a vertical electric field can make the DSD wider compared to a horizontal electric field. Using electric field soundings, Marshall and Rust (1993) and Stolzenburg et al. (1994) showed that the charge in the stratiform region tends to occur in four to six layers. Analysis of 12 soundings of electric field in various types of electrified stratiform cloud by Shepherd et al. (1996) shows strong electric field of magnitude 50–75 kV/m and high charge density near to the 0 °C isotherm. The observations of charge regions situated one above other and high charge density observed near the 0 °C isotherm suggest that the electric field will be predominantly vertical in the base of stratiform cloud. These previous observations support the argument that below the cloud base the atmospheric electric field is predominantly vertical. The significantly increased large drop concentration in case of strongly electrified events compared to weakly electrified events in the present study strongly supports the idea that presence of vertical electric field and electric charge on raindrop modifies the shape of DSD of raindrops in tropical clouds and hence can act as an influential factor in tropical precipitation formation processes.

Moore et al. (1962, 1964) observed echo intensification with vertically scanning radar in a volume of cloud (where electric discharge originated) just after the electric discharge and a gush of rain at the ground with a time delay of 1–3 min after the discharge. In Figures 11a–11d we have plotted electric field and MVD of raindrops in four cases to establish a cause and effect relationship between the lightning and the raindrop size. Surface electric fields and DSDs measured at the AEO at Pune (India), which is about 100 km away from the HACPL, are used in this figure. The optical disdrometer used to measure the MVDs during the reported lightning events is collocated with the field mill at Pune. It should be noted here that the four lightning events reported in this figure are observed over the AEO, Pune, in the premonsoon season of the year 2008. As shown in this figure the large electric field change induced by lightning is followed by a sharp increase in the MVD of raindrops arriving at the surface. The time delay between the lightning discharges and peak MVD is about 2–4 min. Assuming a 7–8 m/s fall speed of 2–3 mm raindrops, in 2–4 min, the drops are expected to traverse a distance of 900–1,200 m. In absence of the vertical structure of reflectivity profiles after the lightning discharge, the altitude of the origin of drops is difficult to ascertain. In Figure 12a, we have plotted magnitudes of electric field changes produced by lightning discharge and a corresponding increase in MVDs for 11 cases observed over AEO with the best fit line. As shown in this figure the two parameters

10.1029/2017JD028205

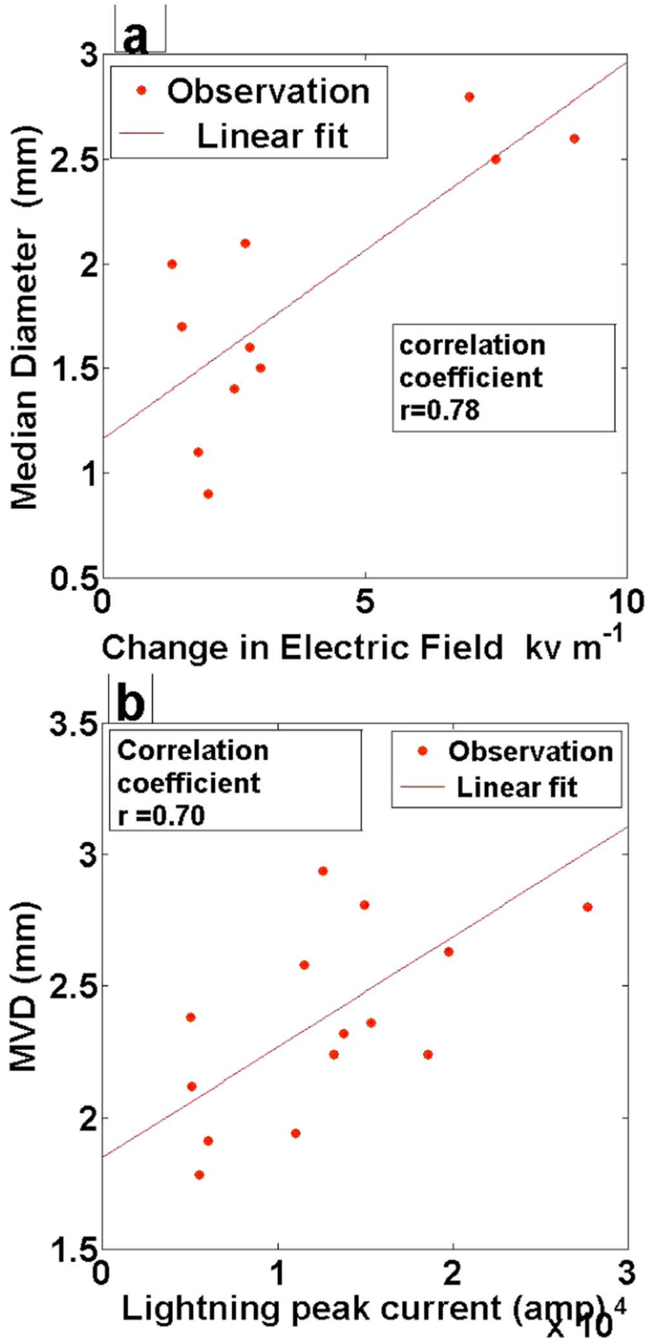

Figure 12. Scatter plot of MVD with (a) change of electric field during electric discharge and (b) lightning peak current (lightning peak currents are measured by MLLN).

show good correlation with each other (*r* = 0.78). In Figure 12b, we have plotted the MVD (measured by JWD at HACPL) against the peak lightning current (extracted from the MLLN) for some isolated lightning events within the 2-km radius of the HACPL site. The JWD measured MVDs are averaged over 3 min each corresponding to the peak value of rain rate, 2–4 min just after the lightning. As seen from the figure the MVDs shows a reasonable correlation (*r* = 0.70) with the electric parameter. As some of the MVDs of Figure 12a and all the MVDs of Figure 12b might be of convective type rain (rain rate $>$ 30 mm/hr), it can be presumed that the electrical forces also play a significant role in convective rain microphysics, which can be dynamically different from the stratiform rain microphysics. The good correlation with electrical parameters suggests that the lightning of higher intensities can produce more ions in the atmosphere, which results in more deviation in DSDs of raindrops. Figures 10 and 12 suggest that MVDs corresponding to certain rain DSDs shows a better dependence on the electrical parameters than the dynamical and microphysical parameters.

Even though our data demonstrate that the strong electrical forces inside clouds can modify the DSD of raindrops, the observed difference in the DSDs of the strongly electrified events and weakly electrified events can also be explained by another hypothesis based on a lightning-ice relationship (ice factory hypothesis). It has been shown that the more electrically active the preceding convection (and the more active the lightning activity with which it is associated), the more vigorous will be the stratiform region and greater the likelihood of lightning flashes in the stratiform region (Williams & Boccippio, 1993). A more vigorous ice factory means larger concentrations of ice crystals, which in turn drive a more vigorous aggregation process. The larger the aggregates, the larger will be the raindrops that result from the melting (E. R. Williams, private communications, 2017). This ice factory hypothesis has a convincing logical basis. The large ice concentration in the lightning-producing stratiform regions may result in broader rain DSD. In stratiform precipitation, the growth of hydrometeors (ice particles) is dominated by vapor diffusion in the upper level and by aggregation just and by aggregation just above the melting level (0 to −15°C). Near the melting level, the aggregates melt resulting in a well-defined radar bright band (Houze, 1997). Studies by Huggel et al. (1996); Sharma et al. (2009) ,and Waldvogel et al. (1993) support this hypothesis of bright band formation. These studies suggest that if the aggregation is more dominant than riming in the ice particle growth, then a well-defined and strong bright band can be achieved.

Some studies like Huggel et al. (1996) and Oue et al. (2015) do not support the ice factory hypothesis. They showed that in the stratiform rain, the mean particle size of raindrops varies much more with precipitation intensity than the aggregation process, and therefore, the presence of higher ice concentration does not guarantee a broader spectrum of rain DSD. Also, DSDs in Figure 9 show that strongly electrified events have fewer smaller drops and larger concentration of bigger drops, which cannot be explained by ice factory hypothesis, because according to this hypothesis, concentrations of all size drops should be higher in case of lightning-producing (strongly electrified) events compared to non-lightning-producing (weakly electrified) events. Figure 9 clearly indicates that the growth rate of larger drops is more significant in the case of strongly electrified events compared to weakly electrified events. To strengthen this point, we have plotted vertical profiles of rain rates and MVDs (Figures 6a–6d) in extended height scale between the 2,000 and 600 m in Figures 13a–13d. These figures clearly show that the MVDs of the raindrops are increasing significantly faster in the case of strongly

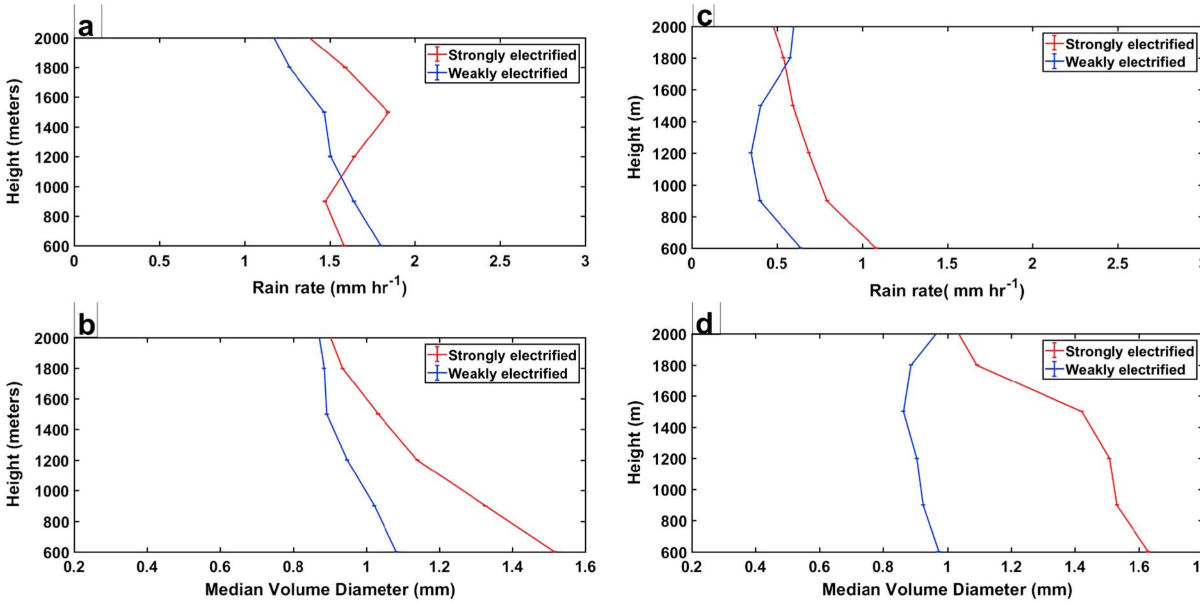

Figure 13. Vertical profiles of rain rates and MVDs in extended scale corresponding to Figures 6a–6d.

electrified events compared to the weakly electrified events, which evidently suggested a higher collection efficiency of drops, falling at their terminal speed below the melting level. From the perspective of the ice factory hypothesis, it is conceivable that presence of larger raindrops will induce faster growth below the melting level and hence produce bigger drops when reaching the surface. Kollias et al. (2002) and Fabry and Zawadzki (1995) studied the vertical evolution of the Doppler spectrum, MVD, and reflectivity at vertical incidence below the melting layer and found that the vertical profiles of MVD and reflectivity do not show significant variability below the melting layer, which is consistent with our present observation of weakly electrified stratiform rain events as can be seen from Figures 13b and 13d. This implies that the raindrops reach the surface from the melting layer without much change in their sizes irrespective of their size of origin. But in the case of strongly electrified events, the vertical profiles of MVD show a significant variability from the melting layer to the surface even though near the melting layer both types of events show approximately similar profiles of drop size (Figures 6b and 6d). Therefore, our study strongly suggests that this observed higher collection efficiency in the case of strongly electrified events can be attributed to the presence of stronger electrical forces among the drops, as the ice factory hypothesis is unable to delineate this faster growth of drops in the strongly electrified stratiform rain events. Also, the higher variability in the MVD values of the strongly electrified events as seen from Figure 8 can be attributed to the highly variable electrical forces inside the strongly electrified cloud.

With all the observational evidence, it is concluded that the electrical forces inside the cloud can modify the DSD by influencing collision, coalescence, and breakup characteristics of raindrops. In the absence of certain observational measurements, which would have given a more conclusive idea about dynamical and microphysical characteristics in all of the 12 stratiform rain events considered for the present analysis, the complete rejection of the ice factory hypothesis is cautiously avoided.

One of the outstanding systematic errors in simulating the observed frequency distribution of tropical rainfall in almost all models is that the models tend to highly overestimate the frequency of very light rain events at the expense of severely underestimating heavy rainfall events (Goswami & Goswami, 2016). One possible reason for this persistent problem of weather and climate models may be some missing physics in the parameterization of microphysical processes in cloud modules. The effect of electrical processes on rain formation is not parameterized in most weather and climate models and could be responsible for some of the biases in simulating precipitation by such models. Our quantification of changes in DSD spectra by the electrified environment in tropical clouds could provide a basis for the parameterization of electrical processes in rain formation in weather and climate models.

Acknowledgments

IITM is funded by the Ministry of Earth Sciences, Government of India. We thank the director of IITM for his continuous support and encouragement. We sincerely acknowledge the efforts of scientific and technical staffs of IITM, Pune, working in High Altitude Cloud Physics Laboratory (HACPL) at Mahabaleshwar, to collect the microrain radar and impact disdrometer data. We are grateful to the Editor, Associate Editor, E. R. Williams (MIT, Cambridge), and other four anonymous reviewers for their critical and constructive comments throughout the review process, which greatly improved the manuscript. Sincere thanks to P. Murugavel and Manoj Domkawale for providing the Maharashtra Lighting Location Network (MLLN) data. The data used in the manuscript are accessible through the link http://www.tropmet.res.in/~majfiles/pawar-JGR-data-2018.html. We are thankful to the University of Washington in Seattle, USA, for making available the WWLLN data (http://wwlln.net/). B. N. G. thanks INSA for a fellowship and CU for hosting.

References

Ausman, E. L., & Brook, M. (1967). Distortion and disintegration of water drops in strong electric fields. *Journal of Geophysical Research*, *72*(24), 6131–6135. https://doi.org/10.1029/JZ072i024p06131

Bateman, M. G., Marshall, T. C., Stolzenburg, M., & Rust, W. D. (1999). Precipitation charge and size measurements inside a New Mexico mountain thunderstorm. *Journal of Geophysical Research*, *104*(D8), 9643–9653. https://doi.org/10.1029/1998JD200118

Bhalwankar, R. V., & Kamra, A. K. (2007). A wind tunnel investigation of the deformation of water drops in the vertical and horizontal electric fields. *Journal of Geophysical Research*, *112*, D10215. https://doi.org/10.1029/2006JD007863

Bhalwankar, R. V., Sathe, A. B., & Kamra, A. K. (2004). The evaporation of the charged and uncharged water drops suspended in a wind tunnel. *Proceedings of the Indian Academy of Science (Earth and Planetary Sciences)*, *113*, 129–138.

Bringi, V. N., & Chandrasekar, V. (2001). *Polarimetric Doppler weather radar: Principles and applications* (p. 636). Cambridge, UK: Cambridge University Press. https://doi.org/10.1017/CBO9780511541094

Christian, H., Holmes, C. R., Bullock, J. W., Gaskell, W., Illingworth, A. J., & Latham, J. (1980). Airborne and ground-based studies of thunderstorms in the vicinity of Langmuir Laboratory. *Quarterly Journal of the Royal Meteorological Society*, *106*(447), 159–174. https://doi.org/10.1002/qj.49710644711

Curic, M., & Janc, D. (2011). Comparison of modeled and observed accumulated convective precipitation in mountainous and flat land areas. *Journal of Hydrometeorology*, *12*(2), 245–261. https://doi.org/10.1175/2010JHM1259.1

Curic, M., Janc, D., & Veljovic, K. (2010). Dependence of accumulated precipitation on cloud drop size distribution. *Theoretical and Applied Climatology*, *102*(3-4), 471–481. https://doi.org/10.1007/s00704-010-0332-5

Davis M. H. (1964). Two charged spherical conductor in a uniform electric field: Forces and Field strength. *Rand Corp. Publ*. (Santa-Monica, California), RM-3860-PR.

Erpul, G., Gabriels, D., & Janssens, D. (2000). The effect of wind on size and energy of small simulated raindrops: A wind tunnel study. *International Agrophysics*, *14*, 1–7.

Fabry, F., & Zawadzki, I. (1995). Long-term radar observations of the melting layer of precipitation and their interpretation. *Journal of the Atmospheric Sciences*, *52*(7), 838–851. https://doi.org/10.1175/1520-0469(1995)052%3C0838:LTROOT%3E2.0.CO;2

Gilmore, M. S., Straka, J. M., & Rasmussen, E. N. (2004). Precipitation and evolution sensitivity in simulated deep convective storms: Comparisons between liquid-only and simple ice and liquid phase microphysics. *Monthly Weather Review*, *132*(8), 1897–1916. https://doi.org/10.1175/1520-0493(2004)132%3C1897:PAESIS%3E2.0.CO;2

Goswami, B. B., & Goswami, B. N. (2016). A road map for improving dry-bias in simulating the South Asian monsoon precipitation by climate models. *Climate Dynamics*, *49*(5-6), 2025–2034. https://doi.org/10.1007/s00382-016-3439-2

Houze, R. A. (1997). Stratiform precipitation in regions of convection: A meteorological paradox? *Bulletin of the American Meteorological Society*, *78*(10), 2179–2196. https://doi.org/10.1175/1520-0477(1997)078%3C2179:SPIROC%3E2.0.CO;2

Hu, Z., & Srivastava, R. C. (1995). Evolution of raindrop size distribution by coalescence, breakup, and evaporation: Theory and observation. *Journal of the Atmospheric Sciences*, *52*, 1761–1783.

Huggel, A. W., Schmid, W., & Waldvogel, A. (1996). Raindrop size distributions and the radar bright band. *Journal of Applied Meteorology*, *35*(10), 1688–1701. https://doi.org/10.1175/1520-0450(1996)035%3C1688:RSDATR%3E2.0.CO;2

Iguchi, T., Kozu, T., Kwiatkowski, J., Meneghini, R., Awaka, J., & Okamoto, K. (2009). Uncertainties in the rain profiling algorithm for the TRMM precipitation radar. *Journal of the Meteorological Society of Japan*, *87*, 1–30.

Islam, T., Rico-Ramirez, M. A., Han, D., Srivastava, P. K., & Ishak, A. M. (2012a). Performance evaluation of the TRMM precipitation estimation using ground-based radars from the GPM validation network. *Journal of Atmospheric and Solar-Terrestrial Physics*, *77*, 194–208. https://doi.org/10.1016/j.jastp.2012.01.001

Islam, T., Rico-Ramirez, M. A., Thurai, M., & Han, D. (2012b). Characteristics of raindrop spectra as normalized gamma distribution from a Joss-Waldvogel disdrometer. *Atmospheric Research*, *108*, 57–73.

Joss, J., & Waldvogel, A. (1967). Ein Spektrograph für Niederschlagstropfen mit automatischer Auswertung. *Pure and Applied Geophysics*, *68*(1), 240–246. https://doi.org/10.1007/BF00874898

Kamra, A. K. (1985). Modification of some microphysical properties in the highly electrified regions of thundercloud. *Archiv fur Meteorologie, Geophysik, und Bioklimatologie Serie A Meteorologie und Geophysik*, *34*(1), 37–50. https://doi.org/10.1007/BF02267394

Kamra, A. K., & Ahire, D. V. (1989). Wind tunnel studies of the shape of charged and uncharged water drops in the absence or presence of an electricfield. *Atmospheric Research*, *23*(2), 117–134. https://doi.org/10.1016/0169-8095(89)90003-3

Kamra, A. K., Bhalwankar, R. V., & Sathe, A. B. (1991). Spontaneous breakup of charged and uncharged water drops freely suspended in a wind tunnel. *Journal of Geophysical Research*, *96*(D9), 17,159–17,168. https://doi.org/10.1029/91JD01475

Kodama, Y.-M., Tokuda, M., & Murata, F. (2006). Convective activity over the Indonesian Maritime Continent during CPEA-I as evaluated by lightning activity and Q1 and Q2 profiles. *Journal of the Meteorological Society of Japan. Series II*, *84A*, 133–149. https://doi.org/10.2151/jmsj.84A.133

Kollias, P., Albrecht, B. A., & Marks, F. Jr. (2002). Why Mie? Accurateobservations of vertical air velocities and raindrops using a cloud radar. *Bulletin of the American Meteorological Society*, *83*, 1471–1483. https://doi.org/10.2151/jmsj.84A

Konwar, M., Das, S. K., Deshpande, S. M., Chakravarty, K., & Goswami, B. N. (2014). Microphysics of clouds and rain over the Western Ghat. *Journal of Geophysical Research: Atmospheres*, *119*, 6140–6159. https://doi.org/10.1002/2014JD021606

Konwar, M., Maheskumar, R. S., Das, S. K., & Morwal, S. B. (2012). Nature of light rain during presence and absence of bright band. *Journal of Earth System Science*, *121*(4), 947–961. https://doi.org/10.1007/s12040-012-0202-x

Lapshin, V. B., Yablolov, M. Y., & Palei, A. A. (2002). Vapor pressure over a charged drop, *Russian. The Journal of Physical Chemistry*, *76*, 1727–1729.

Lhermitte, R. M. (1960). The use of a special pulse Doppler radar in measurement of particles fall velocities. *Proceeding of Eighth Weather Radar Conference, Boston* (pp. 269–275). Boston, MA: American Meteorological Society.

Löffler-Mang, M., & Joss, J. (2000). An optical disdrometer for measuring size and velocity of hydrometeors. *Journal of Atmospheric and Oceanic Technology*, *17*(2), 130–139. https://doi.org/10.1175/1520-0426(2000)017%3C0130:AODFMS%3E2.0.CO;2

MacGorman, D. R., Rust, W. D., Schuur, T. J., Biggerstaff, M. I., Straka, J. M., Ziegler, C. L., et al. (2008). TELEX: The thunderstorm electrification and lightning experiment. *Bulletin of the American Meteorological Society*, *89*(7), 997–1014. https://doi.org/10.1175/2007BAMS2352.1

Marshall, T. C., & Rust, W. D. (1993). Two types of vertical electrical structures in stratiform precipitation regions of mesoscale convective systems. *Bulletin of the American Meteorological Society*, *74*(11), 2159–2170. https://doi.org/10.1175/1520-0477(1993)074%3C2159:TTOVES%3E2.0.CO;2

Moore, C. B., Vonnegut, B., Machado, J. A., & Survilas, H. J. (1962). Radar observations of rain gushes following overhead lightning strokes. *Journal of Geophysical Research*, *67*(1), 207–220. https://doi.org/10.1029/JZ067i001p00207

Moore, C. B., Vonnegut, B., Vrablik, E. A., & McCraig, D. A. (1964). Gushes of rain and hail after lightning. *Journal of the Atmospheric Sciences*, *21*(6), 646–665. https://doi.org/10.1175/1520-0469(1964)021<0646:GORAMA>2.0.CO;2

Morita, J., Takayabu, Y. N., Shige, S., & Kodama, Y. (2006). Analysis of rainfall characteristics of the Madden–Julian oscillation using TRMM satellite data. *Dynamics of Atmospheres and Oceans*, *42*(1-4), 107–126. https://doi.org/10.1016/j.dynatmoce.2006.02.002

Nielsen, J. K., Maus, C., Rzesanke, D., & Leisner, T. (2011). Charge induced stability of water droplets in subsaturated environment. *Atmospheric Chemistry and Physics*, *11*(5), 2031–2037.

Ochs, H. T., III, & Czys, R. R. (1987). Charge effects on the coalescence of water drops in free fall. *Nature*, *327*(6123), 606–608. https://doi.org/10.1038/327606a0

Oue, M., Ohigashi, T., Tsuboki, K., & Nakakita, E. (2015). Vertical distribution of precipitation particles in Baiu frontal stratiform intense rainfall around Okinawa Island, Japan. *Journal of Geophysical Research: Atmospheres*, *120*, 5622–5637. https://doi.org/10.1002/2014JD022712

Pawar, S. D., Gopalakrishnan, V., Murugavel, P., Veremey, N. E., & Sinkevich, A. A. (2017). Possible role of aerosols in the charge structure of isolated thunderstorms. *Atmospheric Research*, *183*, 331–340. https://doi.org/10.1016/j.atmosres.2016.09.016

Pawar, V. S., Domkawale, M. A., Pawar, S. D., Salvekar, P. S., & Pradeep Kumar, P. (2017). Inter annual variability of tropospheric NO2 and tropospheric ozone over Maharashtra (India): The role of lightning. *Remote Sensing Letters*, *8*(11), 1015–1024. https://doi.org/10.1080/2150704X.2017.1346398

Peters, G., Fischer, B., Münster, H., Clemens, M., & Wagner, A. (2005). Profiles of raindrop size distributions by micro rain radars. *Journal of Applied Meteorology*, *44*(12), 1930–1949. https://doi.org/10.1175/JAM2316.1

Pruppacher, H. R., & Klett, J. D. (1996). *Microphysics of clouds and precipitation* (2nd ed.). Springer.

Rasmussen, R., Walcek, C., Pruppacher, H. R., Mitra, S. K., Lew, J., Levizzani, V., et al. (1985). A wind tunnel investigation of the effect of an external, vertical electric field on the shape of electrically uncharged rain drops. *Journal of the Atmospheric Sciences*, *42*(15), 1647–1652. https://doi.org/10.1175/1520-0469(1985)042<1647:AWTIOT>2.0.CO;2

Rayleigh, L. (1879). The influence of electricity on colliding water drops. *Proceedings Royal Society of London*, *28*, 406–409.

Richards, C. N., & Dawson, G. A. (1971). The hydro-dynamic instability of water drops falling at terminal velocity in vertical electric fields. *Journal of Geophysical Research*, *76*(15), 3445–3455. https://doi.org/10.1029/JC076i015p03445

Rutledge, S. A., Lu, C., & MacGorman, D. R. (1990). Positive cloud-to-ground lightning in mesoscale convective systems. *Journal of the Atmospheric Sciences*, *47*(17), 2085–2100. https://doi.org/10.1175/1520-0469(1990)047%3C2085:PCTGLI%3E2.0.CO;2

Rutledge, S. A., & MacGorman, D. R. (1988). Cloud-to-ground lightning activity in the 10–11 June 1985 mesoscale convective system observed during the Oklahoma-Kansas PRESTORM Project. *Monthly Weather Review*, *116*(7), 1393–1408. https://doi.org/10.1175/1520-0493(1988)116%3C1393:CTGLAI%3E2.0.CO;2

Sarma, A. C., Deshamukhya, A., Narayana Rao, T., & Sharma, S. (2016). A study of raindrop size distribution during stratiform rain and development of its parameterization scheme in the framework of multi-parameter observations (2016). *Meteorological Applications*, *23*(2), 254–268. https://doi.org/10.1002/met.1551

Schlamp, R. J., Grover, S. N., & Pruppachcr, H. R. (1976). A numerical investigation of the effects of electric charge and vertical external electric fields on the collision efficiency of cloud drops. *Journal of the Atmospheric Sciences*, *33*(9), 1747–1755. https://doi.org/10.1175/1520-0469(1976)033%3C1747:ANIOTE%3E2.0.CO;2

Schlamp, R. J., Grover, S. N., Pruppacher, H. R., & Hamielec, A. E. (1979). A numerical investigation of the effect of electric charges and vertical external electric fields on the collision efficiency of cloud drops. *Part II. Journal of the Atmospheric Sciences*, *36*(2), 339–349. https://doi.org/10.1175/1520-0469(1979)036%3C0339:ANIOTE%3E2.0.CO;2

Sharma, S., Konwar, M., Sarma, D. K., Kalapureddy, M. C. R., & Jain, A. R. (2009). Characteristics of rain integral parameters during tropical convective, transition and stratiform rain at Gadanki and its application in rain retrieval. *Journal of Applied Meteorology and Climatology*, *48*(6), 1245–1266. https://doi.org/10.1175/2008JAMC1948.1

Shepherd, T. R., Rust, W. D., & Marshall, T. C. (1996). Electric fields and charges near 0°C in stratiform clouds. *Monthly Weather Review*, *124*(5), 919–938. https://doi.org/10.1175/1520-0493(1996)124%3C0919:EFACNI%3E2.0.CO;2

Stolzenburg, M., Marshall, T. C., Rust, W. D., & Smull, B. F. (1994). Horizontal distribution of electrical and meteorological conditions across the stratiform region of a mesoscale convective system. *Monthly Weather Review*, *122*(8), 1777–1797. https://doi.org/10.1175/1520-0493(1994)122%3C1777:HDOEAM%3E2.0.CO;2

Stolzenburg, M., Rust, W. D., & Marshall, T. C. (1998). Electrical structure in thunderstorm convective regions. 1. Mesoscale convective systems. *Journal of Geophysical Research*, *103*, 14,059–14,078.

Taylor, G. (1964). The disintegration of water drops in an electric field. *Proc. R. Proceedings of the Royal Society of London Series A*, *A280*, 383–397.

Testik, F. Y., & Barros, A. P. (2007). Toward elucidating the microstructure of warm rainfall: A survey. *Reviews of Geophysics*, *45*, RG2003. https://doi.org/10.1029/2005RG000182

Testik, F. Y., & Pei, B. (2017). Wind effects on the shape of raindrop size distribution. *Journal of Hydrometeorology*, *18*(5), 1285–1303. https://doi.org/10.1175/JHM-D-16-0211.1

Tokay, A., & Short, D. A. (1996). Evidence from tropical raindrop spectra of the origin of rain from stratiform versus convective clouds. *Journal of Applied Meteorology*, *35*(3), 355–371. https://doi.org/10.1175/1520-0450(1996)035,0355:EFTRSO.2.0.CO;2

Virts, K. S., & Houze, R. A. (2015). Variation of lightning and convective rain fraction in mesoscale convective systems of the MJO. *Journal of the Atmospheric Sciences*, *72*(5), 1932–1944. https://doi.org/10.1175/Jas-D-14-0201.1

Waldvogel. A., Henrich, W., & Mosimann, L. (1993). New insight into the coupling between snow spectra and rain drop size distribution. Preprints, 26th International Conference on Radar Meteorology (pp. 602–604). Norman, OK: American Meteorological Society.

Williams, E. R. (2018). Lightning activity in winter storms: A meteorological and cloud microphysical perspective (review article, ISWL −2017, Japan)

Williams, E. R., & Boccippio, D. J. (1993). Dependence of cloud microphysics and electrification on mesoscale vertical air motion in stratiform precipitation, Conference on atmospheric electricity, St. Louis, MO. *American Meteorological Society*, *1993*, 825–831.

Williams, E. R., Lyons, W. A., Hobara, Y., Mushtak, V. C., Asencio, N., Boldi, R., et al. (2010). Ground-based detection of sprites and their parent lightning flashes over Africa during the 2006 AMMA campaign. *Quarterly Journal of the Royal Meteorological Society*, *136*, 257–271. https://doi.org/10.1002/qj.489

Winn, W. P., Schwede, G. W., & Moore, C. B. (1974). Measurements of electric fields in thunderclouds. *Journal of Geophysical Research*, *79*(12), 1761–1767. https://doi.org/10.1029/JC079i012p01761

Role of Electrical Effects in Intensifying Rainfall rates in the Tropics

Dipjyoti Mudiar, Anupam Hazra, S. D. Pawar, Rama Krishna Karumuri, Mahen Konwar, Subrata Mukherjee, M. K. Srivastava, E. R. Williams and B. N. Goswami

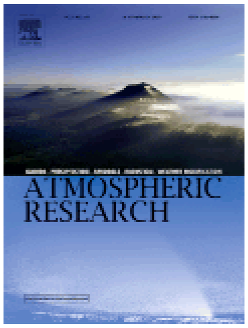

(https://www.sciencedirect.com/science/journal/01698095)

ISSN: 0169-8095

Atmospheric Research

Clouds - Precipitation - Aerosols - Radiation - Climatology, Weather Modification

› **CiteScore: 8.4** ⓘ **Impact Factor: 4.676** ⓘ

Submit Your Paper (https://www.editorialmanager.com/atmosres/default.aspx)

Supports Open Access (https://www.elsevier.com/journals/atmospheric-research/0169-8095/open-access-options)

View Articles (https://www.sciencedirect.com/science/journal/01698095)

Guide for Authors

Gmail

Dipjyoti Mudiar <dmudiar@gmail.com>

Confirming submission to Atmospheric Research

1 message

Atmospheric Research <em@editorialmanager.com> Tue, Aug 11, 2020 at 4:43 AM
Reply-To: Atmospheric Research <atmos@elsevier.com>
To: Dipjyoti Mudiar <d.mudiar@gmail.com>

This is an automated message.

Role of Electrical Effects in Intensifying Rainfall rates in the Tropics

Dear Mr Mudiar,

We have received the above referenced manuscript you submitted to Atmospheric Research.

To track the status of your manuscript, please log in as an author at https://www.editorialmanager.com/atmosres/, and navigate to the "Submissions Being Processed" folder.

Thank you for submitting your work to this journal.

Kind regards,
Atmospheric Research

More information and support

You will find information relevant for you as an author on Elsevier’s Author Hub: https://www.elsevier.com/authors

FAQ: How can I reset a forgotten password?
https://service.elsevier.com/app/answers/detail/a_id/28452/supporthub/publishing/
For further assistance, please visit our customer service site: https://service.elsevier.com/app/home/supporthub/publishing/
Here you can search for solutions on a range of topics, find answers to frequently asked questions, and learn more about Editorial Manager via interactive tutorials. You can also talk 24/7 to our customer support team by phone and 24/7 by live chat and email

---

Role of Electrical Effects in Intensifying Rainfall rates in the Tropics

Dipjyoti Mudiar[a,c], Anupam Hazra[a], S. D. Pawar[a], Rama Krishna Karumuri[b], Mahen Konwar[a], Subrata Mukherjee[1], M. K. Srivastava[c], E. R. Williams[d] and B. N. Goswami[e]

[a]Indian Institute of Tropical Meteorology, Pune, India 411008, Ministry of Earth Sciences, Pune, India, 41100

[b]King Abdullah University of Science and Technology, Thuwal, Saudi Arabia

[c]Banaras Hindu University, Varanasi, India

[d] Massachusetts Institute of Technology, Cambridge, MA USA

[e]Cotton University, Guwahati, India 781001

Corresponding author

Dipjyoti Mudiar

Email id: d.mudiar@gmail.com

IITM, Pune-411008, India

Abstract:

In the backdrop of a revolution in weather prediction with Numerical Weather Prediction (NWP) models, quantitative prediction of the intensity of heavy rainfall events and associated disasters has remained a challenge. Encouraged by compelling evidence of electrical influences on cloud/rain microphysical processes, here we propose a hypothesis that modification of the raindrop size distribution (RDSD) towards larger drop sizes through enhanced collision-coalescence facilitated by cloud electric fields could be one of the factors (The other potential factors include the melting of larger graupel particles in lightning-producing clouds) responsible for intensity errors in weather/climate models. The robustness of the proposed hypothesis is confirmed through a series of simulations of strongly electrified (SE) rain events and weakly electrified (WE) events with a convection-permitting weather prediction model incorporating the electrically modified RDSD parameters in the model physics. This modification of the model physics is encouraged by observed significant influence of in-cloud electric field and lightning on the RDSD slope parameter. The role of ambient aerosol size distribution and melting of graupel particles in intensity modification of surface precipitation also have been tested. Our results indicate a possible roadmap for improving hazard prediction associated with extreme rainfall events in weather prediction models and climatological dry bias of precipitation simulation in many climate models.

Keywords: Numerical Weather Prediction, Rain intensity, Electrical Forces, Lightning, Raindrop Size Distribution

1. Introduction

The revolution in weather forecasting (Boer et al., 2014) has led to significant improvement in the simulation of precipitation in synoptic and mesoscales by Numerical Weather Prediction (NWP) models. However, the quantitative precipitation forecast (QPF) on a smaller scale, required for hydrological forecasts remains a challenge even in the latest high resolution operational models (Shrestha et al., 2013; Wang et al., 2016; Shahrban et al., 2016) with unacceptably large mean absolute error, MAE (Giinaros et al., 2015). The problem of errors in the QPF appears to be related to (a) displacement of the simulated centre of the mesoscale system compared to observed, (b) simulation of the phase of the diurnal cycle of precipitation over land by models a few hours before observed (Dirmeyer et al., 2012) and (c) underestimation of heavy precipitation by almost all climate models even up to a resolution of 12 km (Kendon et al., 2012). As the same factors are also responsible for prediction errors of thunderstorms and extreme rainfall events, it is critical to improve them in models for skillful predictions of hazards associated with increasing frequency of extreme rainfall events (Goswami et al., 2006). While there is a need for improving all three aspects of precipitation simulation in a model, in this study we focus only on the 'intensity' simulation of a convection-permitting NWP model. A simple increase in resolution of a model, however, is not helpful as has been found that it has little impact on the skill of prediction (Shrestha et al. 2013) or produces too intense extreme events (Kendon et al., 2012). It is recognized that high 'resolution' in a climate model is a necessary but not sufficient condition for simulating the variance of high-frequency fluctuations (Goswami and Goswami, 2016). It is also known that an adequate 'cloud microphysics' parameterization is essential for simulation of the organization of mesoscale systems and equatorial waves (Hazra et al., 2017, 2019). However, numerical simulation of electrical forces within clouds associated with extreme rainfall events are only beginning to be addressed in NWP models (Mansell et al.,2009; Dafies et al., 2018). Here, we test a hypothesis that a large part of underestimation of the 'intensity' may be related to modification of the raindrop size distribution (RDSD) by electric fields in the clouds and test the veracity of the hypothesis through simulations of rainfall in several 'strongly' electrified cases and 'weakly' electrified cases in a convection-permitting NWP model.

A substantial fraction of tropical precipitation (57-60%) originates from thunderstorms and electrified shower clouds with 30 dBZ radar echo-top temperature lower than -10^{o}C over land and -17^{o}C over ocean (Liu et al., 2010). The electrified shower clouds, embedded in Mesoscale Convective Systems (MCS) exhibits stronger in-cloud electrical environment but do not produce lightning (MacGorman et al., 2008; Liu et al., 2010). Two dynamically and microphysically distinct cloud regimes are known to contribute to the rainfall in the tropical atmosphere are named convective and stratiform (Houze, 1997). In the convective regime, characterized by stronger updraft, the precipitation particles grow by accretion of cloud liquid water, a process known as *coalescence* in the warm phase of cloud and *riming* in the mixed phase region (Houghton, 1968). In lightning-producing-clouds associated with stronger updraft, larger and numerous graupel particles formed by riming of supercooled water in the mixed phase region of cloud (Palucki et al., 2011; Mattos et al., 2016) where they take part in the electrification of cloud through non-inductive charging process (Bruning et al., 2010). Upon melting (below the melting level) the medium to larger sized graupel particles could contribute a substantial fraction of precipitation at the surface. The radar observations of lightning-producing clouds depict higher reflectivity in the mixed phase region of cloud indicating presence of larger hydrometeors relative to non-lightning-producing clouds (Williams et al., 1992; Mattos et al., 2016). It has been observed that aggregation of ice phase hydrometeors above the melting layer can produce larger raindrops at the surface (Tokay and Short, 1996). In the stratiform regime, where there is not much liquid water, the precipitation particles grow primarily by vapour diffusion and aggregation above the freezing level of cloud (Houze, 1997). Apart from the prevailing dynamics and microphysics, the precipitation formation processes are known to influenced by the ambient aerosol size distribution as well (Khain et al., 1999; Rosenfeld, 2000; Rosenfeld et al., 2002; Rosenfeld and Woodley, 2003), although the relationship between them is observed to be non-linear in intensity modification of precipitation(Khain et al. 2005).

The scientific speculation regarding the electrical influence on the cloud microphysical processes is long-standing, dating back to the time of Lord Rayleigh (1879). The lightning-producing clouds exhibit stronger in-cloud electrical environment with vertical electric field reaching values up to 400 kVm^{-1} (Winn et al,. 1974) with charge densities which could go up to 10^{9} elementary charges (Christian et al., 1980; Bateman et al., 1999). Several laboratories, observational and numerical modeling studies provide compelling evidence suggesting strong electrical influences on cloud/rain microphysical processes inside strongly electrified cloud

(Schlamp et al., 1976 1979; Khain et al., 2004; Bhalwankar and Kamra., 2007; Hortal et al., 2012; Harrison et al., 2015, 2020). Numerical calculation of collision efficiency between two charged cloud droplets in an external electric field (vertically downward if the field points from a positively charged region in the top of the cloud to a negatively charged region in the base of the cloud and downward if vice versa) by Schlamp et al., (1976, 1979) and Khain et al., (2004) reported a significant effect of an external electric field and electrical charges residing on the interacting drops on the collision efficiency of the drops. A few laboratory studies also revealed that the presence of a vertical electric field can broaden the rain RDSD and hence enhance the growth rate of raindrops (Bhalwankar and Kamra, 2007). A laboratory investigation by Ochs and Czys (1987) reported that permanent coalescence results for all impact angles upon collision of two drops if their relative charge exceeds 2×10^{-12} C irrespective of the polarity of the charges they carry. Our recent work of simultaneous field observations of the RDSD and electrification of clouds at the High Attitude Cloud Physics Laboratory (HACPL), India (Mudiar et al., 2018) strongly supports some of the earlier laboratory and modeling studies. The observed similarity in the growth rate of raindrops in the warm phase of stratiform (Mudiar et al., 2018) and more strongly electrified convective cloud (Mattos et al., 2016) indicates a significant influence of electric force on the coalescence growth of raindrops which evidently distinguish the evolutionary track of raindrops below the melting layer in strongly and weakly electrified clouds.

Our hypothesis proposed above has emerged from this compelling and consistent evidence of the electrical influences on the cloud microphysical processes, indicating the urgent need to include the electrical effects on rain formation in NWP models. Intrigued by this possibility, here we have attempted to test an NWP model's fidelity in simulating 8 rain events associated with a stronger in-cloud electrical environment and 5 rain events with a weaker electrical environment using the same model setup. The simulated precipitation fields are compared with the available observed data for validation. The results have been discussed from the perspective of

1. Electrical modification of RDSD parameters through enhanced collision-coalescence growth of raindrop and consequent modification of surface precipitation intensity.
2. Possible modification of surface precipitation by melting of larger ice-phased hydrometeors associated with lightning-producing cloud.

3. The influence of ambient aerosol size distribution in simulated precipitation intensity.

Attempts have also been made to bring in the electrical influences in the model physics schemes through modification of model RDSD parameters.

2. Data & Methodology

All the simulations pertaining to the current study were performed using Advanced Weather Research and Forecasting (WRF-ARW) model version 3.5.1 developed by the National Center for Atmospheric Research (NCAR). The WRF is fully compressible, non-hydrostatic, terrain-following 3D mesoscale model. The simulations are performed considering four nested domain (d01, d02, d03, d04) with a horizontal grid spacing of 27km, 9km, 3km &1km, respectively. Figure 1a shows the geographical coverage of the model domain along with the topographical map (Figure 1b) of the innermost domain. The innermost domain d04 is centered at the HACPL, Mahabaleshwar, (India; 17.92 N, 73.66 E). The initial and boundary conditions are provided from 6 hourly National Centre for Environmental Prediction (NCEP) Final operational global analysis data with $1^{o}\times 1^{o}$ horizontal resolution. The Rapid Radiative Transfer Model (RRTM) has been used for longwave radiation (Mlawer et al., 1997) while the Dudhia scheme (Dudhia, 1989) has been used for short wave radiation. In the model, the sub-grid scale effects of convective and shallow cloud are represented by the cumulus parameterization. The current model set up was tested with the Betts-Miller-Janjic (BMJ), Kain-Fritsch (KF) and Grell-Devenyi ensemble (GD) cumulus schemes (Results of KF and GD are not shown). As compared with the observation, the BMJ convective scheme was found to be better and used for the current study. The cumulus parameterization (BMJ scheme) is used in only the outer two domains (d01 & d02). The cloud-resolving 3rd and 4th domain are treated with explicit convection. The microphysical sensitivity of the model was tested with three bulk microphysical parameterization schemes, namely the WRF Double-Moment (WDM6) (Hong et al., 2010), the Thompson scheme (Thompson et al., 2004) and the Morrison double moment with six classes of hydrometeors (Morrison et al., 2005). After a comparison of simulated precipitation and RDSD with the observations (Figure not shown), the Morrison double moment scheme was found to be better and hence has been used for all the current simulations. More details regarding the experiment design are documented in Table 3.

Out of the 8 events with stronger in-cloud electrical environment considered for simulation experiment, 5 events were observed over the HACPL,(17.92 N,73.66 E) which is located in the Western Ghat (WG) of peninsular India at an altitude of 1.3 Km from mean sea level (MSL) with complex topography. All 5 events with the weaker electric environment were also observed over the HACPL. The pre-monsoon precipitation over the WG is highly convective in nature (Romatschke and Houze, 2011) while shallow convective rain dominates the monsoon season **(**Konwar et al., 2014). A study of deep tropical convection over Darwin, Australia revealed that 'break period' of monsoon exhibits vigorous convection with higher lightning activity, cause of which is assigned to the variation in conditional instability and updraft speed (Williams et al., 1992). The events observed over the HACPL are documented in the Tables 1 & 2 along with some of the available cloud properties and features derived from the Moderate Resolution Imaging Spectroradiometer (MODIS) (Terra platform) collection 6 (Baum et al., 2012) and European Centre for Medium-Range Weather Forecasts (ECMWF) interim reanalysis (ERA-Interim; Dee et al. 2011) at 0.25° × 0.25° resolution datasets. The other 3 events with the stronger in-cloud electrical environment were observed over Solapur (17.72^{o}N, 75.85^{o}E) in the rain shadow of the Western Ghat. The observations over Solapur were made in a ground campaign conducted during the Cloud-Aerosol Interaction and Precipitation Enhancement Experiment (CAIPEEX) (Kulkarni et al., 2012).

The distinction between stronger/weaker electrical environments is ascertained by the presence/absence of lightning discharges in the innermost domain (Figure 1)**.** The spatial distributions of lightning discharges observed over the model domain d04 for all the events over the HACPL are shown in Figure 2. While Figures 2(a-e) show lightning discharges in the area encompassing the model innermost domain, they are conspicuously absent in the events shown in Figures 2(f-j). For the events (a-c) listed in Table 1, lightning data were extracted from the World Wide Lightning Location Network (WWLLN) with detection efficiency of 25% -30% while for the rest; they were extracted from the Maharashtra Lightning Location Network (MLLN) (Pawar et al. 2017) with detection efficiency about 90%. The MLLN operates in the frequency range 1 KHz (VLF) and 10 MHz (HF). As lightning-producing clouds exhibit stronger electrical environment in terms of the magnitude of electric field at the surface as well as inside the cloud and charge distribution inside cloud, we termed these set of events as strongly electrified (SE) events while non-lightning-producing rain events were termed as weakly electrified (WE) events as these kind events are associated with weaker electric field. The in-cloud charging mechanism inside a lightning-producing cloud produces a tripole charge structure creating a stronger electric field between the main negative charge centre (located above the melting layer) and the ground.

The experiments were carried out as discussed below

A set of control (CTL) experiments were carried out for both the SE and WE of events with the WRF-ARW model with the standard physics packages using the same model setup and the simulated precipitation field and the RDSD were validated against available observed variables.

In the WRF-ARW, the precipitation is calculated using a Marshall-Palmer formulation of RDSD with a specified slope parameter, λ. We find that λ, used in the default physics scheme is inadequate to represent precipitation in the SE events. Hence in a second set of experiment; the default minimum value of the RDSD slope parameter, λ, in the physics module has been replaced with a new λ as obtained from observation, averaged over all five SE events observed over the HACPL. It has been observed that the values of λ vary with rain intensity during a storm**,** although non-linearly. Hence, a time**-**averaged value over the entire rainy period for each of the events is considered as a representative value. Abel and Boutle (2012) show that simulated fields are quite sensitive to the time-averaged drop size distributions. The influence of λ on the simulated precipitation has been discussed in the supporting text in details. The value of λ nearest to the mean for a particular storm observed to better simulate the precipitation fields for that storm (Figure S1). A new set of simulations was carried out for the same SE events using the same model setup with the modified physics.

For the rain events recorded in the afternoon or late afternoon hours, the model was initialized with the NCEP FNL 00:00:00 UTC initial conditions (IC) while for the late night or early morning events, initialization was performed using the 12:00:00 UTC ICs. The details of the model design have been tabulated in Table 3.

For comparison with observations, data from a surface-based JW disdrometer (JWD) located at the HACPL and at Solapur were used which record the RDSD and rain intensity (Joss and Waldvogel, 1967). The hourly accumulated rain was extracted from the JWD record and considered for validation of simulated hourly precipitation. The recorded distribution was also used to calculate the RDSD parameters from the gamma distribution fitted to the RDSD. Data recorded by an optical disdrometer installed at the Atmospheric Electricity Laboratory, (AEO) Pune (18.52^{o}N, 73.85^{o}E**),** about 100 km away from the

HACPL was also used to study the geographical variability of the RDSD. The relation between surface-measured electric field and RDSD parameters during storms has been investigated with an electric field-mill located at the AEO which was kept in a pit with its sensor flush to the ground. This field-mill measures the vertical component of the surface electric field produced by internal charging mechanism of cloud. More details of the instruments are given in Pawar et al., (2017b)**.** The aerosol size distribution was observed over the HACPL with a Scanning Mobility Particle Sizer (SMPS) while Cloud Condensation Nuclei (CCN) was measured with a collocated Cloud Condensation Nuclei Counter (CCNC) (Singla et al., 2019).

3. Results

3.1 Comparison of Simulated Precipitation and RDSD with Observation

a) Strongly Electrified Cases

The reported underestimation of simulated rain intensity for the rain events that are associated with lightning discharges suggested the model's inability to reproduce heavy precipitation amount towards higher rain bins. The underestimations of rainfall are linked with the improper representation of the RDSD. In the present study, the 5 SE events observed over the HACPL are simulated and verified for precipitation in comparison with the JWD measured hourly rain rate. As we have not addressed the spatial displacement of the simulated center of mesoscale convection relative to the observation, the simulated precipitation is verified in all the grid points within a 25km × 25 km box, centered at the HACPL. The grid point that shows the closest value of precipitation rate to the observed one is considered as model simulated precipitation and compared with the observation. Figure 3 (a-e) shows the model-simulated rain rate for the events reported in Figure 2(a-e) along with the observed rain rate. Apart from the shift in timing of the peak rainfall, significant underestimation of the observed precipitation can be seen in the simulations for the events 3(a-c) while for events 3(d-e), the model failed to simulate any rain during the event duration. The underestimation of rain intensity is found to be consistent with the earlier reported dry bias in the simulation of heavy precipitation associated with lightning activity (Giinaros et al., 2015; Dafis et al., 2018). In some cases, the model predicted the rainfall 3-4 hours advance while in others the rainfall was delayed by 1-2 hours. This phase difference in the diurnal cycle of the simulated peak and observed peak in precipitation is well recognized (Jeong et al., 2011; Diro et al., 2012; Walther et al., 2013; Gao et al., 2018).

The higher sensitivity of model-accumulated precipitation to the prescribed RDSD was reported in a number of earlier studies (Gilmore et al., 2004; Curic et al., 2010; Morrision, 2012; Kovacevic and Curic, 2015). The prognostic variables like mixing ratios and number concentrations of different species of hydrometeors are expressed as a function of the RDSD parameters. In Figure 3(f-j), the model-simulated RDSDs were compared with the observed RDSD. The observed RDSD was averaged over the entire duration of the rainfall for each event. The simulated RDSD was calculated using the model-predicted rain mixing ratio averaged over the rain period. The double moment microphysics scheme predicts the mass mixing ratios and number concentration of hydrometers assuming a gamma particle size distribution

$$N(D) = N_0\, D^{\mu} e^{-\lambda D} \qquad (1)$$

Where N_0 , λ, μ are the intercept, slope and shape parameters of the size distribution, respectively. D is the diameter of the particles.

With μ=0 for rain (Morrison et al., 2008), the size distribution of rain will take the form of exponential function (Marshall-Palmer distribution)

$$N(D) = N_0\, e^{-\lambda D} \qquad (2)$$

λ & N_0 can be derived from the model-predicted rain number concentration N and rain mixing ratio q

$$\lambda = \left(\frac{\pi \rho_{r}\, N}{q\rho}\right)^{1/4} \qquad (3)$$

$$N_0 = N\,\lambda \qquad (4)$$

Where ρ_r is the density of raindrops (1000 kg m^{-3}) and ρ is the air density.

Consistent with the underestimation of observed rainfall intensity by the model in the events shown in Figure 3(a-c), the simulated RDSD in Figure 3(f-h) shows substantial underestimation in the number concentration of larger raindrops compared to the observation. As the model was unable to reproduce rainfall at the surface for the SE events shown in Figure 3(d-e), the RDSD corresponding to these events only depicts the observed distributions (Figure 3(i-j)). The overestimation of the smaller-size raindrops may be caused by the inherent deficiency of assumed Marshall-Palmer distribution (Gao et al., 2018). It was observed that the underestimation in the drops number concentration increases as drop size increases.

b) Weakly Electrified Cases

It is interesting to note that there is no underestimation of observed rainfall by the model in the WE cases (Figure 4(a-e)). Apart from the generic problem of timing of peak rainfall simulation, the model in fact slightly overestimated the precipitation intensity compared with the observations in three out of five events as shown in Figure 4(a-c). This wet bias in the WE events was found to be in contrast with the reported dry bias in SE events. The temporal spread in the simulated rain was found to be consistent with the observation. For some of the events, the phase shift in the precipitation peak was found to be 1-4 hours.

The right panels of Figure 4(f-j) depict the comparison of the simulated RDSD with the observed ones. Both the sets of RDSD are averaged over the entire rain duration recorded by the model and JWD. The observed RDSD for the WE events primarily found to be exponential in nature and comparable with the simulated ones in almost all the events, as shown in Figure 4(f-j). It is also observed that in both types of events, the model overestimated the number concentration of smaller size drops. In the case of WE events for higher rain intensity, the tail of the distribution was extended towards the larger drop size in the JWD-measured RDSD, while in contrast, broadening of the RDSD towards the larger size range was observed irrespective of the rain intensity for SE events.

Thus, for the WE events, the simulated precipitation and the RDSDs were found to be comparable with the observations while for the SE cases, intensity of rainfall is underestimated consistent with significant underestimation of larger drops indicating a potential limitation in the RDSD parameterization in the Morrison microphysics used in the WRF-ARW model. It is clear that the inability of the model to simulate the intensity of precipitation in the SE cases is related to its bias in simulating the larger drops in the RDSD. The fact that the slope of the simulated RDSD in the WE cases match well with that of observations, indicates that the model specification of ‘slope’ for SE cases is inadequate. A few simulation studies (Gilmore et al., 2004; Curic et al., 2010; Abel and Boutle, 2012; Morrison, 2012; Kovacevic and Curic, 2015) indicated that the simulated precipitation is very sensitive to the prescribed RDSD parameters viz. μ, λ and N_o. Also, these parameters are observed to depend explicitly on prevailing microphysical processes (Konwar et al., 2014).

4. The Electrical Modification RDSD slope parameter, λ

The findings reported in Mudiar et al., (2018) indicate a substantial modification of RDSD by in-cloud electrical forces. The observed broadening of the RDSD in SE events reduces the value of λ for the distribution when compared to the same for WE events. It has been shown that the RDSD achieves this broadening through enhanced collision–coalescence growth of raindrops below the melting layer mediated by in-cloud electrical forces. Figure 5(a) depicts the bar plot representation of the mean value of λ (averaged over the entire rainy periods) for all the events reported in Figure 2. These values of λ are estimated using the method of moments reported in Konwar et al.,(2014). It is notable that values of λ are distinguishable between the SE and WE events with substantially lower values for the SE events. Figure 5(b-c) depicts the observed relation between rain intensity and λ for some more SE and WE events observed over the HACPL. It is interesting to note that for low rain intensity (<10 mm/hr) λ could be high for both SE and WE events. However, for strong rain intensity (>20 mm/hr), the SE events are associated with a much lower value of mean λ (~2.5 mm^{-1}) than the WE ones (~7.0 mm^{-1}), which clearly suggests that broader RDSD spectrum dominates the SE events. The reduction in λ values in SE cases are primarily due to the extension of the RDSD to larger raindrops that also indicate presence of big raindrops.

The observed difference in λ between both the sets of events can be attributed to the prevailing stronger in-cloud electrical environment in SE clouds. This attribution is based on extensive laboratory (Bhalwankar and Kamra., 2007; Hortal et al., 2012; Harrison et al., 2015; Y. Yang *et al*., 2018), numerical (Schlamp et al., 1976, 1979; Khain et al., 2004) and observational (Mudiar et al., 2018; Harrison et al., 2020) evidence regarding the substantial electrical influence in the microphysical properties of cloud/raindrops size distribution. It has been shown that stratiform clouds with a stronger electrical environment are inherently associated with broader RDSD with smaller values of λ.

In order to further investigate the effect of lightning in modification of the value of λ, we have selected some isolated lightning events recorded by the MLLN within 700 m of the HACPL. While selecting these lightning events, it was ensured that no other lightning events were recorded by the MLLN within 3-4 minutes of the selected event. Figure 6(a-d) depicts time evolution of values of λ before and after seven selected lightning events. The interesting observation is that 2-3 minutes after the lightning, λ exhibits a transient dip indicated by the downward arrow. It may be noted here that the dip in the value of λ observed to be inherently associated with a transient amplification in rain intensity as well. It has also been observed that surface RDSD broadens with a 2-3 minutes time lag after an overhead lightning which suggested that lightning could enhance the growth of raindrops in the warm phase of cloud (discussed in details elsewhere) through deposition of ions inside the cloud (Heckman and Williams**,** 1989; Williams and Montanya, 2019**)**. We hypothesize that the broadening of RDSD by electrification of cloud droplets by lightning may be a possible cause of lower value of λ, observed after an overhead lightning. However, we also recognize that the robustness of this decrease in λ following lightning needs to be established with more number of observations.

The evidence presented above strongly indicates that the electrical field within the clouds plays a critical role in broadening the RDSD and in increasing the rainfall. Laboratory experiments mentioned above strongly support this conclusion where the role of dynamics on RDSD could be controlled. A counter argument in the case of observations is that the SE cases are largely associated with strong convective events where dynamics broadens the RDSD and lightning is a result, not the cause. Our view is that indeed the initiation of electrification and lightning could be due to dynamics. However, once electrified, they would broaden the RDSD further (weaken λ) and lead to further increase in rainfall. The question, therefore, is not whether but by how much λ is decreased by the electrical effects? In order to make an estimate of this influence of electrical fields of λ, we investigate the influence of in-cloud electric environment in the modification of λ for the SE event by analyzing a few thunderstorms observed over the AEO. Four thunderstorms were observed over the AEO on 3 June; 31 August; 1 September and 9 September 2008. For all the four storms, the surface electric field was recorded with a surface-based field mill located at the AEO. The simultaneous RDSDs for all the storms were measured with a collocated optical disdrometer. While for the storm observed on 3 June exhibits a peak lightning frequency of 24 flashes min^{-1}, the other three storms are smaller storms with a peak lightning rate of 3-8 flashes min^{-1}. It has been observed that, although the strength of the surface-measured electric field is the summation of fields due to charges in the primary charge centre and space charge in the sub-cloud layer, the variation of the field at the surface remained coupled with the charging processes in the main negative charge centre located in the temperature regime ranging -10^{O}C to -25^{O}C inside a strongly electrified cloud (Standler and Winn,1979; Soula and

Chauzy,1991**)**. Figure 7(a-d) depicts the scatter plot representation of the surface measured-electric field and λ for all the four storms. The two observables have been averaged over every two minutes interval during the rainy periods. For all the storm, λ exhibits a decreasing trend with the increasing magnitude of electric field. This decrease in value of λ is caused by the broadening of the corresponding RDSD. In a cloud chamber experiment, Y. Yang *et al.*,(2018) observed broadening of particle size distribution after applying an electric field. They observed that with higher applied electric field, the size of single water drop increases and propose that presence of electric field can enhance the collision-coalescence processes between water drops. Same observation has been reported by Mudiar et al., (2018) in their observation of SE stratiform rain events. The collective evidence from laboratory experiments and observational analysis confirmed the significant influence of in-cloud electric fields on the microphysical properties (primarily the collision-coalescence process) of SE clouds and hence on the electrical modification of λ. It is noted that the correlations between λ and the electric field are highly significant but not perfect. This may be due to the role of dynamics on λ. The correlations in the Figure indicate that a 20-40% decrease in the value of λ may be attributed to electrical effect. We believe this is an important quantification of broadening of RDSD by electric field.

The collective effect of electric field and lightning on the RDSD modification in the SE events may explain the observed difference in the values of λ observed in Figure 5(b-c). An appropriately modified Morrison scheme for the SE cases and re-simulation of the SE cases with the modified scheme is presented next.

5. Modification of Model RDSD for Strongly Electrified events

By virtue of the microphysical modification of λ through enhanced collision-coalescence growth of raindrops in the presence of stronger in-cloud electric forces, the characteristic value of λ for the SE events is observed to be distinct from the WE ones. Here we demonstrate that the simulated precipitation exhibits significant improvement if modification of the RDSD by electric field is adequately included for the SE events. A modification of the model physics in Morrison scheme is achieved primarily through modification of the slope parameter λ (mm^{-1}). As indicated in the physics module of the WRF (Morrison), an earlier attempt has been made to increase the minimum value of λ for rain in the WRF version 3.2, although as would be seen from the current study, the use of a universal λ may be responsible for the observed discrepancy between simulated and observed rainfall in the case of the SE and WE events. In this sensitivity experiment, the default minimum value for λ in the physics module has been replaced with a new λ averaged over all the five SE events as obtained from observation over the Indian subcontinent. As the values of λ are observed to vary with rain intensity, the time-mean of λ is calculated for each events considering the entire rainy periods as a representative value for each of the SE events. It should be noted here that the value of λ is not predicted from a detailed model for rain formation incorporating the electrical effect in the model microphysical schemes. The modified simulated precipitation is shown in green colors in Figures 8(a-e) indicated as 'Morr(M)' along with the default Morrison indicated as 'Morr' together with the observed ('Obs'). Substantial improvement was observed in rain intensity with the incorporation of the modified λ in all the events. For the events shown in Figure 8(d-e), for which the default Morrison scheme was unable to reproduce any rain for the simulated period, the model with the Morr(M) reproduces a substantial amount of rain albeit with some underestimation still remaining. The right panels of Figure 8 depict the simulated RDSD with the modified scheme along with the default and the observed ones. Substantial improvement in number concentrations of larger raindrops can be observed with the Morr(M) (Figure 8(f-h)). While for the events shown in Figure 8(i-j), the simulated RDSD show some improvement consistent with the larger amount of simulated rainfall, but with underestimation of larger raindrops still persisting. The overestimation of the number concentration of the smaller size drops still persists. The overall improvement in the accumulated rain and RDSD indicate considerable sensitivity of simulated precipitation to λ and establish the benefit of the electrically-modified slope parameter, λ.

In order to ascertain the representativeness of λ derived over the HACPL, we have investigated the spatio-temporal variability of λ for SE events. For this purpose, we have evaluated λ considering some additional SE rain events (other than the events documented in Table 1) associated with lightning over the HACPL as well as another two locations in the state of Maharashtra, e.g., in Pune & Solapur. While the HACPL is located on the windward slope of the WG, Pune and Solapur are located in the leeward side of WG with MSL heights of 560m and 458m respectively. The values are documented in Table S1, S2 and S3 (see supporting tables) and found to be in a similar range as the events reported in Figure 3. Figure 9 depicts the results of simulation of 3 SE events observed over Solapur using the same microphysical and cumulus schemes. The modified simulated precipitation (Morr(M)) corresponds to the same value of λ as over the HACPL. The substantial improvement in the precipitation field as well as in the RDSD with the modified physics over the HACPL as well as over Solapur, a region of significantly lower climatological mean rainfall added confidence to our conclusion that the effect of electrically enhanced coalescence growth of raindrops in precipitation formation inside a SE cloud is valid irrespective of geographical locations. Table S4 depicts several representative values of λ for the WE events over the HACPL, distinguishable from the values in the SE category (Table S1) with higher magnitude & variability.

6. Aerosol and CCN influences on the simulated Rain Intensity:

One factor that could add a certain amount of uncertainty to our primary conclusion is the precipitation modification by aerosol concentrations. Numerous in-depth studies reported significant modification of accumulated precipitation by ambient aerosol concentration, although the relationship between the two observables is quite non-linear in modification of precipitation (Khain et al., 1999; Rosenfeld, 2000; Rosenfeld et al., 2002; Rosenfeld and Woodley, 2003; Andreae et al., 2004; Khain et al., 2005). To gain more confidence in our primary hypothesis of electrical enhancement of precipitation intensity, we further investigated the response of precipitation to the number concentration of aerosol, which can act as Cloud Condensation Nuclei (CCN) over the HACPL. The aerosol size distribution was measured over the HACPL with a Scanning Mobility Particle Sizer (SMPS) while Cloud Condensation Nuclei (CCN) were measured with a collocated Cloud Condensation Nuclei Counter (CCNC) (Singla et al., 2019). The measured CCN number concentration over the HACPL indicated no discernible difference between the SE and WE events (Figure 10a). The measured aerosol concentration shows a slightly higher value (~ 20 cm^{-3}) for SE (157 cm^{-3}) events compared to that of WE (137 cm^{-3}), with both exhibiting a peak around 0.05 μm (*Aitken mode*). When the model physics is perturbed by adding the difference between the mean concentration of aerosol and the one observed for SE events (around 6% of mean), it is observed that an increase in aerosol concentration alone does not substantially change the simulated intensity of precipitation, although it adds a little to the total accumulation (Figure 10b). However, when the aerosol perturbation is added with electric-simulated intensity, simulated intensity shows a discernible improvement while the peak rainfall is delayed by an hour. This delay is expected as a higher concentration of aerosol would reduce the drop sizes inhibiting collision-coalescence growth of drops in the warm phase, thereby suppressing the warm rain by the first aerosol indirect effect (Twomey et al., 1984; Konwar et al., 2012; Hazra et al., 2013). The RDSDs shown in Figure 10(c) also do not indicate a significant change in the number concentration of larger drops with aerosol inclusion, although the modification through electrically-modified λ is quite significant. Results of this experiment (see supporting text for details) adds to our confidence on the primary conclusion of electrical modification of simulated precipitation intensity with a possible contribution from the melting of larger graupel particles associated with SE clouds.

7. Discussions and Conclusion

In quest of better estimation of precipitation for the benefit of meteorological as well as hydrological applications and encouraged by compelling evidences from laboratory as well as field experiments on substantial influences from electrical forces on cloud/rain microphysical processes, here we demonstrate that modeling the RDSD correctly in an NWP model is critical in simulating and predicting the rainfall with fidelity in MCS. A microphysical modification in the model emerged from a set of simulations of 8 SE cases and 5 WE cases with Morrison microphysics and a critical evaluation of their biases. The results suggest that the underestimations of heavy rainfall associated with SE events may be caused by the model's inability to properly reproduce the larger raindrops which get substantially improved with the inclusion of electrically-modified RDSD slope parameter λ. The observational evidence (presented here and elsewhere) establishes that the value of λ gets substantially modified by in-cloud electrical field as well as by lightning. The improvement in the simulated rain intensity with an electrically modified λ reaffirms the idea of substantial influence of in-cloud electric forces in physics of rain formation along with laboratory and observational evidences (Schlamp et al.,1976, 1979; Khain et al., 2004; Bhalwankar and Kamra, 2007; Harrison et al., 2015,2020; Mudiar et al., 2018).

As discussed in the introduction, in SE cloud, melting of larger graupel particles (e.g. Palucki et al., 2011; Mattos et al., 2016) may also have some contribution to the surface rainfall. However, quantification of the same is lacking. The uncertainty in the accurate prediction of ice phase hydrometeors (ice, graupel, and snow) produces major uncertainty in the simulation fields. However, through a WRF simulation of convective storm, Morrison et al., (2009) find that accurate prediction of number concentration of rain has more impact on the simulated fields than the prediction of number concentration of snow and graupel. The vertical profiles of simulated hydrometeors for the two sets of events (SE and WE) observed over the HACPL and selected for the testing of our primary hypothesis have been presented in Figure 11. A little higher cloud ice (~5×10^{-5} kg kg^{-1} for SE and 3.3×10^{-5} kg kg^{-1} for WE) and graupel mixing ratio(~1.8×10^{-4} kg kg^{-1} for SE and 1.6×10^{-5} kg kg^{-1} for WE) (Figure 11a

& 11c) are as expected for the lightning-producing clouds required by the non-inductive charging mechanism of cloud electrification. In case WE events, it is also found that graupel resides at lower altitude in the mixed phase region of cloud compared to the SE events (also see Mattos et al., 2016) suggesting the presence of larger size graupel particles above the melting layer in WE events relative to the SE ones, where they are more numerous. The underestimation in rain intensity in SE events despite having higher graupel and ice mass than the WE events suggest that the underestimation in the observed rain intensity may be caused by some missing microphysical processes influenced by electric forces, which broaden the RDSD and hence enhance the growth rate of raindrops. The improvement in rain intensity with the inclusion of the distinctly different characteristic slope parameter in SE and WE events (Figure 5b-c) suggest that this missing physics is likely to be electrically enhanced collision-coalescence growth of raindrops inside the SE cloud. However, the melting of graupels (more numerous in SE events than the WE) can also contribute to the total rainfall in SE events. But as the result suggests, it is not contributing much to the biases in intensity simulation of SE events.

The simulations presented in the study are short-range predictions and as such sensitive to initial conditions (IC). The coarse resolution ($1^o \times 1^o$) analysis (NCEP-FNL) interpolated to the finer model domain may introduce some uncertainty in the IC over the finer resolution model domain ($0.01^o \times 0.01^o$). To test the robustness of our main result that Morr(M) improves the simulation of rainfall intensity and the RDSD in the SE cases, we have performed an ensemble of simulations with 10 ensemble members for the SE event (b) documented in Table 1 using the default Morrison and Modified Morrison schemes. The ensemble members were generated by adding slight perturbation to the temperature field in NCEP ICs in the range of ±0.05 K, determined based on the standard deviation of hourly mean vertical profiles. It was observed (Figure 12) that neither the rain intensity nor the RDSD show significant sensitivity to the perturbed ICs. In contrast, the sensitivity to the electrically-modified λ is highly significant, suggesting the robustness of our primary conclusion.

We are aware that the modification of the Morrison scheme used in the numerical experiments described here is rather simplistic. The objective has been to use it as a ‘proof of concept’ for improvement of biases in simulation of the pdf of rainfall by prediction models potentially through modification of λ. However, as seen in Fig.5 (b,c), the dependence of λ on electrical forces (or lightning flashes) is much more complex and nonlinear. Therefore, the modification of the Morrison scheme also has to be essentially nonlinear and dynamic. While this is outside the scope of the present work, we hope to attempt it in the future. The results presented here strengthens our optimism that with the improved parameterizations of the electrical effect in the physics module of NWP models, the reported dry bias associated with simulation of heavy precipitation events in the weather/climate models is likely to be minimized and would increase the skill of the models in predicting the intensity of quantitative precipitation.

Declaration of Competing Interest

None.

Acknowledgments

The IITM is funded by the Ministry of Earth Sciences, Government of India. We thank Director, IITM for his continuous support and encouragement. We sincerely acknowledge the efforts of scientific and technical staffs of IITM, Pune, working in the HACPL to collect the JWD data. First author is grateful to Madhuparna Halder for the support in initial model setup. The data used to prepare the manuscript is available in the link https://iitmcloud.tropmet.res.in/index.php/s/g87WJjyayHLw42n. We are thankful to the University of Washington in Seattle, USA for making available the WWLLN data (http://wwlln.net/). BNG thanks the Science and Engineering Research Board, Government of India for the SERB Distinguished Fellowship. The Authors are grateful to CAIPEEX team members for their efforts in collecting data.

References:

Abel, S.J. and Boutle, I.A. (2012), An improved representation of the raindrop size distribution for single-moment microphysics schemes. Q.J.R. Meteorol. Soc., 138: 2151-2162. doi:10.1002/qj.1949.

Andreae, M. O., D. Rosenfeld, P. Artaxo, A. A. Costa, G. P. Frank,K. M. Longo, and M. A. F. Silva-Dias (2004) Smoking rainclouds over the Amazon, Science,303, 1337–1342, doi:10.1126/science.1092779

Bateman, M. G., T. C. Marshall, M. Stolzenburg, and W. D. Rust (1999) Precipitation charge and size measurements inside a New Mexico mountain thunderstorm, *J. Geophys Res (Atmospheres)*, 104, 9643–9654, doi:10.1029/1998JD200118.

Bhalwankar, R. V., and A. K. Kamra (2007) A wind tunnel investigation of the deformation of water drops in the vertical and horizontal electric fields, J. Geophys. Res., 112, D10215, doi: 10. 1029/2006JD007863.

Baum, B. A., W. P. Menzel, R. A. Frey, D. Tobin, R. E. Holz, S. A. Ackerman, A. K. Heidinger, and P. Yang (2012) MODIS cloud top property refinements for Collection 6, J. Appl. Meteorol. Climatol., 51, 1145–1163.

Boers N, Bookhagen B, Barbosa H, Marwan N, Kurths J, Marengo J (2014) Prediction of extreme floods in the Eastern Central Andes based on a complex networks approach. Nat Commun 5:5199. doi: 10.1038/ncomms6199

Bruning, E.C., Rust, W.D., MacGorman, D.R., Biggerstaff, M.I., Schuur, T.J. (2010) Formation of charge structures in a supercell. Mon. Weather Rev. 138, 3740–3761.

Christian H., C. R. Holmes, J. W. Bullock, W. Gaskell, A. J. Illingworth, and J. Latham,(1980) Airborne and ground-based studies of thunderstorms in the vicinity of Langmuir Laboratory, *Q. J. R. Meteorol. Soc*., 106, 159-174.

Curic M., D. Janc, K. Veljovic (2010) Dependence of accumulated precipitation on cloud drop size distribution. Theor. Appl. Climatol. 102, 471–481.

Dafis, S., Fierro, A., Giannaros, T. M., Kotroni, V., Lagouvardos, K., and Mansell, E.(2018) Performance evaluation of an explicit lightning forecasting system. Journal of Geophysical Research: Atmospheres, 123, 5130–5148. https:// doi.org/10.1029/2017JD027930.

Dee, D. P., Uppala, S. M., Simmons, A. J., Berrisford, P., Poli, P., Kobayashi, S., et al. (2011) The ERA-interim reanalysis: Configuration and performance of the data assimilation system. Quarterly Journal of the Royal Meteorological Society, 137(656), 553–597. https://doi.org/ 10.1002/qj.828

Dirmeyer, P. A., et al. (2012) Simulating the diurnal cycle of rainfall in global climate models: Resolution versus parametrization,Clim.Dyn.,39, 399–418.

Diro, G. T., S. A. Raischer, F. Giorgi, and A. M. Tompkins, (2012) Sensitivity of seasonal climate and diurnal precipitation over Central America to land and sea surface schemes in RegCM4. Climate Res., **52**, 31–48, doi:https://doi.org/10.3354/cr01049.

Dudhia, J., (1989) Numerical study of convection observed during the winter monsoon experiment using a mesoscale two dimensional model. J. Atmos. Sci., 46, 3077–3107.

Gao, W., Liu, L., Li, J., and Lu, C. (2018) The microphysical properties of convective precipitation over the Tibetan Plateau by a subkilometer resolution cloud-resolving simulation. Journal of Geophysical Research: Atmospheres, 123, 3212–3227. https://doi.org/10.1002/ 2017JD027812

Gilmore, M. S., Straka, J. M., and Rasmussen, E. N. (2004) Precipitation uncertainty due to variations in precipitation particle parameters within a simple microphysics scheme. Monthly Weather Review, 132(11), 2610–2627. https://doi.org/10.1175/Mwr2810.1

Giannaros, T. M., Kotroni, V., and Lagouvardos, K. (2015) Predicting lightning activity in Greece with the Weather Research and Forecasting (WRF) model. Atmospheric Research, 156, 1–13.

Goswami, B. N., Venugopal, V., Sengupta, D., Madhusoodanan, M. S., and Xavier, P. K. (2006) Increasing trend of extreme rain events over India in a warming environment. Science, **314**(5804),1442– 1445. https://doi.org/10.1126/science.1132027

Goswami B.B., B.N. Goswami (2016) A Road Map for Improving Dry-Bias in Simulating the South Asian Monsoon Precipitation by Climate Models, Climate Dynamics, DOI:10.1007/s00382-016-3439-2

Harrison, R. G., K. A. Nicoll, and M. H. P. Ambaum (2015) On the microphysical effects of observed cloud edge charging, Q. J. R. Meteorol. Soc. ,141 , 2690– 2699, doi:10.1002/qj.2554.

Harrison, R. G., Nicoll, K., Ambaum, M., Marlton, G., Aplin, K., & Lockwood, M. (2020) Precipitation Modification by Ionization. *Physical Review Letters*, *124*(19), 198701-198707. https://doi.org/10.1103/PhysRevLett.124.198701

Hazra, A., B. N. Goswami, and J.-P. Chen (2013) Role of interactions between aerosol radiative effect, dynamics, and cloud microphysics on transitions of monsoon intraseasonal oscillations, J. Atmos. Sci., 70, 2073–2087, doi:10.1175/JAS-D-12-0179.1.

Hazra, A., Chaudhari, H.S., Saha, S.K., Pokhrel, S. and Goswami, B.N. (2017) Progress towards achieving the challenge of Indian summer monsoon climate simulation in a coupled ocean–atmosphere model. Journal of Advances in Modeling Earth Systems, **9**, 2268–2290.

Hazra A., Chaudhari H.S., Saha S.K., Pokhrel S., Dutta U., Goswami B.N. (2019) Role of cloud microphysics in improved simulation of the Asian monsoon quasi-biweekly mode (QBM), Climate Dynamics, DOI:10.1007/s00382-019-05015-5, 1-16

Heckman, S., and E. Williams (1989) Corona envelopes and lightning currents, J. Geophys. Res., 94, 13,287.

Hong, Y.S., Lim, S.K., Lee, Y.H., Ha, J.C., Kim, H.W., Ham, S.J., Dudhia, J.(2010) Evaluation of the WRF double-moment 6-class microphysics scheme for precipitating convection. Adv. Meteorol. http://dx.doi.org/10.1155/2010/707253.

Hortal A.A. Pérez, S.E. García, G.M. Caranti, (2012) Droplet charging by high voltage discharges and its influence on precipitation enhancement, Atmospheric Research, Volume 108.

Houghton, J. G., (1968) On precipitation mechanisms and their artificial modification. J. Appl. Meteor., 7, 851–859.

Houze, R. A. (1997) Stratiform precipitation in regions of convection: A meteorological paradox? Bull. Am. Meteorol. Soc., 78(10), 2179–2196.

Joss, J. and Waldvogel, A. PAGEOPH (1967) 68: 240. doi: 10.1007/BF00874898

Jeong, J.-H., A. Walther, G. Nikulin, D. Chen, and C. Jones,(2011) Diurnal cycle of precipitation amount and frequency in Sweden: Observation versus model simulation. Tellus, **63A**, 664–674, doi:https://doi.org/10.1111/j.1600-0870.2011.00517

Kendon, E. J., Roberts, N. M., Senior, C. A., and Roberts, M. J. (2012) Realism of rainfall in a very high-resolution regional climate model, J. Clim., **25**, 5791– 5806, doi:10.1175/JCLI-D-11-00562.1

Khain, A. P., A. Pokrovsky, and I. Sednev (1999) Some effects of cloud–aerosol interaction on cloud microphysics structure and precipitation formation: Numerical experiments with a spectral microphysics cloud ensemble model, Atmos. Res.,52, 195–220

Khain, A., M. Arkhipov, M. Pinsky, Y. Feldm an, and Y. Ryabov (2004) Rain enhancement and fog elimination by seeding with charged droplets. Part 1: Theory and numerical simulations, J. Appl. Meteorol., 43, 1513–1529, doi:10.1175/JAM2131.1.

Khain, A., D. Roseenfeld, and A. Pokrovsky (2005) Aerosol impact on the dynamics and microphysics of deep convective clouds, Q. J. R. Meteorol. Soc., 131, 2639–2663, doi:10.1256/qj.04.62

Konwar, M., R. S. Maheskumar, J. R. Kulkarni, E. Freud, B. N. Goswami, and D. Rosenfeld (2012) Aerosol control on depth of warm rain in convective clouds, J. Geophys. Res., 117, D13204, doi:10.1029/2012JD017585.

Konwar, M., S. K. Das, S. M. Deshpande, K. Chakravarty, and B. N. Goswami (2014) Microphysics of clouds and rain over the Western Ghat, J. Geophys. Res. Atmos., 119, doi: 10.1002/2014JD021606.

Kovacevic, N. M. Curic (2015) Precipitation sensitivity to the mean radius of drop spectra: comparison of single- and double-moment bulk microphysical schemes Atmosphere, 6 (2015), pp. 451-473, 10.3390/atmos6040451.

Kulkarni, J. R., et al. (2012) The Cloud Aerosol Interactions and Precipitation Enhancement Experiment (CAIPEEX): Overview and preliminary results, Curr. Sci., 102, 413–425.

Liu, C., E. R. Williams, E. J. Zipser, and G. Burns (2010) Diurnal variations of global thunderstorms and electrified shower clouds and their contribution to the global electrical circuit, J. Atmos. Sci.,67, 309–323,doi:10.1175/2009JAS3248.1.

MacGorman, D. R., W. D. Rust, T. J. Schuur, M. I. Biggerstaff, J. M. Straka, C. L. Ziegler, E. R. Mansell, E. C.Bruning, K. M. Kuhlman, N. R. Lund, N. S. Biermann, C. Payne, L. D. Carey, P. R. Krehbiel, W. Rison, K. B. Eack, and W. H. Beasley (2008) TELEX: The thunderstorm electrification and lightning experiment. Bull. Amer. Meteor. Soc., 89, 997–1018.

Mansell, E. R., C. L. Ziegler, and E. C. Bruning (2010), Simulated electrification of a small thunderstorm with two-moment bulk microphysics, J. Atmos. Sci., 67(1), 171–194, doi:10.1175/2009JAS2965.1.

Mlawer, E.J., Taubman, S.J., Brown, P.D., Iacono,M.J., Clough, S.A., (1997) Radiative transfer for inhomogeneous atmosphere: RRTM, a validated correlated-kmodel for the long-wave. J. Geophys. Res. 102, 16663–16682. http://dx.doi. org/10.1029/97JD00237.

Morrison H, Gettelman A. (2008) A new two-moment bulk stratiform cloud microphysics scheme in the community atmosphere model, version 3 (CAM3). Part I: Description and numerical tests. J. Climate 21: 3642–3659.

Morrison, H., G. Thompson, and V. Tatarskii (2009) Impact of cloud microphysics on the development of trailing stratiform precipitation in a simulated squall line: Comparison of one- and two-moment schemes. *Mon. Wea. Rev.*, **137,** 991–1007

Morrison, H., Tessendorf, S. A., Ikeda, K., and Thompson, G. (2012) Sensitivity of a simulated midlatitude squall line to parameterization of raindrop breakup. Monthly Weather Review, 140, 2437–2460.

Morrison, H., Curry, J.A., Shupe,M.D., Zuidema, P., (2005) A new double-moment microphysics parameterization for application in cloud and climate models. Part II: single-column modeling of arctic clouds. J. Atmos. Sci. 62, 1678–1693.

Morrison H, Curry JA, Khvorostyanov VI. (2005) A new double-moment microphysics parameterization for application in cloud and climate models. Part I: Description. J. Atmos. Sci. 62: 1665–1677.

Mudiar, D., Pawar, S. D., Hazra, A., Konwar, M., Gopalakrishnan, V., Srivastava, M. K., and Goswami, B. N. (2018) Quantification of observed electrical effect on the raindrop size distribution in tropical clouds. Journal of Geophysical Research: Atmospheres, 123. https://doi.org/10.1029/2017JD028205

Ochs, H. T., III, and R. R. Czys (1987) Charge effects on the coalescence of water drops in free fall, Nature, 327, 606–608.

Mansell, E. R., C. L. Ziegler, and E. C. Bruning (2010), Simulated electrification of a small thunderstorm with two-moment bulk microphysics, J. Atmos. Sci., 67(1), 171–194, doi:10.1175/2009JAS2965

Mattos, E. V., L. A. T. Machado, E. R.Williams, and R. I. Albrecht (2016) Polarimetric radar characteristics of storms with and without lightning activity, J. Geophys. Res. Atmos., 121,14,201–14,220, doi:10.1002/ 2016JD025

Palucki, J. L., M. I. Biggerstaff, D. R. MacGorman, and T. Schuur (2011) Comparison between low-flash and non-lightning-producing convective areas within a mature mesoscale convective system,Weather Forecasting,26, 468–486, doi:10.1175/WAF-D-10-05012.1.

Pawar V. S. , M. A. Domkawale , S. D. Pawar , P. S. Salvekar and P. Pradeep Kumar, (2017a) Inter annual variability of tropospheric NO2 and tropospheric ozone over Maharashtra (India) : the role of lightning, Remote Sensing Letters, doi.org/10.1080/2150704X.2017.1346398.

Pawar S.D., V. Gopalakrishnan , P. Murugavel , N.E. Veremey , A. A. Sinkevich (2017b) Possible role of aerosols in the charge structure of isolated thunderstorms, Atmospheric Research 183 463 ,331–340.

Rayleigh Lord (1879) The influence of electricity on colliding water drops, Proc. Roy. Soc. London, 28, 406-409.

Romatschke, U., and Houze, R. A. Jr. (2011) Characteristics of precipitating convective systems in the premonsoon season of South Asia. Journal of Hydrometeorology, 12, 157–180

Rosenfeld, D. (2000) Suppression of rain and snow by urban air pollution, Science, 287, 1793–1796

Rosenfeld, D., Lahav, R., Khain, A.and Pinsky, M. (2002) The role of sea spray in cleansing air pollution over ocean via cloud processes. Science, **297,** 1667–1670

Rosenfeld, D. and Woodley, W. L. (2003) Closing the 50-year circle: From cloud seeding to space and back to climate change through precipitation physics. Pp. 59–80 in Cloud systems, HURRICANES, and the Tropical Rainfall Measuring Mission (TRMM). Eds. Wei-Kuo Tao and Robert Adler. Meteorol. Mono., Vol. 51, American Meteorological Society

Rosenfeld, D. (2000) Suppression of rain and snow by urban air pollution, Science,287, 1793–1796

Schlamp, R. J., S. N. Grover, and H. R. Pruppachcr (1976) A numerical investigation of the effects of electric charge and vertical external electric fields on the collision efficiency of cloud drops, J. Atmos. Sci., 33, 1747-1755.

Schlamp, R. J., S. N. Grover, H. R. Pruppacher, and A. E. Hamielec (1979) A numerical investigation of the effect of electric charges and vertical external electric fields on the collision efficiency of cloud drops: Part II, J. Atmos. Sci., 36(2), 339 – 349.

Shahrban, M., J. P. Walker, Q. J. Wang, A. Seed, and P. Steinle (2016) "An evaluation of numerical weather prediction based rainfall forecasts." Hydrol. Sci. J. 61 (15): 2704–2717. https://doi.org/10.1080/02626667.2016.1170131

Shrestha, D. L., D. E. Robertson, Q. J. Wang, T. C. Pagano, and H. A. P. Hapuarachchi, (2013) Evaluation of numerical weather prediction model precipitation forecasts for short-term streamflow forecasting purpose. Hydrol. Earth Syst. Sci., 17, 1913–1931, doi:10.5194/hess-17-1913-2013.

Singla, V., Mukherjee, S., Kashikar, A.S. et al. Environ Sci Pollut Res (2019) 26: 7071. https://doi.org/10.1007/s11356-019-04162-w

Standler, R. B., and W. P. Winn, Effects of coronae on electric field beneath thunderstorms, Q. J. R. Meteorol. Soc., 105, 285-302, 1979.

Soula, S., and S. Chauzy, Multilevel measurement of the electric field underneath a thundercloud, 2. Dynamical evolution of ground space charge, J. Geophys. Res.,96, 22,327-22,336, 1991.

Thompson, G., Rasmussen, R.M., Manning, K. (2004) Explicit forecasts of winter precipitation using an improved bulk microphysics scheme. Part I: description and sensitivity analysis. Mon. Weather Rev. 132, 519–542.

Thompson G, Field PR, Rasmussen RM, Hall WD (2008) Explicit forecasts of winter precipitation using an improved bulk microphysics scheme. Part II: Implementation of a new snow parameterization. Mon. Weather Rev. 136: 5095–5115.

Tokay, A. and D.A. Short, (1996) Evidence from Tropical Raindrop Spectra of the Origin of Rain from Stratiform versus Convective Clouds. *J. Appl. Meteor.*, **35**, 355–371, https://doi.org/10.1175/1520-0450(1996)035<0355:EFTRSO>2.0.CO;2

Twomey, S., M. Piepgrass, and T. L. Wolfe, (1984) An assessment of the impact of pollution on global cloud albedo. Tellus, 36B, 356–366.

Wang, G., Yang, J., Wang, D., and Liu, L.(2016) A quantitative comparison of precipitation forecasts between the storm-scale numerical weather prediction model and auto-nowcast system in Jiangsu, China. Atmospheric Research, 181, 1–11. https://doi.org/10.1016/j.atmosres.2016.06.004

Walther, A., J.-H. Jeong, G. Nikulin, C. Jones, and C. Deliang, (2013) Evaluation of the warm season diurnal cycle of precipitation over Sweden simulated by the Rossby Centre regional climate model RCA3. Atmos. Res., **119**, 131–139, doi:https://doi.org/10.1016/j.atmosres.2011.10.012

Williams, E. R., S. A. Rutledge, S. C. Geotis, N. Renno, E. Rasmussen, and T. Rickenbach, (1992) A radar and electrical study of tropical hot towers, J. Atmos. Sci., 49, 1386–1395.

Williams, E.R.; Joan Montanya (2019)_A closer look at lightning reveals needle-like structures, nature, volume-568, https://doi.org/10.1038/d41586-019-01178-7.

Winn, W. P., G. W. Schwede, and C. B. Moore (1974) Measurements of electric fields in thunderclouds, *J. Geophys. Res*., 79, 1761– 1767

Y. Yang *et al*.(2018) Corona Discharge-Induced Rain and Snow Formation in Air in *IEEE Transactions on Plasma Science*, vol. 46, no. 5, pp. 1786-1792, doi: 10.1109/TPS.2018.2820200.

Figure Captions:

Figure1: (a) Nested model domain, (b) topographical map encompassing domain d04.

Figure2: The spatial distribution of lightning observed in the model domain d04. Panels (a-e) correspond to strongly electrified (SE) events and (f-j) corresponds to weakly electrified events (WE). The labelling of all the events is same as Table 1 and 2. For events 2(a-c) distribution was derived from the World Wide Lightning Location Network (WWLLN) and for the rest from the Maharashtra Lightning Location Network (MLLN).

Figure3: Comparison of simulated rain rate (a-e) and simulated RDSD (f-j) with the observation for the strongly electrified (SE) events observed over the HACPL. N(D) is the number density of drops. The legends in the figure 'Obs' indicated observation (red) while 'Morr' indicated Morrison double moment scheme (blue).

Figure4: As in Figure 3 but for weakly electrified (WE) events.

Figure5: (a) Bar plot representation of the mean value λ for all the SE and WE events reported in Table 1-2. The λ is averaged over the entire rainy periods for each events. Scatter plot of slope parameter λ with rain intensity (b) strongly electrified (SE), (c) weakly electrified (WE) rain events observed over the HACPL. The values of λ are estimated using the method of moments reported in Konwar et al.,(2014).

Figure 6: Time evolution of λ before and after some isolated lightning event recorded within 700m of the HACPL. The vertical dashed bar indicate the time of lightning recorded by the Maharashtra Lightning Location Network (MLLN). The green downward arrow indicates the trough in λ after the lightning. It may be noted here that, the observed dip in the values of λ were inherently associated with a transient amplification in rate intensity.

Figure7: Scatter plot of slope parameter, λ with surface measured electric field (a) 3 June, 2008, (b) 31 August, (c) 1 Sept., (d) 9 Sept., 2008. All the events are observed over the Atmospheric Electricity Laboratory, (AEO) Pune. 'r' indicate correlation coefficient with p-value <0.0001.

Figure8: As in Figure 3 but with modified Morrison scheme. The legends 'Obs' indicated observation, 'Morr' indicated Morrison scheme and 'Morr(M)' indicated modified Morrison scheme.

Figure9: Comparison of simulated precipitation (a-c) and corresponding RDSD (d-f) with the observation for the SE events observed over Solapur documented in table S3. The legends 'Obs' refers to observation, 'Morr' refers to Morrison scheme and 'Morr(M)' refers to modified Morrison scheme.

Figure10: (a) Bar representation of total CCN number concentration for SE and WE events at 0.3% supersaturation measured in pre-storm interval at the HACPL. Labelling is same as Table 1& 2. (b) Comparison of simulated rain intensity with aerosol modification. (c) Comparison of the RDSD. The simulation with aerosol modification alone is indicated as 'Morr+AS' while simulation with both aerosol and λ modification is indicated as 'Morr(M)+AS' where'Morr' indicates Morrison scheme and 'Morr(M)' indicates modified Morrison scheme.

Figure11: Area and time-averaged vertical distribution of simulated (a) Ice mixing ratio (kg kg^{-1}), (b) Snow mixing ratio (kg kg^{-1}), (c) Graupel mixing ratio (kg kg^{-1}) (d) Rain mixing ratio (kg kg^{-1}) for the events observed over the HACPL. The blue and red curves correspond to the WE and SE events, respectively. Each profile has been averaged over 5 events each.

Figure12: Inter-comparison among observation and simulation with NCEP Initial Condition (IC) as well with ensemble mean of 10 member ensemble generated by perturbing the temperature field of NCEP IC, labelled as Obs, NCEP, ENS. Mean (NCEP), respectively. (a-b) precipitation intensity, (c-d) RDSD. The vertical bars indicate the respective standard deviation.

Tables:

Table 1: Some Cloud and Electrical properties of the Strongly Electrified (SE) events.

Dates	Cloud top temperature(K)	Total accumulated rain from JWD (mm)	Total column cloud liquid water (kg m^{-2})	Daily accumulated lightning count in d04
5 October,2012(a)	250	21.64	0.19	98
2 June,2013(b)	-	30.16	0.08	186
10 sept.,2013(c)	-	71.5	0.04	249
15 May,2015(d)	252	6.98	0.002	898
30 May,2015(e)	-	3.74	0.03	173

Note: The lightning counts for the events (a-c) are derived from WWLLN and for (d-e) from MLLN with higher detection efficiency. The total column cloud liquid water was derived from the Era-interim datasets while cloud top temperature was derived from MODIS terra datasets. The labelling for the events is same as Figure 2

Table 2: Some Cloud and Electrical properties of the Weakly Electrified (WE) events.

Dates	Cloud top temperature(K)	Total accumulated rain JWD (mm)	Total column cloud liquid water (kg m^{-2})	Daily accumulated lightning count in d04
31Aug,2014(f)	250	116	0.75	0
26Oct.,2014(g)	-	5.4	0.06	0
14Nov.,2014(h)	-	13.41	0.01	0
2 Oct.,2015(i)	-	22.7	0.01	0
3 Oct.,2015(j)	270	70	0.004	0

Note: The lightning counts for the events (a-e) derived from MLLN. The total column cloud liquid water was derived from the Era-interim datasets while cloud top temperature was derived from MODIS terra datasets. The labelling for the events is same as Figure 2.

Table 3: The WRF Model Experiment Design.

	Name of Experiment			
Physical Processes	Control (CTL) run	Modification of limit of λ in Morrison scheme	Modification of aerosol number concentration	Modification of aerosol number concentration + Modification of λ
Convective process	Betts-Miller-Janjic (BMJ)	Betts-Miller-Janjic (BMJ)	BMJ	BMJ
Microphysics process	Default Morrison Scheme (Morr) following *Morrison et al.*,2005.	Modified Morrison (Morr(M)). The default minimum value of λ in the physics module has been replaced with a new λ, averaged over all the five SE events observed over the HACPL	Default Morrison Scheme (Morr) + change in aerosol number concentration in Mode 1(0.05 μm)	Modified Morrison (Morr(M)) + change in aerosol number concentration in Mode 1(0.05 μm)
Model Initialization	For the events (b-d) documented in the Table 1, (a,c,d,e) in Table 2 and the events (a-b) in Figure 6, the model was initialized with 00:00:00 UTC NCEP ICs while for the events (a & e) in Table 1, (b) in Table 2 and event (c) in Figure 6 , model was initialized with 12:00:00 UTC IC.			

Note: Other physical processes (short and long wave radiation scheme) are kept the same for both sets of sensitivity experiment.

Figure 1

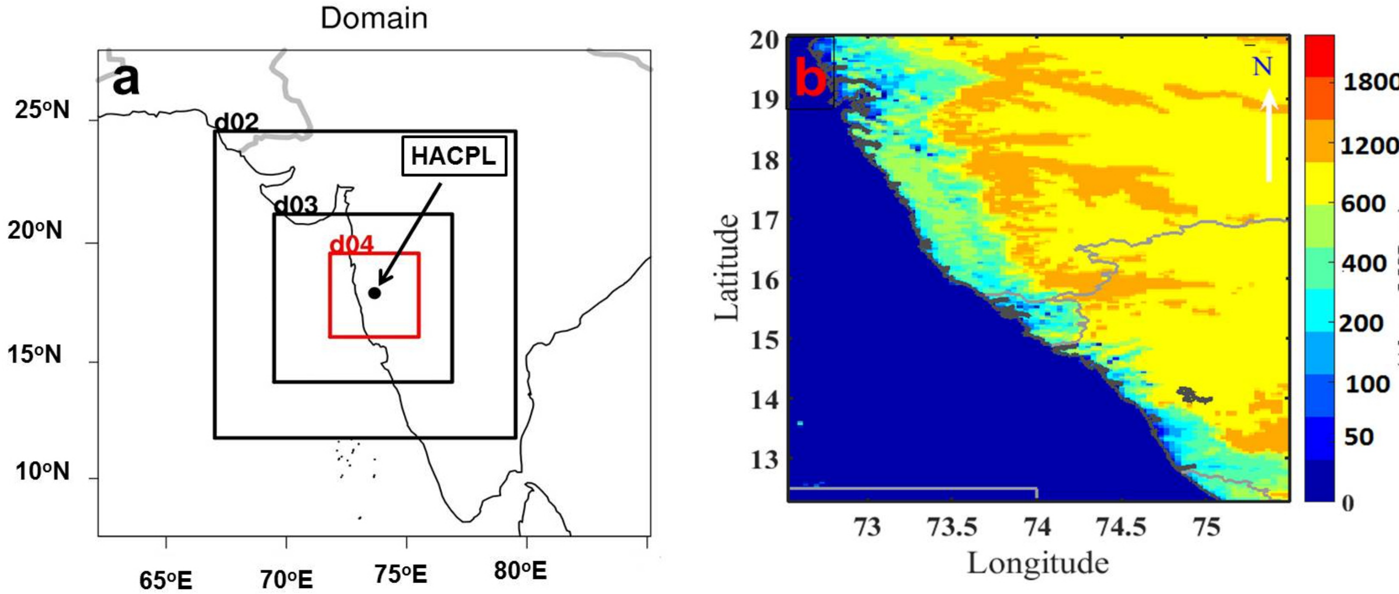

Figure 1:

Figure 2

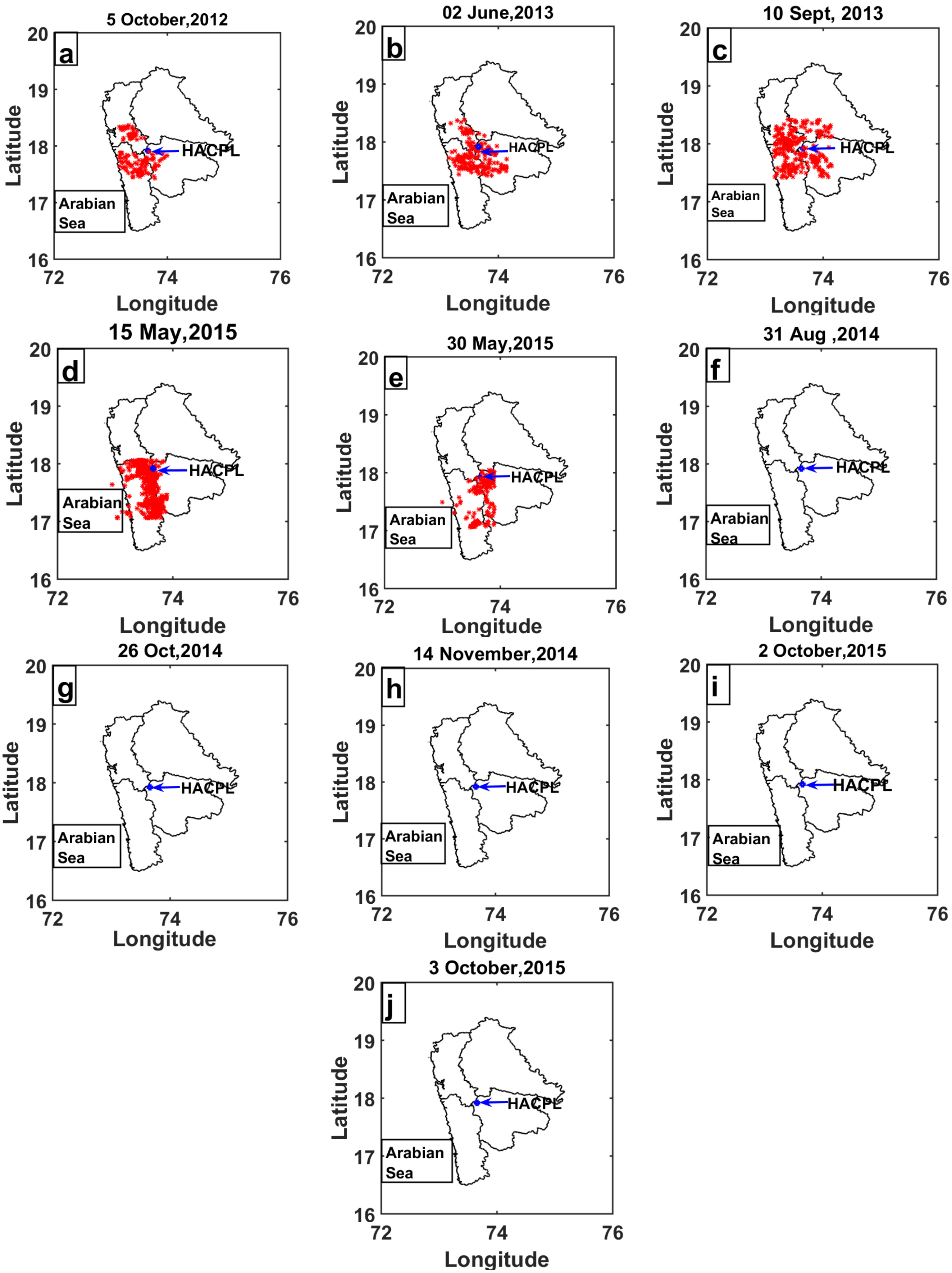

Figure 2:

Figure 3

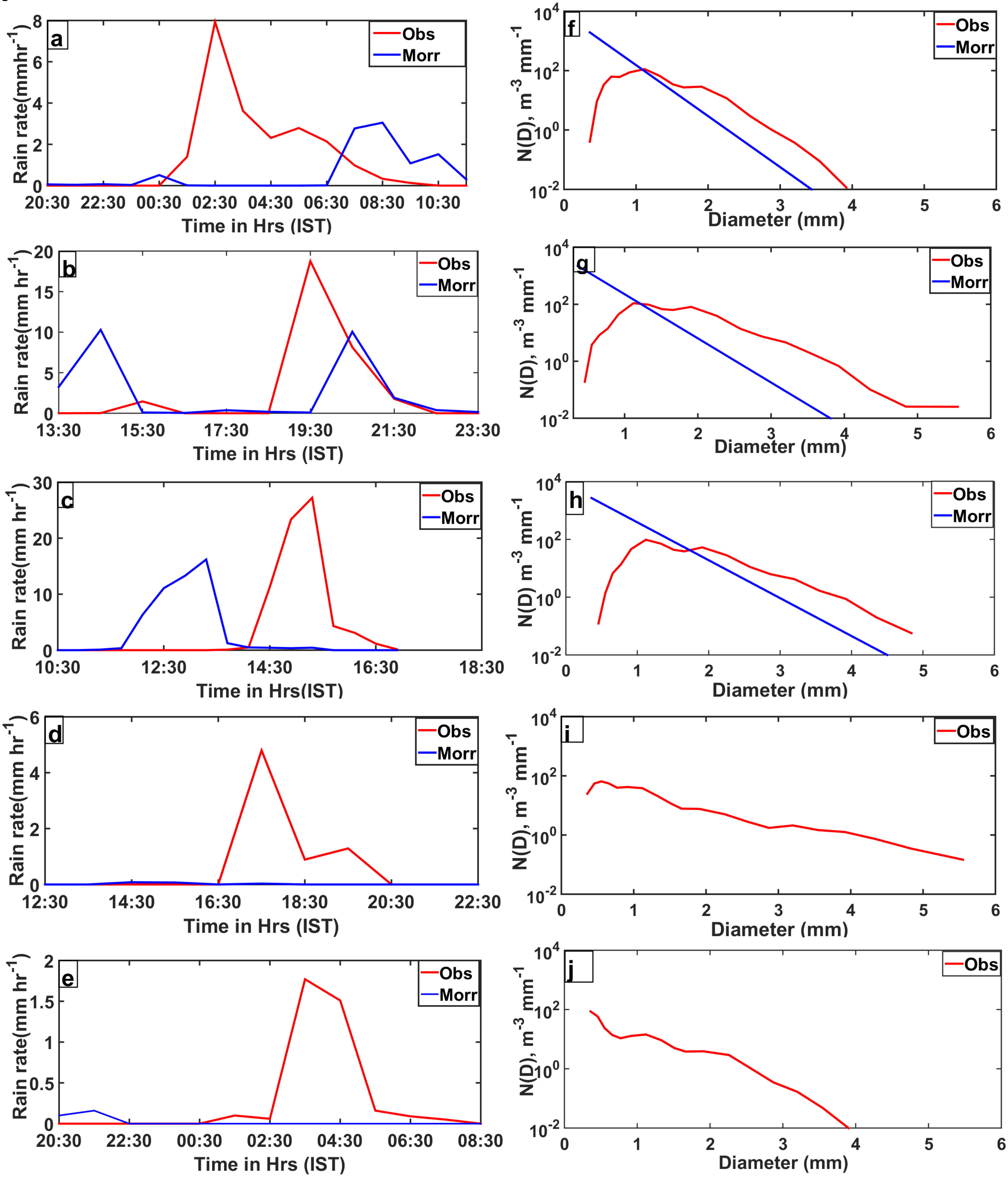

Figure 3:

Figure 4

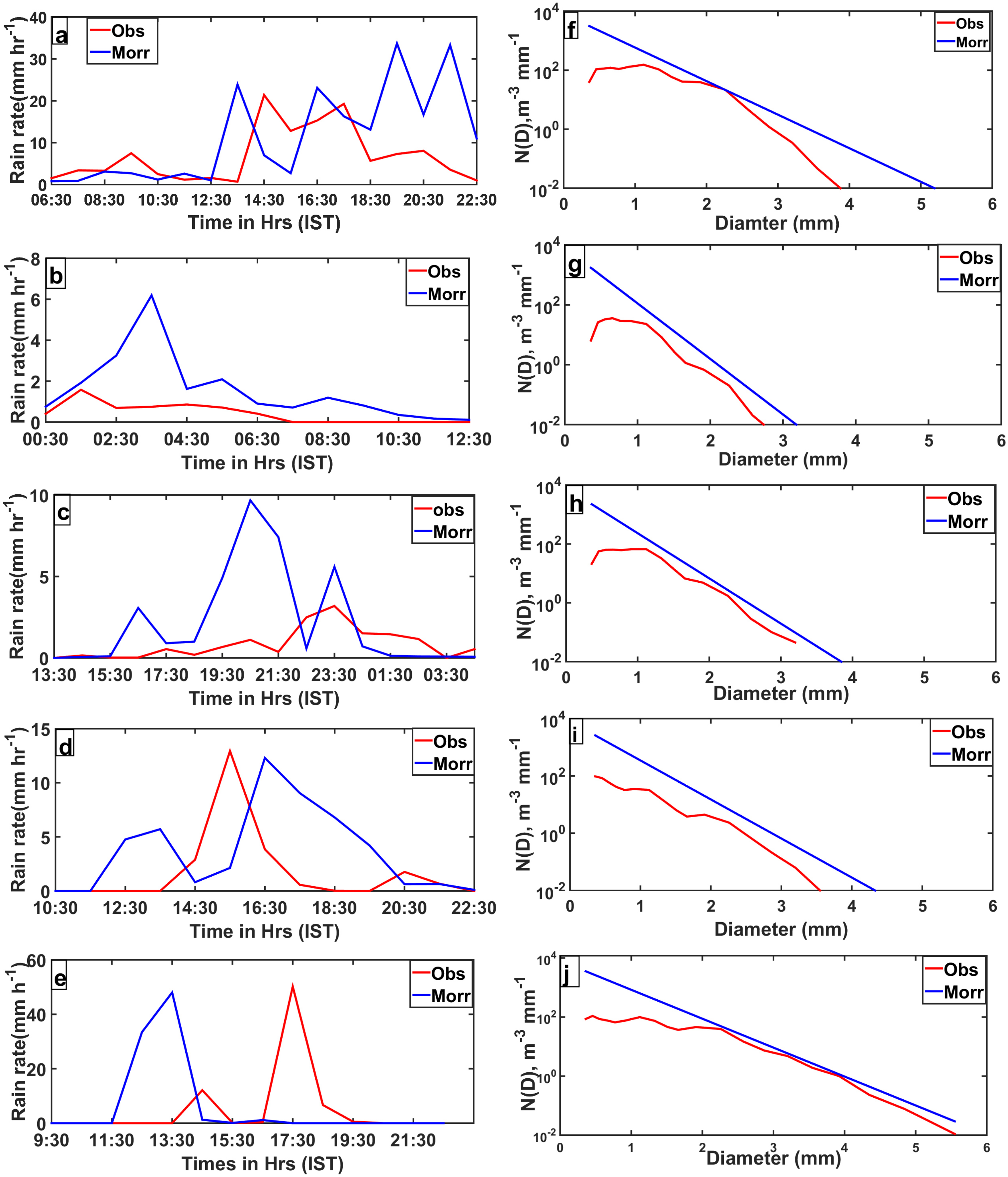

Figure 4:

Figure 5

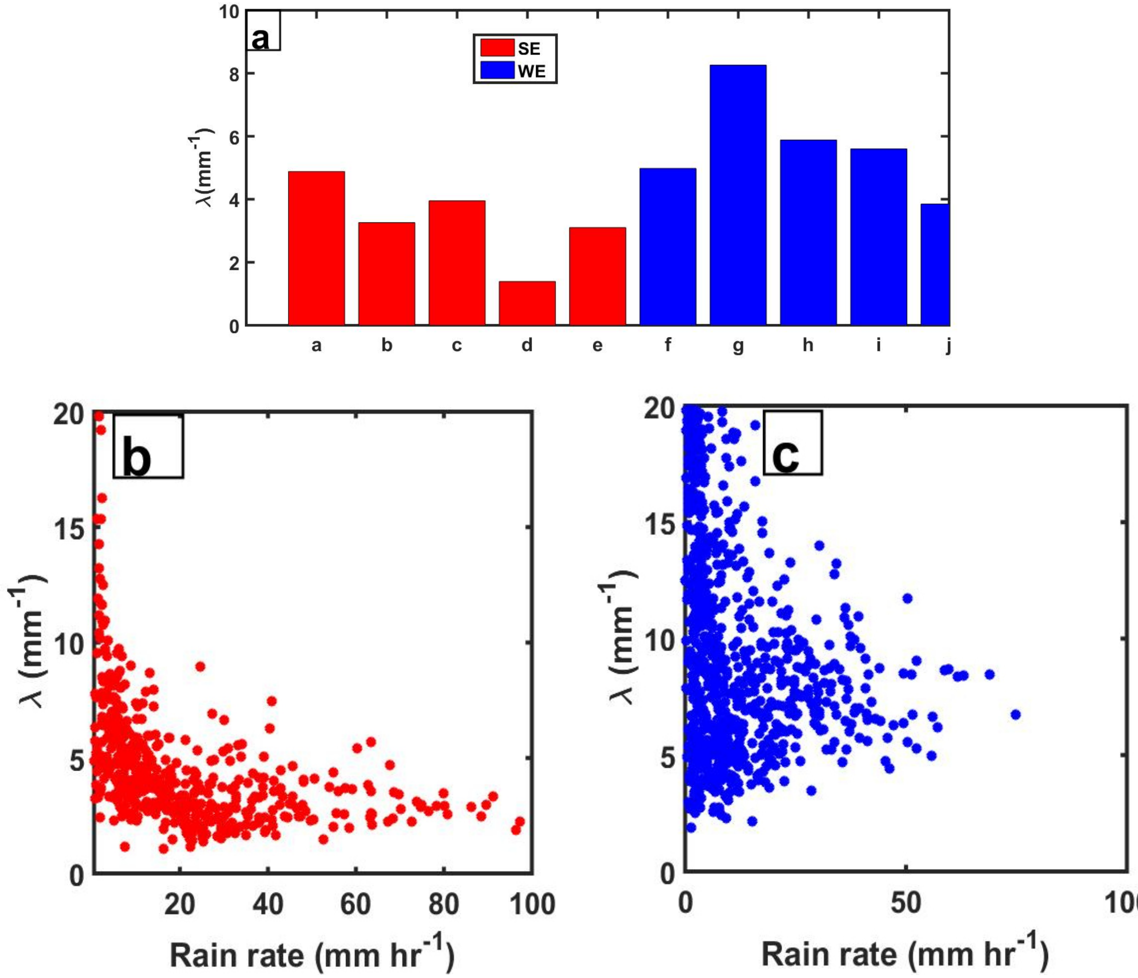

Figure 5:

Figure 6

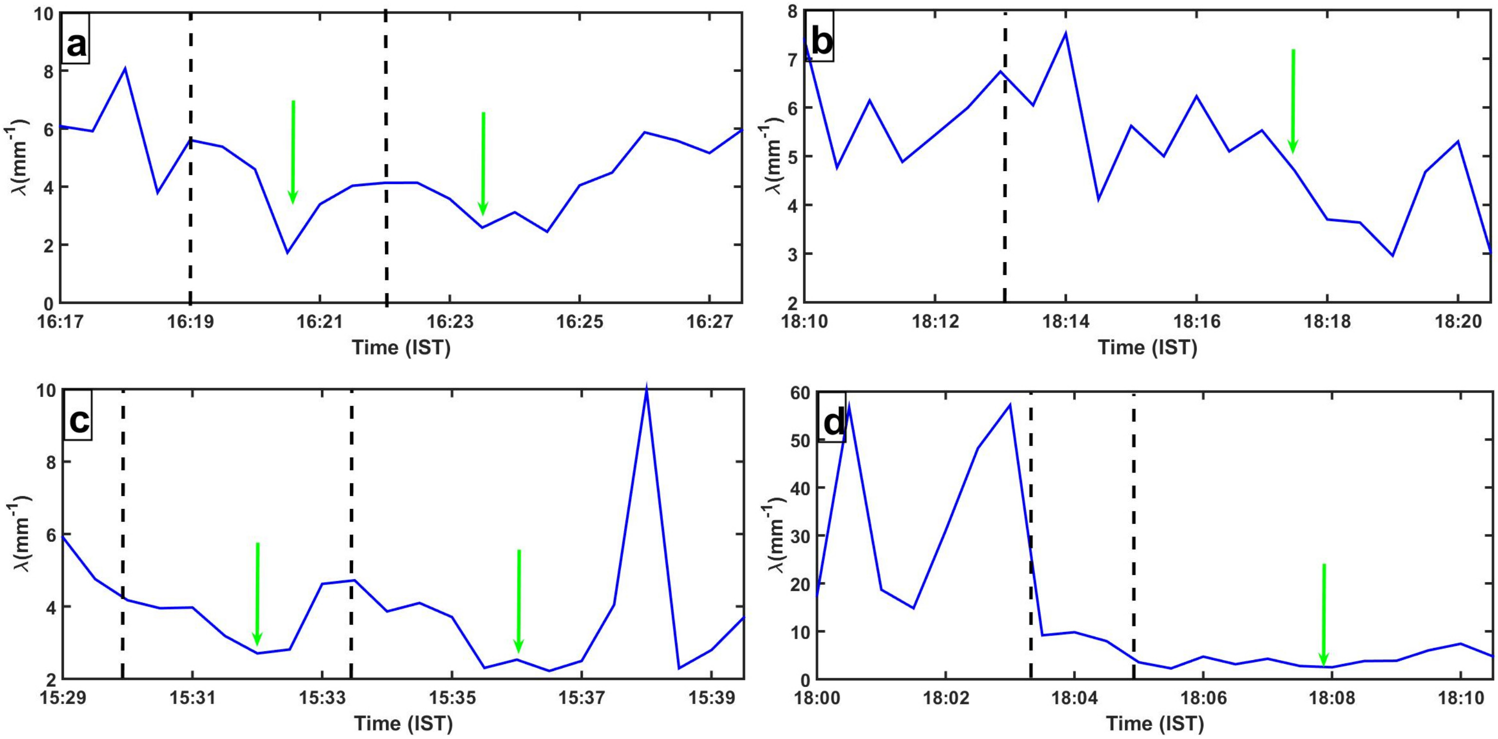

Figure 6:

Figure 7

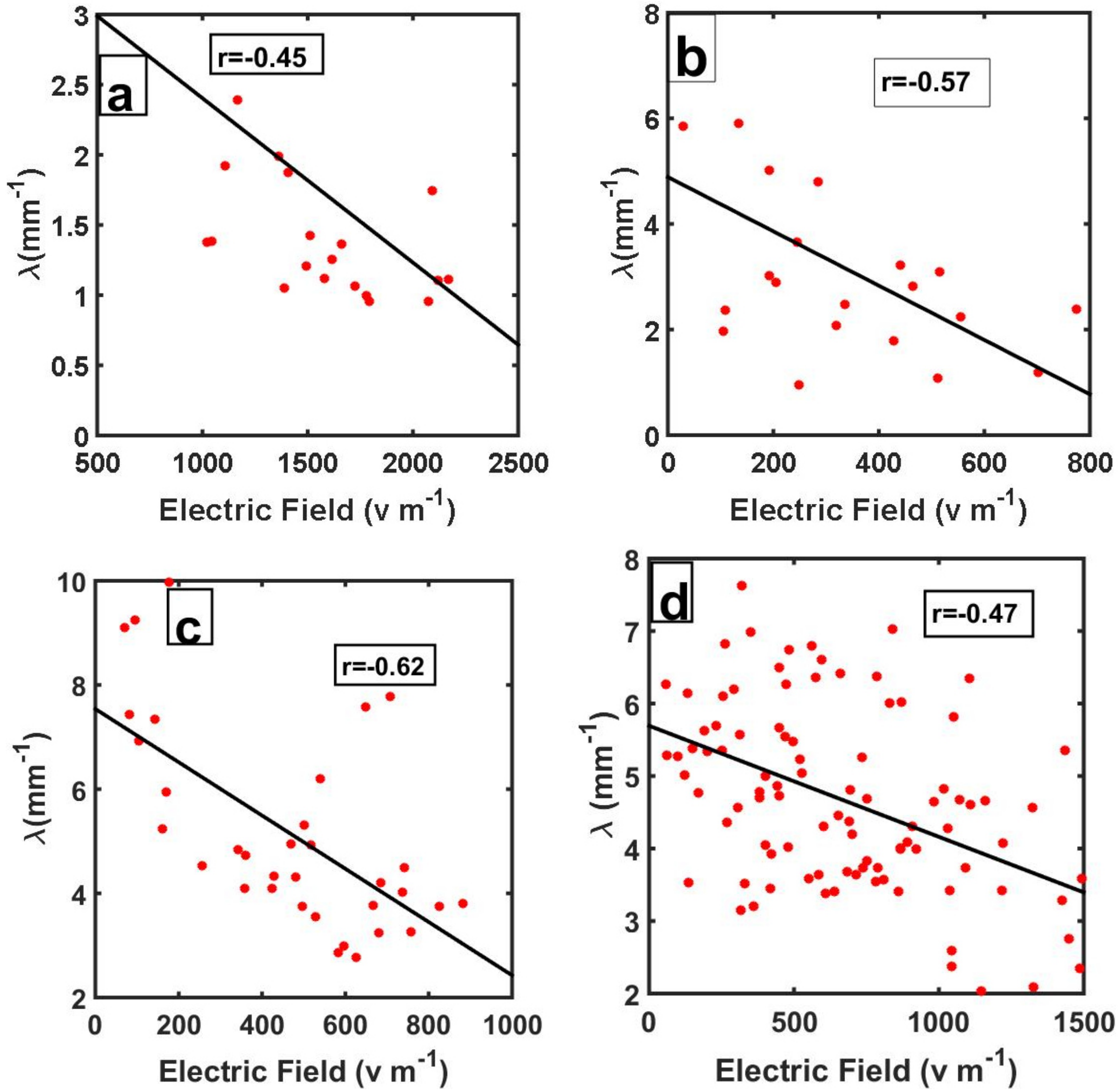

Figure 7:

Figure 8

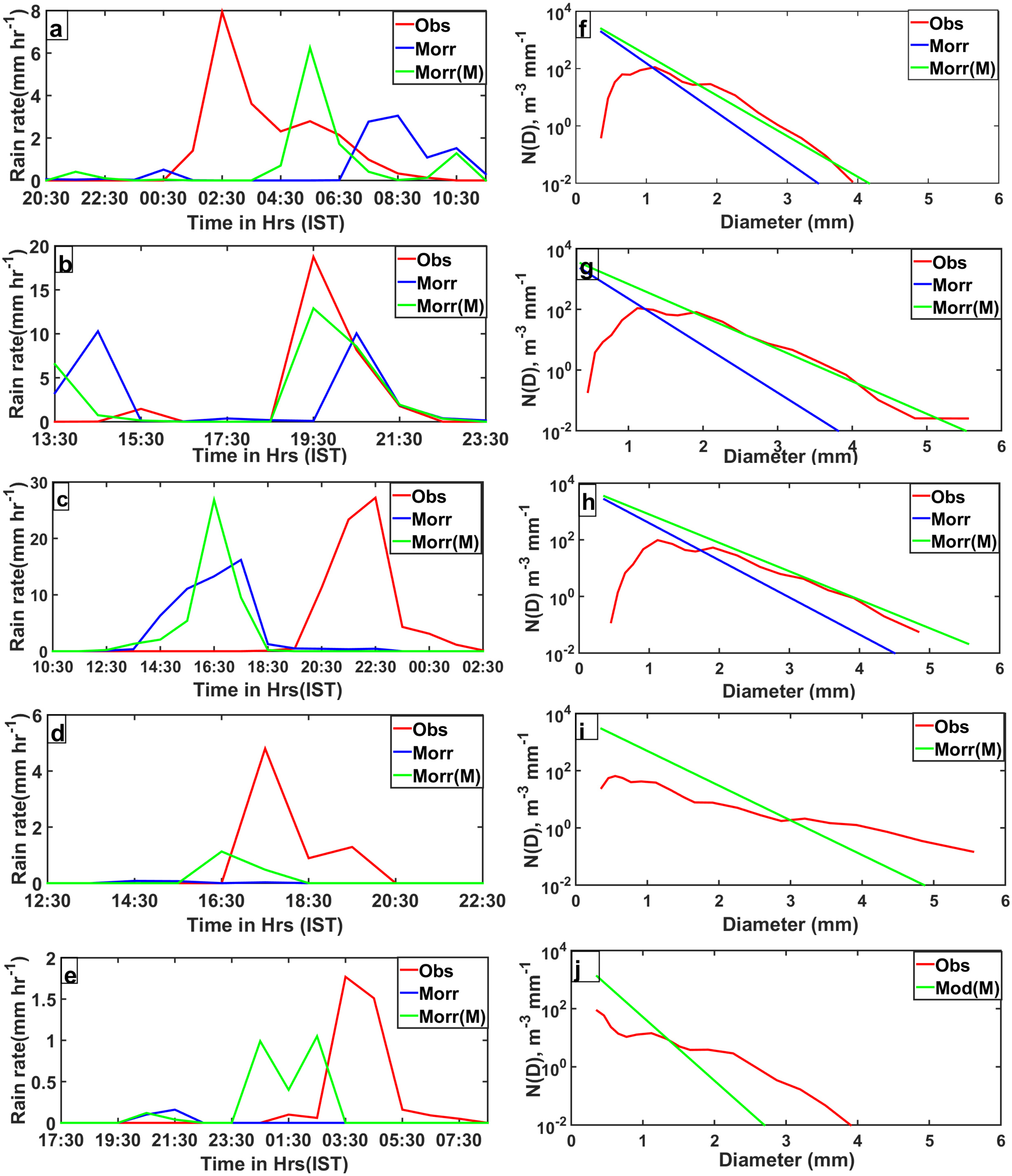

Figure 8:

Figure 9

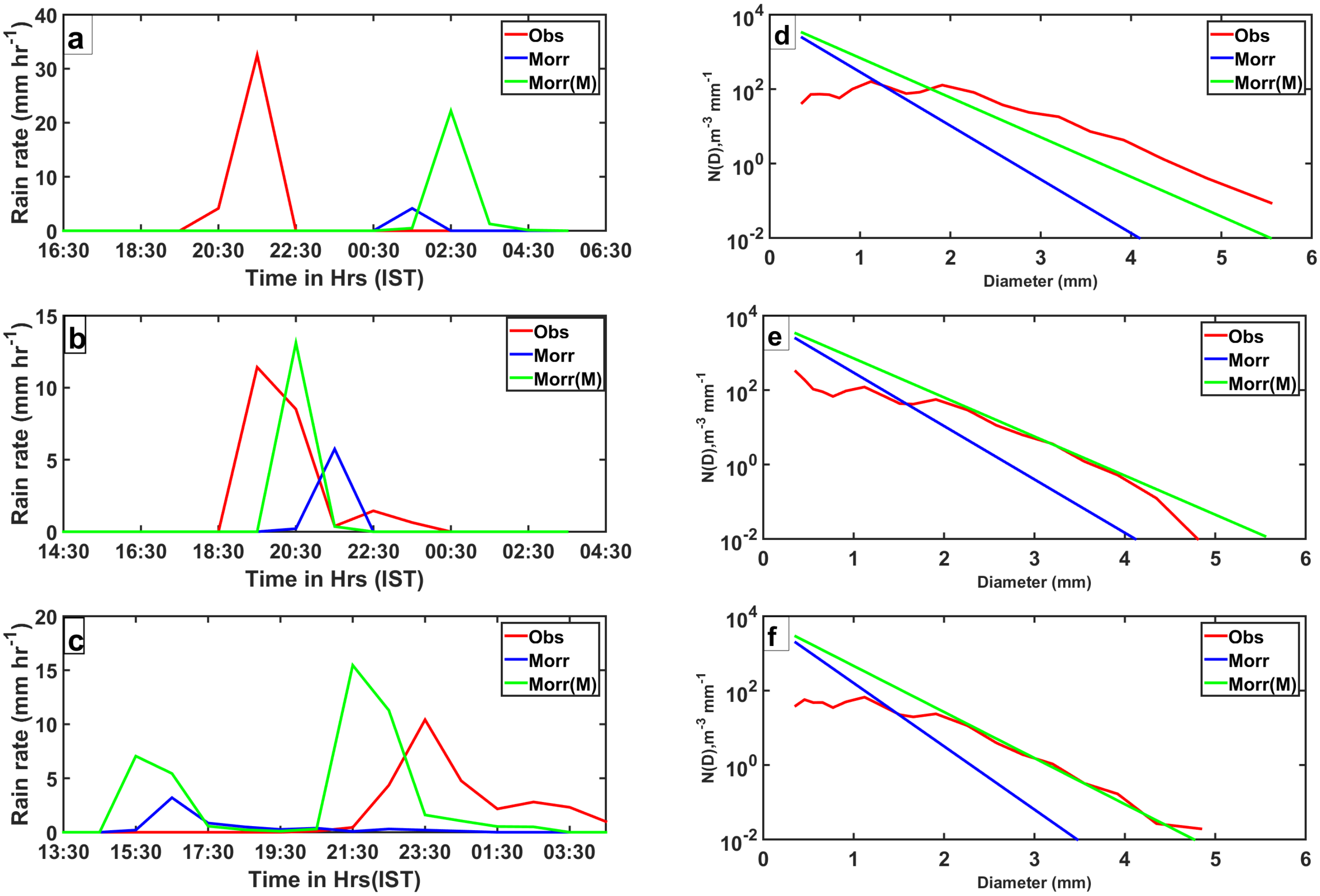

Figure 9:

Figure 10

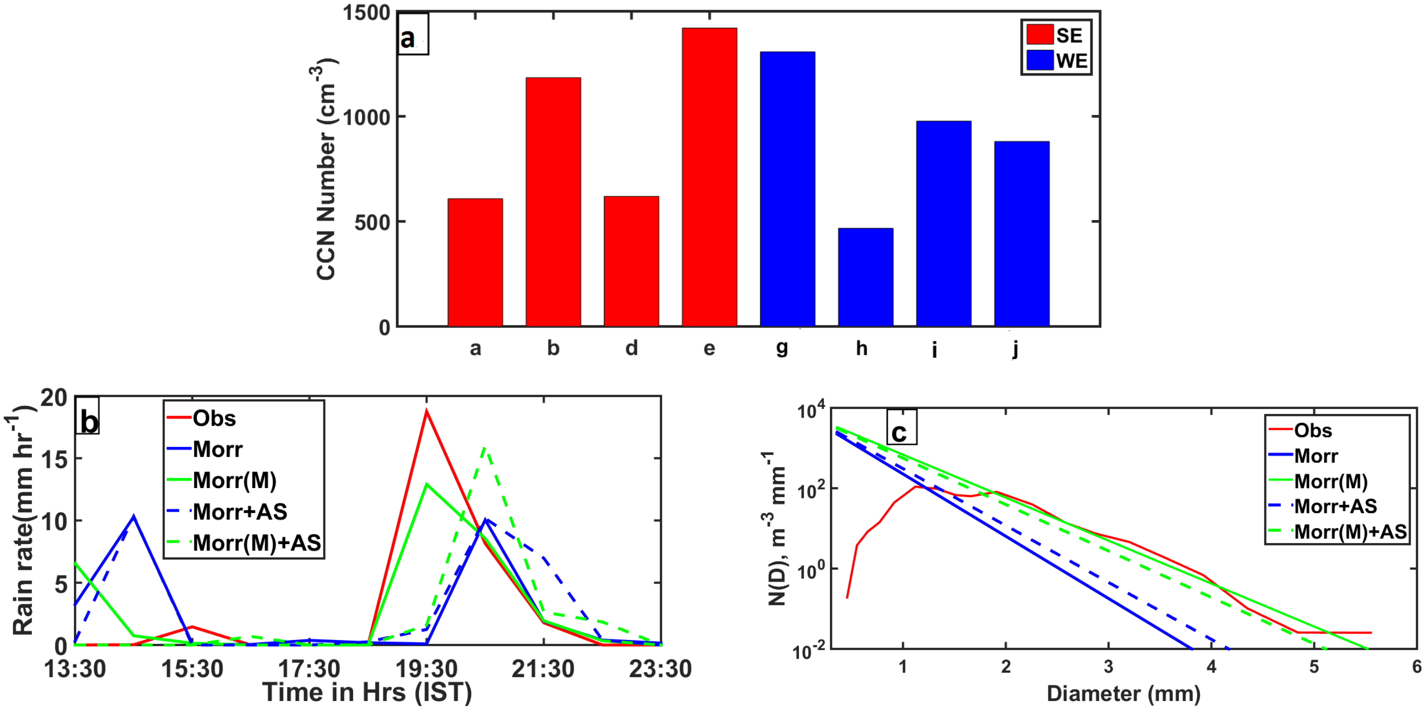

Figure 10:

Figure 11

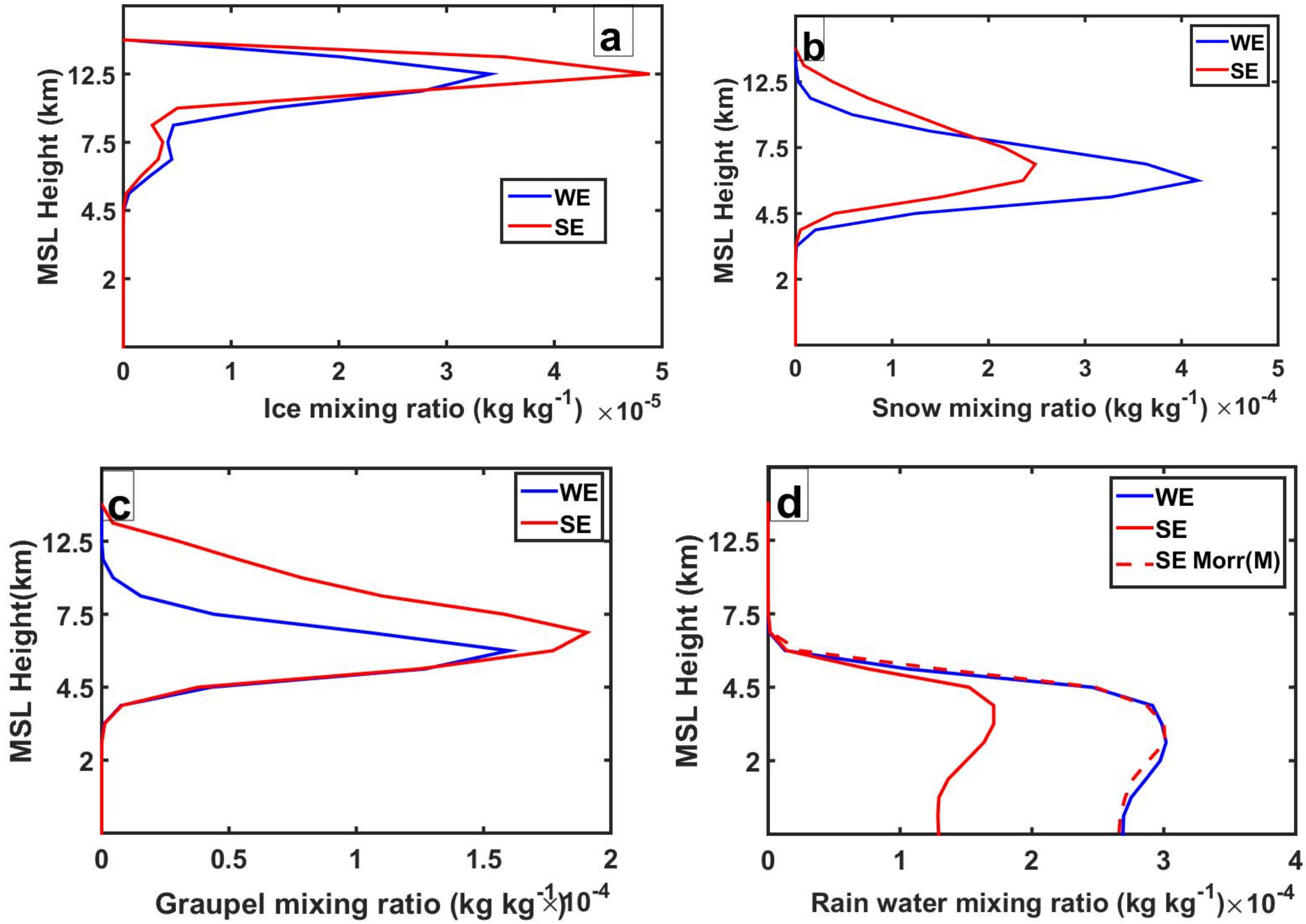

Figure 11:

Figure 12

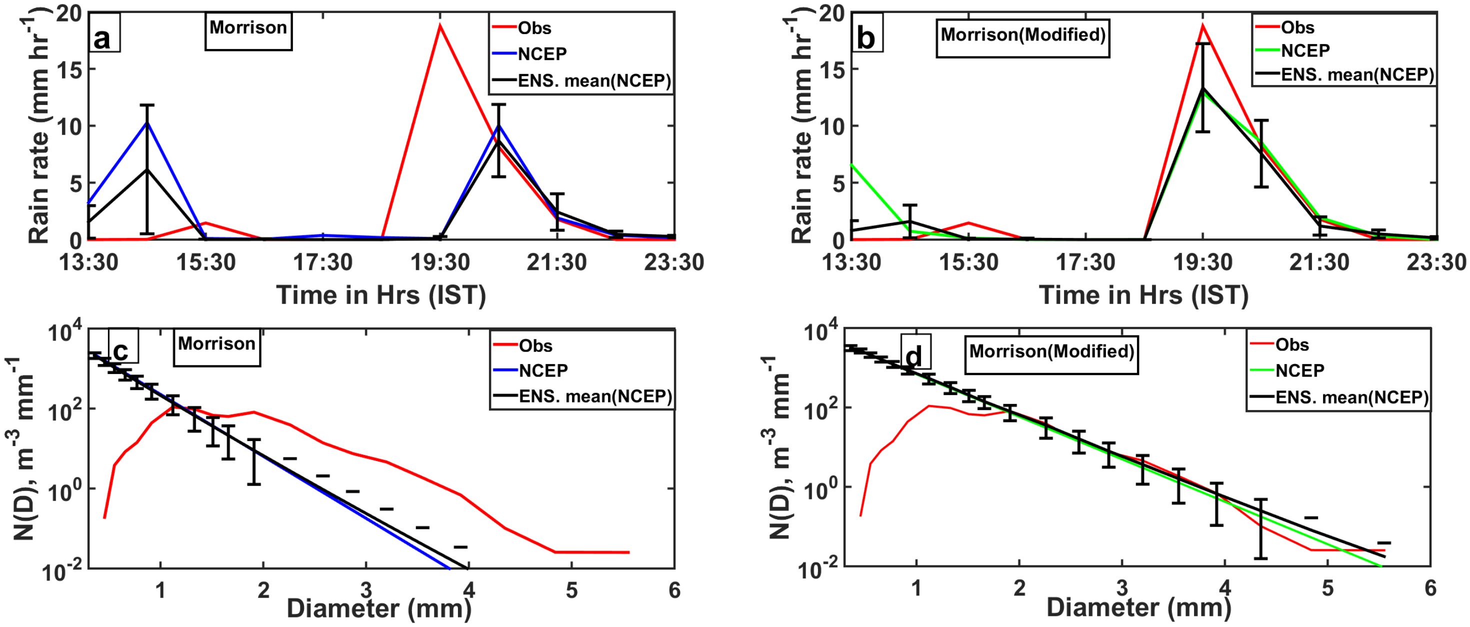

Figure 12:

Declaration of interests

☒ The authors declare that they have no known competing financial interests or personal relationships that could have appeared to influence the work reported in this paper.

☐The authors declare the following financial interests/personal relationships which may be considered as potential competing interests:

None

Click here to access/download
Supplementary Material
Supporting Online Materials.pdf

Personal Profile

Name : Dipjyoti Muidar

Father's Name : Chitramal Mudiar

Mother's Name : Manju Mudiar

Date of Birth : 01 March, 1988

Nationality : Indian

Address of Correspondence: Indian Institute of Tropical Meteorology (IITM), P.O.: NCL Post, Pashan, Pune-411008, India

Permanent Address : Vill.-Tengabari, Post- Solmara, Dist.-Nalbari, Assam, India

Email : d.mudiar@gmail.com, dipjyoti@tropmet.res.in

Academic Qualification:

EXAM PASSED	YEAR OF PASSING	BOARD/UNIVERSITY	SUBJECTS	DIVISON
MSC	2012	GAUHATI UNIVERSITY	**PHYSICS**	FIRST CLASS
BSC	2010	GAUHATI UNIVERSITY	**PHYSICS**(HONORS), MATHS,CHEMISTRY	FIRST CLASS

Number of paper published in peer reviewed journal: 1

Paper Presented in International Conference: 3

Date:

Place: Varanasi Dipjyoti Mudiar